Contributions to adaptive equalization and timing recovery for optical storage systems

Citation for published version (APA):
Riani, J. (2008). *Contributions to adaptive equalization and timing recovery for optical storage systems*. [Phd Thesis 1 (Research TU/e / Graduation TU/e), Electrical Engineering]. Technische Universiteit Eindhoven. https://doi.org/10.6100/IR638300

DOI:
10.6100/IR638300

Document status and date:
Published: 01/01/2008

Document Version:
Publisher's PDF, also known as Version of Record (includes final page, issue and volume numbers)

Contributions to Adaptive Equalization and Timing Recovery For Optical Storage Systems

PROEFSCHRIFT

ter verkrijging van de graad van doctor aan de Technische Universiteit Eindhoven, op gezag van de Rector Magnificus, prof.dr.ir. C.J. van Duijn, voor een commissie aangewezen door het College voor Promoties in het openbaar te verdedigen op woensdag 19 november 2008 om 14.00 uur

door

Jamal Riani

geboren te Tétouan, Marokko

Dit proefschrift is goedgekeurd door de promotor:

prof.dr.ir. J.W.M. Bergmans

Copromotor:
dr. W.M.J. Coene

CIP-DATA LIBRARY TECHNISCHE UNIVERSITEIT EINDHOVEN

Riani, Jamal

Contributions to Adaptive Equalization and Timing Recovery For Optical Storage Systems / by Jamal Riani. - Eindhoven : Technische Universiteit Eindhoven, 2008.
Proefschrift. - ISBN 978-90-386-1436-6
NUR 959
Subject headings: signal processing / adaptive equalizers / timing recovery / Viterbi detection / digital storage systems.

Committee:

prof.dr.ir. J.W.M. Bergmans
Eindhoven University of Technology, The Netherlands.

dr. W.M.J. Coene
ASML Research, Veldhoven, The Netherlands.

prof.dr. D.T.M. Slock
Institut Eurecom, France.

dr. H. Zhang
Shanghai Jiaotong University, China.

prof.dr.ir. P.G.M. Baltus
Eindhoven University of Technology, The Netherlands.

This work has been supported in part via a European IST-project called ‘TwoDOS’
(Project Nr. IST-2001-34168)

Pour Yemma et Baba (que Dieu les préserve).

Contributions to Adaptive Equalization and Timing Recovery For Optical Storage Systems

During the last decades, storage density and data rate of optical storage devices have increased dramatically. This increase arises out of the evolution from the Compact Disc (CD) with a storage capacity of 680 MByte and a user data rate of 1.4 Mbit/s to the recently standardized 3rd generation format called Blu-ray Disc (BD) with a single layer storage density of 25 GByte and a user data rate of around 35 MBit/s.

Although this explosive growth has been mainly due to major advances in the physics, i.e. due to the improvements made in the design of laser diodes with a shorter wavelength and lenses with a higher numerical aperture, rapid advances in coding and signal processing algorithms have also played a significant role.

As storage density and data rate of optical storage systems increase, many system artifacts, e.g. media noise and channel nonlinearities, become important and result in reduction of system margins and signal-to-noise ratio. In order to cope with these artifacts, data receivers for optical storage systems need to employ powerful signal processing methods.

Among the signal processing blocks in data receivers for optical storage systems, the equalizer, data-detector and the timing recovery block are the most important. The way of equalization consists of using one or more filters to mitigate the effect of interference and noise prior to data-detection. The timing recovery block deals with the synchronization of the readback signal with the data written on the disc.

Because of system artifacts at high storage densities, the tasks of equalization and timing recovery become more difficult and, at the same time, increasingly critical for reliable data recovery. Existing equalization and timing recovery algorithms can not cope with these artifacts efficiently.

The objective of this thesis is to push the state of the art in equalization and timing recovery for optical storage systems and propose powerful adaptive equalization and timing recovery algorithms to meet the challenges of future optical storage systems. The thesis contains seven chapters. These chapters are written to be as independent

and as self-contained as possible, so that they can be read separately.

Chapter 1 gives an introduction to optical storage technology and a review of signal processing techniques for optical storage data receivers. It also presents the main challenges in future high-density optical storage systems. This introductory chapter concludes with the motivations, contributions and organization of the thesis.

In Chapters 2 and 3 we introduce a novel adaptive equalization technique that seeks to minimize the probability of detection error. These chapters explain, first, the limitations of the existing adaptive equalization techniques and then propose a new adaptation technique for detection error rate minimization. The key property of the new adaptation technique is its selectivity in the sense that it mainly focuses on the data patterns that have the highest likelihood of detection error. The strength of the proposed technique is not restricted to providing a better performance but extends to allowing very low implementation costs.

Chapter 4 reports an asynchronous adaptive equalization scheme that aims at minimizing latencies inside the timing-recovery loop. The chapter explains the implication of this scheme for equalizer adaptation and proposes a highly simple yet efficient method for asynchronous equalizer adaptation.

Following this, and with respect to the objective of strengthening the timing-recovery loop, Chapter 5 focuses on designing a timing-recovery scheme for channels with data-dependent noise. The applicability of the proposed scheme thus extends well beyond optical storage channels. The chapter exploits the data-dependent and colored nature of noise to improve the performance of timing recovery. It starts by analyzing the maximum-likelihood (ML) timing-recovery criterion and proposes a novel and practical scheme to achieve near ML performance.

As recently all-digital timing recovery is often employed, design of efficient sampling-rate converter (SRC) digital filters is very important for performance optimization and complexity limitation. In this respect, SRC filters that also realize channel equalization can be attractive. Chapter 6 explains first the problem of equalizing SRC filters and then presents algorithms for designing such filters.

Chapter 7 concludes the thesis with some remarks and directions for future work.

The development of all new algorithms presented in the different chapters is supplemented with computer simulation results. These simulation results are used for demonstrating the effectiveness of the proposed algorithms and for validating the analytical developments.

Contents

List of abbreviations

ACS	Add Compare Select
ADC	Analog to Digital Converter
AWGN	Additive White Gaussian Noise
BD	Blu-ray Disc
BER	Bit-Error Rate
CD	Compact Disc
DA	Data-Aided
DD	Decision-Directed
DFE	Decision Feedback Equalization
DVD	Digital Versatile Disc
EBR	Electron-Beam Recording
ECC	Error Correction Code
EFM	Eight-to-Fourteen Modulation
EML	Equalized Maximum Likelihood
FSE	Fractionally Spaced Equalizer
FSR	Fractional Shift Register
ISI	Intersymbol Interference
ISRC	Inverse Sampling Rate Converter
KT	Kuhn-Tucker
LF	Loop Filter
LMS	Least Mean Square
LMSAM	Least-Mean squared SAM
LPF	Low-Pass Filter
LPM	Linear Pulse Modulator
ML	Maximum Likelihood
MLSD	Maximum Likelihood Sequence Detection
MMSE	Minimum Mean Square Error
MRD	Missing-Run Detector
MSE	Mean Square Error

MTF	Modulation Transfer Function
NA	Numerical Aperture
NMBER	Near Minimum-BER
NPML	Noise-Predictive Maximum-Likelihood
NRZ	Non-Return to Zero
NRZI	Non-Return to Zero Inverse
OPU	Optical Pick-up Unit
PDIC	Photo-Detector Integrated Circuit
PGPA	Parallel Generalized Projection Algorithm
PLL	Phase-Locked Loop
PR	Partial Response
PRML	Partial Response Maximum-Likelihood
RLL	Runlength-Limited
RPD	Runlength Pushback Detector
SAM	Sequenced Amplitude Margin
SANR	Signal to Additive Noise Ratio
SMNR	Signal to Media Noise Ratio
SNMBER	Simplified Near Minimum-BER
SNR	Signal to Noise Ratio
SRC	Sampling-Rate Converter
TED	Timing-Error Detector
VA	Viterbi Algorithm
VCO	Voltage Controlled Oscillator
VD	Viterbi Detector
VLP	Video Long Play
VSPM	Vector Space Projection Method
ZC	Zero-Crossing
ZF	Zero Forcing

Chapter 1

Introduction

In this chapter, we first give an overview of optical storage technology. Then we explain the role of signal processing in existing optical storage systems. Following this, we exhibit the key challenges, from the signal processing perspective, of future high-density optical storage systems. The chapter concludes by highlighting the motivations for the work presented in this thesis and by presenting a description of the contribution of each chapter of this thesis.

1.1 Introduction to Digital Optical Storage

In this digital information era, our need for storage is growing explosively because of multimedia requirements for text, images, video and audio. This need has prompted the development of various digital storage systems, such as hard disks, compact discs (CDs), digital versatile discs (DVDs) [31, 115] and magneto-optical disks [155].

Optical storage systems are systems that use light for recording and retrieval of information. Information is recorded on a disc as a change in the material characteristics by modulating the phase, intensity, polarization, or reflectivity of a readout optical beam [10, 42, 111]. In the case of read-only discs, the information is mastered on the media by injection molding of plastics or by embossing of a layer of photopolymer coated on a glass substrate [10, 42]. In other types of optical discs, some information is stamped onto the media and the substrate is coated with a storage layer that can be modified by the user during storage of information.

Compared to the other storage technologies, the most distinguishing feature of optical storage is the removability of the storage medium. In fact, a key difference between existing optical storage and magnetic storage systems is the ease with which

the optical media can be made removable with excellent robustness, archival lifetime and very low cost. The separation between the media surface and the optical pick-up unit (OPU), which includes the laser diode, the lenses and the photo-detector IC (PDIC), excludes all risks of the infamous head crashes experienced in hard disk drives.

The storage density and data rate of optical storage devices have increased dramatically in the last decades. Although this explosive growth has been mainly due to major breakthroughs in the physics, i.e. due to the improvements made in the design of the OPU and storage media, sophisticated coding and signal processing techniques as well as accurate servo control algorithms have also played a significant role [113, 152]. The potential of coding and signal processing techniques to substantially further enhance the storage capacity is becoming evident.

The remaining part of this section provides first a brief historical overview of optical storage technology and then discusses the optical disc readout and digital optical formats.

1.1.1 Optical Storage History and Trends

This section gives a brief historical overview of optical storage technology. A more detailed overview can be found in [74] and the references therein.

The huge popularity of the gramophone record and the growth of television in the 1960's called for techniques for storing video signals on a disc. The use of a disc, as an information carrier, solves the problem of slow accessibility of tape-based storage in the sense that fast access to any part of the programme is made possible. Moreover, using a disc for data storage still presents the low price advantage brought about by production methods similar to that of the gramophone disc [1], i.e. mechanical impressing the information in the disc by using a master stamper.

In this period, research on this subject started at different laboratories. Early investigations showed that optical read out of information has distinct advantages over the mechanical read out as was used in case of the gramophone record. The first edition of 'Philips Technisch Tijdschrift' [151] describes the so-called Philips-Miller-System for optical registration of audio information. The main advantage of this system over the gramophone is that mechanical wear due to read out of the information is eliminated because there is no mechanical contact between the medium

and the readout device. However, the idea could not be made practically viable until the availability of a very bright, and in principle cheap, light source in the form of a laser.

In 1967 the basic idea of storing data on a transparent optical disc was disclosed by D. Gregg [49]. In 1972, a standard established by Philips, Thomson, Music Corporation of America and later on Pioneer described the Video Long Play (VLP) system with the goal of playing back video content on a television set [24, 149]. The system uses discs of a transparent polymer material with standardized diameters of 20 and 30 cm and a thickness of 2.6 mm. The VLP disc resembles a gramophone record but has a mirror-like appearance [1], see Figure 1.1.

Figure 1.1: *'The video disc resembles a gramophone record but has a mirror-like appearance' [1].*

The information on these discs is stored in tracks spiraling outward with a track-to-track distance of 1.6 μm. The discs are manufactured by mechanical impressing of information in the disc using a master stamper to allow a cheap and fast replication process. The master stamper is made by illuminating a 100 μm thin photo-sensitive layer on a glass substrate and developing the photo resist to remove it at positions where it was illuminated. The information is present in the so-called pits and lands (non-pits). The readout of information from the disc is achieved via a laser beam with a wavelength λ of 632.8 nm, which is focused onto the information layer by a so-called objective lens. Explanation of the readout process is presented in Section 1.1.2.

Table 1.1: *Key properties and advantages of optical storage systems.*

Property	**Advantage**
• Mechanical impression of information using a master stamper.	• Cheap replication of discs.
• No mechanical contact between medium and readout device.	• No mechanical wear during readout and easily removable storage medium.
• Protective cover-layer in the form of the disc substrate.	• Robust against dust and scratches.

It was already recognized that the small size of the pits (width of 0.4 μm; average length of 0.6 μm) requires a special protection of the information layer. Small dust particles and scratches on the disc can easily damage the imprinted information layer and lead to signal drop-outs. To solve this problem, the use of a transparent, protective layer on top of the information layer has proven to be necessary. More importantly, the use of the disc substrate itself as this protective layer has proven to be one of the key ideas that made the optical storage system a robust information carrier as we know it today [99]. Table 1.1 shows an overview of the key properties and advantages that make the optical storage system the system of choice for many of today's applications [74].

The major drawback of the VLP system was its limited playing time. This made competition with the video cassette recorder rather difficult [16] and limited the market share of the VLP system. In the meantime, research was done to replace the old gramophone disc by an optical system to distribute audio content. The large increase in areal capacity when going from the mechanical to the optical readout was exploited in two ways. First, the optical disc was reduced considerably in size compared to the gramophone disc. Second, the audio signal was digitized allowing the use of error correction codes (ECC). This made the system even more robust against dust and scratches compared to the VLP.

1.1.2 Readout of Optical Discs

In optical storage systems, the data is written on the disc in the form of marks of various lengths in a track spiraling outwards from an inner radius (R1) towards an outer radius (R2), see Figure 1.2. The separation in the radial direction between adjacent tracks is called track pitch. Read-only systems, such as CD-ROM, employ a pattern of pits and lands to write the information on the disc. In rewritable systems, such as DVD-RW, phase changes due to local differences in material structure are generally used to represent information [150].

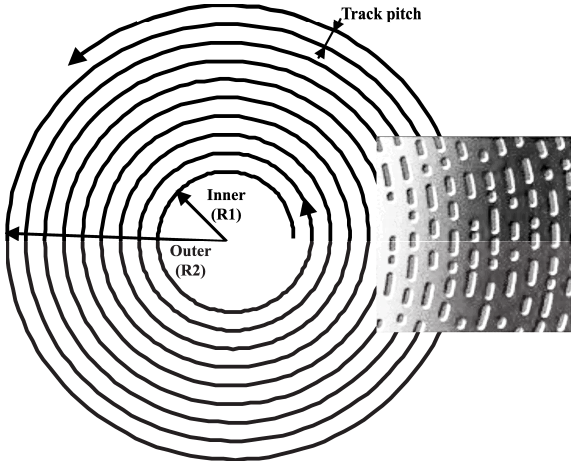

Figure 1.2: *Schematic drawing of the outward spiraling track on an optical disc. In the inset the pits on the disc are shown in detail.*

The data is read out with a focused laser beam. A schematic drawing of the optical light path is shown in Figure 1.3 [74]. A light beam is generated by a semiconductor laser diode. The light is pointed towards a beam-splitting cube and then directed towards the objective lens via a collimating lens that makes a parallel light bundle. The objective lens focuses the parallel bundle onto the rotating storage medium. By actuating the objective lens towards and from the disc, ideal focus can be maintained even when the disc is not ideally flat. Additionally, by actuating it in the radial direction (the direction perpendicular to the along-track direction) the spiraling track can be followed accurately. The focused light beam is reflected by the storage medium, after which the light is collected again by the same objective lens. Via the same optical path and the beam splitter it is now focused onto a photo detector that transfers

the optical signal into an electrical signal. This electrical signal contains information on the pit sequence on the disc from which we can derive the original bit sequence.

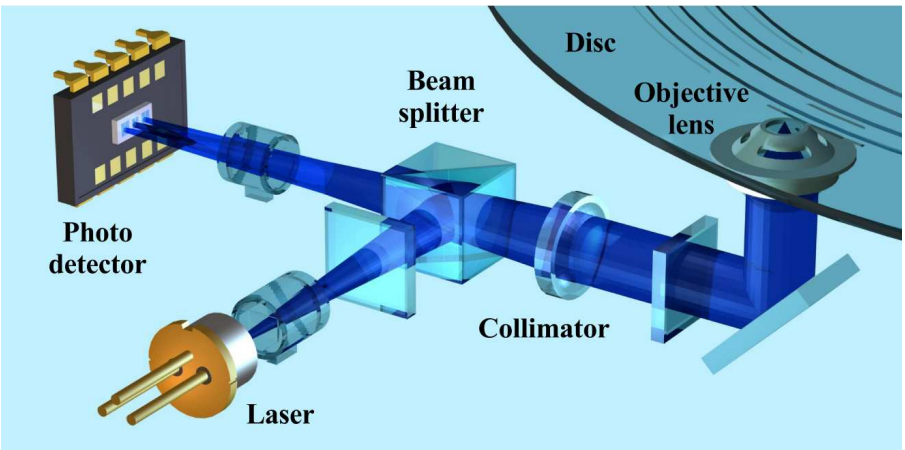

Figure 1.3: *The optical light path.*

1.1.3 Digital Optical Formats

The digital audio long play disc that originated from the VLP system was renamed compact disc (CD). The CD standard was introduced by Philips and Sony in 1980 and was officially brought to the market in Europe and Japan in 1982. Besides the digitization of the data and a change in laser wavelength λ to 780 nm, the basic principle was kept the same. The storage density of 680 MByte on a single layer disc with a diameter of 12 cm was reached using a track pitch of 1.6 μm and a channel bit length of 277 nm. This storage density is directly dependent on the size of the optical spot which is a function of the wavelength and the numerical aperture (NA). The NA is defined as the sine of the opening angle of the light cone that is focused on the storage medium. For CD, NA=0.45. The thickness of the transparent disc (that serves as the protecting cover layer for the data) is 1.2 mm. Figure 1.4 shows an overview of existing optical storage formats together with the main parameters. By reducing the wavelength of the laser light and by increasing the numerical aperture, the storage capacity of the disc has been increased in a few steps. The 'digital versatile disc' (DVD) uses a laser with a wavelength of 650 nm and the NA is increased to 0.6. By further reducing the margins slightly, which is made possible by more advanced

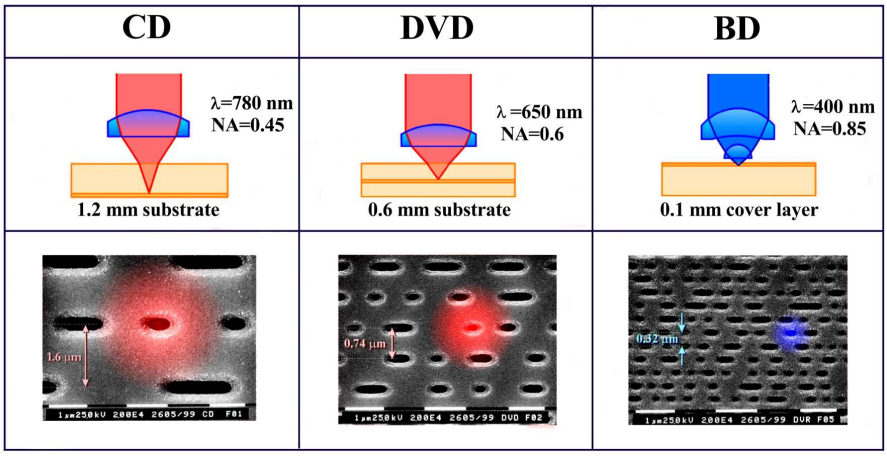

Figure 1.4: *Overview of existing optical storage formats.*

signal processing and manufacturing methods, a storage capacity of 4.7 GB on a single layer is achieved. This has been realized by using a track pitch of 0.74 μm and a bit length of 133 nm (see Table 1.2 for an overview of these parameters [74]). Recently, the Blu-ray Disc (BD) standard was introduced. It offers a capacity of 25 GB and uses a blue-violet laser diode with a wavelength of 405 nm. The NA is 0.85. More recently, but still at the research level, an improvement in storage density has been achieved by going to values of NA that are higher than 1. This is known as near-field storage [74].

Because the tolerance to disc tilt goes with the third power of NA [74], disc tilt becomes a serious issue for systems with a high NA. This is counteracted partially by choosing a thinner protective layer (0.6 mm for DVD and 0.1 mm for BD) at the cost of a decreased robustness against dust and scratches. This has also implications for the receiver architecture and the employed signal processing techniques as we discuss in Section 1.3.

1.2 Signal Processing in Current Optical Storage Systems

The key components in the development of a storage system are optical pick-up units, media, and signal processing. In the past, the main growth in optical storage systems was due to development of shorter-wavelength lasers and stronger lenses, along with

Property	**CD**	**DVD**	**BD**
λ [nm]	780	650	405
NA	0.45	0.6	0.85
(d,k)-constraint	(2,10)	(2,10)	(1,7)
Channel bit length [nm]	280	133	74.5
User bit length [nm]	700	313	137
ECC rate	0.85	0.85	0.8170
Track pitch [μm]	1.6	0.74	0.32
cover layer thickness [mm]	1.2	0.6	0.1
Inner radius (R1) [mm]	24	24	24
Outer radius (R2) [mm]	58	58	58
User Capacity [GB]	0.68	4.7	25.0
Density [Gb/inch^2]	0.40	2.78	14.74

Table 1.2: *Key parameters of various optical storage formats. The user bit length is calculated based on the channel bit length, the overhead for error correction and the rate of the channel modulation code. The (d,k)-constraints (see Section 1.2.1) determine, respectively, the minimum and maximum number of consecutive ones or zeros in the channel bit stream.*

developments in media technologies. However, the role of sophisticated signal processing techniques is increasingly becoming crucial in supporting and augmenting the advancement in media, lasers and lenses technologies. In fact, fuelled by the advances in CMOS technology, digital signal processing is recognized as a cost efficient means for increasing density while satisfying challenging design constraints in terms of data rate, power consumption and implementation cost [33, 66, 79, 113, 152]. Moreover, the necessity of using advanced signal processing techniques becomes even more obvious as the storage density increases and the signal to distortion ratios reduce [22, 42, 86, 113, 142, 145].

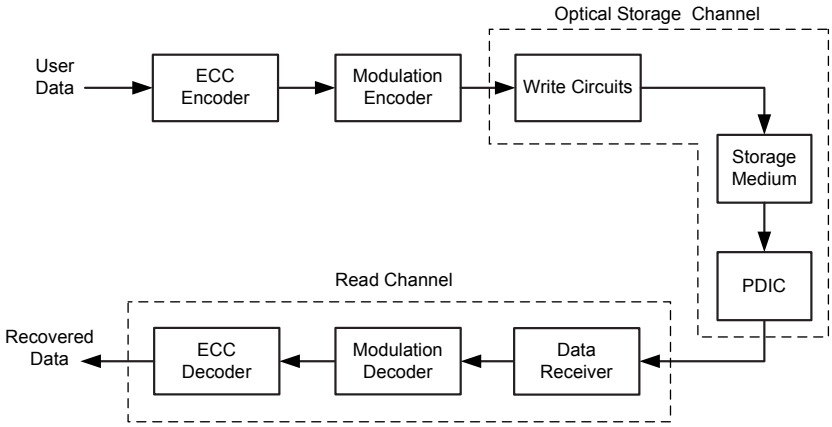

Figure 1.5: *Schematic block diagram of an optical storage system.*

Figure 1.5 shows a schematic diagram with the basic building blocks involved in an optical storage system [42, 86]. The upper part of Figure 1.5 highlights the write part of the system which is analogous to the transmitter part in a communication system. The lower part of Figure 1.5 highlights the read part, commonly referred to as the read channel, which is equivalent to the receiver part in a communication system. The write part involves an error correction code (ECC) encoder which encodes the user data bits to protect the recorded data from channel noise and disc defects [30, 138]. A modulation encoder is then used for matching the data to the storage channel characteristics and to facilitate the operation of the different receiver control loops, e.g. timing recovery [93, 96, 125]. The write circuits transform the binary data to be written on the storage media into a certain format to facilitate the writing. They modulate the laser light according to a so-called write strategy in order to modify or

compensate for distortions that occur while writing the data on the disc, e.g. [57,146].

During the readout process and based on the reflected light from the disc, a photo detector generates an electrical signal, called replay signal and modelled in Figure 1.5 as the output of the photo-detector IC (PDIC). Throughout this thesis, we refer to the combination of the write circuits, the storage medium and the PDIC as the optical storage channel or optical channel for conciseness. The optical channel output or replay signal is processed to recover the recorded data as reliably as possible. This is the task of the data receiver.

A modulation decoder then inverts the modulation encoding step. In this whole process, the erroneously detected user bits will be corrected by the ECC decoder using the redundant information that was added at the transmitting side by the ECC encoder. The replay signal often includes linear and nonlinear distortions and timing variations [8, 22, 61, 86, 100, 101, 145, 148]. To recover the recorded data reliably, a typical data receiver contains an analog front-end circuit, an equalizer, a timing recovery circuit and a bit detector (Figure 1.6). The front-end circuit conditions the replay signal prior to equalization. This includes amplification of the replay signal and limitation of its noise bandwidth [13]. The main task of the equalizer is to suppress noise and to reshape the replay signal in order to simplify bit detection [86, 119, 144]. The purpose of the timing recovery is to ensure that the replay signal, which contains timing variations as caused by disc rotation speed variation, is sampled at the correct sampling instants for bit detection [37, 86, 91, 127].

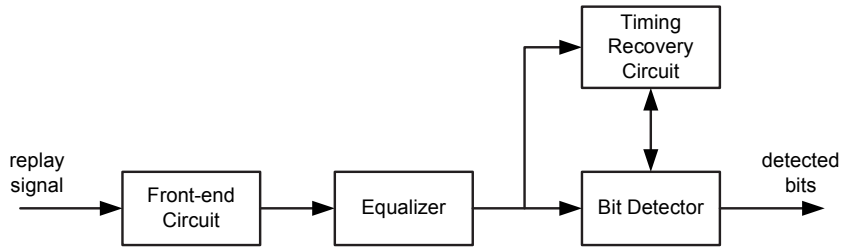

Figure 1.6: *Schematic block diagram of a data receiver.*

In the rest of this section we elaborate on selected parts of the optical storage system, namely, optical channel and modulation codes. We also provide an explanation of the main signal distortion sources, equalization, timing recovery and detection. We put special emphasis on equalization and timing recovery as these functions are

of central interest to this thesis.

1.2.1 Optical channel model and modulation codes

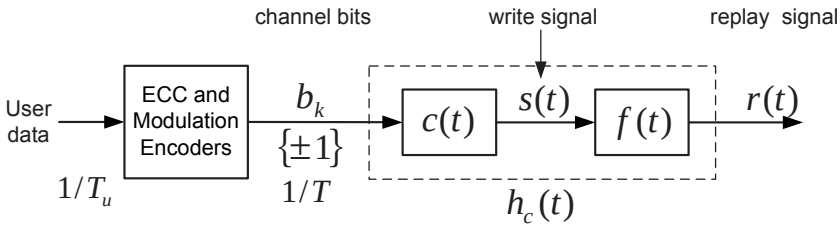

Figure 1.7: *Continuous-time model of the optical storage channel. Noise is omitted.*

Figure 1.7 shows a continuous-time model of the optical storage channel. The user data, at the rate $1/T_u$ bits/second, is applied to the ECC and modulation encoders. These encoders add redundancy to the user data which results in channel bits b_k at the rate $1/T$, where $T = RT_u$, with R being the joint code rate of these encoders.

In optical storage there exist two formats to denote the information bits, namely, the non-return-to-zero-inverse (NRZI) and non-return-to-zero (NRZ) formats. In the NRZI format the bit '1' represents a change in the state of the storage medium and the bit '0' represents no change. In the NRZ format, one state of the medium corresponds to the bit '1' and the other state corresponds to the bit '0'. Usually the output of the different encoders is encoded using the NRZI format and then transformed into NRZ format before being sent to the write circuit [93]. This operation is known as NRZI-to-NRZ *precoding* and can be characterized by a transfer function $1/1 \oplus D$, where '$\oplus$' is the Boolean XOR operator and 'D' is the 1 bit-duration delay operator. The precoder output is then mapped to channel bits $b_k \in \{-1, +1\}$, by assigning $+1$ to '1' and -1 to '0'. The channel bits are then stored on the disc. In this thesis, we associate pits with $b_k = +1$ and lands with $b_k = -1$.

A linear pulse modulator (LPM) [86] transforms the channel bit sequence b_k into a binary write signal $s(t)$ given by

$$s(t) = \sum_k b_k c(t - kT),$$

where the symbol response $c(t)$ of the LPM is given by

$$c(t) = \begin{cases} 1, & |t| < \frac{T}{2}, \\ 0, & \text{otherwise.} \end{cases}$$

For current disc formats, the continuous-time replay signal $r(t)$ can be assumed to be a linearly filtered and noisy version of the write signal $s(t)$. This assumption is not entirely realistic for higher storage densities as we will discuss in Section 1.3. Here we assume linearity as we focus on current optical storage systems. For now we omit channel noise, which will be the subject of Section 1.2.2. The replay signal can then be written as

$$r(t) = (s * f)(t). \tag{1.1}$$

Here $f(t)$ denotes the impulse response of the channel and '$*$' denotes the linear convolution operator. The characteristics of the impulse response $f(t)$ depend on the optics. A model of the impulse response $f(t)$, based on scalar diffraction theory, was developed by Hopkins [42, 68]. In short, the analysis in [68] is based on the concatenation of the following facts. Light, generated by the laser source, propagates through the lens towards the disc surface. Field propagation is described by the Fourier transform of the scalar input field. Then, disc reflectivity is modelled making use of the Fourier analysis for periodic structures. Light is reflected in proportion to the phase profile of the disc, times the incident field. Then the field is back-propagated to the detector, through the same lens as in the forward path. Back-propagation can be modelled by another Fourier transform. Finally, the photodiode converts the incident field into an electrical signal. According to [42], the Fourier transform of $f(t)$, called Modulation Transfer Function (MTF), is given, at a frequency Ω, by

$$F(\Omega) = \begin{cases} \frac{2}{\pi}\left(\cos^{-1}|\frac{\Omega}{\Omega_c}| - \frac{\Omega}{\Omega_c}\sqrt{1-(\frac{\Omega}{\Omega_c})^2}\right), & |\Omega| < \Omega_c, \\ 0, & |\Omega| \geq \Omega_c, \end{cases}$$

where Ω_c denotes the optical cut-off frequency. This expression of the channel MTF $F(\Omega)$ is known in the optical storage signal processing community as the Braat-Hopkins formula [42]. The optical cut-off frequency Ω_c depends on the laser wavelength λ and the numerical aperture NA of the objective lens and is given by

$$\Omega_c = \frac{2\text{NA}}{\lambda}.$$

For an optical storage system using a channel bit length $L_{\text{bit}} = \nu T$ where ν denotes the velocity of the media, the highest frequency that can be represented on the disc, i.e. $1/(2L_{\text{bit}})$, is called the Nyquist frequency. At densities of practical interest, optical storage channels are said to have a negative excess bandwidth [86] meaning that the optical cut-off frequency is below the Nyquist frequency, i.e. $\frac{2\text{NA}}{\lambda} < \frac{1}{2L_{\text{bit}}}$. For example, for a BD channel with $\lambda = 405$ nm, NA $= 0.85$ and $L_{\text{bit}} = 74.5$ nm, we obtain $\Omega_c \approx \frac{0.31}{L_{\text{bit}}} < \frac{1}{2L_{\text{bit}}}$.

For the sake of clarity, we keep the same notations and use throughout the remaining part of this thesis normalized frequencies to the inverse channel bit length $1/L_{\text{bit}}$. The normalized optical cut-off frequency is then given by $\Omega_c = \frac{2\text{NA}}{\lambda} L_{\text{bit}}$. For a given optical channel parameters, the normalized cut-off frequency is a direct measure of the storage density as it is proportional to the channel bit length. The higher the storage density is, the smaller the normalized cut-off frequency becomes.

The channel symbol response $h_c(t)$ is obtained by convolving $f(t)$ with $c(t)$. In the frequency domain, this gives

$$H(\Omega) = \begin{cases} \frac{2T}{\pi} \frac{\sin(\pi\Omega)}{\pi\Omega} \left(\cos^{-1} |\frac{\Omega}{\Omega_c}| - \frac{\Omega}{\Omega_c} \sqrt{1 - (\frac{\Omega}{\Omega_c})^2} \right), & |\Omega| < \Omega_c, \\ 0, & |\Omega| \geq \Omega_c. \end{cases} \tag{1.2}$$

The optical storage channel has a low-pass nature with a normalized cut-off frequency Ω_c and approximately a linear roll-off. By way of illustration we show in Figure 1.8 the transfer functions of the CD and DVD channels according to (1.2). For CD the normalized cut-off frequency is $\Omega_c \approx 0.32$ and for DVD $\Omega_c \approx 0.26$. The low-pass nature of the optical channel is apparent, with an almost linear roll-off.

Because $H(\Omega)$ is bandlimited to normalized frequencies well within $[-0.5, 0.5]$ for storage densities of practical interests, the replay signal $r(t)$ can be sampled at the baud rate $1/T$ without loss of information and the cascade of the continuous-time model in Figure 1.7 with the sampler can then be replaced by the discrete-time model of Figure 1.9. The discrete-time impulse response h_k and the readback signal r_k are the sampled versions of $h_c(t)$ and $r(t)$, respectively, all at the rate of $1/T$ samples/second. The discrete-time counterpart of equation (1.1) then becomes

$$r_k = (h * b)_k = \sum_i h_i b_{k-i}, \tag{1.3}$$

where '$*$' denotes discrete convolution.

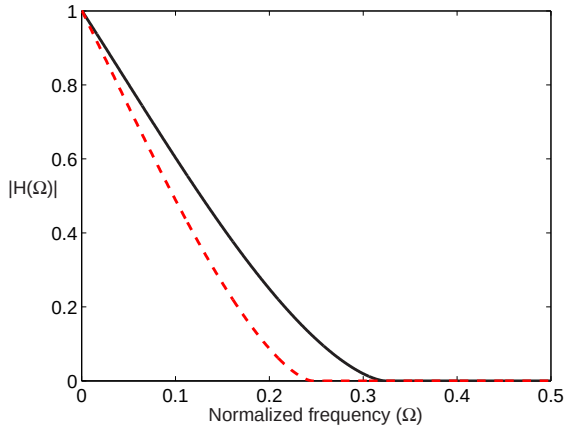

Figure 1.8: *The transfer functions of the CD (continuous line) and DVD (dashed line) channels. Both channels are normalized to have a unit transfer at DC.*

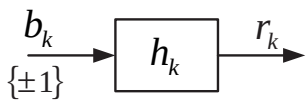

Figure 1.9: *The equivalent discrete-time model of a noiseless optical storage channel.*

The negative excess bandwidth property, i.e. $\Omega_c < 0.5$, has several implications. On the one hand, intersymbol interference increases rapidly as excess bandwidth decreases. At the same time the replay signal comes to contain progressively less timing information. On the other hand, receiver performance tends to become more sensitive to channel parameter variations [86]. These factors have direct consequences on modulation coding, equalization, detection, timing recovery and adaptation as we will explain in the forthcoming sections.

Modulation Codes:

Modulation codes for storage systems [93,96,125], known as runlength-limited (RLL) codes, are commonly used in optical storage to spectrally shape the information written on the disc in accordance with the MTF of the optical channel. This is meant to improve detection performance and to facilitate the operation of control loops in

the receiver. Moreover, the use of RLL codes also helps to considerably reduce the impact of some nonlinear artifacts on system performance, e.g. signal asymmetry as we will discuss in Section 1.2.2.

RLL codes are characterized by so-called (d,k) constraints or runlength constraints where a runlength is the length of runs of consecutive pits and lands on the disc. RLL coded sequences have a minimum runlength of $d+1$ channel bits, and a maximum runlength of $k+1$ channel bits. The d constraint controls the high-frequency content of the data stream and helps to increase the minimum spacing between transitions in the data recorded on the medium. This has an impact on the linear and nonlinear interferences and distortions present in the readback signal. The k constraint controls the low-frequency content of the data stream and ensures frequent transitions in the channel bit-stream for proper functioning of the timing-recovery loop. Modulation codes for optical storage often also include a dc-free constraint [154] in order to reduce interference between data and servo signals and to mitigate the effect of all kinds of low-frequency noise. For a detailed review of RLL codes, we recommend [93].

Typical values of the minimum runlength constraint are $d = 1,2$. In CD systems, an eight-to-fourteen modulation (EFM) code is used [95], with $d = 2$ and $k = 10$. DVD systems use the same runlength constraints and employ the so-called EFMPlus code [94]. In BD systems, the so-called 17PP code [115] is used. This code has $k = 7$ and the minimum runlength constraint has been reduced from $d = 2$ to $d = 1$ to allow a higher code rate and especially to allow a larger tolerance against writing jitter or the so-called mark-edge noise [152].

1.2.2 Signal Distortions and Artifacts in Optical Storage

Readback signals in optical storage systems are corrupted by various noise sources, interferences and nonlinear distortions. The major artifacts in optical storage are Intersymbol Interference (ISI), noise, and signal asymmetry.

One way to visualize system sensitivity and gauge the severeness of the different system artifacts is via the so-called eye pattern or eye diagram [80]. The eye pattern is obtained by overlaying segments of the signal in a phase-aligned manner. The shape of the resulting ‘eye’ indicates the margins of the system against various disturbances, such as timing phase errors, ISI and noise. By way of illustration Figure 1.10 shows

the eye pattern for the noiseless CD channel. The eye pattern in this case shows that data can be detected, at the ideal sampling phase, by means of a simple slicer with zero threshold at the middle of the 'eye'. Referring to the middle of the eye pattern, two key parameters for system sensitivity are shown in Figure 1.10, namely the 'eye width' and 'eye opening'. The eye width is defined as the width of the interval around the optimal phase over which the eye is not closed. The eye width is a straightforward measure of system timing sensitivity or timing phase margins defined as the maximum error in sampling phase that the receiver can tolerate before the performance becomes unacceptable. The eye opening is the opening of the eye pattern at the ideal sampling phase. The eye opening defines the margin of the system against noise.

In the following paragraphs we discuss the different artifacts in optical storage systems.

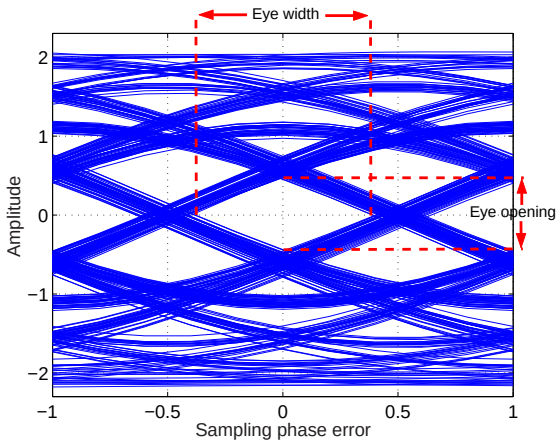

Figure 1.10: *Eye pattern for the CD channel with* (d,k)*=(2,10) RLL data in the absence of noise.*

Intersymbol Interference (ISI):

The bandwidth limitation of the optical storage channel, as described earlier, causes the channel impulse response h_k to be of long duration compared to the bit interval T. Therefore, channel responses due to successive channel bits interfere with each other, resulting in intersymbol interference (ISI) characterized by the linear im-

pulse response h_k. This can be seen from (1.3) where the terms $h_i b_{k-i}$ for $i \neq 0$ cause the readback signal r_k to be also dependent, in a linear fashion, on the neighboring bits of b_k. This ISI increases with density as the cut-off frequency of the optical channel decreases. By way of illustration, Figure 1.11 shows the idealized impulse response of the CD and DVD channels. In terms of eye pattern, the ISI increase results in a reduction of the eye opening and eye width, see Figure 1.12.

As we mentioned earlier, the channel for current optical storage systems behaves essentially linearly. This means that ISI is mainly linear at current densities. The effect of this type of ISI is often mitigated by the use of linear equalization techniques as will be discussed in Section 1.2.4.

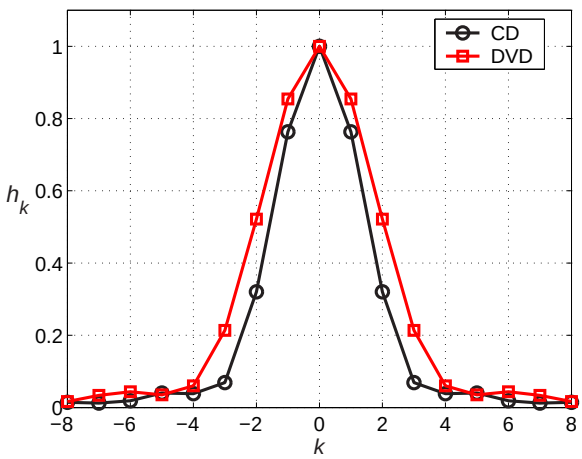

Figure 1.11: *The idealized impulse response h_k corresponding to the CD and DVD channels. Both responses are normalized to have a central tap value of 1.*

Noise in Optical Storage:

There are three main types of noise in optical storage. These are *Electronics Noise*, *Laser Noise* and *Media Noise* [67, 74, 142]. In general, electronics noise is the noise due to the electronics of the system [74]. Laser noise is the noise contributed by the laser due to variations in light intensity, phase and wavelength. Finally, media noise originates from small deviations in the storage medium from its ideal form, e.g. as caused by roughness of the mirror-like surface, variations in reflectivity, and cover-

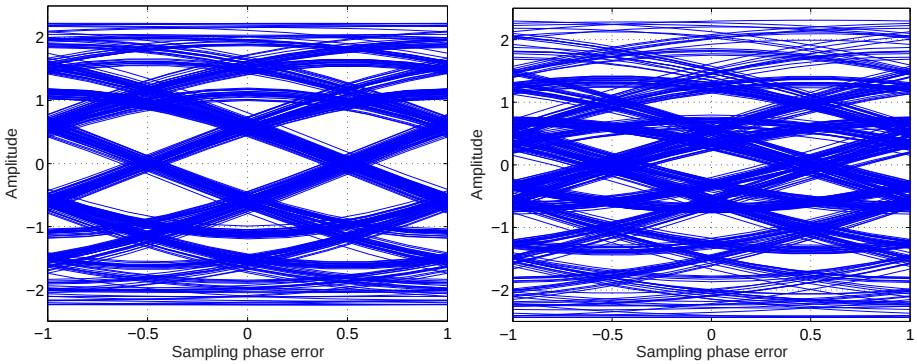

Figure 1.12: *Eye pattern for the CD channel (left plot) and the DVD channel (right plot).*

layer thickness variations. An important source of media noise in optical storage is caused by inaccuracy in the pit-shape. One possible inaccuracy is that the pit size varies from one pit to the other [74], see Figure 1.13.

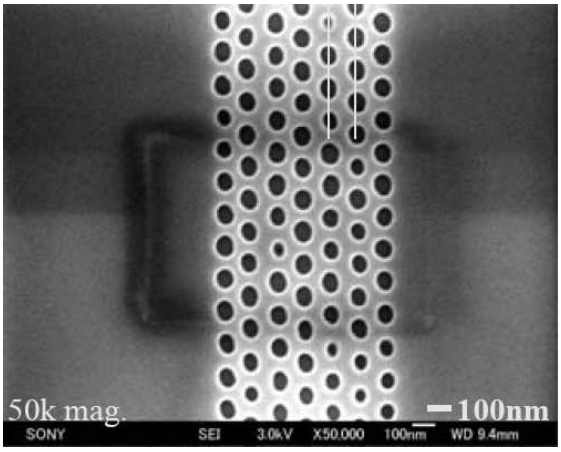

Figure 1.13: *Scanning electron microscope image of an experimental optical disc showing clear pit-size variations [74]. Note that these variations are highly exaggerated with respect to normal operating conditions.*

Whereas electronics noise is often modelled as additive white Gaussian noise (AWGN), laser noise is usually multiplicative, see [67] and the references therein.

However, laser noise power is typically lower than that of electronics noise [74]. For this reason, laser noise is neglected in this thesis.

As far as media noise is concerned, this becomes important only at high storage densities [74]. For this reason, we treat and model media noise in Section 1.3 that deals with challenges in high-density optical storage systems.

Signal Asymmetry:

Although channels for current optical storage systems are essentially linear, there exist several sources of nonlinearities [86]. For read-only systems, the principal source of nonlinearities arises during the writing process and is caused by systematic differences in the size of pits and lands on the disc. This is known as *domain bloom* or *asymmetry* [86] [60] which is the fact that pits can be longer than lands of the same nominal size or vice versa. This causes asymmetry in the signal levels of the replay signal.

In CD and DVD systems, the use of RLL codes with $d = 2$, which makes the minimum pit length to be 3 times the channel bit length, helps to considerably reduce the impact of asymmetry on system performance. For writable or rewritable systems, asymmetry is less significant than for read-only systems [60] because of the finer control of the writing process in rewritable systems. A typical approach to circumvent asymmetry in rewritable systems is to use the so-called *write precompensation* [57, 86] and *write strategies* [74, 145, 146].

1.2.3 Detection Techniques in Optical Storage

First optical storage systems, such as CD and DVD, relied heavily on modulation coding to maintain data integrity. This has enabled the use of simple symbol-by-symbol detection schemes. A common reception scheme for CD includes a fixed prefilter for noise suppression, and a memoryless slicer for bit detection [34]. In order to improve the performance of symbol-by-symbol detectors, an improved scheme, known as Runlength Pushback Detector (RPD), was proposed in [147] [47]. The RPD detects and corrects bit patterns that violate the constraints of the RLL code used. For the $d = 1$ runlength constraint, the RPD can correct only single bit-errors. This becomes problematic as density increases and other bit-errors become important. An improved detector called Missing-Run Detector (MRD) was proposed in [62], and is

based on identifying the most probable bit-errors after single bit-errors and devoting a simple scheme to detect and correct for these errors.

Recently, the threshold detectors have given way to more powerful maximum-likelihood sequence detection (MLSD) schemes [41] which detect the most likely recorded bit sequence [121] [152]. MLSD is implemented via a Viterbi Detector (VD) [41].

The drawback of the VD is that it is bit-recursive, requiring the execution of an Add Compare Select (ACS) operation for every state in the VD trellis and at each bit-interval. This limits the attainable speed of the VD which, however, needs to follow the rapidly increasing data rate of optical storage systems. Substantial simplification of the baseline VD can be obtained by folding the states diagram of the VD via formulating the detection problem as a transition detection problem [89].

Throughout Chapters 2 and 3 we assume the use of a VD for bit detection. The other chapters of this thesis do not depend on the employed detection scheme.

1.2.4 Partial Response Equalization

Among the various methods available to handle ISI and noise, equalization methods, which consist of using one or more filters to mitigate the effect of ISI and noise, play an important role [80, 86, 144].

The earliest roots of equalization can be found in the annals of telegraphy [82]. The notion of full equalization, which consists of using a linear filter to suppress all ISI at the decision instants, stems back to the work of Küpfmüller and Nyquist [58, 59, 92]. Full equalization is widely used in data communications and has long been studied in the past. For a historical perspective and a detailed description, the reader may refer to [80, 86, 106, 144] and the references therein.

Although full equalization allows the use of simple symbol-by-symbol detectors [86], it finds little application in optical storage, because of its noise enhancement penalty, especially at relatively high densities. In fact, because full equalization consists of undoing the effect of the channel, it will severely enhance noise in view of the negative excess bandwidth nature of optical storage channels, see Figure 1.8.

For this reason, another equalization method, known as Partial Response (PR) equalization, was widely accepted and used in storage systems including magnetic storage systems. PR equalization allows a well-defined quantity of ISI to remain

untackled before detection. The remaining untackled ISI is characterized by a linear impulse response g_k that we call target response. This can be seen as providing additional freedom of equalization that can be used to reduce noise enhancement significantly. The origin of this equalization method can be linked to partial-response coding and signaling techniques that aim at spectrum control and signaling rate enlargement [9, 36, 119].

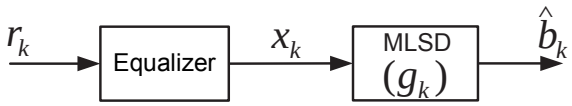

Figure 1.14: *Block diagram of the PRML system. MLSD must be designed for the target response g_k.*

Application of PR equalization to digital storage systems was first reported in the field of magnetic storage where the combination of PR equalization and MLSD was proposed to replace the peak detection technique [124] in order to achieve high reliability and high storage densities [20, 38, 51, 53, 54, 70]. For similar reasons, PR equalization was also employed in optical storage systems. Systems that combine PR equalization and MLSD are known as partial response maximum-likelihood (PRML) systems. A block diagram of the PRML system is shown in Figure 1.14. The MLSD is implemented via a VD whose trellis is tailored to the target response g_k and to the d constraint of the underlying code. Therefore, the performance improvement of PRML systems in comparison to systems employing symbol-by-symbol detection, comes at the price of a more complicated detector whose complexity, in fact, increases exponentially with the target response length.

1.2.5 Timing recovery

For optimum detection performance, receivers for storage systems need to determine the ideal sampling instants of the replay signal. These instants correspond to the instants of maximum opening in the eye pattern of the replay signal. Clearly, errors in the choice of sampling instants will directly translate to poor detection performance as this generates a significant amount of residual ISI. The task of the timing-recovery unit is to estimate the ideal sampling instants and compensate for any random timing uncertainty in the replay signal. The timing uncertainty in optical storage may come,

for example, from differences between the writing and the reading clocks, mechanical motion fluctuation of the media during the writing and reading process or variations in the group delays of the analog front-end filters.

Being a crucial task in digital storage and communication systems, timing recovery has been a subject of investigation for several decades and many timing-recovery schemes have been proposed. A comprehensive exposition and classification of these schemes can be found in [55, 56, 86, 106, 153].

Among the existing timing recovery approaches, we focus in this thesis on the self-timing approach which consists of extracting timing information from the replay signal itself [86, 91, 105, 129]. This approach is of particular interest for read channels for storage systems. At the heart of a self-timing scheme is an objective function of the readout signal samples such that timing errors can be obtained directly and without ambiguity from this function [4, 52, 76, 91, 105]. Figure 1.15 shows a schematic

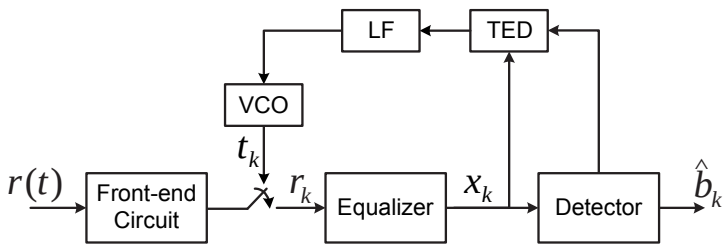

Figure 1.15: *Schematic diagram of the timing-recovery loop.*

of the timing-recovery scheme architecture that is widely used in read channels for storage systems. The replay signal $r(t)$ is first processed and filtered by the front-end circuit to suppress out-of-band noise. The front-end circuit output is first sampled, equalized and then passed to a detector that produces bit decisions $\hat{b}_k$. In order for the detector to operate properly, a timing-recovery subsystem ensures that the sampling instants closely approach their ideal values. Based on the sampled and equalized sequence x_k, the timing-recovery subsystem extracts a clock signal that indicates the sampling instants t_k. The timing-recovery subsystem takes the form of a phase-locked loop (PLL) [45], with a timing-error detector (TED), loop filter (LF), and a voltage controlled oscillator (VCO). The TED produces an estimate of the sampling-phase error. The filtered TED output is used to control the phase and frequency of the VCO. The LF has a significant role in determining the PLL properties in terms of

noise suppression and bandwidth. A detailed description of this role can be found in [45] [86].

A key part in the design of timing recovery is the design of the TED. In the past decades, several techniques were reported. An excellent review and classification of the key contributions can be found in [86].

The TED scheme that is mostly used in current optical storage systems is known as the Zero-Crossing (ZC) technique [11, 34, 140]. This consists of tracking the position of the zero crossings in the replay signal and deriving the TED output by comparing the actual zero crossings with those of a sampling clock signal [34] [11]. Several extensions of this scheme incorporating asymmetry and pattern jitter compensation were reported in [140] and [123]. ZC timing recovery is a non-data aided scheme in the sense that the recorded data is not used in the TED to extract timing information.

However, as storage density increases, ZC timing recovery performs poorly and faces some serious limitations. The next section shows these limitations and exhibits the main signal distortions present at high storage densities, and highlights their main implications for equalization and timing recovery.

1.3 Challenges for High-Density Optical Storage Systems

As density and data rate of optical storage systems increase, many system artifacts become important and result in reduction of system margins and SNR. In order to cope with these artifacts, new coding and signal processing methods must be developed. In this section we give an overview of the main artifacts in high-density optical storage systems, e.g. beyond BD, and explain their implications for equalization and timing recovery. These artifacts can be divided into four main categories: linear ISI, nonlinear ISI, media noise and channel parameter variations.

In the following paragraphs we discuss the different artifacts in high-density optical storage systems.

Linear ISI:

As mentioned in Section 1.1.1, high-density optical storage is mainly achieved by using lasers with short wavelengths λ and lenses with high numerical aperture NA. Since the diameter of the laser spot is proportional to λ/NA, decrements of λ and

increments of NA cause the disc area illuminated by the spot to be smaller, leading to an increased ability to detect small details on the disc surface, i.e. a higher resolution [152]. However, in order to push storage densities to even higher levels, the size of the recorded bits is reduced relative to the size of the laser spot. This increase in density relative to the resolution leads to more ISI. Figure 1.16 shows the impulse response of the Blu-ray Disc (BD) channel at densities of 25 GB, 30 GB and 35 GB. This clearly points out the ISI increase as function of storage density.

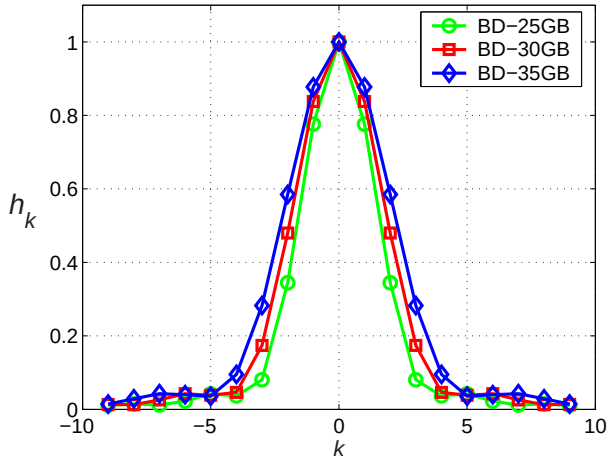

Figure 1.16: *BD channel impulse response at different densities. The time axis is normalized to the bit interval T and the impulse responses are normalized to have a central tap value of 1.*

Nonlinear ISI:

It is often assumed that the readback signal in storage systems can be constructed from linear superposition of isolated impulse responses. In practice, this is true only at low storage densities. As density increases, neighboring bits start to interact in a nonlinear way resulting in significant nonlinear ISI [22, 61, 68, 101, 137, 145]. The sources of nonlinear ISI can be divided into two groups: nonlinearity sources from the write process, as explained in Section 1.2.2, and sources from the readout process. The nonlinear distortion during readout is inherent in the readout process itself. In fact, according to the scalar diffraction theory [22, 68], the propagation of light in the readout process is represented by a chain of linear transformations, e.g. Fourier

transform and inverse Fourier transform, followed by the quadratic operation in the photo detector to obtain light intensity. This causes the readback signal to be non-linearly dependent on the written bits. This dependence is bilinear in the sense that the bilinear terms $b_k b_{k-i},\ i \neq 0$ become visible in the readback signal [22]. The most important nonlinear contribution comes from the immediately neighboring bits to the central bit [22]. For this reason and for simplicity, we consider in the thesis only the bilinear terms $b_k b_{k-1}$ and $b_k b_{k+1}$, although the techniques that we develop are much more generally applicable.

media noise:

At high storage densities, media noise becomes important [142] [74]. This causes noise to be highly data-dependent, correlated and non-stationary. This particularity of storage systems compared to classical communication systems has to be taken into account in the design of signal processing algorithms in order to limit performance degradation at high storage densities.

Unlike electronics noise, which can be modelled as additive white Gaussian noise (AWGN) [74], media noise in optical storage is correlated, data-dependent, non-stationary and non-additive in nature. For read-only systems, the most important sources of media noise are random pit-position and pit-size variations [74]. Pit-position variation is a deviation of the center of gravity of a pit from its nominal position. Pit-size variation is caused by the fact that the pit size depends on the number of pits in a wide neighborhood. For example, for Electron-Beam Recording (EBR), a proximity effect is caused by the scattering of electrons in the resist during mastering which generates a background illumination that increases the size of pits [74].

For rewritable optical storage systems, media noise is caused by fluctuations in the reflectivity of the crystalline state, representing pits. In the amorphous states, representing lands, no such fluctuations arise [18]. This media noise can be modelled as a random disturbance at the channel input that is injected only in the presence of pits [139]. We model this noise as an additive white Gaussian random process u_k with variance σ_u^2 that is injected at the channel input when $b_k = +1$. We introduce then the media noise term as $m_k = \frac{1+b_k}{2} u_k$. This is illustrated in Figure 1.17. The multiplication with $\frac{1+b_k}{2}$, in Figure 1.17, reflects the data-dependent nature of the

media noise. That is, the channel bit b_k is corrupted by $m_k = u_k$ only when $b_k = +1$. When $b_k = -1$ we have $m_k = 0$. The readback signal r_k can then be written as

$$r_k = \sum_i h_i b_{k-i} + \sum_i h_i m_{k-i} + z_k, \tag{1.4}$$

where z_k denotes electronics noise and is modelled as an AWGN with a variance σ_z^2. For clarity of the derivations in this thesis, we denote by n_k the sum of the electronics and media noise, i.e.

$$n_k = \sum_i h_i m_{k-i} + z_k.$$

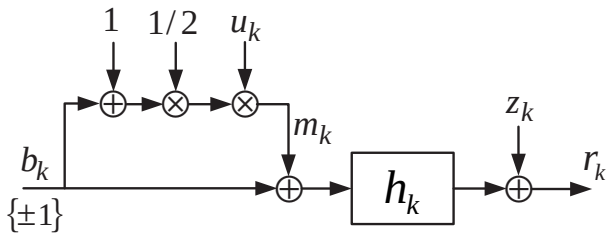

Figure 1.17: *Discrete-time model of the optical storage channel with media noise m_k and electronics noise z_k.*

Because media noise m_k and electronics noise z_k have different characteristics, they introduce different effects on the system performance. For this reason, we adopt in this thesis two different signal-to-noise ratio (SNR) measures: a signal to media noise ratio (SMNR) and a signal to additive noise ratio (SANR) given by

$$\text{SMNR} = \frac{2}{\sigma_u^2}, \tag{1.5}$$

and

$$\text{SANR} = \frac{\sum_k h_k^2}{\sigma_z^2}. \tag{1.6}$$

The SANR in (1.6) is defined according to the matched-filter bound [86]. The normalization by the factor 2 in (1.5) takes into account that $E[b_k^2] = 1$ and that the average media noise variance over pits and lands equals $\sigma_u^2/2$.

The impact of media noise, as modelled in Figure 1.17, on the eye pattern for the 23 GB rewritable BD channel is illustrated in Figure 1.18. This figure shows that media noise mainly affects the upper traces of the eye pattern and that lower traces are less hampered. This is caused by the fact that media noise affects only the pits on the disc.

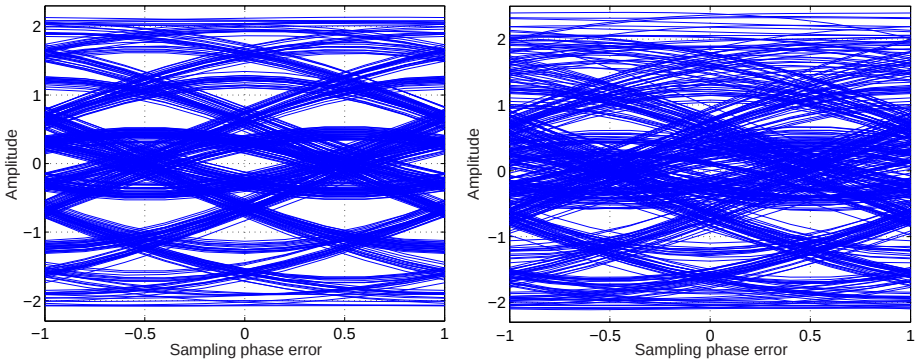

Figure 1.18: *Eye pattern for the 23 GB BD channel with* (d,k)*=(1,7) in the absence of noise (left plot) and in the presence of media noise at* SMNR*=20 dB (right plot).*

Parameter Variations:

The trend of increasing storage densities results in reduced margins and in growing sensitivity of system performance to any variations of storage channel parameters. To counteract these variations, the use of accurate and adaptive techniques, e.g. adaptive equalization, in the data receiver becomes a necessity.

The accuracy in adaptation is especially hard to accomplish for the tracking of rapid variations, and is limited in part by latencies in the adaptation loops. Therefore, minimizing latencies inside the critical adaptation loops becomes crucial for proper functioning of the system [15].

One of the most important sources of rapid variations in high-density optical storage is caused by fast timing variations [74]. This has a direct implication for the structure of the different adaptation loops and especially the equalizer adaptation loop as we will discuss in Chapter 4.

1.3.1 Implications of increasing density on equalization

As storage density increases, adaptive equalization techniques become more and more attractive because of their ability to counteract the reduced system margins. In addition, adaptive equalization presents some other advantages. First, it can compensate for the variations in optics and media that inevitably occur during the manufacturing process. Second, it allows eliminating the need for any manual adjustment

for different discs.

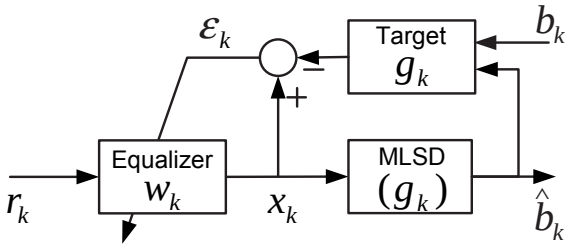

Figure 1.19: *Block diagram of a PRML system with an adaptive equalizer.*

Different equalizer adaptation techniques exist in literature. Among these, the most widely used techniques are the Least Mean Square (LMS) and the Zero-Forcing (ZF) techniques. LMS adaptation is based on minimizing the power of the error signal ε_k, see Figure 1.19, taken as the difference between the detector input x_k and its ideal value $(g * b)_k$. ZF adaptation is based on forcing residual ISI at the detector input to zero [86]. The ZF criterion can be written as forcing the equalizer impulse response w_k to meet on a given span $(w * h)_k = g_k$. Both ZF and LMS adaptation are based on the error signal ε_k. The generation of the error signal obviously assumes knowledge of the channel bits b_k. This mode of operation is known as the Data-Aided (DA) mode [86] where the channel bits are available in the form of a known preamble or as decisions taken from the bit detector. When bit decisions are used inside the adaptation loop we speak about 'decision-directed' (DD) mode of operation [86].

These adaptive equalization techniques date back to the second half of the last century. The LMS equalizer was first reported in [3, 83, 132] and its ZF counterpart was first proposed in [131]. After these pioneering contributions, several publications focused on the behavior of these techniques, in terms of convergence and performance, and dealt with their implementation issues, e.g. [14, 44, 130]. For an excellent review of adaptive equalization we recommend [144] and [86].

A problem associated to adaptive equalization for PR systems relates to the design and adaptation of the target response g_k. In fact, receivers for future high-density storage systems may need to resort to joint equalizer and target-response adaptation because it presents particular advantages. First, in order to cope with the ISI increase at high storage densities, the length of the target response used for detection has to increase. This causes detection complexity to increase substantially as this complex-

ity depends exponentially on the target response length [41]. Therefore, adaptive design and training of powerful short target responses becomes essential at high densities. Second, considering that the optical channel is not completely known until after the entire storage device is manufactured, adaptive equalization and target response adaptation provide a better fitting and tracking of the channel. Third, because the noise in high density storage systems depends heavily on the medium, see Section 1.3, an equalizer and target response that adaptively take the noise characteristics into consideration is very desirable.

Because the target response largely determines PR system performance, several papers attempted to solve the target response design and adaptation problem. In [143], the target response was designed as a truncated version of the channel impulse response and the equalizer was chosen to minimize the Mean Square Error (MSE). The MSE-minimization problem was extended to the target response adaptation in [29] and [27]. An inherent issue in joint equalizer and target-response adaptation is the interaction problem between the equalizer and target-response adaptation. This interaction is usually prevented by employing a constraint on the target response. In [29], a fixed energy constraint for the target response was used, i.e. the target response energy was fixed to unity, while [27] used the monic constraint, i.e. the first nonzero term in the target response was fixed to one. The latter corresponds to a minimum-phase target response that is optimum for decision feedback equalization [106] and thus presents similar noise whitening properties [78]. The minimum MSE (MMSE) target response design and adaptation problem was also discussed in [71] [72].

Although the problem of PR equalization and target response adaptation received a lot of attention in the past decades, several challenges remain unsolved. In fact, because all existing adaptation algorithms are based on the LMS or ZF criteria, they are not necessarily optimum in terms of minimizing detection bit-error rate (BER) as we will show in Chapters 2 and 3. Referring to Figure 1.19, the BER reflects the frequency of occurrence of bit errors at the detector output and is defined as

$$\text{BER} = \frac{\text{number of error bits at detector output}}{\text{number of channel bits}}.$$

Moreover, nonlinear ISI and data-dependent noise, which are inevitable at high densities, see Section 1.3, degrade the performance of existing adaptation schemes. Important improvements in system performance and robustness can then be accomplished by applying more sophisticated adaptation schemes such as those that we propose in

Chapters 2 and 3.

Note that the new adaptation techniques that we develop in Chapters 2 and 3 are quite general in the sense that they are not restricted to optical storage and are applicable to a wide range of communication and storage systems, e.g. to magnetic storage systems.

1.3.2 Implications of increasing density on timing recovery

The increase in ISI caused by increased density translates into a reduced timing phase margin. This latter is defined as the maximum error in sampling phase that the receiver can tolerate before the performance becomes unacceptable. The timing phase margin can be gauged by examining the eye pattern of the signal at the input of the decision device within the receiver [80]. Figure 1.20 shows eye patterns in the noiseless case for the CD channel and the 23 GB BD channel. This illustrates that the higher the density is, the smaller the eye width becomes which implies a decreased timing phase margin. One should note that the eye width decreases further at higher BD densities and that the eye pattern becomes completely closed which excludes the simple threshold detector for data-detection.

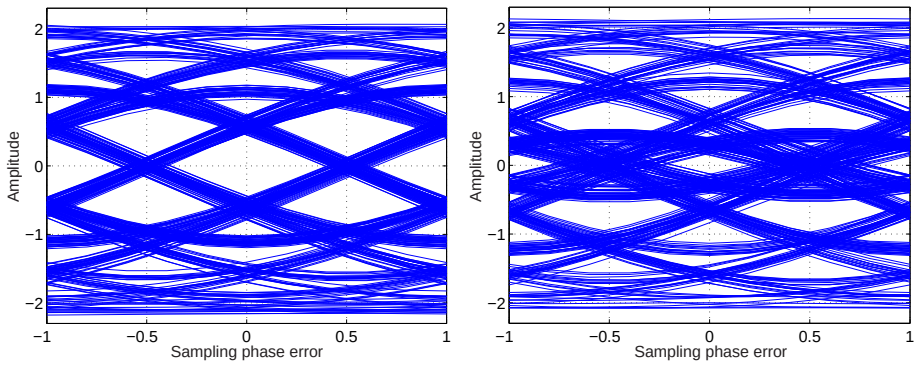

Figure 1.20: *Noiseless eye pattern for the CD channel with (d,k)=(2,10) RLL data (left plot) and the 23 GB BD channel with (d,k)=(1,7) RLL data (right plot).*

Besides the fact that sampling-phase errors become increasingly critical for reliable data detection at high densities, extracting accurate timing information from the incoming signal becomes comparatively difficult. In fact, because the readback

signal conveys fewer high-frequency components at high densities, the amount of timing information in the readback signal per unit of time and SNR, i.e. the timing efficiency, decreases rapidly [87].

Because at high storage densities, the replay signal contains more ISI and fewer high-frequency components, i.e. because of the absence of sharp transitions in the replay signal, Zero-Crossing (ZC) timing recovery becomes unfeasible [11]. Moreover, as mentioned earlier, the eye pattern becomes closed at high storage densities. This implies that non-data aided timing-recovery schemes, e.g. the ZC schemes, where no information on the transmitted data is exploited by the TED, become impractical at such densities [86]. For this reason, Data Aided (DA) timing recovery must be used. In a DA timing recovery technique, the recorded bits are assumed to be available to the TED in the form of a known preamble, or as decisions, taken from the detector, see Figure 1.21. The latter mode of operation is called Decision-Directed (DD) and is useful to track timing variations once the PLL has locked up.

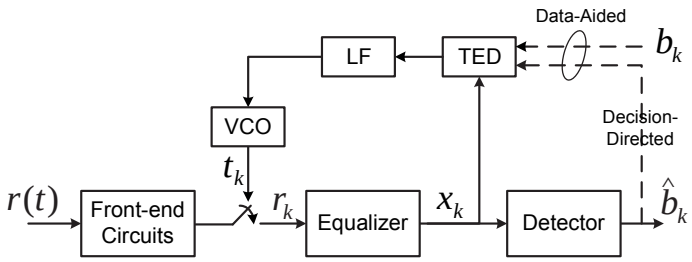

Figure 1.21: *Schematic diagram of the data-aided and decision-directed timing-recovery loops.*

Another problem for timing recovery for high-density optical storage systems is caused by the data-dependent media noise and nonlinearities. In fact, this data-dependency translates into a replay signal that contains more distortions for specific bit patterns than for other patterns. In order to achieve the best performance, the timing recovery has to be 'selective' in the sense that it should extract timing information primarily from data patterns with less noise. This can be achieved by designing a TED that incorporates knowledge about the data-dependent nature of noise. Existing TED algorithms do not incorporate this knowledge because they generally assume stationary and additive noise. For this reason, Chapter 5 proposes and analyzes a new practical timing-recovery scheme that exploits the nature of data-dependent noise in

optical storage. This new scheme is not restricted to optical storage channels but extends naturally to magnetic storage and is applicable to a wide range of communication channels with data-dependent noise.

The above mentioned aspects have motivated the research work reported in this thesis. In the next section, we summarize the contributions in each of the chapters.

1.4 Outline and contributions of the thesis

As it can be seen from Section 1.2, most of the adaptive signal processing techniques used in todays optical storage systems originate from different communication systems and are quite basic in the sense that they do not fully exploit the nature of the optical storage channel in terms of key artifacts such as noise and nonlinearities. This thesis is devoted to the development of new adaptive equalization and timing recovery techniques that are meant to meet the future challenges in high-density optical storage systems as presented in Section 1.3.

This thesis contains seven chapters. The work in this thesis has resulted in several publications and patent applications, see the list of publications at the end of this chapter. The different chapters are written to be as independent and as self-contained as possible, so that they can be read separately. Chapter 1 gives an introduction to optical storage technology and a review of signal processing techniques for read channels. It also presents the main challenges in future high-density optical storage systems. This introductory chapter concludes with the motivations, contributions and organization of the thesis.

In Chapter 2 we introduce a novel adaptive equalization technique that seeks to minimize detection bit-error rate for PRML systems. Although the idea behind this chapter, i.e. basing equalizer adaptation/design on minimizing BER, is not entirely new, we are the first to propose a practical and simple adaptive algorithm that achieves a near minimum-BER performance. The chapter explains, first, the limitations of the existing equalization techniques and then proposes a new adaptive algorithm for BER optimization. The superiority of the proposed algorithm is first demonstrated analytically and then verified based on computer simulations. The key property of the new adaptation scheme is its selectivity in the sense that it mainly focuses on the data patterns that have the highest likelihood of detection error. The strength of the proposed algorithm is not restricted to providing a better performance but extends

to allowing very low implementation costs. Further simplification of the proposed algorithm for different channels and extension to diverse detection schemes is also discussed and validated in Chapter 2.

Because target-response adaptation is an important problem for high density storage systems, as explained earlier, Chapter 3 generalizes and applies the near minimum-BER adaptation technique to joint target response and equalizer adaptation. This is achieved by focusing target-response adaptation on the most likely bit-error events and by acting towards decreasing their corresponding probability of occurrence. Analysis of the near minimum-BER technique for target-response adaptation is presented in Chapter 3 to prove its superiority with respect to existing techniques. Also simulation results for optical storage channels with electronics and media noise and channel nonlinearities are provided. Relative to the existing adaptation methods, the near minimum-BER scheme is comparable in terms of implementation complexity. However, in terms of performance, it allows significant improvements especially for short target or equalizer lengths or in the presence of nonlinear ISI and media noise. This is of great importance for high-density storage systems. On the one hand, this can be used to reduce system complexity, by allowing the use of a short target response without significant performance degradation. On the other hand, it can help mitigating nonlinearities and media noise without increasing complexity.

With respect to the objective of minimizing latencies inside the timing-recovery loop to allow tracking of the fast variations, Chapter 4 reports an asynchronous equalization scheme for storage systems. It involves an equalizer that operates at a sampling-rate asynchronous to the data rate [28, 112, 114]. Chapter 4 explains the implication of this scheme for equalizer adaptation and proposes a highly simple yet efficient method for asynchronous equalizer adaptation. For simplicity, Chapter 4 focuses on LMS adaptation. However, the results of this chapter carry over to other adaptation criteria as well, e.g. the near minimum-BER criterion proposed in Chapter 2.

With respect to the objective of strengthening the timing-recovery loop, Chapter 5 focuses on designing an optimal timing-recovery scheme for channels with data-dependent noise. The key benefits of the proposed scheme is its simplicity, generality and near-optimality. The applicability of the proposed algorithm extends well beyond optical storage channels. The chapter exploits the data-dependent and colored nature of noise to improve the performance of timing recovery. It starts by

analyzing the maximum-likelihood (ML) timing-recovery criterion and proposes a practical scheme to achieve near-ML performance. It presents both theoretical and numerical evidences of the performance gain provided by the scheme compared to existing schemes.

As recently all-digital timing recovery is often employed, e.g. [112, 121], design of efficient sampling-rate converter (SRC) digital filters is very important for performance optimization and complexity limitation. More precisely, design of SRC filters that also realize channel equalization presents a two-fold attractive property. First, it helps to reduce complexity by shifting a big part of channel equalization (amplitude equalization) towards the SRC filters and thus shortens significantly the equalizer length for the same performance. Second, for systems employing a digital synchronous equalizer, shortening the equalizer length limits the delay inside the timing-recovery loop which is crucial for the latter to function properly [15]. Chapter 6 explains first the problem of equalizing SRC filters and then presents algorithms for designing such filters.

Chapter 7 concludes the thesis with some remarks and directions for future work.

The development of all new algorithms presented in the different chapters is supplemented with computer simulation results. These simulation results are used for demonstrating the effectiveness of the proposed algorithms and for validating the analytical developments.

1.4.1 About author's publications and patent applications

During the course of this Ph.D. work, the author worked first on a two-dimensional optical storage system called TwoDOS [17, 73–75]. Inspired by the work on TwoDOS, the author then focused, in the second part of his Ph.D. period, on equalization and timing recovery for optical storage systems.

The TwoDOS period was, for the author, a great opportunity for learning on several levels. During this period, the author published different papers, coauthoring with his supervisor and project partners (see the list of publications below).

In the after-TwoDOS period, the author published several papers and filed two patent applications related to equalization and timing recovery. The totality of this thesis relates to this period. The following list contains the publications and patent applications by the author.

Papers:

[P-1] J. Riani, S. van Beneden, J.W.M. Bergmans, A.H.J. Immink, “Near Minimum BER Equalizer Adaptation for PRML systems”, *Accepted for publication in IEEE Trans. on Communications*, 2007.

[P-2] J. Riani, A.H.J. Immink, J.W.M. Bergmans, S. Van Beneden, “Near Minimum-BER All-Adaptive Partial Response Equalization for Recording Systems”, *IEEE Global Telecommunications Conference (GLOBECOM)*, 28 Nov.-2 Dec 2006.

[P-3] J. Riani, A.H.J. Immink, J.W.M. Bergmans, S. Van Beneden, “Near Minimum-BER All-Adaptive Partial Response Equalization for Recording Systems”, *Submitted for publication to IEEE Trans. on Magn.*, 2007.

[P-4] J. Riani, J.W.M. Bergmans, S. Van Beneden, A. Immink, “Data-Aided Timing Recovery for Recording Channels with Data-Dependent Noise”, *IEEE Trans. on Magn.*, Vol. 42, Issue 11, pp. 3752 - 3759, Nov. 2006.

[P-5] J. Riani, S. Van Beneden, J.W.M. Bergmans, “Equalizing Sampling Rate Converters for Storage Systems”, *IEEE International Conference on Acoustics, Speech, and Signal Processing (ICASSP)*, Vol. 3, pp. III-392 - III-395, 21-24 May 2006.

[P-6] J. Riani, J.W.M. Bergmans, A.H.J. Immink, “Asynchronous LMS Adaptive Equalization: Analysis and Efficient Realization,” *Submitted for publication to IEEE Trans. on Sign. Proc.*, 2006.

[P-7] J. Riani, S. van Beneden, J.W.M. Bergmans, A.H.J. Immink, “Near Minimum-BER Equalizer Adaptation for PRML systems”, *IEEE Global Telecommunications Conference (GLOBECOM)*, Vol. 4, pp. 2123-2128, 2005.

[P-8] J. Riani, S. Van Beneden, J.W.M. Bergmans, “Data-aided Timing Recovery in the presence of Data-Dependent Noise”, *European Signal Processing Conference, Eusipco*, 4-8 Sept. 2005.

[P-9] J. Riani, J.W.M. Bergmans, A.H.J. Immink, R. Otte, “Efficient Realization of Asynchronous LMS Adaptive Equalization”, *IEEE Benelux Sig. Proc. Symposium*, April 15-16, 2004.

[P-10] J. Riani, J.W.M. Bergmans, S.J.L. v. Beneden, W.M.J. Coene, A.H.J. Immink, "Equalization and Target Response Optimization for High Density Two-Dimensional Optical Storage," *Proc. 24-th Symp. Inf. Th. Benelux, ed. L. Tolhuizen, ISBN 90-71048-18-7*, pp. 141-148, 2003.

[P-11] S. Van Beneden, J. Riani, J.W.M. Bergmans, "Adaptive Decomposition of Noise Sources in Digital Recording Systems with Media Noise", *IEEE Trans. on Magn.*, Vol. 43, Issue 2, Part 1, pp. 561 - 571, Feb. 2007.

[P-12] S. van Beneden, J.W.M. Bergmans, J. Riani, A.H.J. Immink, "Minimum Latency Tracking of Rapid Variations in Two-Dimensional Storage Systems," *IEEE Trans. on Magn.*, Vol. 43, Issue 1, Part 1, pp. 67 - 78, Jan. 2007.

[P-13] S. Van Beneden, J. Riani, J.W.M. Bergmans, "Data-Dependent Noise Estimation in Digital Recording Systems", *Accepted for publication at the IEEE Global Telecommunications Conference (GLOBECOM)*, 28 Nov.-2 Dec 2006.

[P-14] S. Van Beneden, J. Riani, J.W.M. Bergmans, A.H.J. Immink, "Cancellation of Linear Intersymbol Interference for Two-Dimensional Storage Systems", *IEEE Trans. on Magn.*, Vol. 42, Issue 8, pp. 2096 - 2106, Aug. 2006.

[P-15] S. Van Beneden, J. Riani, J.W.M. Bergmans, "Cancellation of Linear Intersymbol Interference for Two-Dimensional Storage Systems", *IEEE International Conference on Communications (ICC)*, Vol. 7, pp. 3173 - 3178, June 2006.

[P-16] S. Van Beneden, J. Riani, J.W.M. Bergmans, "Characterization of Two-Dimensional Storage Systems", *International Conference on Acoustics, Speech, and Signal Processing (ICASSP)*, Vol. 4, pp. IV-801 - IV-804, 2006.

[P-17] J.J.M. Kierkels, J. Riani, J.W.M. Bergmans, G.J.M. van Boxtel, L.L.M. Vogten, "Using an eye tracker for accurate eye movement artifact correction", *Accepted for publication at IEEE Trans. on Biomedical Engineering*, 2006.

[P-18] W.M.J. Coene, D.M. Bruls, A.H.J. Immink, A.M. van der Lee, A.P. Hekstra, J. Riani, S. van Beneden, M. Ciacci, J.W.M. Bergmans, M. Furuki,

"Two-dimensional optical storage", *International Conference on Acoustics, Speech, and Signal Processing (ICASSP)*, Vol. 5, pp. 749-752, March 2005.

[P-19] D.M. Bruls, A.H.J. Immink, A.M. van der Lee, W.M.J. Coene, J. Riani, S.J.L. van Beneden, M. Ciacci, J.W.M. Bergmans, M. Furuki, "Two-Dimensional Optical Storage: High-Speed Read-Out of a 50 GByte Single-Layer Optical Disc with a 2D Format Using λ=405 nm and NA=0.85," *Jpn. J. Appl. Phys.*, Vol. 44, No. 5B, pp. 3547-3553, 2005.

[P-20] A.H.J. Immink, J.Riani, S.J.L. v. Beneden, J.W.M. Bergmans, M. Ciacci, A. Nowbakht Irani, W.M.J. Coene, A.M. van der Lee, D. Bruls, "Adaptation and Timing Recovery for Two-Dimensional Optical Storage," *Optical Data Storage, Proceedings of SPIE*, vol. 5380, pp. 90-104, 2004.

[P-21] A. Nowbakht Irani, J.W.M. Bergmans, S. v. Beneden, W.M.J. Coene, M. Ciacci, A.H.J. Immink, J. Riani, "Improved Correlation Receiver for Frame Synchronization," *Proceedings of the 25-th Symp. Inf. Th. Benelux. Ed. R. Pellikaan*, pp. 65-72, 2004.

[P-22] M. Ciacci, J. Riani, J.W.M. Bergmans, A.H.J. Immink, "Equalizer Based Tilt Estimation for Two-Dimensional Optical Storage," *Proc. 25-th Symp. Inf. Th. Benelux, ISBN 90-71048-20-9*, pp. 249-256, 2004.

[P-23] S. van Beneden, J.W.M. Bergmans, J. Riani, M. Ciacci, A. Nowbakht, A.H.J. Immink, "Minimum Loop-Delay Adaptation and Timing Recovery for Two-Dimensional Optical Storage," *Proc. 25-th Symp. Inf. Th. Benelux, ISBN 90-71048-20-9*, pp. 257-264, 2004.

[P-24] A.H.J. Immink, W.M.J. Coene, A.M. van der Lee, C. Busch, A.P. Hekstra, J.W.M. Bergmans, J. Riani, S.J.L. van Beneden, T. Conway, "Signal Processing and Coding for Two-Dimensional Optical Storage," *Global Telecommunications Conference, GLOBECOM, IEEE*, vol.7, pp. 3904-3908, 2003.

Patent Applications:

[PA-1] J. Riani, S.J.L. v. Beneden, J.W.M. Bergmans, A.H.J. Immink, *Near-minimum bit-error rate equalizer/target adaptation*, patent application No. 05 300939.5, filing date : 18 Nov. 2005

[PA-2] J. Riani, S.J.L. v. Beneden, J.W.M. Bergmans, A.H.J. Immink, *Data Dependent Timing Recovery*, PHNL 000669, filing date: 13 Jul. 2005.

[PA-3] J.W.M. Bergmans, S.J.L. v. Beneden, A.H.J. Immink, J. Riani, *Feedback Control Loop for bit detection in an N-dimensional data block*, PHNL040117, filing date 20 Jan. 2005.

[PA-4] A.H.J. Immink, W.M.J. Coene, J.W.M. Bergmans, J. Riani, *Channel Synchronization for Two-Dimensional Optical Recording*, WO 2004/112019, publication date: 23 Dec. 2004.

Chapter 2

Minimum Bit-Error Rate Equalization

Receivers for Partial Response Maximum-Likelihood systems typically use a linear equalizer followed by a Viterbi detector. The equalizer tries to confine the channel intersymbol interference to a short span in order to limit the implementation complexity of the Viterbi detector. Equalization is usually made adaptive in order to compensate for channel variations. Conventional adaptation techniques, e.g. LMS, are in general suboptimal in terms of bit-error rate. In this chapter we present a new equalizer adaptation algorithm that seeks to minimize bit-error rate at the Viterbi detector output. The algorithm extracts information from the Sequenced Amplitude Margin (SAM) histogram and incorporates a selection mechanism that focuses adaptation on particular data and noise realizations. The selection mechanism is based on the reliability of the Add Compare Select (ACS) operations in the Viterbi detector. From a complexity standpoint, the algorithm is essentially as simple as the conventional LMS algorithm. Moreover, we present a further simplified version of the algorithm that does not require any hardware multiplications. Simulation results, for an idealized optical storage channel, confirm a substantial performance improvement relative to existing adaptation algorithms.

2.1 Introduction

The optimal receiver for estimating a data sequence in the presence of intersymbol interference (ISI) and additive Gaussian noise [41] can generally not be realized because of its excessive complexity. This fact has led to a development of a variety of suboptimal and lower complexity receivers.

In many practical systems, a linear equalizer is first used to shape the channel

symbol response to an acceptably shorter target response. A Viterbi detector (VD), suitable for the target response [143], subsequently estimates the transmitted data sequence. Such systems are known as Partial Response Maximum-Likelihood (PRML) systems. PRML systems are widely used in digital storage systems [20] to combat the extensive ISI, caused by the channel, especially at high storage densities. The extensive ISI at high densities precludes the application of full Maximum Likelihood Sequence Detection (MLSD) [41] because of system complexity and data rate constraints.

Equalization in PRML systems is usually made adaptive in order to compensate for channel variations. One of the most popular adaptation methods is based on the Minimum Mean Square Error (MMSE) criterion [86]. This method minimizes the power of the error signal, with the error signal being the difference between the actual and the ideal (noiseless) VD input. This minimization is achieved regardless of correlation or data-dependency of the error signal, as caused, for example, by residual ISI (RISI) due to mis-equalization. However, it is known that RISI or correlated noise can cause considerable bit-error rate (BER) degradation when compared to a system operating with a comparable amount of additive white Gaussian noise (AWGN) and no RISI. Therefore, MMSE equalization does not guarantee, in general, optimum BER performance. To minimize BER, the equalizer must minimize RISI for data patterns that are critical for bit detection and might tolerate more RISI for less critical data patterns. In other words, the effort of equalization must be focused primarily on critical data patterns, by improving their corresponding detection Signal to Noise Ratio (SNR). As far as noise correlation is concerned, the equalizer must seek an appropriate trade-off between noise correlation and RISI in order to achieve the best BER. These requirements cannot, in general, be fulfilled with MMSE equalization.

Adaptive minimum-BER equalization has been already studied for the case of full response equalization and sample-by-sample detection [19] and decision-feedback equalization [134]. However, in the context of PRML systems, no such studies have been reported. A step towards minimum-BER adaptive equalization was reported in [117] where a new equalizer adaptation criterion was derived from the Sequenced Amplitude Margin (SAM) [122] [118]. The novel idea in [117], known as least-mean squared SAM error (LMSAM), is to base equalizer adaptation on minimizing the ‘variance’ of the SAM for particular bit patterns and error events. The error events considered by the LMSAM technique are single bit-errors at transitions in the

data. This restriction to single bit-errors makes the LMSAM technique suboptimal for channels where other error events are important. Moreover, basing the equalizer adaptation on minimizing the SAM variance only is in general not optimal in terms of BER, as will be shown in this chapter.

This chapter presents a new equalizer adaptation algorithm that seeks to minimize BER. The algorithm incorporates a selection mechanism that focuses equalizer adaptation only on a particular region of the SAM histogram. The selection mechanism is based on the reliability of the Add Compare Select (ACS) operation in the VD. From an implementation standpoint, our algorithm is essentially as simple as the LMS algorithm. Moreover, a further simplified version of the algorithm that does not require any multiplications is proposed.

The remainder of this chapter is organized as follows. Section 2.2 describes the system model and nomenclature. Section 2.3 provides analytical steps needed to understand the behavior of the VD as a function of the error signal at its input. This allows us to propose a cost function for equalizer adaptation. Section 2.4 explains the new equalizer adaptation schemes. Simulation results, presented in Section 2.6, show the merits of our algorithm compared to existing ones.

2.2 System Model and Problem Definition

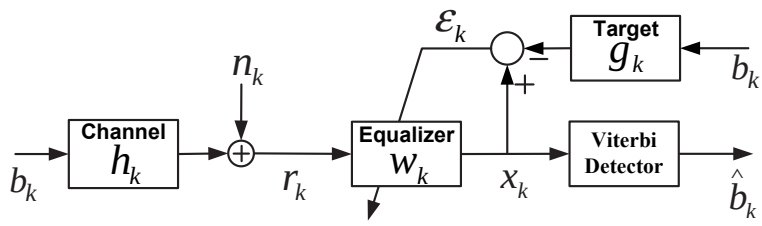

Figure 2.1: *A discrete-time model of a PRML system.*

A discrete-time model of a PRML system is shown in Figure 2.1. A binary sequence $b_k \in \{\pm 1\}$ is transmitted, at a rate $1/T$, over a linear dispersive channel with finite impulse response h_k. The channel output is corrupted by additive zero-mean noise n_k. The reasoning in this chapter is quite general and does not assume any prior knowledge of the nature of the noise n_k, e.g. the noise n_k is not necessarily Gaussian and can be data-dependent. The readback signal r_k is the noisy channel output and is

given by

$$r_k = (h * b)_k + n_k,$$

where `$*$´ denotes linear convolution. The channel impulse response is in general quite long and may be time-varying. For this reason adaptive Partial Response (PR) equalization [86] is used in order to transform the channel response to a shorter and well defined impulse response. The equalizer impulse response w_k is optimized so that the overall impulse response, at its output, is as close as possible to a prescribed short impulse response that we refer to as the target response g_k. The equalizer output x_k serves as input to a VD that is matched to the target response g_k and that produces bit decisions $\widehat{b}_k$. The detector input x_k is ideally equal to the reference signal $(g * b)_k$. However, because of channel noise, RISI and the different channel artifacts, x_k can be written as

$$x_k = (g * b)_k + \varepsilon_k,$$

where ε_k denotes the error signal at the detector input and contains contribution of channel noise and RISI caused by mis-equalization.

Before proceeding with equalizer adaptation that minimizes BER, let us first understand, in the next section, the dependency of the VD performance on the error signal ε_k. This is then used in order to derive a practical equalizer adaptation criterion that is directly linked to BER.

For mathematical convenience we omit the delays of the different modules and the latency of the bit detector and assume that $\widehat{b}_k = b_k$.

2.3 Derivation of the adaptation criterion

The VD in Figure 2.1 operates on a trellis that is matched to the target response g_k. Every path in this trellis corresponds to an admissible bit sequence. The detector selects the sequence that leads to the smallest path metric in the trellis [41]. The metric of a bit sequence a_k is given by the Euclidian metric

$$\mathcal{M}(a) = \sum_i (x_i - (g * a)_i)^2, \tag{2.1}$$

where the above summation is taken over all readback symbols indices.

An example of a 4-state trellis is shown in Figure 2.2. At time kT the VD employs, for every state, an Add Compare Select (ACS) operation to select the best path arriving at each state; the other path is discarded. Let us assume for the sake of the argument that the path corresponding to the transmitted bit sequence b_k arrives at state S_0 at time kT. We denote by b_k^0 and b_k^1 the selected and discarded paths by the ACS operation at state S_0 and time kT. An erroneous ACS decision will occur at time kT when the correct path, corresponding to b_k, is discarded, i.e. when $b^1 = b$. The selected path in this case is $b^0 = b + 2e$ where $e = \frac{b^0 - b}{2}$ ($e_k \in \{0, \pm 1\}$) is referred to as the bit-error sequence. This erroneous ACS decision occurs with a probability:

$$\Pr(\text{ACS error}|b, e) = \Pr(\mathcal{M}(b + 2e) - \mathcal{M}(b) < 0). \tag{2.2}$$

The left part of (2.2) represents the probability that the ACS operation induces a decision error, by discarding the correct path, given the transmitted bit sequence b_k and an admissible bit-error sequence e_k, i.e. a sequence in $\{0, \pm 1\}$ for which $b_k + 2e_k$ is an admissible bit sequence.

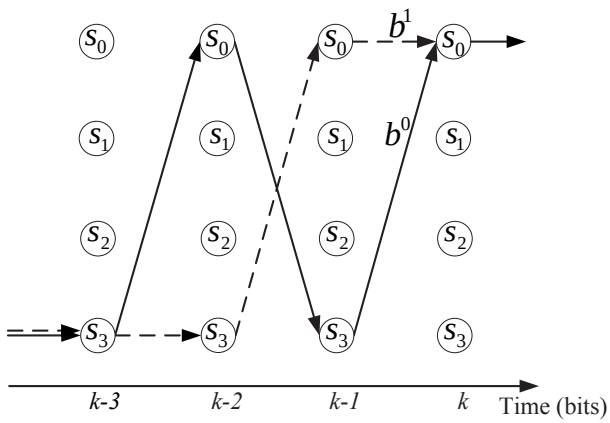

Figure 2.2: *An example of a 4-state trellis.*

With the assumption of an infinitely long backtracking depth in the VD, the overall BER is directly related to the probability of ACS errors over all possible data patterns and admissible bit-error sequences. Minimization of the probability of ACS error for a given bit-error sequence leads to minimization of BER for that specific bit-error sequence, i.e. of the contribution of this sequence to the overall BER.

The variable $S(e) = \mathcal{M}(b + 2e) - \mathcal{M}(b)$ is known in literature as the Sequence Amplitude Margin (SAM) and was first introduced in [122]. Upon invoking (2.1),

$S(e)$ can be written as

$$\begin{aligned} S(e) &= 4\sum_i (g*e)_i^2 - (g*e)_i\varepsilon_i \\ &= 4(\underline{\delta}_e^T\underline{\delta}_e - X_e), \end{aligned} \tag{2.3}$$

where $\underline{\delta}_e$ is a column vector given by $\underline{\delta}_{e,i} = (g*e)_i$, $\underline{\delta}_e^T\underline{\delta}_e$ is the Euclidian weight of the bit-error sequence e_k, and $X_e = \underline{\delta}_e^T\underline{\varepsilon}$ denotes the correlation between $\delta_{e,k}$ and the error signal ε_k. Using (2.3), Eq. (2.2) can be rewritten as:

$$\Pr(\text{ACS error}|b,e) = \Pr(\underline{\delta}_e^T\underline{\delta}_e < X_e). \tag{2.4}$$

In order to minimize (2.4) for a particular bit-error sequence e_k, optimal equalization must shape ε_k, or equivalently the variable X_e, such that $\Pr(\underline{\delta}_e^T\underline{\delta}_e < X_e)$ is minimized. A first attempt towards this goal is to minimize $E[X_e^2]$ according to the LMSAM algorithm as suggested, for single bit-errors, in [117]. However, this is not optimal because minimization of $E[X_e^2]$ yields no control on the sign of $E[X_e]$ whereas this sign is of capital importance for $\Pr(\underline{\delta}_e^T\underline{\delta}_e < X_e)$.

By way of illustration, we consider in Appendix A the case when the channel noise n_k is additive and Gaussian and study the impact of linear residual ISI on the SAM. We show mainly two points. First, $E[X_e]$ and $E[X_e^2]$ are both function of the equalizer response w_k (2.20)(2.21). Second, $E[X_e]$ affects (2.4) differently than the variance $\sigma_{X_e}^2 = E[X_e^2] - E[X_e]^2$ of X_e. The average of X_e, when positive, causes a degradation in effective Euclidian weight of the bit-error sequence e_k. The variance of X_e can be seen as an increase in channel noise power. Thus minimizing $E[X_e^2]$ is suboptimal because, on the one hand, this does not provide the optimal trade-off between $E[X_e]$ and σ_{X_e} and on the other hand, this does not constrain the sign of $E[X_e]$ whereas the latter is of capital importance for (2.4). This sign tells whether the residual ISI is constructive or destructive in terms of (2.4).

Because Appendix A assumes the prior knowledge of the channel response and noise characteristics, its results cannot be directly used in the context of adaptive equalization. In order to come up with a simple criterion on X_e that is directly linked to minimization of (2.4) we make the following observations:

- First, an ACS error occurs only when $\underline{\delta}_e^T\underline{\delta}_e < X_e$. Therefore, it is natural to consider the values of X_e only in a certain interval of interest, namely when X_e is higher than a certain threshold around $\underline{\delta}_e^T\underline{\delta}_e$.

- Second, although the distribution of X_e is in general not Gaussian, its tail above $\underline{\delta}_e^T \underline{\delta}_e$, or equivalently the tail of $S(e)$ below zero, can be approximated with a Gaussian tail. This argument has been first used and validated in [118] in order to extract BER estimates from the SAM distribution. The validation of this argument in [118] was based on both simulated data and experimental replay signals taken from different optical disk systems.

Example 2.1 :
In order to provide a simple explanation of the Gaussian tail approximation, let us consider the case where the channel noise n_k has a Gaussian distribution. The error signal ε_k can be written as $\varepsilon_k = (q*b)_k + v_k$ where $q_k = (w*h)_k - g_k$ and $v_k = (w*n)_k$ is Gaussian as it is a filtered version of a Gaussian noise. The variable X_e, which is written as

$$X_e = \sum_k (g*e)_k (q*b)_k + \sum_k (g*e)_k v_k,$$

can then be interpreted as a superposition of different Gaussian distributions; one distribution per bit sequence. For a given bit sequence b_k, the mean of the corresponding Gaussian distribution is given by $E[X_e|b] = \sum_k (g*e)_k (q*b)_k$ and its variance by $\underline{\delta}_e^T R_{vv} \underline{\delta}_e$ where R_{vv} denotes the autocorrelation matrix of v_k. Because the variance of these Gaussian distributions is independent of b_k, the tail of X_e, above $\underline{\delta}_e^T \underline{\delta}_e$, is mainly determined by the bit sequence $\overline{b}$ for which $\sum_k (g*e)_k (q*b)_k$ is the biggest, i.e. $\overline{b} = \arg\max_b \sum_k (g*e)_k (q*b)_k$. This justifies the Gaussian tail approximation on the distribution of X_e. Note that the bit sequence $\overline{b}$ corresponds to the sequence with most destructive ISI for the bit-error sequence e_k. $\diamondsuit$

Following the above mentioned observations, we introduce the truncated version of X_e over the interval $]T_e, +\infty[$ where the positive threshold T_e is smaller than $\underline{\delta}_e^T \underline{\delta}_e$, i.e. $0 < T_e \leq \delta_e^T \underline{\delta}_e$. The truncated version of X_e is denoted by X_e' and is defined as

$$X_e' \doteq X_e \mathbf{1}_{\{X_e > T_e\}} = \begin{cases} X_e & \text{if } X_e > T_e, \\ 0 & \text{otherwise,} \end{cases} \tag{2.5}$$

where the function $\mathbf{1}_{\{Y\}}$ takes the value 1 if the Boolean variable Y is true and 0 otherwise.

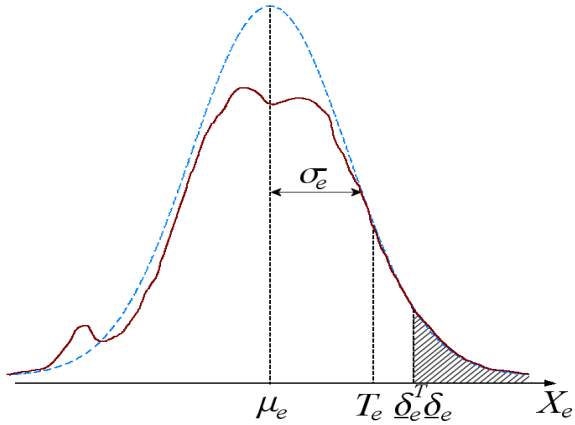

Figure 2.3: *A conceptual plot of the distribution of X_e (solid). The dashed curve corresponds to the Gaussian fitting of the tail of X_e on $]T_e, +\infty[$. The hashed area corresponds to* $\Pr(\underline{\delta}_e^T\underline{\delta}_e < X_e)$.

Under the assumption that the tail of the distribution of X_e over $]T_e, +\infty[$ can still be approximated as a tail of a Gaussian, we will show that, for a judicious choice of T_e, $\Pr(\underline{\delta}_e^T\underline{\delta}_e < X_e)$ is an increasing function of $E[X_e']$. In other words, increasing $E[X_e']$ leads necessarily to an increase in $\Pr(\text{ACS error}|b,e)$ and vice versa. In fact, if we denote by μ_e and σ_e^2, respectively, the average and the variance of the Gaussian distribution that fits best the tail of the distribution of X_e over $]T_e, +\infty[$, see Figure 2.3, then one can write:

$$\Pr(\underline{\delta}_e^T\underline{\delta}_e < X_e) \simeq \mathrm{Q}\left(\frac{\underline{\delta}_e^T\underline{\delta}_e - \mu_e}{\sigma_e}\right), \tag{2.6}$$

where the Q-function is defined as $\mathrm{Q}(x) = \frac{1}{\sqrt{2\pi}}\int_x^\infty e^{\frac{-t^2}{2}}dt$. Besides, it can be shown that

$$E[X_e'] \;=\; \mu_e \mathrm{Q}\left(\frac{T_e - \mu_e}{\sigma_e}\right) \;+\; (2\pi)^{-1/2}\sigma_e \exp\{-\frac{(T_e-\mu_e)^2}{2\sigma_e^2}\}.$$

This expression can be further simplified, over the SNR range of practical interest, by using the approximation $\mathrm{Q}(x) \simeq (2\pi x^2)^{-1/2}\exp\{-x^2/2\}$ for $x > 2$. This leads to

$$E[X_e'] \simeq T_e \mathrm{Q}\left(\frac{T_e - \mu_e}{\sigma_e}\right). \tag{2.7}$$

In order to make the argument of the Q-function in (2.7) proportional to that in (2.6), an obvious choice of T_e is $T_e = \underline{\delta}_e^T\underline{\delta}_e$. However, this choice of T_e implies that

X'_e is nonzero only when the VD makes a detection error. Accordingly any equalizer adaptation in this case can only operate in a Data-Aided (DA) mode where prior knowledge of the transmitted bits is available. In order to be able to also operate in the Decision-Directed (DD) mode, where the detected bits are used in the adaptation loop, the threshold T_e has to be taken strictly smaller than $\underline{\delta}_e^T \underline{\delta}_e$. To this aim, one can readily show that thresholds T_e of the form

$$T_e = (1-\alpha)\underline{\delta}_e^T \underline{\delta}_e + \alpha\mu_e, \tag{2.8}$$

where $\alpha \in [0,1]$, make the argument of the Q-function in (2.7) proportional to that of (2.6). In fact, such a choice of T_e leads to

$$\frac{E[X'_e]}{T_e} \simeq \mathrm{Q}\left((1-\alpha)\frac{\underline{\delta}_e^T \underline{\delta}_e - \mu_e}{\sigma_e}\right). \tag{2.9}$$

It is apparent that minimizing (2.6) is equivalent to minimizing (2.9). Thus, in order to minimize BER for a particular bit-error sequence e_k, equalizer adaptation can be based on minimizing the following cost function:

$$\Delta_e = \frac{E[X'_e]}{T_e}, \tag{2.10}$$

where the threshold T_e is given by (2.8). The value of α is chosen such that the Gaussian tail approximation holds on $]T_e, +\infty[$. Typical values of α are in the interval $[0, 0.5]$. The dependence of T_e on μ_e (2.8) implies that in practice the variables μ_e for the different bit-error sequences must be estimated and adapted. However, because at reasonable SNRs, $\mu_e \simeq E[X_e] = E[\underline{\delta}_e^T \underline{\varepsilon}] \ll \underline{\delta}_e^T \underline{\delta}_e$, one can simply neglect the dependency of T_e on μ_e. Unless specified otherwise, we fix a value of α and consider the threshold T_e to be equal to $(1-\alpha)\underline{\delta}_e^T \underline{\delta}_e$.

Example 2.2 :

For the sake of illustration, let us consider the error signal ε_k as a zero-mean Gaussian noise signal and denote its autocorrelation matrix by R_ε. This is especially true if residual ISI at the detector input is negligible.

For a given bit-error sequence e_k, the variable X_e is then Gaussian with a mean $\mu_e = 0$ and a variance $\sigma_e^2 = \underline{\delta}_e^T R_{\varepsilon\varepsilon} \underline{\delta}_e$. The threshold T_e in (2.8) is then given by

$T_e = (1-\alpha)\underline{\delta}_e^T \underline{\delta}_e$ and one can show, after few straightforward mathematical steps, that (2.10) boils down to

$$\Delta_e = f\left(\frac{T_e}{\sigma_e}\right)$$

where the function f is given by $f(x) = \frac{1}{\sqrt{2\pi x^2}} \exp\left\{-\frac{x^2}{2}\right\}$.

Because f is a strictly decreasing function for $x > 0$, one concludes that minimizing Δ_e is equivalent to maximizing the ratio $\frac{T_e}{\sigma_e} = (1-\alpha)\frac{\underline{\delta}_e^T \underline{\delta}_e}{\sqrt{\underline{\delta}_e^T R_\varepsilon \underline{\delta}_e}}$ which is proportional to the root square of the effective SNR, i.e. $\frac{\underline{\delta}_e^T \underline{\delta}_e^2}{\underline{\delta}_e^T R_\varepsilon \underline{\delta}_e}$, [41]. This example illustrates once more that designing an equalizer that minimizes Δ_e is equivalent to maximizing the effective SNR, i.e. minimizing BER for a given bit-error sequence.$\diamondsuit$

2.4 Near minimum-BER equalizer adaptation

In the previous section, a cost function (2.10), which is directly related to the BER for a given bit-error sequence, was derived. In this section we employ (2.10) in order to derive the Near Minimum-BER (NMBER) equalizer adaptation. The basic idea of the NMBER adaptation is to minimize (2.10) for all relevant bit-error sequences. The different functions Δ_e for the different bit-error sequences are then combined with different weights so as to achieve the best overall BER. For clarity, let us first focus on a given bit-error sequence e_k and develop an adaptive equalization scheme that minimizes (2.10). The second part of this section combines the different minimizations of the different functions Δ_e such that the overall BER, approximated by its union bound expression, is optimized.

For a given bit-error sequence e_k, an equalizer adaptation scheme that minimizes (2.10) can be based on the steepest descent algorithm. This consists of following at each iteration the opposite direction of the gradient of Δ_e with respect to the equalizer coefficients. The adaptation of the pth equalizer tap can be written as follows:

$$w_p^{(k+1)} = w_p^{(k)} - \eta'(e)\left.\frac{\partial \Delta_e}{\partial w_p}\right|_{\underline{w}=\underline{w}^{(k)}}, \tag{2.11}$$

where $w_p^{(k)}$ is the pth equalizer tap at time kT. The coefficient $\eta'(e)$ denotes the equalizer adaptation constant. Note that this adaptation constant is, in general, dependent

on the error sequence e_k. The reasons for this dependency are explained in the next paragraph. By using (3.2) and the equality $\frac{\partial \varepsilon_i}{\partial w_p} = r_{i-p}$, one can prove that

$$\left.\frac{\partial X'_e}{\partial w_p}\right|_{\underline{w}=\underline{w}^{(k)}} = \left(\sum_{i \leq k} \delta_{e,i} r_{i-p}\right) \mathbf{1}_{\{X_e > T_e\}}.$$

Upon replacing the expectation of X'_e in (2.10) by its instantaneous realization, (2.11) can be rewritten as:

$$w_p^{(k+1)} = w_p^{(k)} - \eta(e) \left(\underline{\delta}_e^T \underline{r}_{k-p}\right) \mathbf{1}_{\{\mathcal{M}(b+2e)-\mathcal{M}(b)<T_h(e)\}} \tag{2.12}$$

where $\eta(e) = \eta'(e)/T_e$, $\underline{r}_{k-p} = [r_{k-p}, r_{k-p-1}, \ldots]^T$ and $T_h(e) = 4\alpha \underline{\delta}_e^T \underline{\delta}_e$ and where the selection condition, i.e. $\mathbf{1}_{\{X_e > T_e\}}$, was rewritten in terms of path metrics in the VD trellis using (2.3).

Now, if we consider a set of bit-error sequences, the overall BER can be seen as the accumulation of conditional bit-error rates for each bit sequence and admissible bit-error sequence, weighted differently for every bit sequence and bit-error sequence. More precisely, if we assume that transmitted sequences are of length N, then a union bound on the BER can be obtained using Bayes' rule. This is written as

$$\text{BER} \leq \sum_{b,e} p(b,e) \frac{H_w(e)}{N} \Pr(\underline{\delta}_e^T \underline{\delta}_e < X_e), \tag{2.13}$$

where the summation is taken over all possible bit sequences b of length N and bit-error sequences e. The probability that a bit sequence b is transmitted and that e is an admissible bit-error sequence is denoted by $p(b,e)$. The Hamming weight of the bit-error sequence e, i.e. the number of non-zeros in e, is denoted by $H_w(e)$. In order to derive a near optimal expression of the weights $\eta(e)$, we use the union bound expression to approximate BER.

Averaging over all bit sequences and admissible bit-error sequences, one can see that the NMBER adaptation in (2.11) seeks to minimize the total cost function

$$\overline{\Delta} = \sum_{b,e} p(b,e) \eta'(e) \Delta_e. \tag{2.14}$$

Note that the averaging operation is inherited in the equalizer adaptation loop. If we first consider the case where $\alpha = 0$, then we have $T_e = \underline{\delta}_e^T \underline{\delta}_e$ and $\Delta_e = \Pr(\underline{\delta}_e^T \underline{\delta}_e < X_e)$ using (2.6), (2.9) and (2.10). It follows that, in order to make the minimization of

(2.14) equivalent to that of the right hand expression of (2.13), it is sufficient to take $\eta'(e) = \eta(e)T_e$ to be proportional to $H_w(e)$, or equivalently

$$\eta(e) = \eta_0 \frac{H_w(e)}{\underline{\delta}_e^T \underline{\delta}_e}, \tag{2.15}$$

where η_0 is a constant independent of the bit-error sequence e_k. Therefore, in order to minimize BER, the minimization of the different cost functions Δ_e should be weighted differently for different bit-error sequences according to (2.15). The division by $\underline{\delta}_e^T \underline{\delta}_e$ in (2.15) can be omitted in practice because the dominant bit-error sequences have approximately similar Euclidian weights, which are close to the minimal Euclidian weight.

When $\alpha > 0$ then the expression of $\eta(e)$ given in (2.15) becomes sub-optimal in general. However, from our simulations, no noticeable improvement in BER was provided by further optimization of $\eta(e)$. For this reason, we consider the expression of $\eta(e)$ given by (2.15) in the sequel.

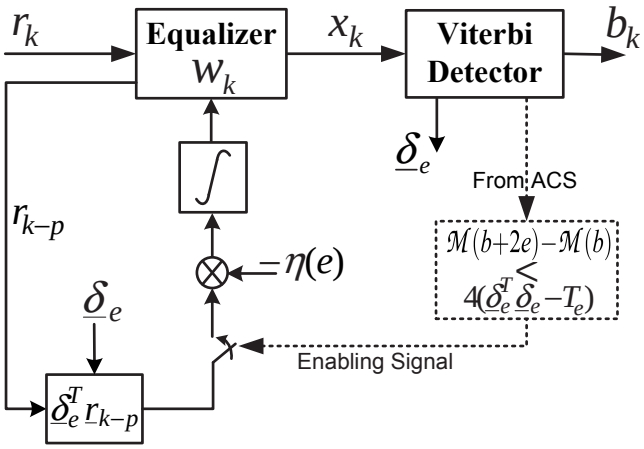

Figure 2.4: *The NMBER adaptation. Only the adaptation of the pth equalizer tap is shown.*

The overall adaptation of the pth equalizer tap value is depicted in Figure 2.4. At every clock cycle kT, an ACS operation is employed at every state. At every state, two quantities are derived. First, the difference in path metrics between the selected and the discarded paths is taken. Second, a bit-error sequence e_k is derived as the bitwise difference between the two sequences corresponding to the discarded and the

selected paths. The bit-error sequence e_k, taken from the state where the best path ends, is used to compute the vector $\underline{\delta}_e = [(g * e)_k, (g * e)_{k-1}, ...(g * e)_{k-L}]^T$, where the integer value L depends on the maximum length of relevant bit-error sequences. In the sequel, we simply fix L to the backtracking depth of the VD. The equalizer adaptation is enabled only when the difference in path metrics is smaller than $T_h(e) = 4\alpha\underline{\delta}_e^T\underline{\delta}_e$. For simplicity, one can fix $T_h(e)$ to

$$T_h(e) = T_h = 4\alpha \min_e \underline{\delta}_e^T \underline{\delta}_e$$

without any significant loss in performance. When the adaptation is enabled, the scalar product of the vector $\underline{\delta}_e$ with the equalizer input vector $\underline{r}_{k-p} = [r_{k-p}, ...r_{k-p-L}]^T$ is computed, scaled with $-\eta(e)$ and then passed to an ideal discrete-time integrator that produces the updated p^{th} equalizer tap value.

A geometrical interpretation of the NMBER algorithm, which provides an intuitive explanation, is given in Section 2.5.

2.4.1 Efficient realization of near minimum-BER adaptation

In Figure 2.4 the scalar product operation $\underline{\delta}_e^T \underline{r}_{k-p}$ can be interpreted as focusing equalizer adaptation on the frequency region that is of interest for the bit-error sequence e_k. The amplitude response of g_k in the calculation of $\underline{\delta}_e^T \underline{r}_{k-p}$ can be interpreted as only a modification of the adaptation open loop gain per frequency. Therefore, one can replace, in $\underline{\delta}_e^T \underline{r}_{k-p}$, g_k by any response g'_k that has the same phase response as g_k. This degree of freedom in the choice of the amplitude response of g'_k can be used to simplify further the NMBER algorithm.

Because target responses for optical storage systems are often symmetric, a simple response $g'(z) = z^{-D_g}$, where D_g denotes the delay in bits of the target response g_k, can be used to compute $\underline{\delta}_e^T \underline{r}_{k-p}$.

Remark :

For longitudinal magnetic storage systems, the target response is antisymmetric and is of the form $g(z) = (1-z^{-1})(1+z^{-1})^n$ where $n = 1$, $n = 2$ or $n = 3$ corresponding to PR4, EPR4 and E2PR4 classes of targets. In this case, the response $g'(z) = (1-z^{-1})z^{-n/2}$ if n is even and $g'(z) = (1-z^{-2})z^{-(n-1)/2}$ if n is odd captures the phase response of the target response $g(z)$. This choice of $g'(z)$ can thus be used to

compute $\underline{\delta}_e^T \underline{r}_{k-p}$.

The Simplified NMBER (SNMBER) equalizer adaptation rule is then obtained by replacing in (2.12) g_k by $g'_k = \delta(k - D_g)$. This can be written as:

$$w_p^{(k+1)} = w_p^{(k)} - \eta(e)\left(\underline{e}_{k-D_g}^T \underline{r}_{k-p}\right) \mathbf{1}_{\{\mathcal{M}(b+2e)-\mathcal{M}(b)<T_h\}}, \tag{2.16}$$

Where D_g is the delay of the target response g_k and $\underline{e}_{k-D_g}^T = [e_{k-D_g}, ..., e_{k-D_g-L}]$. The SNMBER equalizer adaptation algorithm is shown in Figure 2.5. This adaptation algorithm presents the advantage of further improved efficiency. In fact, because, in practice, relevant bit-error sequences span only few bits, the scalar products with $\underline{e}$ can be realized with only few additions. As an example, single bit-errors are given by $e = \pm[1,0,0]$, the simplified equalizer update boils down, except for the selection mechanism, to $\underline{e}_{k-D_g}^T \underline{r}_{k-p} = \pm\, r_{k-p+D_g}$. In the case of a double bit-error given by $e = [1,0,-1]$, the equalizer update is simply given by $\underline{e}_{k-D_g}^T \underline{r}_{k-p} = r_{k-p+D_g} - r_{k-p-2+D_g}$.

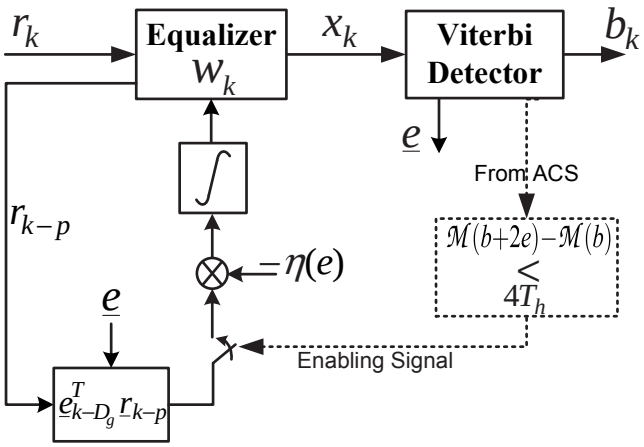

Figure 2.5: *The SNMBER equalizer adaptation for a linear phase target response.*

2.4.2 Extension of the NMBER algorithm to NPML systems

Noise-Predictive Maximum-Likelihood (NPML) detectors arise by imbedding a noise prediction/whitening process into the branch metric computation of the Viterbi detector [32] [23]. This boils down to modifying the path metric in (2.1) by replacing the target response by $g'_k = g_k - \sum_{i=1}^{M} p_i g_{k-i}$ and the detector input by $y_k =$

$x_k - \sum_{i=1}^{M} p_i x_{k-i}$ where p_i denotes an M-tap noise prediction filter. The NPML path metric becomes $\mathcal{M}'(a) = \sum_i (y_i - (g' * a)_i)^2$. Therefore the NMBER algorithm in this case can be derived by simple analogy to the PRML case. One can check that the NMBER adaptation for NPML systems can be obtained by simply replacing in (2.12) g_k by g'_k and applying a whitening filter to the delayed equalizer input, i.e. by replacing in (2.12) r_{k-p} by $r'_{k-p} = r_{k-p} - \sum_{i=1}^{M} p_i r_{k-p-i}$. The equalizer adaptation rule becomes then

$$w_p^{(k+1)} = w_p^{(k)} - \eta(e) \left(\underline{\delta}'^T_e \underline{r}'_{k-p} \right) \mathbf{1}_{\{\mathcal{M}'(b+2e) - \mathcal{M}'(b) < T_h(e)\}},$$

where $\underline{\delta}'_{e,i} = (g' * e)_i$ and $\underline{r}'_{k-p} = [r'_{k-p}, r'_{k-p-1}, ..., r'_{k-p-L}]^T$.

2.4.3 The NMBER algorithm for symbol-by-symbol detection

In the case of a receiver employing a symbol-by-symbol detector, the NMBER equalizer adaptation can be simplified further. In order to illustrate this, let us consider a system employing uncoded binary data taken from the alphabet $\mathcal{A} = \{-1, 1\}$. The receiver is composed of a linear equalizer that tries to undo the effect of the channel and a threshold detector or slicer that outputs bit decisions $\hat{b}_k$, see Figure 2.6. Based on the equalized sample x_k, the threshold detector outputs its closest symbol from the alphabet $\mathcal{A}$.

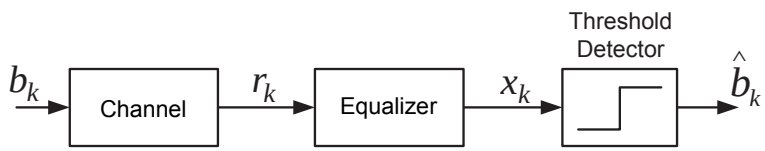

Figure 2.6: *model of the symbol-by-symbol detection system.*

As the threshold detector is equivalent to a VD with a full target response, i.e. $g_0 = 1$ and $g_i = 0$ for $i \neq 0$, the NMBER algorithm we derived earlier applies thus to this simple case. Because the NMBER algorithm contains three main building blocks: the error sequence generation block, the enabling signal generation block and the correlation block, we are going to describe these blocks for systems of Figure 2.6.

- The error sequence generation block produces at every clock cycle the most likely error sequence. In the case of symbol-by-symbol detection only single symbol errors are to be considered. Similarly to the Viterbi detection case, the

threshold detector is slightly modified to output not only the closest symbol to x_k but also the second closest symbol. We denote b_k^1 and b_k^2 the closest and the second closest symbols to x_k, respectively. We have $b_k^2 = -b_k^1$. The derivation of the symbol error sequence e_k differs from the DD to the non-DD modes. In the DA but non-DD mode the bits b_k are known and the derivation of e_k is given by

$$2e_k = \begin{cases} b_k^1 - b_k & \text{if } b_k^1 \neq b_k \quad \text{(case of a detection error)} \\ b_k^2 - b_k^1 & \text{if } b_k^1 = b_k \quad \text{(no detection error)} \end{cases}$$

In the DD mode the detector is assumed to output correct decisions and the derivation of e_k is given by

$$2e_k = b_k^2 - b_k^1.$$

- The enabling signal generation block is also simpler than in the case of Viterbi detection. Given the error event e_k, the general expression of the enabling condition is given by $\mathcal{M}(b+2e) - \mathcal{M}(b) < T_h$ in the non-DD mode and by $\mathcal{M}(b^1+2e) - \mathcal{M}(b^1) < T_h$ in the DD mode. Using $\mathcal{M}(b) = (x_k - b_k)^2$ for the threshold detector and $T_h = 4\alpha e_k^2 = 4\alpha$, it is easy to show that the enabling condition boils down to

$$\begin{aligned} (1-\alpha) &\leq e_k(x_k - b_k) \quad \text{(non-DD)} \\ (1-\alpha) &\leq e_k(x_k - b_k^1) \quad \text{(DD)} \end{aligned}$$

- the correlation of the equalizer input signal with the error sequence simplifies in this case to $e_k r_{k-p}$ for the adaptation of w_p.

The NMBER algorithm applies as well to systems employing threshold detection and leads to a very simple multiplication-free implementation.

2.5 A geometrical interpretation of the NMBER algorithm

In order to develop an intuitive understanding of the NMBER algorithm, let us collect the readback samples r_k in a vector $\underline{r} = [r_0, ..., r_{N-1}]^T$ that we call the readback vector. We denote by $\underline{x} = [x_0, ..., x_{N-1}]^T$ the column vector of equalized samples $x_k = (w * r)_k$. For simplicity, let us focus on one admissible bit-error sequence e_k. This means that we consider for detection only the two sequences b_k and $(b+2e)_k$.

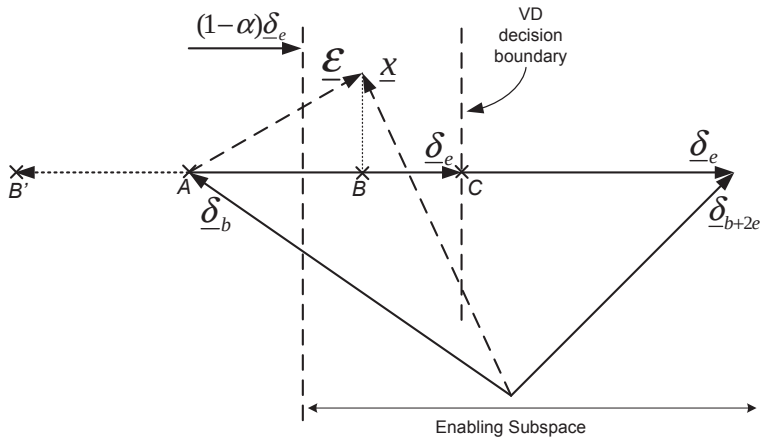

Figure 2.7: *a geometrical representation of the NMBER algorithm enabling condition.*

The VD will decide for the bit sequence b_k if and only if the vector $\underline{x}$ is closer to $\underline{\delta}_b$ than to the vector $\underline{\delta}_{b+2e}$, where $\underline{\delta}_a = [(g*a)_0, ..., (g*a)_{N_b-1}]^T$ for a bit sequence a_k (see Figure 2.7). The distance between two vectors is computed using the L2-norm given by: $\|\underline{X}\|^2 = \underline{X}^T\underline{X}$. Figure 2.7 shows also the vector $\underline{\delta}_e = \frac{1}{2}(\underline{\delta}_{b+2e} - \underline{\delta}_b)$ and the boundary decision of the VD. Let us then see what happens to the vector $\underline{x}$ after the NMBER equalizer adaptation. For this purpose let us assume that we receive a vector $\underline{r}$ and that the NMBER equalizer adaptation is enabled. The same vector $\underline{r}$ is assumed to be received again after equalizer adaptation.

First of all, one needs to note that what matters for detection is the orthogonal projection of $\underline{\varepsilon} = \underline{x} - \underline{\delta}_b$ over the vector $\underline{\delta}_e$, i.e. $\overline{AB} = \underline{\delta}_e^T\underline{\varepsilon}$.

The NMBER adaptation is enabled when $\underline{\delta}_e^T\underline{\varepsilon} > (1-\alpha)\underline{\delta}_e^T\underline{\delta}_e$. This defines an enabling subspace as shown in Figure 2.7. When the vector $\underline{x}$ falls in the enabling subspace, the adaptation is enabled and the equalizer tap values are changed according to (2.12). A correction response ∂w, given by $\partial w_p = -\eta(e)\underline{\delta}_e^T\underline{r}_{k-p}$, is then added to the equalizer response. After adaptation and reception of the same vector $\underline{r}$, the vector $\underline{x}$ will change with $\underline{\partial x}$ and more importantly its orthogonal projection on $\underline{\delta}_e$ changes as follows

$$\partial\overline{AB} = \underline{\delta}_e^T\underline{\partial x}.$$

Using the fact that $\partial x_k = \sum_p \partial w_p r_{k-p}$ and that $\partial w_p = -\eta(e)\sum_k \delta_{e,k} r_{k-p}$, one can eas-

ily prove that

$$\partial\overline{AB} = -\eta(e)\sum_p (\underline{\delta}_e^T \underline{r}_{k-p})^2 \leq 0. \tag{2.17}$$

It is then visible that NMBER adaptation tries to shift the vector $\underline{x}$ outside the enabling subspace and as far as possible from the VD decision boundary such as to increase detection reliability (reliability can be seen, here, as the distance BC in Figure 2.7, between $\underline{x}$ and the VD decision boundary). When the vector $\underline{x}$ falls outside the enabling subspace, the VD will output the bit sequence b_k with a high reliability. In this case the NMBER equalizer adaptation is disabled. However, because the LMSAM minimizes $E[\underline{\delta}_e^T \underline{\varepsilon}^2]$ (for single bit-errors), it does not make any distinction, in Figure 2.7, between the point B ($\underline{\delta}_e^T \underline{\varepsilon} > 0$) and its mirror B' with respect to A ($\underline{\delta}_e^T \underline{\varepsilon} < 0$) whereas these points correspond to completely different reliabilities.

Compared to LMSAM or LMS, the NMBER algorithm does not spend equalization effort when this does not improve detection reliability and moreover, it is clear from (2.17) that when the NMBER adaptation is enabled, it always acts towards improved reliability.

2.6 Simulation Results

By way of illustration we consider an idealized optical storage channel according to the Braat-Hopkins model [42], see Chapter 1,

$$H(\Omega) = \begin{cases} \frac{2T}{\pi}\frac{\sin(\pi\Omega)}{\pi\Omega}\left(\cos^{-1}|\frac{\Omega}{\Omega_c}| - \frac{\Omega}{\Omega_c}\sqrt{1-(\frac{\Omega}{\Omega_c})^2}\right), & |\Omega| < \Omega_c, \\ 0, & |\Omega| \geq \Omega_c. \end{cases}$$

where Ω_c denotes the normalized optical cut-off frequency. Data b_k is taken to be run-length-limited [93] with run-length parameters $(\mathrm{d},\mathrm{k}) = (1,7)$. In this section we consider only electronics noise modelled as Additive White and Gaussian (AWG) with a variance σ_n^2. Simulation results in the presence of media noise and channel nonlinearities are presented in Chapter 3 as this requires the target response to be designed appropriately. Channel SNR is defined as $\mathrm{SNR} = \frac{\sum_k h_k^2}{\sigma_n^2}$. This is the same as the SANR defined in Section 1.2.2 as we focus in this section only on additive electronics noise.

We use here the Blu-ray optical parameters, i.e. NA $=$ 0.85, a laser wavelength $\lambda =$ 405 nm and a track pitch of 320 nm [135]. We consider two different

disk capacities that are 23 GB and 30 GB on a single layer 12 cm disk. The corresponding channel bit-lengths are, respectively, $T_{\text{bit}} = 81$ nm and $T_{\text{bit}} = 62$ nm and the resulting normalized cut-off frequencies are respectively $\Omega_c = 0.34$ and $\Omega_c = 0.26$. The comparison of the NMBER with respect to the LMS algorithm is done at both capacities. To compare the NMBER and the LMSAM algorithms, the 30 GB channel is considered where a more pronounced improvement can be pointed out. To allow fair comparison between the different adaptation algorithms, all schemes are run first in the DA mode where the prior knowledge of the transmitted bit sequence is used in all adaptation loops. For LMS this is used to extract the error signal ε_k and for the NMBER and the SNMBER it is used to select the state that corresponds to the correct bits from where to extract the bit-error sequence e_k. Simulation results of NMBER performances in the DD mode are then shown at the end of this section.

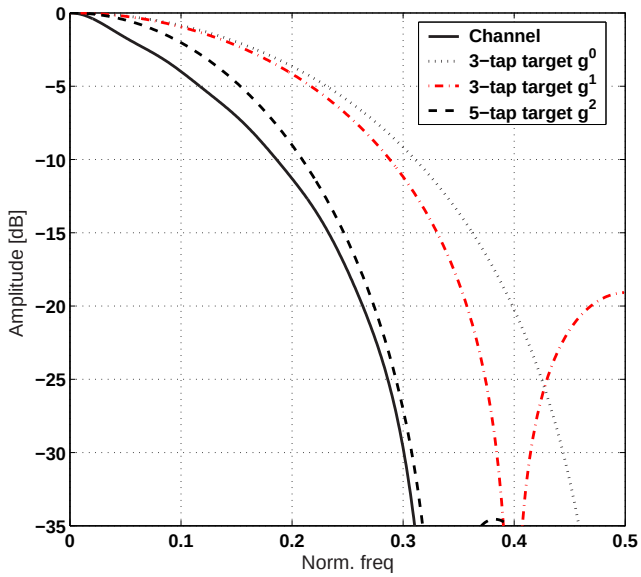

Figure 2.8: *Amplitude-frequency of idealized optical channel having a normalized cut-off* $\Omega_c = 0.34$*, 3-tap targets* $g^0 = [1,2,1]$ *and* $g^1 = [1,1.6,1]$ *and 5-tap target* $g^2 = [0.17,0.5,0.67,0.5,0.17]$*. For clarity of the plot the different targets are normalized to have the same DC.*

In order to demonstrate the benefits gained by employing the NMBER equalizer adaptation over the conventional LMS adaptation, three target responses are con-

sidered. The first one is a 3-tap target response with integer coefficients given by $g^0 = [1,2,1]$. The second one, $g^1 = [1,1.6,1]$, provides a better match to the channel response. A 4-state VD is employed for g^0 and g^1. The third target response is a 5-tap response, which corresponds, because of the d=1 constraint, to a 10-state VD, given by $g^2 = [0.17,0.5,0.67,0.5,0.17]$. The response of g^2 approximates the in-band characteristics and cut-off frequency of the channel quite well. Amplitude responses of $h(t)$, g_k^0, g_k^1 and g_k^2 are depicted in Figure 2.8.

To illustrate the concept of the NMBER adaptation, Figure 2.9 shows the SAM histograms for both LMS and NMBER adaptations using the target response g^1. The SAM histogram is the accumulation of the different probability distribution functions of $S(e)$ for the different bit-error sequences. The area below the tail of this histogram below zero determines the BER. It can be seen already that, below zero, the SAM histogram with NMBER adaptation is below the one with LMS adaptation. Moreover, because the SAM distribution on the positive axis is irrelevant for BER, our adaptation scheme uses this degree of freedom and does not spend any equalization effort there.

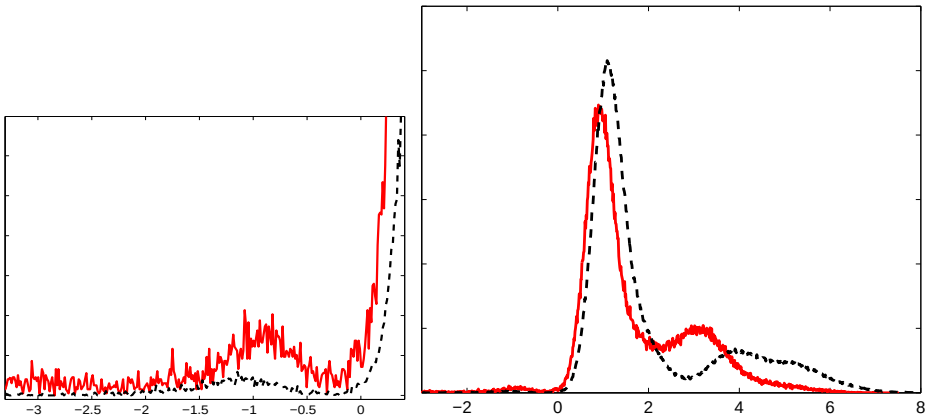

Figure 2.9: *The SAM distribution, at* SNR $= 13$ *dB, is shown in the right plot for LMS adaptation (solid) and NMBER adaptation (dashed). A zoom of the SAM histogram around zero is shown in the left plot.*

For the 23 GB channel, Figure 2.10 shows the simulated BER as function of SNR for the different targets and adaptation algorithms. The equalizer length N_w is fixed to 9 and $\alpha = 0.4$.

For the target response g^0, Figure 2.10 shows that, on the one hand, the NMBER algorithm outperforms the LMS algorithm by 1.5 dB at BER $= 10^{-5}$. On the other hand, the simplified algorithm SNMBER is indistinguishable, in terms of BER, from the NMBER algorithm. For the target response g^1, the NMBER algorithm outperforms LMS by 0.6 dB. Moreover, whereas with the latter the difference in SNR between g^0 and g^1 is $\sim$1 dB, it is reduced to less than 0.1 dB using the NMBER algorithm. The SNR difference between the two targets in the case of LMS is explained by the fact that g^1 is better matched to the channel than g^0 in the in-band frequencies, i.e. for $\Omega < \Omega_c$.

The 5-tap target response g^2 presents a good match to the channel response as shown in Figure 2.8. For this reason, the LMS adaptation is already very close to optimal in the case of additive white noise. In this case, the NMBER algorithm is practically identical to its LMS counterpart over the whole SNR range. In addition, using LMS the 3-tap target g^1 presents a loss in SNR of 1 dB compared to the 5-tap target g^2. This gap in SNR between g^1 and g^2 is reduced to only 0.4 dB using the NMBER algorithm. Such improvement in SNR for short target responses, i.e. less states in the VD trellis, makes the NMBER algorithm very attractive for practical systems.

For the 30 GB channel, Figure 2.11 shows the simulated BER as function of SNR for the different targets and adaptation algorithms. The parameter α is here fixed to $\alpha = 0.3$. Figure 2.11 shows clearly that as density increases, the short lengths target response g^0 and g^1 become completely impractical using the LMS algorithm. Nevertheless, using the NMBER algorithm allows significant performance improvements for these short target responses. This improvement amounts to 3.4 dB for g^1 and to even more for g^0. However, because of their short length, g^0 and g^1 still lag few dBs behind the 5-tap target response g^2. Furthermore, for the target g^2, the NMBER allows an improvement of 1.2 dB in SNR with respect to the LMS algorithm.

It is apparent from Figure 2.10 and Figure 2.11 that the NMBER algorithm can be very useful in practice. First, in order to limit detection complexity, which grows exponentially with the target length, short target responses are preferably employed. For these targets, LMS adaptation becomes suboptimal and the NMBER adaptation allows significant performance improvements. Second, at a given complexity, i.e. target length, the SNR improvement of the NMBER equalization with respect to LMS increases with storage density. This should help to achieve higher storage densities

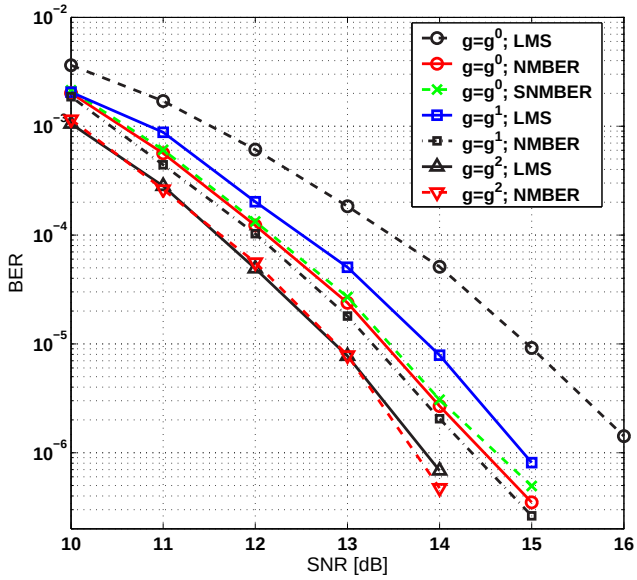

Figure 2.10: *Simulated BER versus SNR for the different target responses and adaptation schemes at a disk capacity of 23 GB.*

without sacrificing complexity.

Next, also the LMSAM is taken into account. The LMSAM scans the data for particular patterns and adapts the equalizer in order to minimize $E[X_e^2]$ for single bit-errors at data transitions. However, as storage capacity increases, other error events, e.g. the double bit-errors $e = \pm[1,0,-1]$, become substantial. The difference in pre-detection SNR between LMSAM and NMBER becomes then more pronounced. In order to illustrate the sub-optimality of the LMSAM algorithm, Figure 2.12 shows simulated BER as function of SNR for the target response g^0 at a disk capacity of 30 GB and $N_w = 9$. The LMSAM algorithm is implemented in the DA mode where the transmitted data is scanned for the patterns $(--++++)$, $(----++)$, $(+++---)$ and $(++----)$. LMSAM equalizer adaptation is implemented as explained in [117]. For NMBER and SNMBER adaptations, α is taken to be equal to 0.3. Figure 2.12 shows that the LMSAM algorithm yields a loss of 1.4 dB compared to the NMBER or the SNMBER algorithm at the capacity of 30 GB. This loss will increase at higher storage capacities.

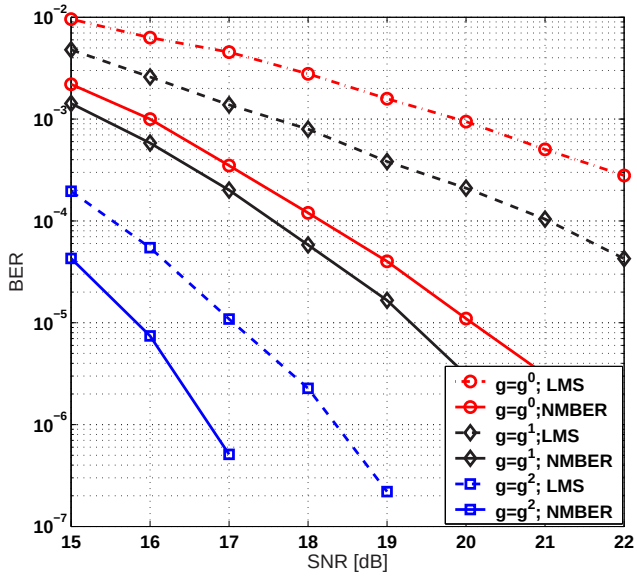

Figure 2.11: *Simulated BER versus SNR for the different target responses and adaptation schemes at a disk capacity of 30 GB.*

2.6.1 Stability and convergence behavior of the NMBER algorithm

Because of the nonlinear and selective nature of the NMBER algorithm, a theoretical analysis of its stability and convergence behavior is quite fastidious. The convergence behavior of the NMBER algorithm depends on the adaptation constant η_0 and on the threshold T_h. The higher the threshold T_h becomes, the more frequent the NMBER adaptation is enabled and the smaller η_o should be taken in order to ensure convergence of the algorithm. In order to highlight the dependence of the NMBER performance as function of η_0, Figure 2.13 and Figure 2.14 show BER as function of η_0 for the 30 GB channel at different SNR values for the target responses $g = g^0$ and $g = g^2$, respectively. The threshold, or equivalently α, is optimized to achieve the best BER for the smallest value of η_0. Figures 2.13 and 2.14 illustrate that the performance of the NMBER algorithm is basically independent of η_0 if this latter is smaller than a given value $\eta_{\max}$ ($\approx 10^{-3}$, in this case) and that if $\eta_0 > \eta_{\max}$, the NMBER algorithm can become unstable.

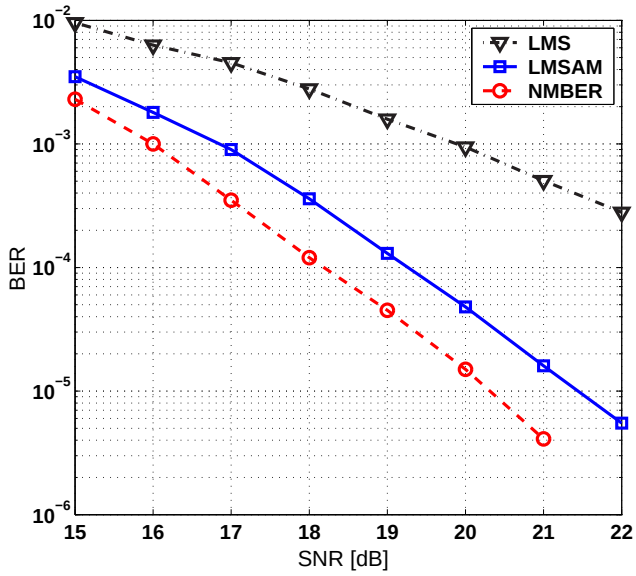

Figure 2.12: *Simulated BER versus SNR for $g = g^0$ and the different adaptation schemes at a disk capacity of 30 GB.*

2.6.2 Behavior of the NMBER algorithm in the decision-directed mode

The previous simulation results were conducted in the DA mode where the prior knowledge of the transmitted bits was used to extract the necessary control signals for the different algorithms. In many practical systems, prior knowledge about the transmitted bits is not available and (preliminary) VD decisions have to be used instead, i.e. the scheme must be run in DD mode.

In the DD mode, the choice of α is crucial. In fact, if $\alpha \approx 0$, then the NMBER algorithm will mainly adapt on wrong decisions which causes the algorithm to diverge. From this perspective, α has to be as high as possible to minimize the probability of adapting on wrong decisions. However, in order to limit BER degradations, α has to be chosen as small as possible such that the Gaussian tail approximation holds. Therefore, α must realize a trade-off between these two criteria.

To implement the NMBER algorithm in the DD mode, a bit-error sequence and a Boolean variable need to be stored at every state of the trellis up to the decision backtracking depth L. The Boolean variable tells whether the difference in path metrics between the selected and discarded paths by the ACS unit is smaller or bigger than

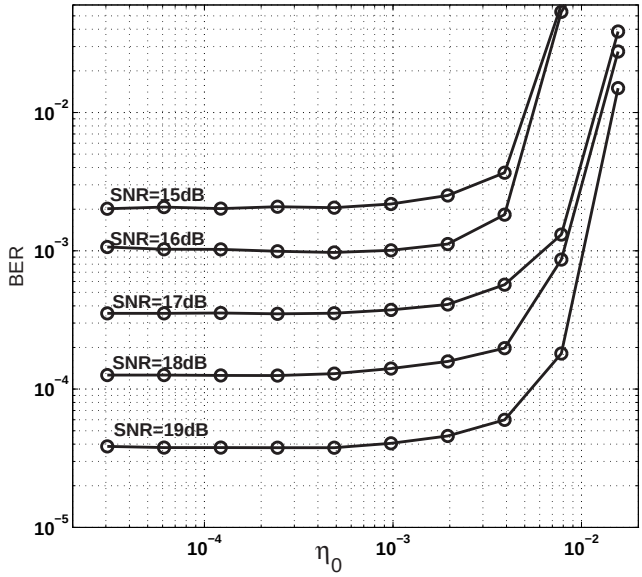

Figure 2.13: *Simulated BER versus η_0 at a capacity of 30 GB and different SNR values for the target response $g = g^0$.*

the threshold T_h. At every clock cycle, a bit decision is taken from the VD trellis, at a decoding state, following a selected path at a depth L. The decoding state is also used to extract a bit-error sequence and one Boolean variable. The equalizer adaptation is then performed according to Figure 2.4 where the equalizer input r_{k-p} is delayed to compensate for the backtracking delay prior to correlation with δ_e.

Figure 2.15 and Figure 2.16 show the simulated BER for the target responses $g = g^0$ and $g = g^2$ and, respectively, the 23 and 30 GB channel using the NMBER adaptation in both DA and DD modes. This shows that the performance of the NMBER adaptation in the DD mode is within a fraction of a dB from its DA counterpart, which proves the practical value of the NMBER algorithm. The SNMBER algorithm has a similar behavior. The performance degradation of the DD mode, compared to the DA mode, increases with storage density as illustrated in Figure 2.15 and Figure 2.16. This is not surprising as system sensitivity increases with density [86], i.e. performance becomes more sensitive to small system parameter deviations.

Remark :

In a practical optical storage system, choosing the threshold to be very small, can

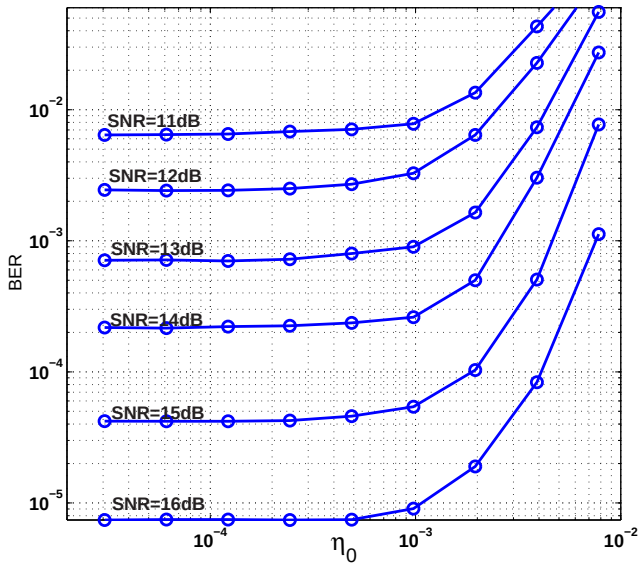

Figure 2.14: *Simulated BER versus η_0 at a capacity of 30 GB and different SNR values for the target response $g = g^2$.*

cause serious problems to the NMBER algorithm. In fact, small values of the difference in VD path metrics can be caused for example by media defects, scratches or finger prints. Adapting the equalizer when these artifacts occur, will cause the NMBER algorithm to diverge. A simple remedy to this issue is to add a second smaller threshold $T_{h2} < T_h$ and freeze the NMBER adaptation when the VD path metrics difference is smaller than T_{h2}. This threshold should serve also to freeze all adaptation loops, e.g. DC, AGC, PLL, to prevent them from divergence.

2.7 Conclusions

A new equalizer adaptation scheme has been proposed for PRML systems. This new scheme seeks to minimize directly the bit-error rate. Based on an analysis of Viterbi detection performance, we highlighted a practical cost function for equalizer adaptation. This function was used to realize a remarkably simple equalizer adaptation scheme. The proposed scheme incorporates a selection mechanism that enables equalizer adaptation only if the difference in path metrics, between selected and discarded paths from the Viterbi trellis, is smaller than a prescribed threshold. The actual

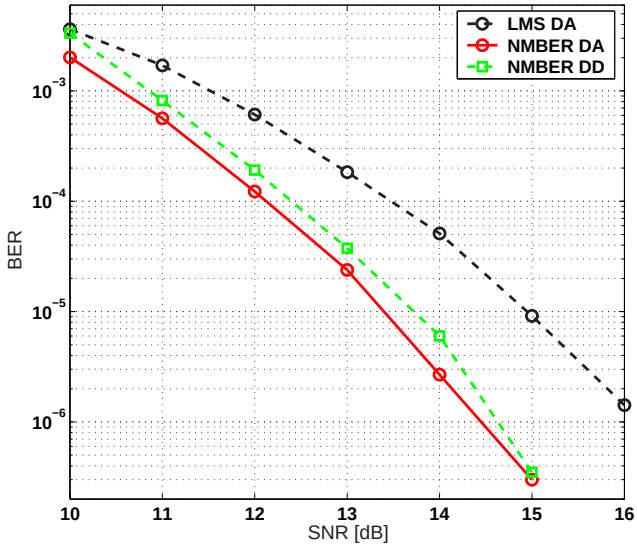

Figure 2.15: *Simulated BER versus SNR using the NMBER algorithm in both DA and DD modes for $g = g^0$ and the 23 GB channel ($\alpha = 0.4$). As a basis of reference, also the LMS performance in DA mode is shown.*

version of the new adaptation scheme is essentially as simple as LMS. A simplified scheme that allows a further improved efficiency was also presented. Because of the selection mechanism, the proposed schemes present an advantage in terms of power consumption especially for long equalizers.

Simulation results for an idealized optical storage system showed that our scheme outperforms significantly the existing adaptation schemes especially at high storage densities or short target response lengths.

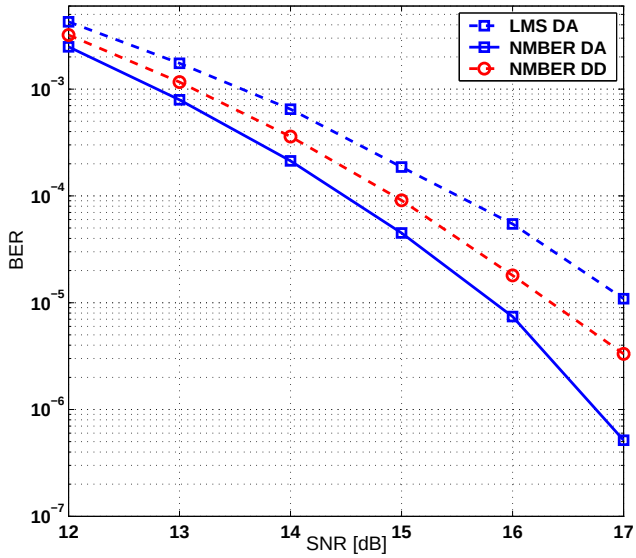

Figure 2.16: *Simulated BER versus SNR using the NMBER algorithm in both DA and DD modes for $g = g^2$ and the 30 GB channel ($\alpha = 0.3$). As a basis of reference, also the LMS performance in DA mode is shown.*

Appendix A: Impact of residual ISI on the sequenced amplitude margin

In order to develop a better understanding of the impact of residual linear ISI on the SAM, let us consider the case where the channel noise n_k is data-independent, additive and Gaussian. In this case, the error signal ε_k is composed of two components. The first component is time-invariant and linearly dependent on the bit sequence b_k, i.e. RISI, and the second one is a data-independent zero-mean and Gaussian noise. For simplicity of the analysis, we assume that the binary data is uncoded. The error signal is given by

$$\varepsilon_k = (q * b)_k + v_k, \tag{2.18}$$

where $v_k = (w * n)_k$ denotes the noise component. The RISI component is characterized by the impulse response q_k, where $q_k = (w * h)_k - g_k$.

In order to evaluate $\Pr(\underline{\delta}_e^T \underline{\delta}_e < X_e)$, let us consider a bit-error sequence e_k and compute $E[X_e]$ and $E[X_e^2]$, where the expectations are taken over all possible realiza-

tions of u_k and b_k such that $b+2e$ is an admissible bit sequence. Plugging (2.18) in $X_e = \underline{\delta}_e^T \underline{\varepsilon}$ and substituting $\delta_{e,k}$ by $(g*e)_k$, we can write

$$X_e = \sum_k (g*e)_k (q*b)_k + \sum_k (g*e)_k v_k. \tag{2.19}$$

Since v_k is independent of e_k and is zero on average, we have $E[\sum_k (g*e)_k v_k] = 0$. The average of X_e is then equal to

$$E[X_e] = E[\sum_k (g*e)_k (q*b)_k] = \sum_{k,i,j} g_{k-i} q_{k-j} E[e_i b_j].$$

In order to evaluate $E[e_i b_j]$ we introduce the set $I(e)$ of indices i such that $e_i \neq 0$, i.e. $(i \in I(e) \Leftrightarrow e_i \neq 0)$. The summation over j in the previous equality is split into two terms depending on $j \in I(e)$ or not:

$$E[X_e] = \sum_{k,i,j \in I(e)} g_{k-i} q_{k-j} E[e_i b_j] + \sum_{k,i,j \notin I(e)} g_{k-i} q_{k-j} E[e_i b_j].$$

When $j \in I(e)$, b_j becomes deterministic. In fact, because $b+2e$ is an admissible bit sequence, the only possibility for b_j, when $e_j \neq 0$, is $b_j = -e_j$. In this case $E[e_i b_j] = -e_i e_j$. However, when $j \notin I(e)$, it is easy to prove that $E[e_i b_j] = 0$ because the data is assumed to be uncoded. It follows that

$$E[X_e] = -\sum_{k,i,j \in I(e)} g_{k-i} q_{k-j} e_i e_j.$$

Because $e_j = 0$ for $j \notin I(e)$, the previous summation can be taken over all values of j. It is then straightforward to show that

$$E[X_e] = -\sum_k (g*e)_k (q*e)_k = -\underline{\delta}_e^T \underline{q}_e \tag{2.20}$$

where the vector $\underline{q}_e$ is given by $(\underline{q}_e)_k = (q*e)_k = (w*h*e)_k - (g*e)_k$.

In a similar manner as we derived (2.20), one can prove that $E[X_e^2]$ can be written as follows:

$$E[X_e^2] = (\underline{\delta}_e^T \underline{q}_e)^2 + \underline{\delta}_e^T (M^e + R_{vv}) \underline{\delta}_e, \tag{2.21}$$

where R_{vv} is the autocorrelation matrix of v_k and the matrix M^e is defined by:

$$M^e_{k,k'} = \sum_{j \notin I(e)} q_{k-j} q_{k'-j} = (q*q^*)_{k-k'} - \sum_{j \in I(e)} q_{k-j} q_{k'-j},$$

where q^* is defined by $q_i^* = q_{-i}$.

Equations (2.20) and (2.21) give a closed form expression of $E[X_e]$ and $E[X_e^2]$. In order to link these quantities to ACS error probabilities, let us assume that the distribution of X_e can be approximated by a Gaussian. This assumption is not valid in general because of the data-dependent component of the error signal ε_k. However, in the limiting case of a small amount of residual ISI, this approximation is acceptable. Note that the approximation is only used at this part of this section to provide more insights and that the other results of this chapter are more general. With this assumption, one can write

$$\Pr(\text{ACS error}|e) \simeq \mathrm{Q}\left(\frac{\underline{\delta}_e^T \underline{\delta}_e + \underline{\delta}_e^T \underline{q}_e}{\sqrt{\underline{\delta}_e^T (M^e + R_{vv}) \underline{\delta}_e}}\right), \tag{2.22}$$

where $\Pr(\text{ACS error}|e)$ equals the average of $\Pr(\text{ACS error}|b,e)$ over all possible bit sequences b_k such that $b+2e$ is an admissible bit sequence.

The impact on $\Pr(\text{ACS error}|e)$ of the RISI differs significantly from the impact of the channel noise. The RISI has basically two different impacts. First, compared to the case of $q=0$, it induces a modification in the nominator of the Q-function argument in (2.22). We name this nominator the effective Euclidian weight of the bit-error sequence e_k. The effective Euclidian weight can be either bigger or smaller than $\underline{\delta}_e^T \underline{\delta}_e$ (constructive or destructive ISI for the bit-error sequence e_k) depending on the sign of $\underline{\delta}_e^T \underline{q}_e = -E[X_e]$. Second, the denominator of the argument of the Q-function in (2.22) is also modified. One can check that the matrix M^e is positive and therefore the denominator increases when $q \neq 0$ compared to $q=0$. The impact of M^e in (2.22) can be seen as an increase in effective channel noise power.

An expression of the effective predetection SNR ρ_{VD} can be extracted from (2.22):

$$\sqrt{\rho_{\mathrm{VD}}} = \min_e \frac{\underline{\delta}_e^T \underline{\delta}_e + \underline{\delta}_e^T \underline{q}_e}{\sqrt{\underline{\delta}_e^T (M^e + R_{vv}) \underline{\delta}_e}} \tag{2.23}$$

Note that if there is no residual ISI, i.e. $q=0$, and v_k is white with a variance σ^2, ρ_{VD} boils down to the known expression $\rho_{\mathrm{VD}} = \min_e \frac{\underline{\delta}_e^T \underline{\delta}_e}{\sigma^2}$.

Application to equalizer adaptation: Designing the equalizer response to minimize $E[X_e^2]$ (2.21) does not necessarily minimize $\Pr(\text{ACS error}|e)$ because of two reasons. First, the impact of $\underline{\delta}_e^T \underline{q}_e$ on $\Pr(\text{ACS error}|e)$ is different than that of $\underline{\delta}_e^T (M^e +$

$R_{vv})\underline{\delta}_e$ as explained earlier. Thus minimizing (2.21) would not, in general, be optimal because this does not provide the optimal trade-off between $\underline{\delta}_e^T \underline{q}_e$ and $\underline{\delta}_e^T (M^e + R_{vv})\underline{\delta}_e$. Second, and more important, minimizing $E[X_e^2]$ does not provide any constraint on the sign of $E[X_e]$, i.e. the opposite sign of $\underline{\delta}_e^T \underline{q}_e$, whereas it has been shown that this sign is of capital importance for $\Pr(\text{ACS error}|e)$. We conclude that minimizing $E[X_e^2]$, as suggested in [117], is not optimal in general. Simulation results of Figure 2.12 confirm this conclusion.

Chapter 3

Minimum Bit-Error Rate Target Response Adaptation

In order to reduce the implementation complexity of maximum likelihood sequence detectors, equalized maximum likelihood receivers are often used. This consists of employing an equalizer to transform the channel response to a short target response to which the Viterbi detector is matched. Existing equalizer and target adaptation schemes are often based on the minimum mean-square error (MMSE) criterion which is not always optimal in terms of detection bit-error rate at the Viterbi detector output. In this chapter we consider minimum bit-error rate joint adaptation of equalizer and target response and present a practical adaptation algorithm that achieves near minimum bit-error rate performance. This chapter can be seen as a generalization of the results of Chapter 2 to include target response adaptation. The proposed algorithm extracts control information from within the Viterbi detector and focuses adaptation on those bit sequences, bit-error events and noise realizations that lead to non-reliable decisions in the Viterbi detector. Simulation results for an optical storage channel, show that, compared to the MMSE-based adaptation methods, the new scheme allows significant performance improvements especially for short target or equalizer lengths or in the presence of channel nonlinearities and media noise. This is very promising for high-density storage systems in terms of system complexity reduction or in terms of fighting nonlinearities and media noise. Moreover, the proposed algorithm is no more complex than the existing MMSE-based algorithms.

3.1 Introduction

The optimal receiver for estimating a data sequence in the presence of intersymbol interference (ISI) and additive Gaussian noise [41] can generally not be realized because of its excessive complexity. This fact has led to a development of a variety of suboptimal and lower complexity receivers. In many practical systems, e.g. storage systems, a combination of partial response equalization with Viterbi detection is used to achieve a simplification of the optimal Maximum-Likelihood Sequence Detection (MLSD) [25, 27, 29, 143]. This consists of using a linear equalizer to shape the channel to a short target response, which allows for a practical use of the Viterbi algorithm (VA), whose computational complexity increases exponentially with the target response length.

In receivers for digital storage systems, equalizer and eventually target response adaptation is usually employed because it presents particular advantages. First, considering that the channel response may be time varying and is not known until after the entire storage device is manufactured, adaptive equalization and target response design provide a better fitting and tracking of the channel response. Second, because the noise in high density storage systems depends on the medium and the data throughput, e.g. this relates to the disc mastering quality and disc rotation speed for optical storage systems, and thus an equalizer and target response that adaptively take the noise characteristics into consideration is very desirable.

Because the target response plays a key role in system performance determination, several papers attempted to solve the target response design and adaptation problem. In [143], the target response was chosen as a truncated version of the channel response and the equalizer was chosen to minimize the Mean Square Error (MSE). The MSE-minimization problem was extended to the target response design and adaptation in [29] and [27]. Because joint equalizer and target adaptation inevitably inherits an issue of interaction between the two adaptation loops, several solutions were reported in literature. In [29], a fixed energy constraint for the target response was used while [27] used the monic constraint, i.e. the first nonzero term in the target response is fixed to one. The latter corresponds to a minimum-phase target response that is optimum for decision feedback equalization [106]. The minimum MSE (MMSE) target response design and adaptation problem was also discussed in [71] for a fixed energy constraint and in [72] for a monic constraint.

All existing target adaptation techniques are based on the MMSE criterion with different constraints. Among the different constraints, the monic constraint was shown to lead to very close to optimal performance, in the bit-error rate sense, for a linear channel [78]. This is especially true if the target and the equalizer are long enough to handle noise coloration. However, for short target or equalizer lengths, as constrained by complexity limitations for example, residual ISI and remaining noise coloration may hamper system performance severely.

Moreover, an important problem at high storage densities, either for optical or magnetic storage systems, is the occurrence of nonlinear intersymbol interference [22, 120]. Applying noise whitening, via monic target adaptation, for such channels will cause the nonlinear ISI after equalization to be spread over many symbols. This causes a memory increase of the nonlinear ISI and leads overall performance degradation. Furthermore, noise tends to become strongly data-dependent at high storage densities. This makes specific bit patterns especially vulnerable to noise. These artifacts are neglected by the MMSE-based adaptation techniques because they do not discriminate vulnerable bit patterns and bit-error events but consider an average MSE over the different bit patterns.

In this chapter we present a new equalizer and target adaptation algorithm that seeks to minimize bit-error rate (BER). The proposed algorithm incorporates a selection mechanism that focuses adaptation on those particular bit patterns and bit-error events that are relevant in terms of predetection SNR or BER. Compared to existing schemes, the new adaptation scheme shows an important performance improvement for short target response and equalizer lengths and in the presence of channel nonlinearities and media noise. Moreover, from an implementation standpoint, the new technique is not more complex than existing techniques.

The remainder of this chapter is organized as follows. Section 3.2 describes the system model. Section 3.3 presents the adaptation criterion that will be used in Section 3.4 to derive the new adaptation algorithm. Simulation results, presented in Section 3.6, show the merits of our algorithm compared to existing ones.

3.2 System Model and Problem Definition

A discrete-time model of an Equalized Maximum Likelihood (EML) system is shown in Figure 3.1. An NRZ sequence $b_k \in \{\pm 1\}$ is transmitted, at a rate $1/T$, over

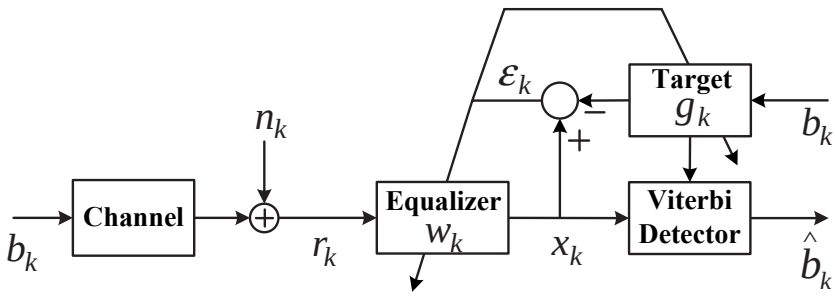

Figure 3.1: *A discrete-time model of an adaptive equalized maximum likelihood system.*

a dispersive channel (linear or nonlinear) whose output at time kT is denoted by $h(b)_k = h(\ldots, b_{k-1}, b_k, b_{k+1}, \ldots)$. In the case of a linear channel, the channel output boils down to $h(b)_k = (h * b)_k$ where h_k is the channel impulse response. The channel output is corrupted by additive noise n_k which can be either white, colored or data-dependent as caused by media noise, see Section 1.2.2 for explanation. The readback signal r_k is the noisy channel output and is given by

$$r_k = h(b)_k + n_k.$$

Because the channel may be time-varying and its memory span is in general quite long, adaptive Partial Response (PR) equalization [86] is used in order to shorten the channel memory. Equalization can be either linear or nonlinear as it is the case for Volterra filter-based equalization [26, 102]. For simplicity, we focus in the sequel on linear equalization. The results of this chapter can be easily generalized to the case of Volterra filter-based equalization.

The equalizer impulse response w_k is optimized so that the overall impulse response, at its output, is as close as possible to a short linear impulse response that we refer to as the target response g_k. The equalizer output x_k serves as input to a Viterbi detector (VD) that produces bit decisions $\hat{b}_k$. In the case of a nonlinear channel, the VD employs pattern-dependent offsets in order to account for nonlinear ISI [116]. These offsets are combined with the linear target values in order to produce the branch metrics in the VD. The number of required offsets equals the number of branches in the VD trellis; one offset is used for each branch. Training and adaptation of the pattern-dependent offsets is also explained in [116].

Contrary to Partial Response Maximum Likelihood (PRML) systems [20] where

the target response is considered to be fixed, EML systems optimize both the equalizer and the target response simultaneously in order to achieve better performance. In [78], adaptive techniques are employed to simultaneously find the target g_k and the equalizer response w_k by minimizing the Mean-Squared Error (MSE) $E[\varepsilon_k^2]$ between the equalizer output x_k and the desired signal $(g*b)_k$, where $\varepsilon_k = x_k - (g*b)_k$ denotes the error signal. In this case, a constraint must be applied to solve the interaction between the equalizer and target adaptation and prevent the system from reaching the trivial solution $g_k = w_k = 0$. The monic constraint on the target response, i.e. $g_0 = 1$, was used in [78]. Applying the monic constraint to the target response and minimizing the MSE was shown to result in an equalizer that is equivalent to the forward equalizer of the MMSE solution of Decision Feedback Equalization (DFE) [106]. This provides similar noise-whitening ability especially if the target and the equalizer are long enough to handle noise coloration and residual ISI. However, for a short target or small equalizer lengths, minimizing the MSE with the monic constraint does not guarantee the best tradeoff between noise coloration and residual ISI. This is illustrated in Section 3.6.

Furthermore, although the MMSE target adaptation with monic constraint showed very close to optimal performance, in the BER sense, for a linear channel and additive noise [78], its robustness in the presence of channel nonlinearities was not considered earlier. In fact, applying noise whitening in the presence of nonlinearities causes the nonlinear ISI after equalization to be spread over many symbols, potentially causing its memory to increase beyond the span of the target response. This, obviously, causes performance degradation as will be seen in Section 3.6. The choice of the (linear) target response is thus still a key issue for high density storage systems with nonlinear ISI.

This chapter presents a joint equalizer and target adaptation scheme that seeks to minimize BER. The adaptation criterion and the corresponding near-minimum bit-error rate (NMBER) equalizer adaptation for a fixed target were presented in Chapter 2. Because the equalizer adaptation used in this chapter is similar to that in Chapter 2, we focus in the sequel primarily on target adaptation. Moreover, we initially omit the pattern-dependent offsets in the VD. These are considered in Section 3.6 to account for channel nonlinearities.

Before proceeding with target adaptation, let us briefly recapitulate, in the next section, the NMBER adaptation criterion. For mathematical convenience we omit

the delays of the different modules and the latency of the bit detector. We use the following notations: $\underline{\delta}_z = [(g*z)_{N_b-1},\ldots,(g*z)_0]^T$ for any sequence z_k and $\underline{\varepsilon} = [\varepsilon_{N_b-1},\ldots,\varepsilon_0]^T$ where N_b denotes the length of transmitted sequence.

3.3 The Minimum-BER Adaptation Criterion

The VD in Figure 3.1 operates on a trellis that is matched to the linear target response g_k. Every path in this trellis corresponds to an admissible bit sequence. The detector selects the sequence that leads to the smallest path metric in the trellis [41]. The performance of the VD depends on the nature of the error signal ε_k, i.e. its coloration and the amount of residual ISI. The probability of detection error is mainly determined by the bit sequences for which the difference between the best and second best paths in the VD trellis is small. Moreover, for a given bit sequence b_k and an admissible bit-error event e_k, i.e. an event for which $b_k + 2e_k$ is an admissible bit sequence, the difference in path metrics between the paths corresponding to b_k and $b_k + 2e_k$ depends on the Euclidian weight of e_k and on the orthogonal projection of the error signal over $\underline{\delta}_e$. In Chapter 2, an analysis of the performance of the VD was presented and a criterion, which was shown to be directly linked to the probability of detection error, was highlighted. For a given bit sequence b_k and an admissible bit-error event e_k this criterion was written as minimizing the following variable

$$\Delta_e = \frac{E[X_e']}{T_e}, \tag{3.1}$$

where

$$X_e' = X_e \mathbf{1}_{\{X_e \geq T_e\}} = \begin{cases} X_e = \underline{\delta}_e^T \underline{\varepsilon} & \text{if } \underline{\delta}_e^T \underline{\varepsilon} > T_e, \\ 0 & \text{otherwise,} \end{cases} \tag{3.2}$$

and

$$T_e = (1-\alpha)\underline{\delta}_e^T \underline{\delta}_e + \alpha\mu_e, \tag{3.3}$$

where $\mu_e = E[\underline{\delta}_e^T \underline{\varepsilon}]$ and α is a fixed value in the interval $[0,1]$.

The cost function Δ_e involves the variable $X_e = \underline{\delta}_e^T \underline{\varepsilon} = \sum_k (g*e)_k \varepsilon_k$, which reflects the fact that, when considering the bit-error event e_k, only the projection of $\underline{\varepsilon}$ over $\underline{\delta}_e$ matters for detection. In other words, the difference in path metrics between the sequences b_k and $b_k + 2e_k$ depends on the error signal only via X_e. The denominator of Δ_e relates to the Euclidian weight of the bit-error event e_k, i.e. $\underline{\delta}_e^T \underline{\delta}_e$, (3.3). It can be

seen already that optimization of the target response based on Δ_e will tend to decrease error signal coloration in the direction of $\underline{\delta}_e$ (noise whitening if one considers all directions $\underline{\delta}_e$) and increase the Euclidian weight of the bit-error event e_k.

The thresholding in (3.2) expresses the focusing of adaptation on bit sequences, bit-error events and noise realizations that correspond to the less reliable decisions in the VD. In terms of path metrics in the VD trellis, the enabling condition $\{X_e > T_e\}$ can be expressed as $\{\mathcal{M}(b+2e) - \mathcal{M}(b) < 4(\underline{\delta}_e^T \underline{\delta}_e - T_e)\}$, where $\mathcal{M}(b) = \sum_k (x_k - (g * b)_k)^2$ denotes the path metric of the sequence b_k. Therefore, the thresholding in (3.2) selects automatically the set of worst bit sequences and bit-error events which are determinant for BER. For example, if we consider mis-equalization ISI then the thresholding is equivalent to focusing the adaptation effort only on bit sequences and bit-error events for which ISI is destructive, i.e. leads to degradation of predetection SNR.

Example 3.1 :
For the sake of illustration, let us consider a linear channel, neglect residual ISI at the detector input and treat the error signal ε_k as a zero-mean Gaussian noise signal and denote its autocorrelation matrix by R_ε. For a given bit-error event e_k, the variable $\underline{\delta}_e^T \underline{\varepsilon}$ is then Gaussian with a mean $\mu_e = 0$ and a variance $\sigma_e^2 = \underline{\delta}_e^T R_\varepsilon \underline{\delta}_e$. The threshold T_e in (3.3) is then given by $T_e = (1-\alpha)\underline{\delta}_e^T \underline{\delta}_e$ and one can easily show, in this case, that (3.1) boils down to

$$\Delta_e = \frac{1}{\sqrt{2\pi}\frac{T_e}{\sigma_e}} \exp\left\{ -\frac{1}{2}\left(\frac{T_e}{\sigma_e}\right)^2 \right\}.$$

Because the function $x \longmapsto \frac{1}{x}\exp\left\{-\frac{1}{2}x^2\right\}$ for $x > 0$ is a strictly decreasing function, one concludes that minimizing Δ_e is equivalent to maximizing the ratio $\frac{T_e}{\sigma_e} = (1-\alpha)\frac{\underline{\delta}_e^T \underline{\delta}_e}{\sqrt{\underline{\delta}_e^T R_\varepsilon \underline{\delta}_e}}$ which is proportional to the root square of the effective SNR [41, 63, 77]. This example illustrates clearly that designing a target response that minimizes Δ_e is equivalent to maximizing the effective SNR, i.e. minimizing BER.$\diamondsuit$

The dependence of the threshold T_e on μ_e in (3.3) implies that in practice the variables μ_e for the different bit-error sequences must be estimated. However, because at reasonable SNRs, $\mu_e = E[\underline{\delta}_e^T \underline{\varepsilon}] \ll \underline{\delta}_e^T \underline{\delta}_e$, one can simply neglect the dependency of T_e on μ_e. In the sequel, we fix a value of α and consider the threshold T_e to be

equal to $(1-\alpha)\underline{\delta}_e^T\underline{\delta}_e$. The cost function Δ_e can then be rewritten, after omission of the constant factor $(1-\alpha)$ in the denominator which is independent of g_k, as

$$\Delta_e = \frac{E[X_e']}{\underline{\delta}_e^T\underline{\delta}_e}. \tag{3.4}$$

and the enabling condition can be simplified as $\{\mathcal{M}(b+2e)-\mathcal{M}(b) < 4\alpha\underline{\delta}_e^T\underline{\delta}_e\}$.

In order to minimize the overall BER, it was shown in Chapter 2 that the different cost functions Δ_e should be combined with different weights for different bit-error events. The weight for a bit-error event e_k was shown to be proportional to its Hamming weight $H_w(e)$, i.e. the number of non-zeros in e_k.

Extraction of the relevant bit-error sequences:

Because the cost function (3.4) involves knowledge of admissible bit-error events, one needs to extract from the received signal information about the most likely bit-error events. Instead of considering all minimum distance bit-error events, ending at a particular time, one can consider at most one bit-error event at each time. This is achieved by considering, at time kT, only the bit-error event that corresponds to the second best path in the Viterbi trellis that merges with the best path at time kT. This reduces significantly the computational complexity without sacrificing performance.

The dominant bit-error event is extracted as follows. At every Add Compare Select (ACS) operation in the VD, a bit-error event is derived as the bitwise difference between the two sequences corresponding to the selected and discarded paths. For every state the corresponding bit-error event is stored in memory. At the decoding state, i.e. the state used to output the detected data, the corresponding bit-error event is extracted and is input to the equalizer and target adaptation loops.

We should point out that knowledge about the dominant bit-error events is not only needed for adaptation but can also be used to improve system performance at a moderate cost via employing a reduced complexity post-processor, e.g. [98].

3.4 Target Response Adaptation

The basic idea of the Near Minimum-BER (NMBER) adaptation is to minimize the cost function Δ_e for all relevant bit-error sequences. The different functions Δ_e for the different bit-error sequences are combined with different weights so as to achieve

the best overall BER. For clarity, let us first focus on a given bit-error sequence e_k and develop an adaptive target response scheme that minimizes (3.4). The different functions Δ_e for different bit-error events are subsequently weighted such that the overall BER is optimized.

For a given bit-error sequence e_k, a target adaptation scheme that minimizes (3.4) can be based on the steepest descent algorithm. This consists of following at each iteration the opposite direction of the gradient of Δ_e with respect to the target coefficients. The adaptation of the pth target tap can be written as follows:

$$g_p^{(k+1)} = g_p^{(k)} - \eta'(e) \left. \frac{\partial \Delta_e}{\partial g_p} \right|_{\underline{g}=\underline{g}^{(k)}}, \tag{3.5}$$

where $g_p^{(k)}$ is the pth target tap at time kT. The coefficient $\eta'(e)$ denotes the target adaptation constant and is ideally proportional to the Hamming weight of the bit-error event e_k, i.e. $\eta'(e) = \eta_0 H_w(e)$ where η_0 is a positive constant value, see Chapter 2.

It should be noted that using the steepest decent algorithm can cause the target adaptation scheme of (3.5) to converge to a local minimum, especially if the initial target response is far off. This is inherent in the BER minimization problem because one can check that BER as a function of the target response is non-convex and can have several local minima. One possible way to find a global minimum is via the use of simulated annealing techniques [104] or genetic algorithms [48]. However, the complexity of these algorithms restricts their use for a real time adaptation of the target response. In this chapter we simply stick to the steepest decent algorithm for its simplicity and assume that the initial target response $g^{(0)}$ is well chosen, e.g. by setting $g^{(0)}$ to be equal to the MMSE solution [78].

Upon replacing the expectation of X_e' in (3.4) by its instantaneous realization and taking its gradient with respect to the pth target tap, an expression of the adaptation rule (3.5) can be derived. This can be written as

$$g_p^{(k+1)} = g_p^{(k)} - \eta(e)\Gamma_p^{(k)} \mathbf{1}_{\left\{\frac{\underline{\delta}_e^{\mathrm{T}}\underline{\varepsilon}}{\underline{\delta}_e^{\mathrm{T}}\underline{\delta}_e} > (1-\alpha)\right\}} \tag{3.6}$$

$$\Gamma_p^{(k)} = \left\{ \underline{e}_{k-p}^{\mathrm{T}}\underline{\varepsilon} - \underline{\delta}_e^{\mathrm{T}}\underline{b}_{k-p} - 2\frac{\underline{\delta}_e^{\mathrm{T}}\underline{\varepsilon}}{\underline{\delta}_e^{\mathrm{T}}\underline{\delta}_e}\underline{\delta}_e^{\mathrm{T}}\underline{e}_{k-p} \right\}, \tag{3.7}$$

where $\eta(e) = \eta_0 \frac{H_w(e)}{\underline{\delta}_e^{\mathrm{T}}\underline{\delta}_e}$, $\underline{b}_{k-p} = [b_{k-p}, b_{k-p-1}, \ldots]$, $\underline{e}_{k-p} = [e_{k-p}, e_{k-p-1}, \ldots]$ and $\underline{\varepsilon} = [\varepsilon_k, \varepsilon_{k-1}, \ldots]$.

The term $\frac{\underline{\delta}_e^{\mathrm{T}}\underline{\varepsilon}}{\underline{\delta}_e^{\mathrm{T}}\underline{\delta}_e}$ in the right hand expression of (3.7) can be interpreted as a weighing factor in the maximization of the Euclidian distance $\underline{\delta}_e^{\mathrm{T}}\underline{\delta}_e$ with respect to the minimization of $\underline{\delta}_e^{\mathrm{T}}\underline{\varepsilon}$. In order to simplify (3.7), this term can be simply fixed to a value β that meets the enabling condition, i.e. $\beta > 1-\alpha$. This is taken to be equal to 1 in the sequel. From our simulations, no noticeable degradation was observed with this approximation. Moreover, depending on the dominant bit-error events, the ratio $\frac{H_w(e)}{\underline{\delta}_e^{\mathrm{T}}\underline{\delta}_e}$ in the expression of the adaptation constant $\eta(e)$ can be assumed to be approximately independent of e_k. This would further simplify (3.6).

Using the above mentioned approximations and expressing the enabling condition in terms of the VD path metrics, (3.6) and (3.7) can be rewritten as

$$\begin{aligned} g_p^{(k+1)} &= g_p^{(k)} - \eta(e)\Gamma_p^{(k)}\mathbf{1}_{\{\mathcal{M}(b+2e)-\mathcal{M}(b)<4\alpha\underline{\delta}_e^{\mathrm{T}}\underline{\delta}_e\}} \\ \Gamma_p^{(k)} &= \underline{e}_{k-p}^{\mathrm{T}}\underline{\varepsilon} - \underline{\delta}_e^{\mathrm{T}}\left(\underline{b}_{k-p} + 2\underline{e}_{k-p}\right). \end{aligned} \tag{3.8}$$

The overall target adaptation can be explained as follows. At every clock cycle, an ACS operation is employed at every state. At the decoding state, two quantities are derived. First, the difference in path metrics between the selected and the discarded paths is taken. Second, a bit-error sequence e_k is derived as the bitwise difference between the two sequences corresponding to the discarded and the selected paths. This derivation of the bit-error sequence reflects the Decision Directed (DD) mode where the transmitted data is not known to the receiver. In the Data Aided (DA) mode where the transmitted data is available to the receiver as a known preamble, the derivation of the bit-error event is simpler because the state that corresponds to the transmitted data is known at every clock cycle. In this case, the bit-error sequence corresponds to the discarded path by the ACS operation if the ACS decision is correct and to the selected path otherwise.

The bit-error sequence e_k is used to compute the vector $\underline{\delta}_e = [(g*e)_k, \ldots (g*e)_{k-L}]^T$, where the integer value L depends on the maximum length of relevant bit-error sequences. In the sequel, we simply fix L to the backtracking depth of the VD. The target adaptation is enabled only when the difference in path metrics is smaller than $4\alpha\underline{\delta}_e^T\underline{\delta}_e$. When the adaptation is enabled, the expression $\Gamma_p^{(k)}$ in (3.8) is evaluated, scaled with $-\eta(e)$ and then passed to an ideal discrete-time integrator that produces the updated p^{th} target tap value. One should note that evaluation of $\Gamma_p^{(k)}$ does not require real multiplications.

Remark :

Storage systems usually employ parity-check (PC) and error correction codes (ECC) in order to tackle the remaining bit-errors at the VD output. The performance of these codes depends on the dominant bit-error events after the VD. Therefore, to optimize sector error rate (SER) after PC and ECC decoding, the adaptation constants $\eta(e)$ *can be better chosen such that the target and equalizer adaptation focuses primarily on the error events that are not covered or 'less covered' by the PC and ECC. In other words, the scheme presented in this chapter can be generalized to achieve SER minimization through optimization of the adaptation constants* $\eta(e)$.

Example 3.2 :

In order to illustrate the way NMBER target adaptation works, let us consider a simple case where only two bits b_0 *and* b_1 *are transmitted over a linear channel* $h(D) = 1 + h_1 D$ *with additive Gaussian noise, assume that the equalizer is fixed to* $w(D) = 1$ *and consider only target responses of the form* $g(D) = 1 + \gamma D$ *where* D *denotes the unit delay operator. Let us also focus only on the single bit-error event on the bit* b_1*, i.e.* $e_0 = 0$ *and* $e_1 = -b_1$*. Because the equalizer is fixed, designing a target response in this case is equivalent to defining a constellation of four points corresponding to the four possible bit sequences* $(b_0, b_1) \in \{(+1,+1),(+1,-1),(-1,+1),(-1,-1)\}$.

The NMBER adaptation of γ *is given by (3.8). It can be shown easily that the NMBER enabling condition is written as* $b_1 x_1 < \alpha + \gamma b_0 b_1$ *and that* $\Gamma_1 = b_0 b_1$*. For example if* $b_0 = b_1 = 1$*, the enabling condition becomes* $x_1 < \alpha + \gamma$ *which means that the NMBER algorithm focuses adaptation on realizations of* x_1 *that are close to the decision boundary given by* $b_1 x_1 = \gamma b_0 b_1$*. An example of how the constellation changes in such case is shown in Figure 3.2. The constellation points change so that the detector input vector* $\underline{x}$ *is farther from the new decision boundary.*

When the adaptation is enabled, then $\gamma^{(k+1)} = \gamma^{(k)} - \eta(e) b_0 b_1$*. Therefore, when enabled, the NMBER algorithm increases* γ *if* $b_0 b_1 = -1$ *and decreases it with the same absolute value if* $b_0 b_1 = 1$*. For simplicity, let us consider only the two upper points of the constellation corresponding to* $b_0 = 1$ *and* $b_1 = \pm 1$*. One can check that the convergence is reached when*

$$\Pr(x_1 < \gamma + \alpha | b_1 = 1) = \Pr(x_1 > \gamma - \alpha | b_1 = -1). \tag{3.9}$$

Because $b_0 = 1$*, we have* $x_1 = b_1 + h_1 + n_1$ *where* n_1 *denotes the noise component*

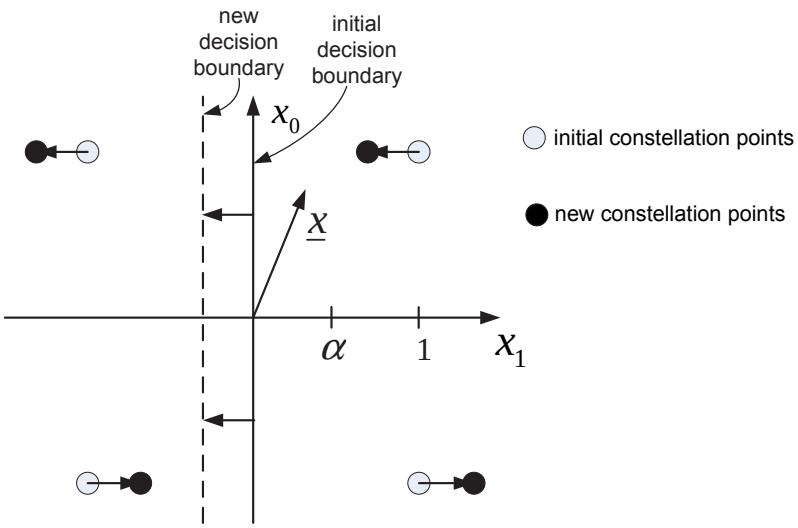

Figure 3.2: *An example of adaptation of γ for a transmitted sequence $b_0 = b_1 = 1$ and a detector input vector $\underline{x}$. The gray constellation points correspond to $\gamma^{(0)} = 0$ and the black ones correspond to $\gamma^{(1)} = -\eta(e)$.*

of x_1. The MMSE solution for γ is given by $\gamma_{\text{mmse}} = h_1$. The NMBER solution of γ is given by (3.9) which can be written as $\Pr(n_1 < \gamma + \alpha - 1 - h_1) = \Pr(n_1 > \gamma - \alpha + 1 - h_1)$. One can easily show that this is equivalent to $\gamma + \alpha - 1 - h_1 = -(\gamma - \alpha + 1 - h_1)$ which leads to $\gamma_{\text{nmber}} = h_1$. Therefore, in this case the MMSE and NMBER solutions are identical, i.e. $\gamma_{\text{nmber}} = \gamma_{\text{mmse}}$.$\diamondsuit$

Example 3.3 :

Let us consider in this example the same scenario of Example 3.2 at the exception of the channel. The channel output x_1 for $b_1 = 1$ is assumed to take in the absence of noise two possible values: $x_1 = 1 - \upsilon$ or $x_1 = 1 + \upsilon$ with equal probabilities. The channel output in the absence of noise for $b_1 = -1$ is $x_1 = -1$. This can be a result of nonlinear ISI for example or can be seen as a simple model of media noise in optical storage channels, where the ones on the disc are either a bit oversized or undersized. In this case, it is easy to prove that the MMSE target response is given by $\gamma_{\text{mmse}} = 0$.

The derivations provided in Example 3.2 of the steady state NMBER equation apply also to this case. The NMBER solution γ_{nmber} can be derived from (3.9) and

can be written as the solution of

$$\Pr(n_1 > \gamma - \alpha + 1) = \frac{1}{2}\left[\Pr(n_1 < \gamma + \alpha - \upsilon - 1) + \Pr(n_1 < \gamma + \alpha + \upsilon - 1)\right]$$

It can be shown after some algebraic manipulations that $\gamma_{\text{nmber}} \simeq \frac{-\upsilon}{2} \neq \gamma_{\text{mmse}}$. *For a given* γ, *the BER is given by*

$$\text{BER}(\gamma) = \frac{1}{2}\text{Q}\left(\frac{1+\gamma}{\sigma_n}\right) + \frac{1}{4}\text{Q}\left(\frac{1-\gamma-\upsilon}{\sigma_n}\right) + \frac{1}{4}\text{Q}\left(\frac{1-\gamma+\upsilon}{\sigma_n}\right),$$

where σ_n *denotes the variance of* n_1. *Figure 3.3 shows the BER of the NMBER and MMSE targets as a function of* υ *for different* $\text{SNR} = 1/\sigma_n^2$ *values. It is apparent that the NMBER target has a superior BER performance than the MMSE one. Moreover, the gain in BER increases with* υ *and decreases with SNR.*$\diamondsuit$

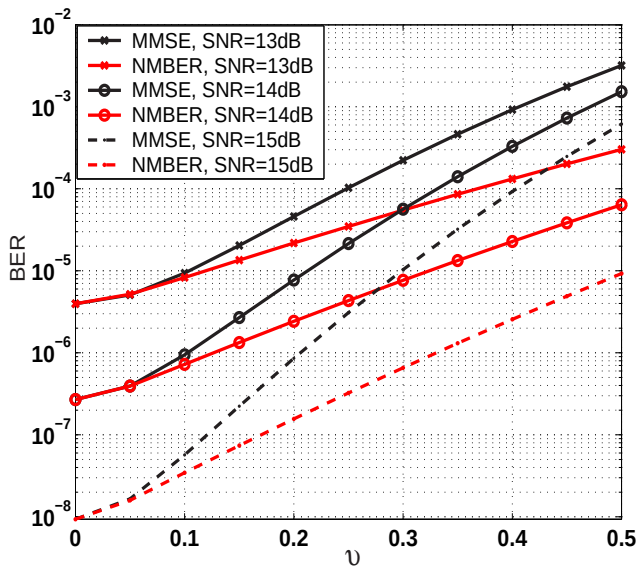

Figure 3.3: *BER versus* υ *for different* SNR *values.*

3.4.1 interaction between the equalizer and target adaptation

The BER of the EML system of Figure 3.1 does not change if the equalizer and target responses are scaled with the same factor. This interaction can cause the equalizer

and target energy to drift to big values or decrease to very small values which leads to saturation or quantization problems in fixed-point implementations. A simple way to solve this interaction problem is to fix the energy of the target response. The target adaptation rule (3.8) is then modified so that after every adaptation the target is scaled to have a unit energy.

Another interaction problem arises from the fact that, for a linear channel and long equalizer, BER is independent of the phase response of the target response. Contrary to the minimum phase target response that arises from MMSE adaptation with a monic constraint, the simplest practical choice of the target response phase for storage channels is linear phase. In fact, a linear phase target presents the following advantages:

- Because both magnetic and optical storage channels have nominally a linear phase, a linear phase target implies that no phase equalization is required, i.e. the nominal equalizer needs only to handle amplitude channel distortions. This relaxes the requirement on the equalizer complexity.

- It avoids automatically the interaction problem that arises between the target adaptation and the timing recovery loop.

- It allows simplifications of the VD without loss in BER because the total number of branch metrics that need to be computed at every clock cycle is roughly halved. Complexity reduction can also be obtained by folding the VD trellis [69].

- Only half of the total number of target taps needs to be adapted. This halves the target adaptation complexity and improves its tracking capabilities compared to a situation where all the target taps need to be adapted. In fact, for a symmetric target response of length N_g, the adaptation rule (3.8) can be written as

$$\begin{aligned}
&\forall p,\ 0 \leq p \leq \tfrac{N_g-1}{2}, \quad p' = N_g - 1 - p \\
&{\Gamma'}_p^{(k)} = (\underline{e}_{k-p} + \underline{e}_{k-p'})^{\mathrm{T}} \underline{\varepsilon} - \underline{\delta}_e^{\mathrm{T}} \left(\underline{b}_{k-p} + \underline{b}_{k-p'} + 2(\underline{e}_{k-p} + \underline{e}_{k-p'}) \right) \\
&g_p^{(k+1)} = g_p^{(k)} - \eta(e) {\Gamma'}_p^{(k)} \mathbf{1}_{\{\mathcal{M}(b+2e) - \mathcal{M}(b) < 4\alpha \underline{\delta}_e^{\mathrm{T}} \underline{\delta}_e\}} \\
&g_{p'}^{(k+1)} = g_p^{(k+1)}.
\end{aligned}$$

A similar adaptation rule can be derived for antisymmetric target responses. This boils down to replacing in the above equations, $\underline{e}_{k-p} + \underline{e}_{k-p'}$ and $\underline{b}_{k-p} +$

$\underline{b}_{k-p'}$ by $\underline{e}_{k-p} - \underline{e}_{k-p'}$ and $\underline{b}_{k-p} - \underline{b}_{k-p'}$ respectively and changing the last equation to $g_{p'}^{(k+1)} = -g_p^{(k+1)}$.

We make a distinction between optical and magnetic storage channels. For optical channels and perpendicular magnetic storage channels, the target is constrained to be symmetric and its energy is fixed to 1. For longitudinal magnetic storage channels, the target is constrained to be antisymmetric with a unit energy.

3.5 Stability Analysis of the NMBER target adaptation

In order to derive stability conditions of the NMBER adaptation, let us for the sake of simplicity assume that the equalizer is fixed and focus only on the NMBER target adaptation. Let us also consider only one bit sequence b_k and a given admissible bit-error sequence e_k. Let us consider first the case where channel noise is absent. A discussion on the impact of noise is provided afterwards.

The NMBER target adaptation was given in (3.8). One can rewrite this adaptation rule using the vector $\underline{g} = [g_0, \ldots, g_{N_g-1}]^{\mathrm{T}}$, where N_g denotes the target length, as

$$\underline{g}^{(k+1)} = \underline{g}^{(k)} - \eta(e)(\mathbf{M}_{b,e}\underline{g}^{(k)} + \underline{c}_{b,e})\mathbf{1}_{\{\frac{1}{2}\underline{g}^{(k)\mathrm{T}}\mathbf{M}_{b,e}\underline{g}^{(k)} + \underline{c}_{b,e}^{\mathrm{T}}\underline{g}^{(k)} > 0\}}, \tag{3.10}$$

where $(\underline{c}_{b,e})_p = \underline{e}_{k-p}^{\mathrm{T}}\underline{x}$, $\underline{x} = [x_k, x_{k-1}, \ldots]^{\mathrm{T}}$, and the symmetric matrix $\mathbf{M}_{b,e}$ is given by

$$(\mathbf{M}_{b,e})_{p,q} = -\underline{e}_{k-p}^{\mathrm{T}}\underline{b}_{k-q} - \underline{e}_{k-q}^{\mathrm{T}}\underline{b}_{k-p} - 2\underline{e}_{k-p}^{\mathrm{T}}\underline{e}_{k-q}. \tag{3.11}$$

As mentioned earlier, the NMBER algorithm can converge to a local minimum because of the non-convex nature of the cost function that it minimizes, i.e. the non-convex nature of BER as a function of the target coefficients. The possible existence of local minima can also be seen by the fact that the matrix $\mathbf{M}_{b,e}$ is not necessarily positive definite for all bit sequences b_k. In fact, if we consider single bit-error events, it can be easily shown that $E[\mathbf{M}_{b,e}] = \mathbf{0}$, where the expectation is taken over all possible bit sequences. This means that there exist at least one bit sequence b_k such that the matrix $\mathbf{M}_{b,e}$ is not positive.

We will qualify then the NMBER algorithm of being stable if and only if $\underline{g}^{(k)}$ converges to a finite target $\underline{g}^{(\infty)}$ regardless of the initialization point $\underline{g}^{(0)}$.

Before deriving the condition for stability of (3.10), let us first rewrite (3.10) in a simpler form. Let us introduce the vector $\underline{\hat{c}}_{b,e}$ such that $\mathbf{M}_{b,e}\underline{\hat{c}}_{b,e} = \underline{c}_{b,e}$. Using the

vector $\underline{\hat{c}}_{b,e}$, one can prove that (3.10) can be rewritten as:

$$\underline{\hat{g}}^{(k+1)} = \underline{\hat{g}}^{(k)} - \eta(e)\mathbf{M}_{b,e}\underline{\hat{g}}^{(k)}\mathbf{1}_{\{\underline{\hat{g}}^{(k)\mathrm{T}}\mathbf{M}_{b,e}\underline{\hat{g}}^{(k)} > \underline{\hat{c}}_{b,e}^{\mathrm{T}}\mathbf{M}_{b,e}\underline{\hat{c}}_{b,e}\}}, \tag{3.12}$$

where $\underline{\hat{g}}^{(k)} = \underline{g}^{(k)} + \underline{\hat{c}}_{b,e}$. In order to derive stability conditions of (3.10) or equivalently (3.12), let us start by considering an eigenvalue λ of $\mathbf{M}_{b,e}$ and initialize $\underline{\hat{g}}$ to a corresponding eigenvector $\underline{v}_\lambda$, i.e. $\underline{\hat{g}}^{(0)} = \underline{v}_\lambda$. Generalization to any initial vector $\underline{g}^{(0)}$ is discussed afterwards. With this initialization, the adaptation rule (3.12) becomes

$$\underline{\hat{g}}^{(k+1)} = \underline{\hat{g}}^{(k)} - \lambda\eta(e)\underline{\hat{g}}^{(k)}\mathbf{1}_{\{\lambda\underline{\hat{g}}^{(k)\mathrm{T}}\underline{\hat{g}}^{(k)} > \underline{\hat{c}}_{b,e}^{\mathrm{T}}\mathbf{M}_{b,e}\underline{\hat{c}}_{b,e}\}}.$$

If $\lambda > 0$ and initially the enabling condition is met, then one can show that the only case the algorithm diverges is when $|1-\lambda\eta(e)| \leq 1$. In fact, when $|1-\lambda\eta(e)| \leq 1$ then it is easy to show that the enabling condition is always met because $\forall k$ $\underline{\hat{g}}^{(k)\mathrm{T}}\underline{\hat{g}}^{(k)} \geq \underline{\hat{g}}^{(0)\mathrm{T}}\underline{\hat{g}}^{(0)}$. In such case, the adaptation rule becomes: $\underline{\hat{g}}^{(k+1)} = (1-\lambda\eta(e))\underline{\hat{g}}^{(k)}$ which does not converge when $|1-\lambda\eta(e)| \leq 1$.

If $\lambda < 0$ then it can be shown that the algorithm will always converge. In fact, instability can only occur if the enabling condition is always met. The algorithm freezes as soon as the enabling condition is not met. If one supposes that the enabling condition is always met, then $\underline{\hat{g}}^{(k+1)} = (1-\lambda\eta(e))\underline{\hat{g}}^{(k)}$ will diverge because $\lambda < 0$. We would have then $\lim_{k\to\infty}\underline{\hat{g}}^{(k)\mathrm{T}}\underline{\hat{g}}^{(k)} = +\infty$ which is contradictory to the fact that the enabling condition met, i.e. $\lambda\underline{\hat{g}}^{(k)\mathrm{T}}\underline{\hat{g}}^{(k)} > \underline{\hat{c}}_{b,e}^{\mathrm{T}}\mathbf{M}_{b,e}\underline{\hat{c}}_{b,e}$, because $\lambda < 0$. Therefore, the enabling condition is not always met and the algorithm does not diverge in this case.

In the case $\lambda = 0$ it is trivial that there is no divergence problem. Therefore the stability condition can be written

$$\forall\lambda > 0 \text{ eigenvalue of } \mathbf{M}_{b,e},\ |1-\lambda\eta(e)| < 1. \tag{3.13}$$

Now, considering any initialization vector $\underline{\hat{g}}^{(0)}$, it can be easily shown by decomposing $\underline{\hat{g}}^{(0)}$ on the basis of eigenvectors of $\mathbf{M}_{b,e}$ that (4.21) is a sufficient condition for stability. The demonstration follows the same reasoning as that presented above.

Impact of noise:

In the noiseless case, the NMBER algorithm freezes as soon as the enabling condition is met. In the presence of noise, the enabling condition in (3.10) becomes

dependent on noise realizations. This can be equivalently seen as changing the adaptation loop gain which becomes proportional to the enabling rate of the NMBER algorithm $\mathrm{EnR} = E\left[\mathbf{1}_{\{\Delta\mathcal{M}_{b,e} \leq 4\alpha\underline{\delta}_e^{\mathrm{T}}\underline{\delta}_e\}}\right] = \Pr(\underline{\delta}_e^{\mathrm{T}}\underline{\varepsilon} \geq (1-\alpha)\underline{\delta}_e^{\mathrm{T}}\underline{\delta}_e)$. The impact of noise on stability can be derived from the noiseless case by replacing $\eta(e)$ with $\eta(e)\mathrm{EnR}$. The stability condition of (4.21) is then written as

$$\forall\lambda > 0 \text{ eigenvalue of } \mathbf{M}_{b,e},\ |1-\lambda\eta(e)\mathrm{EnR}| < 1. \tag{3.14}$$

Because $\mathrm{EnR} \leq 1$ then the stability condition in the noiseless case (4.21) becomes a sufficient condition for stability in the noisy case.

3.6 Simulation Results

By way of illustration we consider an idealized optical storage channel according to the Braat-Hopkins model [42], see Chapter 1,

$$H(\Omega) = \begin{cases} \frac{2T}{\pi}\frac{\sin(\pi\Omega)}{\pi\Omega}\left(\cos^{-1}|\frac{\Omega}{\Omega_c}| - \frac{\Omega}{\Omega_c}\sqrt{1-(\frac{\Omega}{\Omega_c})^2}\right), & |\Omega| < \Omega_c, \\ 0, & |\Omega| \geq \Omega_c. \end{cases}$$

where Ω_c denotes the normalized optical cut-off frequency. We consider a capacity of 30 GB on a single layer 12 cm disc. The corresponding channel bit-length is $T_{\mathrm{bit}} = 62$ nm and the resulting normalized cut-off frequency, given by $\Omega_c = \frac{2\mathrm{NA}}{\lambda}T_{\mathrm{bit}}$, equals $\Omega_c = 0.26$.

The channel output is corrupted by two different noise components. The first one is data-dependent noise media noise u_k and the second one is additive white Gaussian electronics noise z_k with zero mean and variance σ_z^2. We recall the two SNR measures defined in Chapter 1: a signal to media noise ratio (SMNR) and a signal to additive noise ratio (SANR) given by

$$\mathrm{SMNR} = \frac{2}{\sigma_u^2}[\mathrm{dB}] \quad \text{and} \quad \mathrm{SANR} = \frac{\sum_k h_k^2}{\sigma_z^2}[\mathrm{dB}].$$

3.6.1 Impact of channel nonlinearities

At high storage densities, the optical channel exhibits bilinear ISI as shown in [22]. In order to mimic the bilinear ISI in the channel we introduce bilinear ISI components

caused by the central bit b_k and its two neighboring bits b_{k+1} and b_{k-1}, i.e. the replay signal is written as

$$r_k = (h * b)_k + \gamma(b_k b_{k-1} + b_k b_{k+1} + b_{k-1} b_{k+1}) + m_k + z_k,$$

where γ denotes the bilinear ISI parameter. Throughout the simulations, the data b_k is taken to be run-length-limited with run-length parameters $(\mathrm{d}, \mathrm{k}) = (1, 7)$.

In this subsection, the length of the target response is fixed to 5-taps which corresponds to a 10-state VD and the equalizer length is fixed to 11. Throughout the simulation results the value of the parameter α for the NMBER adaptation is fixed to $\alpha = 0.25$.

In order to assess the performance of the NMBER target adaptation, we consider, for comparison, the MMSE target adaptation with the monic and energy constraints. All adaptation algorithms are run in the data-aided mode where the data b_k is used in the different adaptation loops.

By way of comparison, let us first consider the case where only the additive electronic noise is present, i.e. no media noise. Figure 3.4 and Figure 3.5 show simulated BER as function of SANR for $\gamma = 0$ and $\gamma = 0.1$, respectively. In the absence of nonlinearities, the different target adaptation schemes yield a similar performance because noise is white. However, they behave differently in the presence of channel nonlinearities. For clarity, we distinguish here between the first case where the branch metrics in the VD are based only on the linear target and the second case where also the pattern-dependent offsets (PD-offsets) are employed as in [116].

- In the first case, it is apparent from Figure 3.5 that MMSE adaptation with the monic constraint behaves slightly better than that with the energy constraint. The NMBER adaptation allows, however, an important gain in SANR of 1.8 dB with respect to MMSE adaptation with the monic constraint.

- When the PD-offsets are employed in the VD, the performance of MMSE adaptation with the energy constraint outperforms that with the monic constraint. NMBER adaptation still outperforms MMSE adaptation with both constraints. The gain in SANR of the NMBER adaptation with respect to the MMSE adaptation with energy constraint is about 0.7 dB. In order to understand the behavior of the monic constraint and the relatively poor performance in the presence

of nonlinearities, Figure 3.6 shows the bilinear RISI components at the detector input. The first bilinear RISI component results from the ISI terms of the form $b_k b_{k-1}$ and the second bilinear RISI results from the ISI terms of the form $b_k b_{k-2}$. Figure 3.6 shows clearly that, because of the phase equalization involved, the monic constraint causes a spreading of the nonlinear ISI. This spreading causes the nonlinear ISI component to span bits that are outside the linear target response span (VD span). However, the energy constraint and the NMBER adaptation keep most nonlinear components within the VD span which allows a performance improvement using the PD-offsets in the VD.

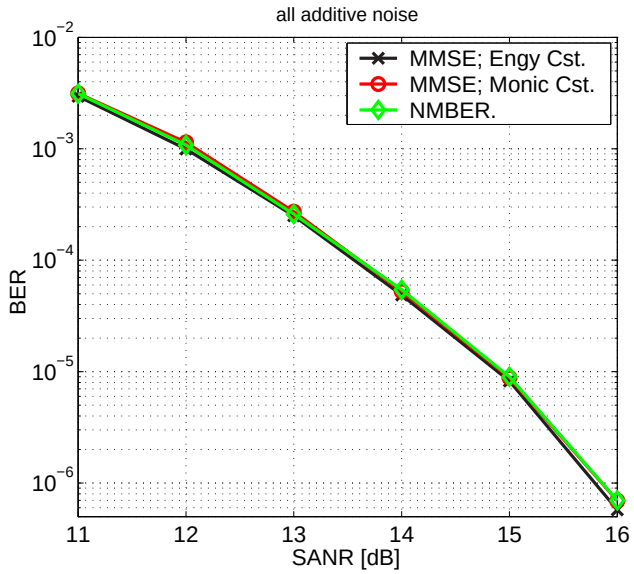

Figure 3.4: *Simulated BER vs SANR in the absence of media noise for* $\gamma = 0$.

In the case where only the media noise is present, i.e. no electronic noise, Figure 3.7 and Figure 3.8 show BER as function of SMNR. In the absence of nonlinearities (Figure 3.7), MMSE adaptation with the monic constraint allows similar performance as the NMBER adaptation because of its known noise whitening abilities. The energy constraint has, however, a penalty of 0.9 dB in SMNR compared to the monic constraint. In the presence of nonlinearities, $\gamma = 0.1$ in Figure 3.8, the monic constraint suffers from spreading the nonlinearities similarly to Figure 3.5 and Figure 3.6. The NMBER adaptation in this case allows a gain of around 1.3 dB in SMNR with respect

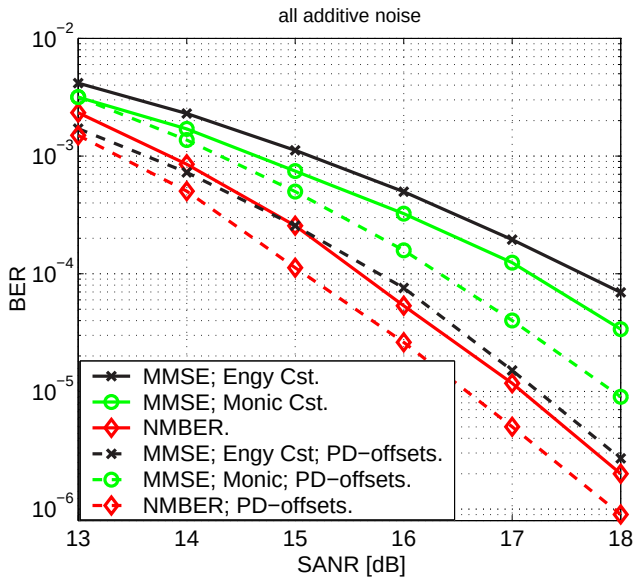

Figure 3.5: *Simulated BER vs SANR in the absence of media noise for* $\gamma = 0.1$.

to MMSE adaptation with the monic constraint. As far as the gap in SMNR between the monic and energy constraint is concerned, this depends on the amount of media noise with respect to channel nonlinearities. As shown in Figure 3.8, the monic constraint allows a better performance in the presence of media noise and the energy constraint is superior in the presence of nonlinearities as shown in Figure 3.5. As the amount of channel nonlinearity increases, the gap between the monic and energy constraints becomes bigger. Figure 3.9 shows BER as function of SMNR for $\gamma = 0.15$. Because of the spreading of nonlinearities, the monic constraint performs very poorly in this case and is outperformed by the energy constraint. The NMBER adaptation in this case allows an important improvement of around 2.8 dB with respect to the energy constraint.

3.6.2 NMBER adaptation performance as function of the equalizer and target lengths

In Section 3.6.1 the length of the target response was fixed to 5 and that of the equalizer to 11. We observed that in the absence of nonlinear ISI, the MMSE target adap-

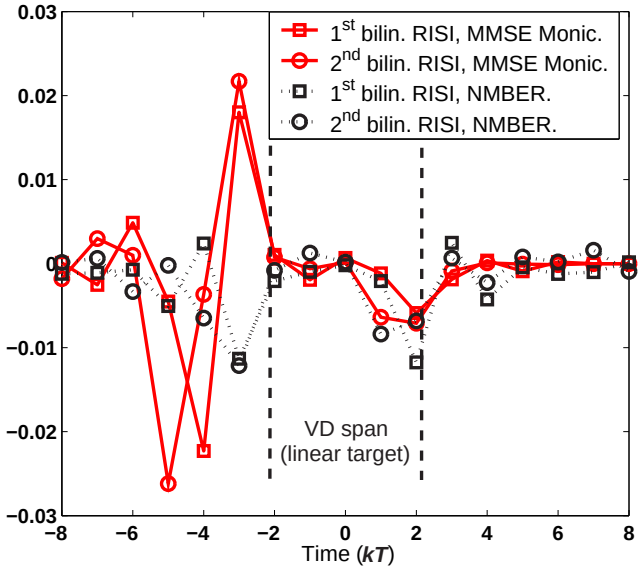

Figure 3.6: *Bi-linear RISI at the detector input for the MMSE adaptation with the monic constraint and NMBER adaptation for* $\gamma = 0.1$.

tation with the monic constraint provided a similar performance than the NMBER target adaptation. As the equalizer and target lengths decrease the two schemes behave differently. Figure 3.10 shows BER as a function of the equalizer length in the absence of nonlinearities. In the presence of media noise the monic target requires the use of relatively longer equalizers than the NMBER target because of the noise whitening. Contrary to the monic target adaptation, the NMBER adaptation is quite robust to equalizer length reduction. This implies an important reduction in equalizer implementation complexity. Similar observations hold in the presence of additive noise although the reduction of equalizer length is smaller than in the presence of media noise. This is mainly because only little equalization is required with a 5-tap target and additive white noise.

As the length of the target decreases, the amount of residual ISI at the detector input becomes more pronounced. Figure 3.11 shows BER versus SMNR for a 2 and 3 tap target in the absence of channel nonlinearities. The performance of a 3-tap target in this case is very close to that of a 5-tap target. This is not surprising as the noise spectrum in the media noise environment follows the signal spectrum very closely and there is no noise enhancement penalty of one target relative to the other.

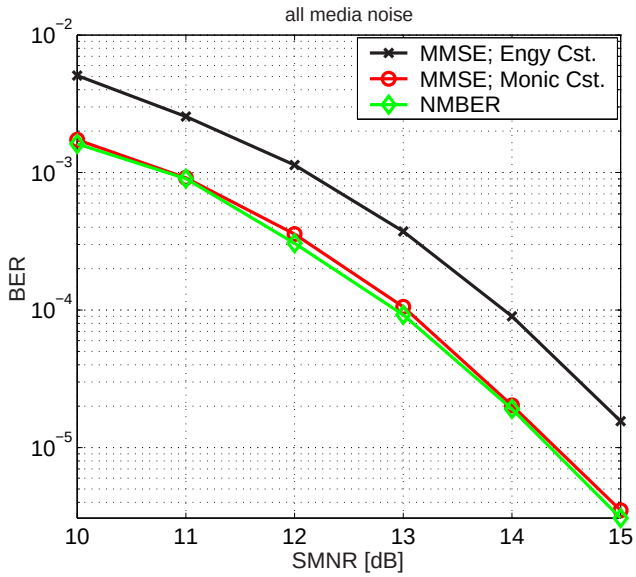

Figure 3.7: *Simulated BER vs SMNR at the absence of electronic noise for* $\gamma = 0$.

Figure 3.11 shows that the NMBER adaptation outperforms the monic constraint for a 2-tap target. Figure 3.10 shows also the robustness of the NMBER against target length reduction.

3.6.3 Convergence Behavior of NMBER adaptation scheme

Because of the highly nonlinear nature of the NMBER adaptation, a full theoretical analysis of the convergence behavior of the equalizer and target adaptation is not straightforward. A typical convergence behavior of the NMBER target adaptation algorithm is captured in Figure 3.12 at SANR=14 dB and in the absence of media noise and channel nonlinearities. The upper plot in Figure 3.12 shows the convergence of the first tap of the target g_0 for different values of the adaptation constant η_0. The lower plot shows the adaptation enabling rate EnR for $\eta_0 = 4 \times 10^{-4}$ where it is apparent that at the start of adaptation, EnR is high and that the closer the target gets to its steady state solution, the smaller EnR becomes. Because the adaptation loop gain is proportional to EnR, the NMBER adaptation presents the advantage that its adaptation gain is high at the start of adaptation, or if the channel changes, which

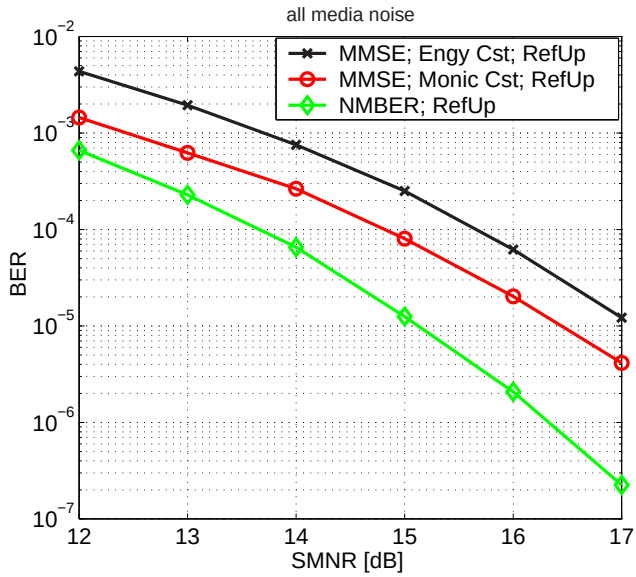

Figure 3.8: *Simulated BER vs SMNR at the absence of electronic noise for* $\gamma = 0.1$.

allows a fast adaptation and becomes smaller as the target gets close to its steady state which in turn allows a fine tracking of small channel variations. The MMSE-based adaptation algorithms do not share this property as their loop gain is fixed over time.

Another appealing property of the $\mathrm{EnR} = \Pr(\underline{\delta}_e^{\mathrm{T}}\underline{\varepsilon} \geq (1-\alpha)\underline{\delta}_e^{\mathrm{T}}\underline{\delta}_e)$ is its direct relation to BER. In fact, using the Gaussian approximation of the error signal at the steady state target, one can write

$$\mathrm{EnR} = \mathrm{Q}\left((1-\alpha)\frac{\underline{\delta}_e^T\underline{\delta}_e}{\sqrt{\underline{\delta}_e^T R_\varepsilon \underline{\delta}_e}}\right) \tag{3.15}$$

where R_ε denotes the autocorrelation matrix of the error signal. The argument of the Q-function in (3.15) is proportional to that in the expression of bit-error rate given by $\mathrm{BER} \propto \mathrm{Q}\left(\frac{\underline{\delta}_e^T\underline{\delta}_e}{\sqrt{\underline{\delta}_e^T R_\varepsilon \underline{\delta}_e}}\right)$. Therefore, measuring EnR, which comes for free with the NMBER algorithm, provides a direct and quick indication of BER. Whereas measuring BER is usually time consuming, measuring EnR can be fast and is very straightforward. Observing EnR is thus a simple mean for system performance evaluation. This is similar to the sequence amplitude margin method presented in [118]

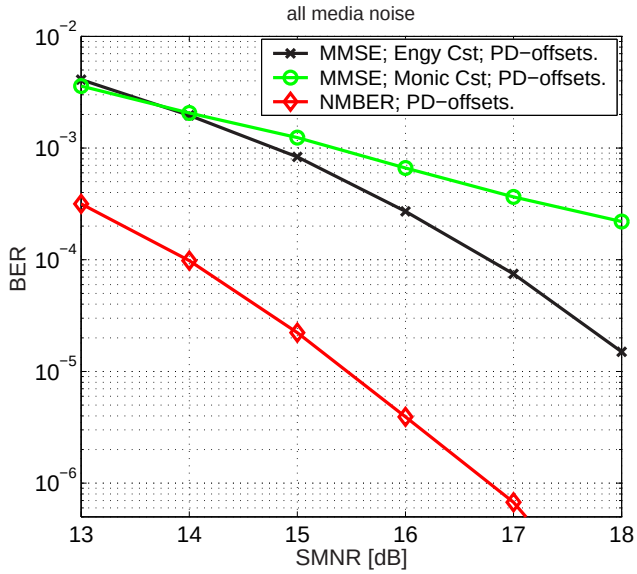

Figure 3.9: *Simulated BER vs SMNR at the absence of electronic noise for the 30GB Blu-ray channel and* $\gamma = 0.15$.

but however comes for free with the NMBER target adaptation.

Remark :
The simulation results presented in this chapter relate to optical storage channels, however the result of this chapter carry over directly to longitudinal and perpendicular magnetic storage channels. The generalization to perpendicular magnetic storage channels is more straightforward because of their similarities to optical storage channels.

3.6.4 Discussion on gradient noise

Because the NMBER algorithm attempts to minimize BER, it will also minimize the EnR because this latter is a monotonous function of BER (3.15). Therefore, because the gradient of EnR is zero at steady state, a first order approximation of the target adaptation rule (3.10) near steady state can be written as

$$\underline{g}^{(k+1)} = \underline{g}^{(k)} - \eta(e)(\mathbf{M}_{b,e}\underline{g}^{(k)} + \underline{c}_{b,e})\mathrm{EnR}(g^{\infty}).$$

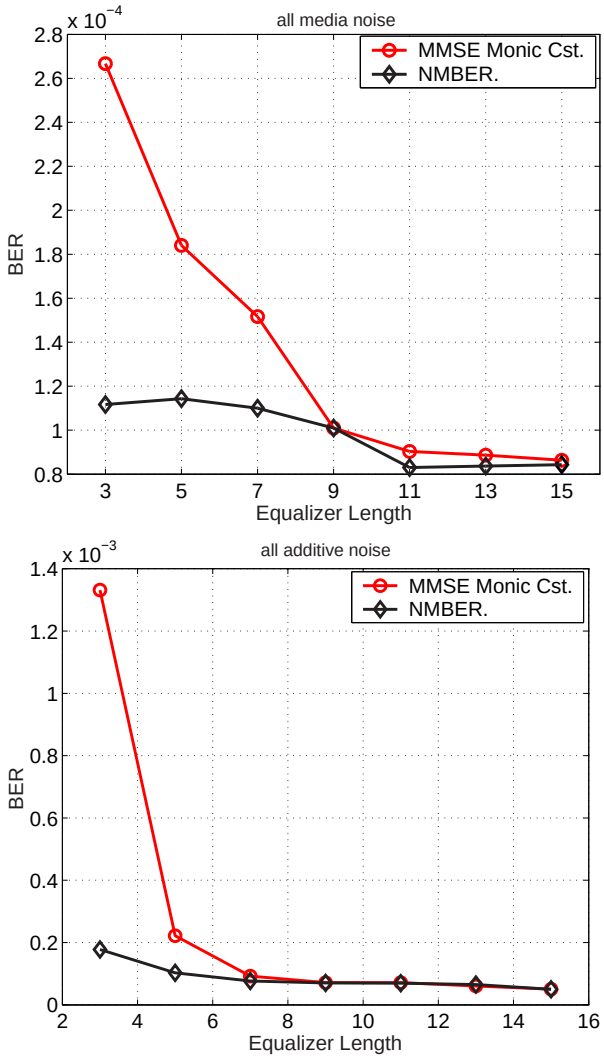

Figure 3.10: *BER vs the equalizer length at the absence of nonlinearities, i.e.* $\gamma = 0$*, for the all media noise case at SMNR=13 dB (upper plot) and all additive noise case at SANR=14 dB (lower plot).*

Therefore the NMBER target adaptation behaves asymptotically as a linear first order adaptation loop. Therefore, by analogy to a linear first order loop [86] the total loop gain of the NMBER adaptation is proportional to $\eta(e)\mathrm{EnR}(g^{\infty})$ and the adaptation gradient noise is also proportional to $\eta(e)\mathrm{EnR}(g^{\infty})$, i.e. $\sigma_g^2 \propto \eta(e)\mathrm{EnR}(g^{\infty})$.

Because EnR is also a function of the gradient noise σ_g^2 and thus of $\eta(e)$, the

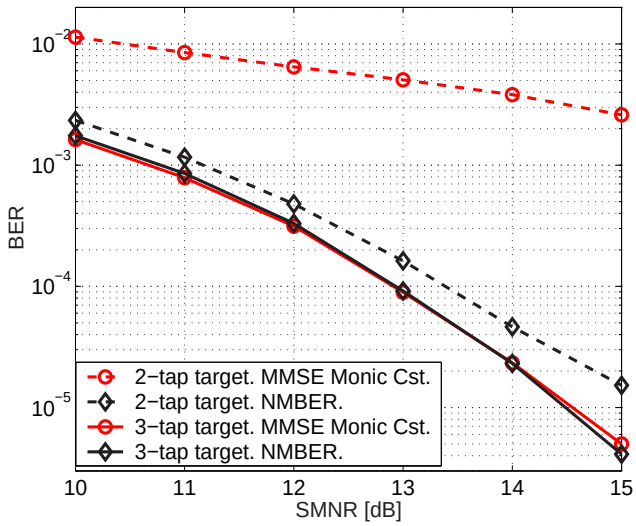

Figure 3.11: *Simulated BER vs SMNR for different target lengths at the absence of channel nonlinearities and electronic noise.*

gradient noise in the NMBER adaptation is not a linear function of $\eta(e)$ as it is the case for a linear first order loop. This could also be seen from Figure 3.12 where multiplying $\eta(e)$ by a factor 2 leads to an increase in gradient noise by a facto higher than two.

However, similarly to a linear first order loop, the efficiency of the NMBER adaptation scheme, which is, roughly speaking, defined as the ratio between gradient noise and total loop gain, is independent on the adaptation constant $\eta(e)$.

3.7 Conclusions

In this chapter a new equalizer and target adaptation scheme has been proposed for equalized maximum likelihood systems. This new scheme seeks to minimize directly the bit-error rate. The proposed scheme incorporates a selection mechanism that enables equalizer and target adaptation only if the difference in path metrics, between the selected and discarded paths from the Viterbi trellis, is smaller than a prescribed threshold. The new adaptation scheme is not more complex than MMSE-based schemes. Simulation results for an optical storage system showed that our

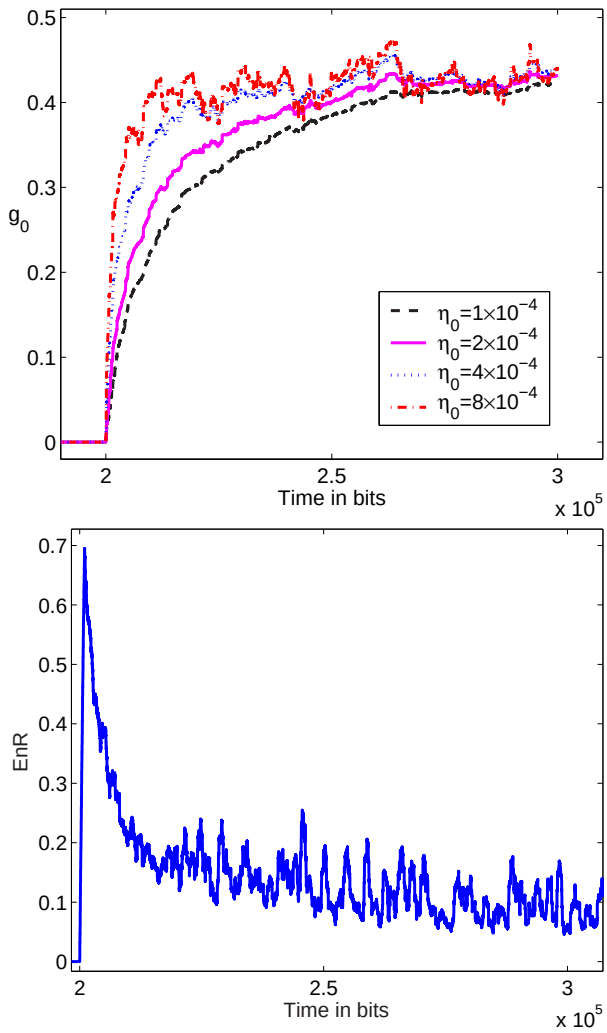

Figure 3.12: *The NMBER target convergence behavior and the corresponding enabling rate for* $\eta_0 = 4 \times 10^{-4}$ *computed over the last 1000 samples.*

scheme outperforms significantly the existing scheme especially for short target or equalizer lengths or in the presence of media noise and channel nonlinearities.

Chapter 4

Asynchronous Adaptive Equalization

Advanced data receivers for storage systems often operate at a sampling rate $1/T_s$ that is asynchronous to the baud rate $1/T$. A digital equalizer will then also operate in the asynchronous clock domain. The adaptation of this equalizer is based on an error signal ε_k that is produced in the synchronous clock domain. Existing adaptation techniques, derived from LMS, require the use of a complex sampling rate converter or inverse sampling rate converter in the adaptation path. The objective of this chapter is to analyze and design an alternative topology that is simpler from an implementation standpoint and still close to optimal. Whereas this chapter focuses on LMS adaptation for simplicity, its main results generalize to other adaptation techniques, e.g. NMBER adaptation of Chapter 2. The proposed asynchronous LMS topology is comparable to its synchronous counterpart in terms of complexity. Numerical results are provided for an idealized optical channel. They show the merits of our scheme compared to the state of the art.

4.1 Introduction

Most modern data receivers for storage and transmission systems operate in the digital domain in order to profit from advanced digital signal processing techniques. An adaptive equalizer is commonly used in these systems as a key part of the receiver. In early transmission systems, symbol-spaced equalization, in the form of a transversal filter with variable tap gains and tap spacing equal to the symbol spacing T, was used. For automatic adjustment of the tap gains in an adaptive manner during the entire period of transmission, the least mean-square (LMS) error algorithm has become a standard method, e.g. [133].

Already in early telephone line modems, equalizers with tap spacing that is less than the symbol interval were suggested. These Fractionally Spaced Equalizers (FSE) [103], [43], [144] offered many improvements over symbol-spaced equalizers in terms of performance insensitivity to sampling phase and ability to compensate for more severe delay and amplitude distortions with less noise enhancement [144].

A different equalization trend arises from receivers for digital storage systems. In these systems, symbol-spaced equalization was first employed and applied to the digitized and synchronized analog replay signal [20]. This requires the analog signal to be first sampled at the baud rate $1/T$ prior to equalization, where the sampling instants are defined by a timing-recovery circuit. A major drawback of symbol-spaced equalization is that the equalizer is inside the timing-recovery loop. This causes the equalizer latency to contribute to the timing-recovery loop delay which has a significant impact on its stability margin and convergence speed [85]. This can be especially dramatic for systems where fast timing variations occur, e.g. for high-density optical storage systems. In order to reduce loop delay, the digital equalizer is shifted out of the timing-recovery loop [21], [112], [35]. A common baseband topology is depicted in Figure 4.1.

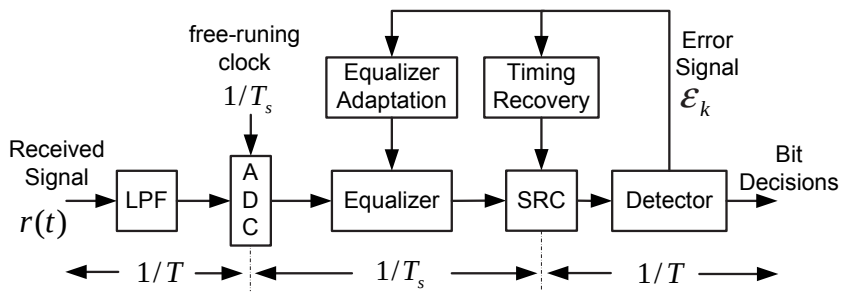

Figure 4.1: *Baseband receiver with asynchronous equalizer. Asynchronous and synchronous clock domains are indicated with the symbols $1/T_s$ and $1/T$, respectively.*

The replay signal $r(t)$ is filtered with an analog low-pass filter (LPF) which suppresses out of band noise. The LPF output is then digitized by an analog to digital converter (ADC) which is operating at a free-running frequency $1/T_s$ that is asynchronous to the baud rate $1/T$, where $1/T_s$ is chosen to be high enough to prevent aliasing. The ADC output is applied to an equalizer which controls intersymbol inter-

ference (ISI) and noise. This equalization is called asynchronous because it operates on samples that are asynchronous to the bit clock in both frequency and phase. A sampling rate converter (SRC) [40] [86], re-samples the equalizer output signal at the correct rate and phase. The SRC is controlled by an all digital timing-recovery circuit that defines the re-sampling instants. The re-sampled sequence serves as input to a bit detector that produces bit decisions and an error signal ε_k. This error signal serves as a basis to adjust the equalizer taps and the re-sampling instants of the timing-recovery as we will see in Chapter 5.

Although an asynchronous equalizer and a FSE look similar, there are two fundamental differences that have significant impacts on adaptation. First, synchronization in systems employing FSEs is normally achieved at the front-end of the receiver by controlling the sampling phase and frequency of the ADC. This makes the FSE adaptation quite simple because alignment (in phase and frequency) of the error and the equalizer input signal is straightforward in contrast to asynchronous equalization as we will see in the continuation of this chapter. However, this causes the FSE to be part of the timing-recovery loop and thus affecting its stability margin and convergence speed as mentioned earlier. Second, whereas FSEs are normally used for channels with positive excess bandwidth, i.e. the channel cut-off frequency Ω_c is bigger than the Nyquist frequency $1/2T$, asynchronous equalization is usually applied to channels with negative excess bandwidth, i.e. $\Omega_c < 1/2T$, where timing-recovery becomes critical for system performance as it is the case for high-density optical storage systems [86]. Besides, in asynchronous equalization, the sampling rate $1/T_s$ may be lower than $1/T$ in the case of a negative excess bandwidth channel, i.e. $\Omega_c \leq 1/2T_s < 1/2T$. This allows the asynchronous equalizer to have fewer taps than its synchronous counterpart without any loss in performance.

To achieve the advantages of asynchronous equalization, it is necessary to develop an asynchronous adaptation scheme that can achieve near optimal performance while being realizable by means of simple circuits. These advantages have motivated several research activities.

In [35] an equalizer adaptation scheme that is based on the synchronous error signal ε_k was proposed. The error signal is converted to the asynchronous clock domain via an inverse sampling rate converter (ISRC) before cross-correlation with a delayed equalizer input. This conversion is meant to align the error signal and the equalizer input both in sampling rate and phase.

In [28] the equalizer adaptation was obtained by converting the equalizer input to the synchronous clock domain via an auxiliary sampling rate converter (SRC) and a fractional shift register (FSR) prior to cross-correlation with the error signal.

Because the first scheme [35] is quite complex and the second [28] can only handle a limited range of oversampling ratios T/T_s, this chapter focuses on developing an alternative adaptation topology that overcomes these two disadvantages while affording near-optimum performance.

The basic idea compared to [28] is that the combination of the auxiliary SRC and the FSR is replaced by a very simple form of interpolation to re-sample the equalizer tap signals at the correct instants. The re-sampling instants are determined by the timing-recovery circuit.

The remainder of this chapter is organized as follows. Section 4.2 describes the system model and nomenclature. Section 4.3 presents analytical results for asynchronous MMSE equalization and Sections 4.4 and 4.5 analyze the problem of adaptive asynchronous equalization. A simple solution is then presented in Section 4.6. Section 4.7 provides numerical results that illustrate the performance of the proposed adaptation scheme for an idealized optical storage system.

4.2 System Model and Nomenclature

In Figure 4.2, a binary data sequence b_k of baud rate $1/T$ is applied to a linear dispersive channel with symbol response $h(t)$ and additive noise $z(t)$ with power spectral density equal to N_0. In this chapter we consider channels without excess bandwidth, i.e. channels that have no transfer beyond the Nyquist frequency $1/2T$.

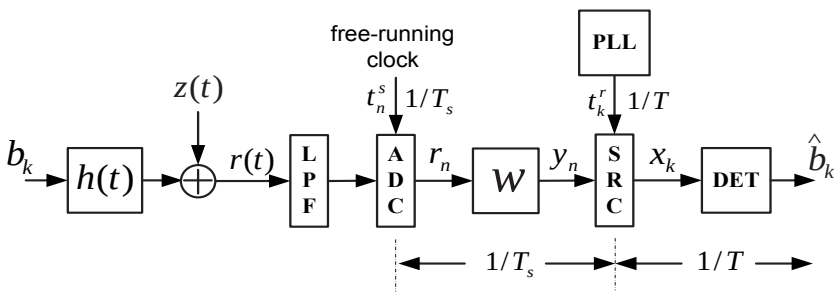

Figure 4.2: *The system model. Timing-recovery loop is not shown.*

The output of the channel is a continuous-time signal

$$r(t) = \sum_k b_k h(t - kT) + z(t).$$

This output is applied to an ideal low-pass filter (LPF) to prevent aliasing and then digitized via an ADC at a free-running frequency $1/T_s$. We denote by r_n the ADC output at the sampling instant $t_n^s = nT_s$. This output may be written

$$r_n = \sum_k b_k h(t_n^s - kT) + z_n \tag{4.1}$$

where z_n is pre-filtered and sampled noise. For simplicity, the noise in this chapter is assumed to be uncorrelated and to have a variance $\sigma_z^2 = N_0/T_s$ which corresponds to considering only electronics noise in an optical storage channels.

The sequence r_n is applied to a transversal equalizer with coefficients w_p, $p \in \{0, ..., N_w - 1\}$, where N_w is the length of the equalizer. The equalizer output $y_n = (r * w)_n$, where $*$ denotes discrete convolution, is used as input of an SRC that serves to re-samples the asynchronous signal y_n at the correct frequency and phase. The SRC is part of a timing-recovery loop [40], [112], [86]. Throughout the chapter we assume that the timing-recovery is ideal and denote the re-sampling instants by $t_k^r = t_0^r + kT$ where t_0^r denotes the time instant at which the SRC output sample with index 0 becomes available. For simplicity we set $t_0^r = 0$. The SRC output may be written as

$$x_k = \sum_n y_n c(t_k^r - nT_s),$$

where $c(t)$ is the equivalent continuous-time symbol response of the SRC. Following [40], we express t_k^r as a sum of an integer multiple and a fraction of T_s, i.e. $t_k^r = (m_k + \mu_k)T_s$ where $m_k = \lfloor t_k^r/T_s \rfloor$ and $\mu_k = t_k^r/T_s - m_k$. Clearly $0 \leq \mu_k < 1$. We will refer to m_k and μ_k as the basepoint index and the fractional interval respectively. It is easy to recast x_k in terms of m_k and μ_k, which gives $x_k = \sum_n y_{m_k - n} c((n + \mu_k)T_s)$. This can be written as a discrete time convolution

$$x_k = (c^{\mu_k} * y)_{m_k} \tag{4.2}$$

where $c_n^{\mu_k} = c((n + \mu_k)T_s)$ is the discrete version of the SRC symbol response, sampled with the fractional delay $\mu_k T_s$. The SRC is driven by a phase-locked loop (PLL), that is part of the timing-recovery circuit, and that provides at each synchronous clock

cycle the values of m_k and μ_k. The SRC output x_k is fed to a bit detector (DET) that produces bit decisions $\widehat{b}_k$. For mathematical convenience we neglect the delays of the different modules and the latency of the bit detector and assume that $\widehat{b}_k = b_k$.

4.3 Asynchronous MMSE Equalization

The task of the Minimum Mean Square Error (MMSE) equalizer in the system model of Figure 4.2 is to minimize the power of the error signal at the bit detector input. The error signal is derived as the mismatch between the actual detector input x_k and the ideal input for bit detection called reference signal. In the case of a partial-response maximum-likelihood (PRML) receiver [20], see Chapter 1, the detector has a prescribed target response g_k, and all the signal processing modules act to make the detector input look as much as possible similar to the corresponding reference signal. This reference signal d_k, as function of the target response g_k, can be written $d_k = (g * b)_k$. The error signal ε_k is then given by $\varepsilon_k = x_k - (g * b)_k$. Replacing y_n by $(w * r)_n$ in (4.2) yields

$$\varepsilon_k = \sum_{p=0}^{N_w-1} w_p (c^{\mu_k} * r)_{m_k - p} - (g * b)_k. \tag{4.3}$$

The MMSE coefficients w_p are obtained by minimizing the cost function $J = E[\varepsilon_k^2]$, where $E[.]$ denotes the expectation operation. This problem has been studied in [114]. It has been shown in particular that the MMSE equalizer tap vector $\underline{w} = [w_0, ..., w_{N_w-1}]^{\mathrm{T}}$, where $[\cdot]^{\mathrm{T}}$ denotes matrix transposition, is characterized by the following linear system:

$$(\mathbf{F}\mathbf{R}_b\mathbf{F}^{\mathrm{T}} + \mathbf{C}\mathbf{R}_z\mathbf{C}^{\mathrm{T}})\underline{w} = \mathbf{F}\mathbf{R}_b\underline{g}, \tag{4.4}$$

where the matrix $\mathbf{F}$ has entries $\mathbf{F}_{p,q} = \sum_n c(nT_s - pT_s)h(qT - nT_s)$, $\mathbf{C}$ is given by $\mathbf{C}_{p,q} = c(-pT_s - qT_s)$ and the autocorrelation matrices of the input data and noise are denoted by $\mathbf{R}_b$ and $\mathbf{R}_z$ respectively. The vector $\underline{g} = [g_0, g_1, ...]^{\mathrm{T}}$ contains the target response coefficients.

Due to the presence of the anti-aliasing filter and the low pass nature of $c(t)$, the system (4.4) may not be well defined, i.e. the matrix $(\mathbf{F}\mathbf{R}_b\mathbf{F}^{\mathrm{T}} + \mathbf{C}\mathbf{R}_z\mathbf{C}^{\mathrm{T}})$ can be singular. This can occur in particular if the oversampling ratio $\frac{T}{T_s}$ is high and the equalizer is long. A near-optimal solution to this problem has been proposed

in [114] and consists of introducing a small correction term to regularize the MMSE equation (4.4). This is achieved by replacing the matrix $(\mathbf{F}\mathbf{R}_b\mathbf{F}^{\mathrm{T}}+\mathbf{C}\mathbf{R}_z\mathbf{C}^{\mathrm{T}})$ in (4.4) by $(\mathbf{F}\mathbf{R}_b\mathbf{F}^{\mathrm{T}}+\mathbf{C}\mathbf{R}_z\mathbf{C}^{\mathrm{T}}+\varepsilon\mathbf{I})$ where $\mathbf{I}$ is the identity matrix and ε is a small non-negative value. In the sequel we will take this regularized solution as a basis of reference.

4.4 Adaptive Asynchronous Equalization

In the previous section we assumed prior knowledge of the channel and reported the closed form solution of the MMSE asynchronous equalization problem. In practical systems the channel is subject to parameter variations, e.g. due to tilt in optical storage systems. Therefore equalization should be made adaptive.

The equalizer adaptation scheme studied in this chapter makes use of the LMS technique that consists of minimizing the instantaneous power of the error. LMS equalizer adaptation consists of adding to the equalizer taps, at each iteration, a change proportional to the negative gradient of the instantaneous squared error. The equalizer adaptation is then written as follows:

$$w_p^{(k+1)} = w_p^{(k)} - \frac{1}{2}\eta \left.\frac{\partial \varepsilon_k^2}{\partial w_p}\right|_{\underline{w}=\underline{w}^{(k)}},$$

where $w_p^{(k)}$ is the pth tap of the equalizer at time kT. The coefficient η denotes the equalizer adaptation constant. The expression of the error signal as a function of the equalizer taps has been given in equation (4.3). Using expression (4.3) to calculate the above partial derivatives leads to the following adaptation equation:

$$w_p^{(k+1)} = w_p^{(k)} - \eta\varepsilon_k(c^{\mu_k} * r)_{m_k-p}. \tag{4.5}$$

This equation describes the asynchronous LMS adaptation rule and suggests that LMS adaptation may be based on correlating the error signal with a synchronous version of the equalizer input. This version is obtained using an auxiliary sampling rate converter in the adaptation loop. For clarity of the sequel and in order to make a clear distinction with the main SRC, we designate this auxiliary sampling rate converter SRC2 and denote its symbol response by $c_2(t)$. Equation (4.5) is then re-written as

$$w_p^{(k+1)} = w_p^{(k)} - \eta\varepsilon_k(c_2^{\mu_k} * r)_{m_k-p}. \tag{4.6}$$

The LMS adaptation scheme is depicted in Figure 4.3. The auxiliary sampling rate converter SRC2 aligns, both in frequency and phase, the error signal and the equalizer input. In particular the overall delay from the point denoted *A* in Figure 4.3 to point *B*, through SRC2, should match the delay from *A* to *C* through the equalizer and the main SRC. The result of correlation between the error signal and the re-sampled equalizer input is first scaled with the adaptation constant η and then passed to a digital integrator. Since this integrator produces an output at the synchronous clock rate and the equalizer operates in the asynchronous clock domain, a form of inverse sampling rate conversion is needed. Moreover, since equalizer tap values change only slowly with respect to both sampling rates, this inverse sampling rate conversion can be achieved in the simplest conceivable manner, namely via a bank of latches (or, equivalently zeroth-order interpolation).

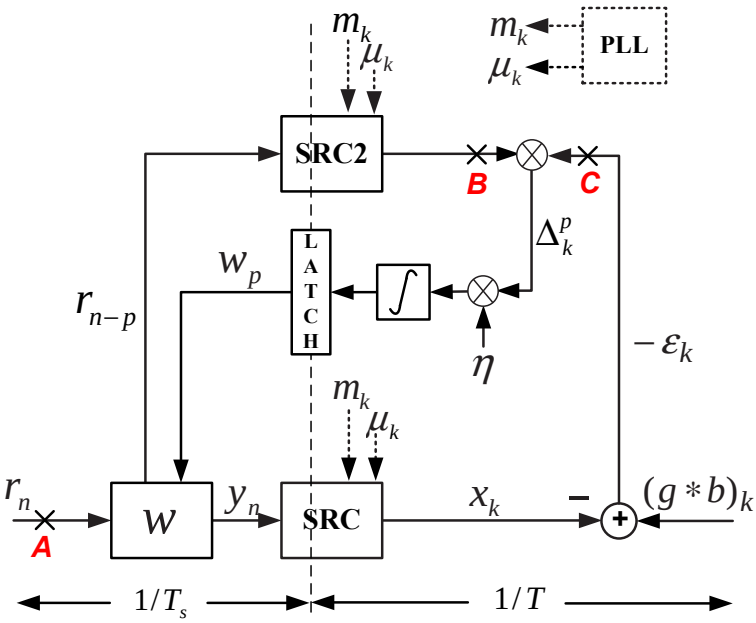

Figure 4.3: *The LMS adaptation of the* p^{th} *equalizer tap.*

A direct implementation of this scheme is, however, quite complex for practical systems. In fact, equation (4.6) requires us to compute all the gradient signals $(c_2^{\mu_k} * r)_{m_k-p}$ for $p \in \{0 \ldots N_w - 1\}$, i.e. the re-sampled signal r at the instants $t_k^r - pT_s$. Therefore, in order to adapt all the equalizer taps at the rate $\frac{1}{T}$, N_w duplications of

SRC2 would in principle be needed.

A solution to this problem has been proposed in [28]. It consists of using one auxiliary SRC2, identical to the main SRC, to re-sample the equalizer input at the instant t_k^r. This is followed by a set of linear interpolators, in the synchronous domain, to produce the gradient signals. Explicitly, it consists of linearly interpolating between the samples $(c_2^{\mu_k} * r)_{m_k} \approx r(t_k^r) = r(kT)$ to build approximations of $(c_2^{\mu_k} * r)_{m_k-p} \approx r(t_k^r - pT_s) = r(kT - pT_s)$. However, this solution is still complex in that it requires an additional sampling rate converter and more importantly it has been shown to be applicable to only limited ranges of oversampling ratios.

In the following section we first analyze the impact of SRC2 on the equalizer adaptation, derive a set of criteria to design $c_2(t)$ and describe a very simple choice that achieves close to MMSE performance. This simple choice renders the topology of Figure 4.3 practical while being applicable to a wide range of oversampling ratios.

4.5 Effect of The Auxiliary SRC on LMS Adaptation

The proper design of $c_2(t)$ is a key element in the realization of the asynchronous LMS adaptation scheme. A straightforward choice is $c_2(t) = c(t)$. However, in this section we will highlight a set of degrees of freedom for the design of $c_2(t)$. Such degrees of freedom will be exploited to simplify the asynchronous LMS adaptation scheme. In the first two subsections we consider the case where SRC2 does not introduce aliasing. In the third subsection, we will focus on the effect of aliasing in SRC2 on the equalizer adaptation.

4.5.1 Effect of the auxiliary SRC on the steady-state solution

A theoretical analysis of the behavior of the LMS adaptation scheme, for an aliasing-free SRC2, is presented in Appendix A. It reveals that the average update signal for the adaptation of the pth equalizer tap, $\Delta_k^p = \varepsilon_k (c_2^{\mu_k} * r)_{m_k-p}$ (see Figure 4.3), can be written as

$$E[\Delta_k^p] = \frac{1}{T_s} \int_{-\infty}^{+\infty} \left[\frac{1}{T_s} \left(\frac{|H|^2}{T} + N_0 \right) CW - H^* G \right] C_2^* e^{j2\pi p T_s \Omega} d\Omega, \tag{4.7}$$

where we have suppressed all dependencies on Ω for notational convenience. In this expression H is the channel transfer function, $W(e^{j2\pi\Omega T_s})$ and $G(e^{j2\pi\Omega T})$ denote the

discrete Fourier transforms of w_n and g_k respectively. The notation X^* denotes the complex conjugate of the transfer function X. The expectation operation in (4.7) is taken over all data and noise realizations.

The equalizer steady-state response is characterized by the set of equations $E[\Delta_k^p] = 0$, $\forall p < N_w$. In order to understand the impact of $c_2(t)$ on this steady-state response, let us first consider the case where the equalizer is infinitely long. In this case, the steady-state response is obtained when the integrand in the right hand side of (4.7) is zero at all frequencies, i.e.

$$\left[1/T_s\left(|H|^2/T + N_0\right)CW - H^*G\right]C_2^* = 0. \tag{4.8}$$

The latter expression shows that if $C_2(\Omega_0) = 0$, for Ω_0 within the channel pass-band, the steady-state equalizer transfer function is ill-defined at $\Omega = \Omega_0$. If, however, C_2 has no spectral nulls within the channel pass-band, the steady-state W is unambiguously defined by H, G and C and is independent of C_2. Conversely, spectral nulls that are outside the channel pass-band do not alter equalizer steady-state solution.

As the length of the equalizer decreases, (4.8) can be met at an increasingly limited set of frequencies. As a result the degeneracy problem becomes smaller.

We may conclude that, if $C_2(\Omega) \neq 0$ for each frequency in the channel pass-band, the equalizer steady-state solution is not affected by the amplitude and phase responses of $c_2(t)$. However, the impact of $c_2(t)$ on loop stability still needs to be explored. The following subsection deals with this issue.

4.5.2 Stability analysis

Stability analysis of the equalizer adaptation loop is presented in Appendix B. It is found that, for long equalizer lengths, the loop is stable if and only if the following condition is met:

$$\forall\Omega \in B_C \quad \eta\frac{1}{T_s}\left(\frac{|H|^2}{T} + N_0\right)\frac{|C(\Omega)||C_2(\Omega)|}{T_s^2} < 2\cos[\varphi_{C_2}(\Omega) - \varphi_C(\Omega)], \tag{4.9}$$

where B_C is the pass-band of $C(\Omega)$ (i.e. $\forall\Omega \notin B_C$ $C(\Omega) = 0$), and $\varphi_C(\Omega)$ and $\varphi_{C_2}(\Omega)$ denote the phase responses of $c(t)$ and $c_2(t)$ respectively. Equation (4.9) provides a condition that links the adaptation constant η, the amplitude response $|C_2(\Omega)|$ and the phase mismatch $\varphi_{C_2}(\Omega) - \varphi_C(\Omega)$ in order to ensure stability. In particular, it shows that by fixing η and $|C_2(\Omega)|$, a range of phase mismatches between $c_2(t)$ and $c(t)$ can

be tolerated. Similarly, fixing η and $\varphi_{C_2}(\Omega)$ defines a range of acceptable amplitude responses that ensure stability.

As the length of the equalizer decreases, inequality (4.9) becomes a sufficient condition for stability as will be seen from simulations.

In many practical systems, equalizer adaptation is often designed to be slow, i.e. $\eta \ll 1$. The left hand side of (4.9) is then close to zero. This implies that the phases of $c_2(t)$ and $c(t)$ must be within $\frac{\pi}{2}$ throughout B_C. In other words, a necessary condition for loop stability is that the phase mismatch between $c_2(t)$ and $c(t)$ is smaller than $\pi/2$ throughout B_C.

Example 4.1 :
Let us consider a channel with a cut-off frequency $\Omega_c \leq 1/(2T)$. In order to suppress out-of-band noise, the transfer function of the ideal SRC is zero outside the interval $[-\Omega_c, \Omega_c]$. Assume that there is a delay mismatch of δ seconds between the two SRCs, i.e. that $\varphi_C(\Omega) - \varphi_{C_2}(\Omega) = 2\pi\delta\Omega$. A necessary condition on δ to ensure stability is that $2\pi|\delta\Omega| < \pi/2 \ \forall|\Omega| < \Omega_c$. The maximum tolerable delay mismatch $\delta_{\max}$ is thus given by

$$\delta_{\max} = \frac{1}{4\Omega_c}.$$

The closer the delay mismatch δ gets to $\delta_{\max}$, the slower the loop must be in order to guarantee stability.

4.5.3 Effect of aliasing in the auxiliary SRC

The impact of aliasing, introduced by SRC2, is a key potential issue in the design of practical asynchronous LMS equalizer adaptation. Actually, it is still not clear from the previous subsections how the equalizer adaptation behaves when $c_2(t)$ does not reject out-of-band frequencies. We will prove, in particular that aliasing in SRC2 does not hamper the LMS adaptation for channels without excess bandwidth. In this case, following similar steps as in Appendix A, one can show that the average update signal for a general symbol response $c_2(t)$ is given by

$$E[\Delta_k^p] = \frac{1}{T_s}\int \left[\frac{1}{T_s}\left(\frac{|H|^2}{T} + N_0\right)CW - H^*G\right] C_b^*(\Omega)e^{j2\pi pT_s\Omega}d\Omega, \tag{4.10}$$

where the expectation operation is taken over all data and noise realizations, and where

$$C_b(\Omega) = \sum_n e^{-j2\pi n \frac{t_k^r}{T_s}} C_2(\Omega - \frac{n}{T_s}). \tag{4.11}$$

Equation (4.10) is analog to (4.7) where the factor $C_2(\Omega)$ is replaced by its aliased version $C_b(\Omega)$. This aliased version is now time dependent, more precisely it depends on the re-sampling instant t_k^r. This implies that the adaptation loop gain [86] is now time-varying and depends on the sampling instants t_k^r. The same reasoning as in Section 4.5.1 holds here if one can ensure that, in average over time, $C_b(\Omega)$ does not have zeros within the channel pass-band and that the phase mismatch relative to $C(\Omega)$ of the average $C_b(\Omega)$ obeys (4.9). In that case the steady-state equalizer will not depend on $c_2(t)$ and the adaptation loop will be stable.
Now replacing in (4.11) the re-sampling instant by its expression $t_k^r = (m_k + \mu_k)T_s$ leads to

$$C_b(\Omega) = \sum_n e^{-j2\pi n \mu_k} C_2(\Omega - \frac{n}{T_s}).$$

The fractional interval μ_k ($\in [0,1[$) depends on the oversampling ratio and on the channel delay that can vary randomly. As a consequence we can assume μ_k to be uniformly distributed in $[0,1[$. In this case it can be proven that $E_{\mu_k}[e^{-j2\pi n \mu_k}] = \delta_n$, where δ_n denotes the Kronecker delta function. Therefore the average over all the sampling instants t_k^r of the function $C_b(\Omega)$ is simply given by

$$E_{t_k^r}[C_b(\Omega)] = C_2(\Omega). \tag{4.12}$$

From (4.10) it can be seen that the influence of aliasing on the LMS adaptation manifests itself as a time-varying loop gain per frequency that is proportional to $C_b^*(\Omega)$. From (4.12) it is apparent that the loop gain, in average over time, is not influenced by aliasing. More precisely, in average over time, the LMS adaptation loop gain at frequency $\Omega = \Omega_0$ is proportional to $C_2^*(\Omega_0)$. An intermediate consequence of the above reasoning is that a spectral null in $C_2(\Omega)$ in the channel pass-band cannot be tolerated.

From (4.12) one can also see that the phase of the average over time of $C_b(\Omega)$ is equal to the phase of $C_2(\Omega)$. Therefore stability is ensured if the phase of $C_2(\Omega)$ satisfies (4.9) within the channel pass-band.

The above considerations suggest that the symbol response $c_2(t)$ needs only to meet (4.9) and to have no spectral nulls in the channel pass-band. In this case the

steady-state equalizer will not be altered by aliasing and the adaptation loop will be stable.

4.6 Simplified Asynchronous LMS Adaptation

In the previous section the relationship between SRC2 and the equalizer adaptation has been discussed. First, we showed that amplitude distortions in SRC2 do not alter equalizer steady-state solution if $C_2(\Omega)$ has no zeros within the channel pass-band. Second, adaptation stability is preserved as long as the phase mismatch between $C_2(\Omega)$ and $C(\Omega)$ is kept below a defined stability bound. Finally, it has been shown that aliasing in SRC2 does not hamper equalizer adaptation. A summary of design criteria for SRC2 can now be presented as follows:

1. The transfer function $C_2(\Omega)$ must not have any spectral zeros within the pass-band of the channel.

2. The phase mismatch between $c_2(t)$ and $c(t)$ must be kept as small as possible according to (4.9).

The design of SRC2 is now made simpler. This can be used to simplify the complete asynchronous LMS adaptation. In order to meet the second design criterion, the simplest possible choice is to consider a symmetric response $c_2(t)$ with the same symmetry point as $c(t)$. The first criterion is also met with very simple waveforms. For example, a rectangular function on the interval $[-T_s/2, T_s/2]$, i.e.

$$c_2(t) = \begin{cases} 1, & |t| < T_s/2, \\ 0, & \text{otherwise}, \end{cases} \tag{4.13}$$

satisfies both conditions. Its transfer function $C_2(\Omega) = T_s \text{sinc}(\pi\Omega T_s)$ has a first spectral null at $\Omega = 1/T_s$ that is always outside the channel pass-band ($\Omega_c < 1/T_s$). This choice of $c_2(t)$ corresponds to an implementation of SRC2 via nearest neighbor interpolation (0th order interpolation). The support $[-T_s/2, T_s/2]$ is the shortest interval that permits adaptation at every synchronous clock cycle independent of the value of μ_k. In fact, if the support of $c_2(t)$ has a shorter length than T_s then $c_{2,n}^{\mu_k}$ is zero for a range of fractional interval μ_k, which implies that the equalizer is not adapted at these instants.

With the mentioned choice of $c_2(t)$, the equalizer adaptation (4.6) can be rewritten as

$$w_p^{(k+1)} = w_p^{(k)} - \eta \varepsilon_k r_{m_k + \lfloor \mu_k + 0.5 \rfloor - p}, \tag{4.14}$$

where

$$r_{m_k + \lfloor \mu_k + 0.5 \rfloor - p} = \begin{cases} r_{m_k - p} & \text{if } \mu_k < 0.5, \\ r_{m_k + 1 - p} & \text{if } \mu_k \geq 0.5. \end{cases} \tag{4.15}$$

This adaptation rule leads to the simplified scheme presented in Figure 4.4.

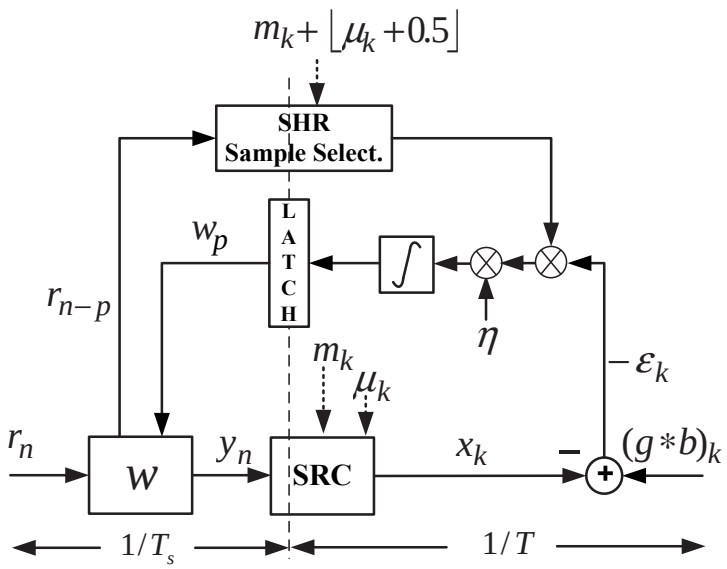

Figure 4.4: *The simplified adaptation of the* pth *equalizer tap.*

At each asynchronous clock cycle, a value of the equalizer tap signal r_{n-p} is fed into a shift register (SHR). At each synchronous clock cycle, the PLL produces the basepoint index m_k and the fractional interval μ_k. The latter serves to select the sample $r_{m_k - p}$ or $r_{m_k - p + 1}$ according to (4.15). The selected sample is correlated with the error signal, scaled by η and passed to an integrator. With the proposed simplified asynchronous LMS scheme, the auxiliary SRC reduces to a very simple sample selector. This makes the proposed scheme no more complex than a completely synchronous LMS adaptation scheme while allowing the benefits of asynchronous equalization as mentioned in the introduction.

4.7 Simulation Results

By way of illustration we consider in this section an idealized optical storage channel according to the Braat-Hopkins model as presented in Chapter 1. In terms of normalized frequencies to the baud rate $1/T$, the channel transfer function is given by

$$H(\Omega) = \begin{cases} \frac{2T}{\pi}\frac{\sin(\pi\Omega)}{\pi\Omega}\left(\cos^{-1}|\frac{\Omega}{\Omega_c}| - \frac{\Omega}{\Omega_c}\sqrt{1-(\frac{\Omega}{\Omega_c})^2}\right), & |\Omega| < \Omega_c, \\ 0, & |\Omega| \geq \Omega_c \end{cases}$$

where the normalized optical cut-off frequency Ω_c is fixed at $1/3$ in this section. Data b_k is taken to be run-length-limited with run-length parameters $(\mathrm{d},\mathrm{k}) = (1,7)$. The target response has 5 taps $g = [0.17, 0.5, 0.67, 0.5, 0.17]$. These choices reflect the system described in [115]. We consider here only electronics noise and fix channel SANR (defined as in Chapter 1) at the value of 15 dB. Similar conclusions can be drawn in the presence of media noise.

Amplitude response of $h(t)$ and g_k are depicted in Figure 4.5. The target response approximates the in-band characteristics and cut-off frequency of the channel quite well. However, because of its finite length it has some transfer above the cut-off frequency.

Since the channel passes no normalized frequencies above $1/3$, we can choose $1/T_s$ as low as $2/(3T)$ without any loss of information. The upper limit of $1/T_s$ is set to $2/T$ in the sequel. The SRC is implemented via a six-tap Lagrange interpolator [110]. At the SRC output, beyond the cut-off frequency Ω_c almost no spectral components are present. The error signal in this band will be negligible irrespective of the equalizer transfer function. As a result, the equalizer steady-state solution tends to become ill-defined, and regularization will be needed. For this purpose we incorporate tap leakage [46] into the equalizer adaptation. Equation (4.6) is then written as

$$w_p^{(k+1)} = (1-\alpha)w_p^{(k)} - \eta\varepsilon_k(c_2^{\mu_k} * r)_{m_k-p} \tag{4.16}$$

where α is a small and positive tap leakage factor.

To illustrate the impact of tap leakage we consider the case of $1/T_s = 1.25/T$. The amplitude response of various equalizers of length $N_w = 15$ are depicted in Figure 4.6. The amplitude response of the theoretical regularized MMSE solution, described in Section 4.3, is plotted together with the simulated equalizer transfer function in the

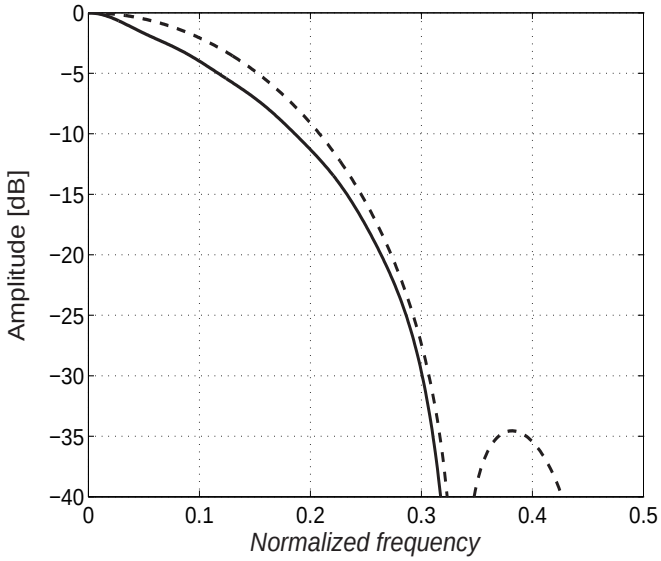

Figure 4.5: *Amplitude-frequency characteristics of idealized optical channel having a normalized cut-off* $\Omega_c = 1/3$ *(solid) and 5-tap target response* $g_k = [0.17, 0.5, 0.67, 0.5, 0.17]$ *(dashed).*

absence and presence of leakage. This figure shows that tap leakage is needed to regularize the equalizer transfer function in the out of band region. Besides, the steady-state solution of the simplified LMS scheme is indiscernible, in the in-band region, from the theoretical MMSE solution.

To highlight the merit of the simplified LMS scheme compared to MMSE, Figure 4.7 shows the normalized MSE, i.e. the MSE divided by the average power of the reference signal, as a function of the oversampling ratio T/T_s for an equalizer length $N_w = 15$. This proves that the simplified scheme is on the one hand equivalent to the full LMS adaptation scheme from MSE point of view and on the other hand leads to close to MMSE performance over the complete range of oversampling ratios. The penalty in MSE with respect to MMSE is less than 0.08 dB.

LMS equalizers tend to be, in general, quite insensitive to variations of the sampling phase. The proposed simplified LMS scheme is no exception. Normalized MSE of the simplified LMS as a function of sampling phase variations is shown in Figure 4.8.

In order to illustrate the impact of a delay mismatch between SRC2 and SRC

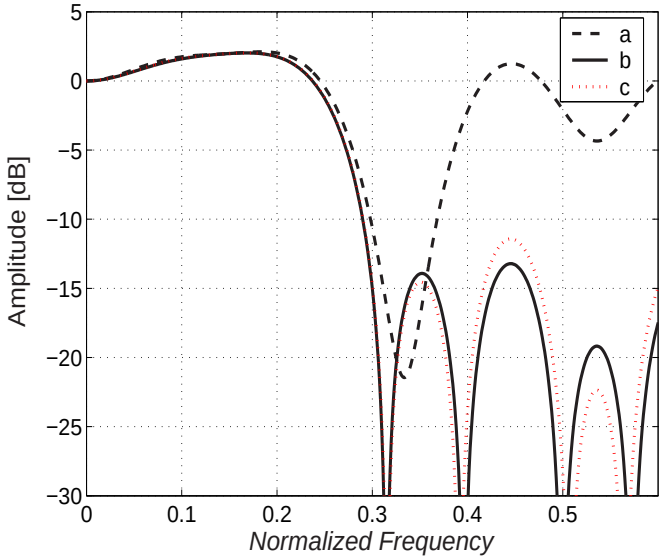

Figure 4.6: *Amplitude response of various equalizers for $\frac{1}{T_s} = \frac{1.25}{T}$. a) simulated LMS, no tap leakage (dashed); b) (regularized) theoretical MMSE solution (solid); c) The simplified LMS with tap leakage (dotted).*

on the equalizer adaptation, and validate the theoretical analysis of Section 4.5.2, we measured simulated MSE as a function of the delay δ between $c_2(t)$ and $c(t)$ for different values of N_w. For every value of N_w, the equalizer adaptation constant is tuned to have optimum MSE at $\delta = 0$ and then fixed for other values of δ. The simulation result is shown in Figure 4.9.

According to the theoretical analysis of Section 4.5.2, the maximum tolerable delay for $\Omega_c = 1/(3T)$ is given by $\delta_{\max} = \frac{1}{4\Omega_c} = \frac{3}{4}T$. This gives a limit that is in particular valid for a very slow adaptation and a very long equalizer. Figure 4.9 shows that, especially for a big N_w, the adaptation is unstable if $\delta > \delta_{\max} = 0.75T$. However, and more importantly, the equalizer adaptation is not affected when $\delta < 0.6T$. For this range of δ, the steady-state equalizer responses are also not affected.

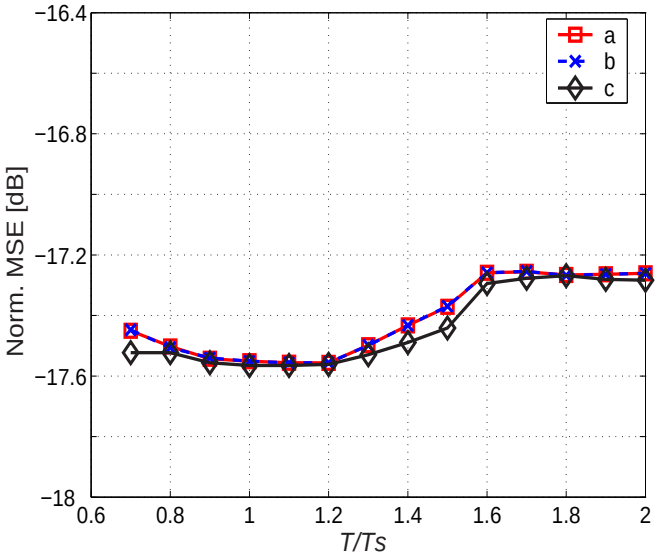

Figure 4.7: *Normalized MSE as a function of oversampling ratio for* $N_w = 15$*: a) Simulated full asynchronous LMS, i.e.* $c_2 = c$*; b) Simulated simplified LMS; c) Theoretical MMSE (4.4).*

4.8 Conclusions

Design and implementation considerations may favor digital equalization to be performed in a clock domain that is asynchronous to the baud rate $1/T$. Such a consideration arises, for example, in systems where asynchronous equalization has to be employed to minimize the delay inside the timing-recovery loop. In this chapter we have studied the asynchronous LMS adaptation and provided its stability analysis. We highlighted a set of interesting degrees of freedom for the design of asynchronous equalizer adaptation. These allowed us to propose a simple asynchronous adaptation scheme that is comparable from a complexity standpoint to the synchronous LMS algorithm. Indeed, compared with the latter, our method requires no true extra complexity apart from a sample selection mechanism.

Simulation results for an idealized optical storage system showed that, on the one hand, the proposed algorithm leads very close to MMSE performance. On the other hand, it is applicable to a wide range of oversampling ratios and is insensitive to sampling phase variations.

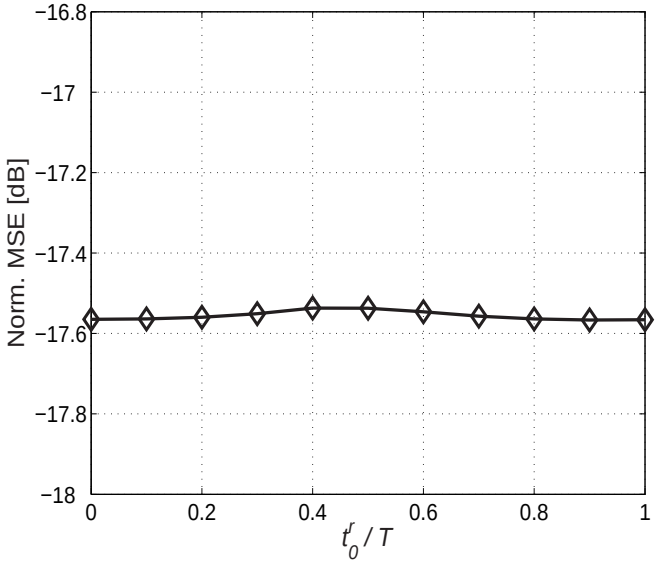

Figure 4.8: *Simulated mean-square error of the simplified LMS scheme as a function of sampling phase variations, at $T/T_s = 1$ and $N_w = 15$.*

Appendix A: Derivation of equality (4.7)

The expression of the average update signal expressed in (4.7) holds for uncoded binary data. A similar expression applies in the case of coded data by simply replacing in (4.7) $|H|^2$ by $P_b|H|^2$ and HG^* by P_bHG^* where P_b denotes the power spectral density of the input data. However because the conclusions of Section 4.5 are independent of the power spectral density of the data, we will, for simplicity, analyze the average update signal for uncoded data.

The update signal, for the pth equalizer tap, Δ_k^p is given by $\Delta_k^p = \varepsilon_k(c_2^{\mu_k} * r)_{m_k-p}$. Taking into account (4.3) we can write

$$E[\Delta_k^p] = \sum_{q=0}^{N_w-1} w_q E[(c^{\mu_k} * r)_{m_k-q}(c_2^{\mu_k} * r)_{m_k-p}] - E[(c_2^{\mu_k} * r)_{m_k-p}(g * b)_k]. \qquad (4.17)$$

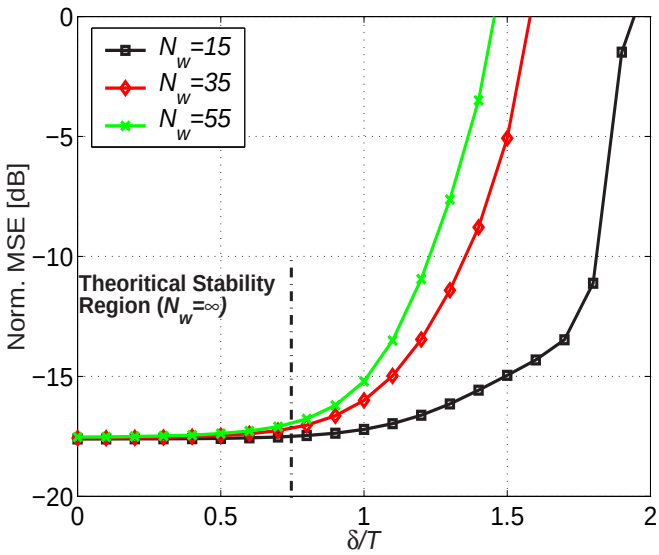

Figure 4.9: *Simulated MSE as a function of the delay mismatch between $c_2(t)$ and $c(t)$ for different values of N_w. The oversampling ratio is $T/T_s = 1$.*

Let us first simplify the expression of $E_1 = E[(c^{\mu_k} * r)_{m_k-q}(c_2^{\mu_k} * r)_{m_k-p}]$. Upon replacing r with (4.1) we get:

$$\begin{aligned} E_1 &= \sum_{n,m,n',m'} E[c_{2\,m_k-p-n}^{\mu_k} c_{m_k-q-n'}^{\mu_k} h(nT_s - mT)h(n'T_s - m'T)b_m b'_m] \\ &+ \sum_{n,n'} E[c_{2\,m_k-p-n}^{\mu_k} c_{m_k-q-n'}^{\mu_k} z_n z'_n]. \end{aligned}$$

In view of the fact that the noise is assumed to be white and the data is uncoded, we may express the last equality as

$$E_1 = \sum_{n,m,n'} E[c_{2\,m_k-p-n}^{\mu_k} c_{m_k-q-n'}^{\mu_k} h(nT_s - mT)h(n'T_s - mT)] + \sigma_z^2 \sum_n E[c_{2\,m_k-p-n}^{\mu_k} c_{m_k-q-n}^{\mu_k}].$$

By changing the order of summations, the last equality can be rewritten as

$$\begin{aligned} &E_1 = \\ &\textstyle\sum_m E[\sum_n c_2((m_k+\mu_k-n-p)T_s)h(nT_s - mT)\sum_{n'} c((m_k+\mu_k-n'-q)T_s)h(n'T_s - mT)] \\ &+ \tfrac{N_0}{T_s}\textstyle\sum_n E[c_2((m_k+\mu_k)T_s - (n+p)T_s)c((m_k+\mu_k)T_s - (n+q)T_s)] \end{aligned}$$

where we used $\sigma_z^2 = \frac{N_0}{T_s}$ and $c_n^{\mu} = c((n+\mu)T_s)$.
Now the remaining steps in this proof use the following equalities derived from the Poisson summation formula:

$$\sum_n x(t_1 - nT_s)h(t_2 + nT_s) = \frac{1}{T_s}\sum_n e^{-j2\pi n\frac{t_1}{T_s}} \int X(\Omega - \frac{n}{T_s})H(\Omega)e^{j2\pi(t_1+t_2)\Omega}d\Omega \quad (4.18)$$

and

$$\sum_n x_1(t_1 - nT_s)x_2(t_2 - nT_s) = \frac{1}{T_s}\sum_n e^{j2\pi n\frac{t_1}{T_s}} \int X_1(\frac{n}{T_s} - \Omega)X_2(\Omega)e^{j2\pi(t_2-t_1)\Omega}d\Omega \quad (4.19)$$

where $X(\Omega)$ is the Fourier transform of $x(t)$. By substituting $c(t)$ for $x(t)$ on one hand and $c_2(t)$ on the other hand, the argument of the right hand summation in equation (4.18) is non-zero only for $n = 0$. This is justified by the fact that c and c_2 are designed such that no aliasing occurs. It follows that

$$\begin{aligned} s_{1,m} &= \sum_n c_2((m_k+\mu_k)T_s - (n+p)T_s)h(nT_s - mT) \\ &= \frac{1}{T_s}\int C_2(\Omega)H(\Omega)e^{j2\pi\Omega((m_k+\mu_k)T_s - pT_s)}e^{-j2\pi m\Omega T}d\Omega \end{aligned}$$

and

$$\begin{aligned} s_{2,m} &= \sum_{n'} c((m_k+\mu_k)T_s - (n'+q)T_s)h(n'T_s - mT) \\ &= \frac{1}{T_s}\int C(\Omega)H(\Omega)e^{j2\pi\Omega((m_k+\mu_k)T_s - qT_s)}e^{-j2\pi m\Omega T}d\Omega \end{aligned}$$

Using the integration Fubini rule we can be write:

$$\sum_m s_{1,m}s_{2,m} = \frac{1}{T_s^2}\iint C(\Omega_1)H(\Omega_1)e^{j2\pi\Omega_1((m_k+\mu_k)T_s - qT_s)}C_2(\Omega_2)H(\Omega_2)e^{j2\pi\Omega_2((m_k+\mu_k)T_s - pT_s)} \times \sum_m e^{-j2\pi m(\Omega_1+\Omega_2)T}d\Omega_1 d\Omega_2$$

Now if we make use of $\sum_m e^{-j2\pi m(\Omega_1+\Omega_2)T} = \frac{1}{T}\sum_m \delta(\Omega_1 + \Omega_2 - \frac{m}{T})$ we get after removing the aliasing terms, which are filtered out by $C(\Omega)$ and $C_2(\Omega)$

$$\sum_m s_{1,m}s_{2,m} = \frac{1}{T_s^2}\int \frac{|H(\Omega)|^2}{T}C(\Omega)C_2^*(\Omega)e^{j2\pi(p-q)T_s\Omega}d\Omega.$$

Now replacing in equation (4.19) $x_1 = c_2$ and $x_2 = c$ and using the fact that the argument of the right hand summation in (4.19) is non-zero only for $n = 0$ due to the

absence of aliasing, one can show that

$$\begin{aligned}&\textstyle\sum_n E[c_2((m_k+\mu_k)T_s-(n+p)T_s)c((m_k+\mu_k)T_s-(n+q)T_s)]\\&=\tfrac{1}{T_s}\textstyle\int C(\Omega)C_2^*(\Omega)e^{j2\pi(p-q)T_s\Omega}d\Omega.\end{aligned}$$

Grouping these last two equations together leads to

$$E_1=\frac{1}{T_s^2}\int(\frac{|H(\Omega)|^2}{T}+N_0)C(\Omega)C_2^*(\Omega)e^{j2\pi(p-q)T_s\Omega}d\Omega.$$

In a similar way one can show that

$$E[(c_2^{\mu_k}*r)_{m_k-p}(g*b)_k]=\frac{1}{T_s}\int H^*(\Omega)G(e^{j2\pi T\Omega})C_2^*(\Omega)e^{-j2\pi\Omega((m_k+\mu_k)T_s-kT)}e^{j2\pi pT_s\Omega}d\Omega.$$

The last step that remains at this point is $(m_k+\mu_k)T_s=t_k^r=kT$. Now plugging the last three equalities into (4.17) leads to (4.7).

Appendix B: Stability Analysis of the Asynchronous Equalizer Adaptation

Ensuring stability of an adaptation loop is very crucial for its proper functioning. This appendix provides stability conditions of the asynchronous equalizer adaptation loop as function of the adaptation constant η, the SRC2 amplitude and phase responses and the oversampling ratio T/T_s. For simplicity of the analysis of this appendix we make the assumption of a big equalizer length. When the length of the equalizer is small, our stability conditions become sufficient conditions for stability.

In order to derive the stability condition, let us first rewrite equation (4.7) using matrix notations as follows:

$$\underline{\Delta} = \mathbf{M}(\underline{w} - \underline{\widetilde{w}}),$$

where $\underline{\widetilde{w}}$ is the equalizer steady-state vector solution, $\underline{\Delta} = [\Delta_0, ..., \Delta_{N_w-1}]^{\mathrm{T}}$ and the matrix $\mathbf{M}$ is given by

$$\mathbf{M}_{p,q} = \frac{1}{T_s^2} \int_{-1/2T_s}^{1/2T_s} \left(\frac{|H|^2}{T} + N_0 \right) C(\Omega) C_2^*(\Omega) e^{j2\pi(p-q)T_s\Omega} d\Omega \quad 0 \leq p, q < N_w. \tag{4.20}$$

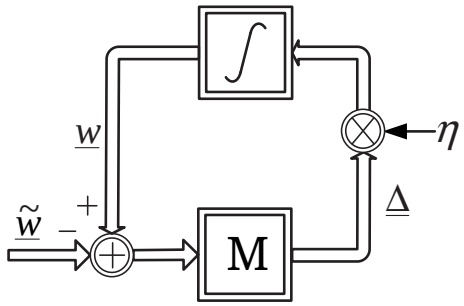

Figure 4.10: *Equivalent equalizer adaptation. Gradient noise is neglected.*

The equivalent equalizer adaptation is shown in Figure 4.10. This adaptation is stable if and only if

$$\lim_{k \to +\infty} (\mathbf{I} - \eta \mathbf{M})^k = \mathbf{0}. \tag{4.21}$$

where the convergence to zero is taken in the Frobenius norm sense, i.e. $\lim_{k\to+\infty} \|\mathbf{I} - \eta \mathbf{M}^k\|_{\mathrm{F}} = 0$. In such a case the equalizer misadjustment error will be always brought

to zero by the adaptation loop. Equation (4.21) gives a constraint on the matrix $\mathbf{M}$ and the adaptation constant η to ensure stability. In order to express the stability condition (4.21) as a function of $C_2(\Omega)$ few steps are needed.
Let us denote by $\mathbf{N}$ the matrix $\mathbf{I}-\eta\mathbf{M}$. One can easily show that

$$\begin{aligned}\mathbf{N}_{p,q} &= \int_{-1/2T_s}^{1/2T_s}\left(T_s-\eta\frac{1}{T_s^2}\left(\frac{|H|^2}{T}+N_0\right)C(\Omega)C_2^*(\Omega)\right)e^{j2\pi(p-q)T_s\Omega}d\Omega\\ &= \int X(\Omega)e^{j2\pi(p-q)T_s\Omega}d\Omega\end{aligned}$$

where $X(\Omega)=T_s-\eta\frac{1}{T_s^2}\left(\frac{|H|^2}{T}+N_0\right)C(\Omega)C_2^*(\Omega)$.
In order to express the stability condition in terms of $X(\Omega)$ we need to compute $\mathbf{N}^k$ and check when it converges to zero for k going to infinity. For that let us first compute $\mathbf{N}^2$. We have

$$\begin{aligned}\mathbf{N}^2_{p,q} &= \sum_l \mathbf{N}_{p,l}\mathbf{N}_{l,q}=\sum_l\iint X(\Omega_1)e^{j2\pi(p-l)T_s\Omega_1}X(\Omega_2)e^{j2\pi(l-q)T_s\Omega_2}d\Omega_1 d\Omega_2\\ &= \iint X(\Omega_1)X(\Omega_2)e^{j2\pi(pT_s\Omega_1-qT_s\Omega_2)}\sum_l e^{-j2\pi lT_s(\Omega_1-\Omega_2)}d\Omega_1 d\Omega_2.\end{aligned}$$

Now if we make use of $\sum_l e^{-j2\pi l(\Omega_1-\Omega_2)T_s}\simeq\frac{1}{T_s}\sum_l\delta(\Omega_1-\Omega_2-\frac{l}{T_s})$ (this approximation is an equality if N_w is infinite) and take into account the fact that the support of $X(\Omega)$ is in $[\frac{-1}{2T_s},\frac{1}{2T_s}]$, we can write, removing the aliasing terms, i.e. $l\neq 0$,

$$\begin{aligned}\mathbf{N}^2_{p,q} &\simeq \frac{1}{T_s}\iint X(\Omega_1)X(\Omega_2)e^{j2\pi(pT_s\Omega_1-qT_s\Omega_2)}\delta(\Omega_1-\Omega_2)d\Omega_1 d\Omega_2\\ &= \frac{1}{T_s}\int X^2(\Omega_1)e^{j2\pi(p-q)T_s\Omega_1}d\Omega_1.\end{aligned}$$

Following a similar computation one can prove that the kth power of the matrix $\mathbf{N}$ is given by

$$\mathbf{N}^k_{p,q}\simeq\frac{1}{T_s^{k-1}}\int X^k(\Omega)e^{j2\pi(p-q)T_s\Omega}d\Omega.$$

Now one can see that $\lim_{k\to+\infty}\mathbf{N}^k_{p,q}=0\ \forall p,q$ is equivalent to $\frac{|X(\Omega)|}{T_s}<1\ \forall\Omega$. This is equivalent to

$$\left|1-\eta\frac{1}{T_s}\left(\frac{|H|^2}{T}+N_0\right)\frac{C(\Omega)C_2^*(\Omega)}{T_s^2}\right|<1. \tag{4.22}$$

By taking the square of the left hand side and subtracting 1 from both sides, one can prove that the following inequality

$$\eta \frac{1}{T_s}\left(\frac{|H|^2}{T}+N_0\right)\frac{|C(\Omega)||C_2(\Omega)|}{T_s^2} < 2\cos[\varphi_{C_2}(\Omega)-\varphi_C(\Omega)],$$

holds on the bandwidth of c that we denote B_C and define as ($\forall \Omega \notin B_C\ C(\Omega)=0$). The phase responses of $c(t)$ and $c_2(t)$ are denoted by $\varphi_C(\Omega)$ and $\varphi_{C_2}(\Omega)$ respectively.

Chapter 5

Timing Recovery For Data-Dependent Noise Channels

In high density data storage systems, noise becomes highly correlated and data-dependent as a result of media noise and channel nonlinearities. In such environments, conventional timing recovery schemes will exhibit large residual timing jitter and especially data-dependent timing jitter. This chapter presents a new data-aided timing recovery algorithm for data storage systems with data-dependent noise. Based on a data-dependent Gauss-Markov model of the noise, a maximum-likelihood timing recovery scheme is derived. The proposed timing recovery algorithm incorporates data-dependent noise prediction parameters in the form of linear prediction filters and prediction error variances. Moreover, because noise can be nonstationary in practice, an adaptive algorithm is proposed in order to estimate and track the noise prediction parameters. Simulation results, for an idealized optical storage channel incorporating media noise, illustrate the merits of the proposed algorithm.

5.1 Introduction

Timing recovery is one of the critical functions for reliable data detection in digital storage systems. The key problem in timing recovery is the determination of time instants at which the replay signal should be sampled for reliable data recovery. This problem has been a subject of investigation for many decades. Among the existing solutions [86], data-aided (DA) timing recovery schemes, e.g. [20, 88, 91, 127], are known to be more powerful. DA schemes use the transmitted data sequence as side information to facilitate timing recovery. This information is available to the receiver either in the form of a known preamble pattern preceding the user data, or as decisions

taken from the bit detector.

Timing recovery becomes more critical as storage density increases because of increasing system performance sensitivity to timing jitter on the one hand and increasing bandwidth limitations, signal to noise ratio (SNR) degradation, noise nonstationarity and data-dependency on the other hand. Although the problem of data detection in such noise environments has received considerable attention, e.g. see [7] [6], much less attention has been devoted to the problem of timing recovery. Conventional timing recovery schemes assume that the noise at their input is stationary and that noise statistics are independent of the transmitted data. However, in high density storage systems, noise becomes colored and data-dependent [5] [81]. This data-dependent nature of the noise significantly deteriorates the performance of timing recovery. It increases timing jitter, i.e. the difference between the ideal and the estimated sampling instants, for a given bandwidth of the timing recovery loop. Large timing jitter leads to an increased bit-error rate and possibly even to loss of lock.

A simple form of timing recovery for data-dependent noise was reported in literature for optical communication channels where noise was modelled as additive white and Gaussian (AWG) with a noise variance dependent on the transmitted symbol [2]. This algorithm is not based on an optimal timing function but is derived as a modification of the well-known Mueller and Müller algorithm [91].

In this chapter we derive an optimal timing recovery algorithm for data-dependent correlated noise. The key to the new timing recovery approach is the modelling of noise as a data-dependent finite-order Markov process [5]. Based on this model Maximum-Likelihood (ML) timing recovery is addressed. The resulting structure is a timing recovery scheme with a new timing error detector (TED) that incorporates, on the one hand, data-dependent noise prediction and on the other hand a data-dependent weighing that depends on the remaining unpredictable noise variance. Moreover, because in practice noise can be nonstationary, an adaptation algorithm that estimates and tracks noise model parameters is proposed. This estimation algorithm is simpler than that presented in [5].

Although this chapter assumes that the transmitted data is known to the timing recovery scheme, its results can be easily extended to the case where soft information is available [64] and in the context of iterative timing recovery [12] [84] where an iterative soft decoder is used. In fact, this would boil down to simply substituting the TEDs in [64] and [12] with the one presented in this chapter.

The remainder of this chapter is organized as follows. Section 5.2 describes the system model and nomenclature. Section 5.3 presents the ML timing recovery for data-dependent noise. Efficiency analysis of the ML timing recovery is addressed in Section 5.4. Section 5.5 presents a simple sample by sample based adaptation of the data-dependent noise parameters. Simulation results for a partial response maximum-likelihood (PRML) system are presented in Section 5.7 and show the important merits of the new scheme of this chapter.

5.2 System Model and Problem Definition

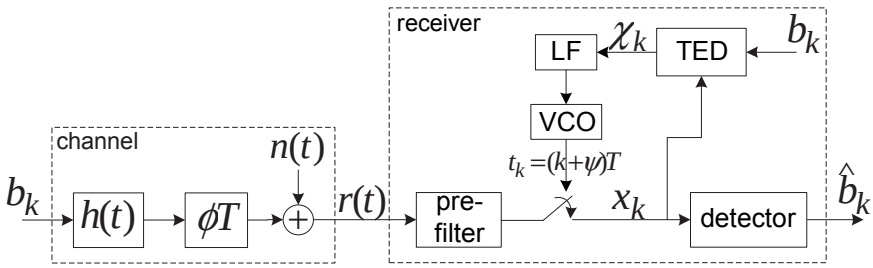

Figure 5.1: *system model*

In Figure 5.1, a zero-mean data sequence $b_k \in \{\pm 1\}$ of length N, i.e. b_1,b_2,...b_N, of data rate $1/T$ is applied to a channel with symbol response $h(t)$, additive noise $n(t)$ and an a priori unknown and possibly time varying delay ϕ (in bit intervals T). Prior to detection, the receiver performs prefiltering that serves to suppress noise and may also condition intersymbol interference (ISI). The prefilter output is first sampled and then passed to a detector that produces bit decisions. For clarity of this chapter, we assume that excess bandwidth at the prefilter output is negligible and consider only baud-rate sampling. The results of this chapter can be easily extended to the over-sampled case. The sampling instants are expressed as $t_k = (k+\psi)T$ where ψ is a sampling phase (normalized in units T). Based on the sampled sequence x_k, the receiver produces bit decisions $\hat{b}_k$ as well as a clock signal that indicates the sampling instants t_k. In order for the detector to operate properly, a timing recovery subsystem ensures that the sampling phase ψ closely approaches ϕ. The timing recovery subsystem takes the form of a phase-locked loop (PLL) with a timing-error detector (TED), loop filter (LF), and a voltage controlled oscillator (VCO). The TED produces an esti-

mate χ_k of the sampling-phase error $\Delta = \phi - \psi$. In this chapter we restrict attention to data-aided (DA) TEDs where b_k is assumed to be available to the receiver in the form of a known preamble, or as decisions, taken from the detector, when bit-error rates are small. PLL behavior depends also on the LF and VCO. A detailed description of this dependence can be found in [45].

To simplify the forthcoming analysis we assume, first, that the timing recovery loop has a sufficiently high bandwidth to enable the variations of ϕ to be tracked. This means that we can take ϕ to be fixed. Second, the sampling-phase errors Δ are restricted to a fraction of a symbol interval T (this reflects the situation when the PLL is in lock; PLL acquisition properties are beyond the scope of this chapter). In this case, the equivalent discrete impulse response q_k^Δ of the system up until the detector input can be linearized as $q_k^\Delta \simeq q_k^0 + \Delta q_k'$, where q_k' is the derivative of q_k^Δ with respect to Δ at $\Delta = 0$. Both responses q_k^0 and q_k' are assumed to be known to the receiver. The detector input sequence can be written as

$$x_k \simeq (q^0 * b)_k + \Delta(q' * b)_k + n_k, \tag{5.1}$$

where `$*$´ denotes linear convolution and n_k is the equivalent noise sequence at the detector input, i.e. $n_k = x_k - (q^\Delta * b)_k$. Unless specified otherwise, we assume that q_k^0 corresponds to the ideal ISI structure assumed by the detector. Any misequalization ISI (linear or nonlinear) at ideal sampling phase, i.e. due to a mismatch between q_k^0 and the ideal detector response, is embedded in the noise n_k. The noise n_k includes also channel noise that may be linearly or nonlinearly data-dependent. The key to the new timing recovery approach is the modelling of the noise as proposed in [5]. We recapitulate the assumptions on the properties of the noise n_k as follows:

1. *Finite correlation length*: The noise n_k is assumed to be independent of past samples before some length $L \geq 0$ (finite Markov memory length). This independence implies that

$$p(n_k | n_{k-1}, ..., n_1, \underline{b}_1^N) = p(n_k | n_{k-1}, ..., n_{k-L}, \underline{b}_1^N) \tag{5.2}$$

   where $p(.)$ denotes the probability density function (pdf) of n_k conditioned on the past noise samples and on the data $\underline{b}_1^N$ where $\underline{b}_{k_1}^{k_2} = [b_{k_1}, b_{k_1+1}, ..., b_{k_2}]$ for $k_2 \geq k_1$. The conditioning on $\underline{b}_1^N$ is meant to take into account the data-dependent correlation of the noise n_k.

2. *Finite data-dependent span*: The noise n_k depends only on its first K-neighbor symbols, i.e. $\underline{b}_{k-K_1}^{k+K_2}$, that we call symbol cluster, where $K = K_1 + K_2 + 1$. The conditioned noise pdf given in Eq. (5.2) becomes

$$p(n_k|n_{k-1},...,n_{k-L},\underline{b}_1^N) = p(n_k|n_{k-1},...,n_{k-L},\underline{b}_{k-L-K_1}^{k+K_2}) \tag{5.3}$$

3. *Joint Gaussian pdf's*: The joint pdf $p(n_k,n_{k-1},...,n_{k-L}|\underline{b}_{k-L-K_1}^{k+K_2})$, conditioned on the data sequence, is Gaussian with a covariance matrix $\mathbf{C}_k = \mathbf{C}(\underline{b}_{k-L-K_1}^{k+K_2})$ of size $(L+1)\times(L+1)$, i.e.

$$p(n_k,...,n_{k-L}|\underline{b}_{k-L-K_1}^{k+K_2}) = \frac{\exp[-\underline{N}_k^{\mathrm{T}}\mathbf{C}_k^{-1}\underline{N}_k]}{\sqrt{(2\pi)^{L+1}\det\mathbf{C}_k}}, \tag{5.4}$$

where $[.]^{\mathrm{T}}$ denotes the transpose operation and the $(L+1)\times 1$ vector $\underline{N}_k = [n_k,...,n_{k-L}]^{\mathrm{T}}$.

It is implicitly assumed here that, given the data sequence, the noise n_k has zero mean. This assumption is not entirely true in general, e.g. in the presence of channel nonlinearities, see [65] and Chapter 1, or in the presence of mis-equalization linear ISI. In such case the vector $\underline{N}_k$ throughout the chapter has to be replaced with $\underline{N}_k - E[\underline{N}_k|\underline{b}_{k-L-K_1}^{k+K_2}]$. For clarity, we omit the mean of n_k in the sequel.

5.3 Maximum-Likelihood Timing-Error Detector

Data-aided ML timing recovery is optimum when no prior statistical knowledge about the phase-error Δ is available. Before developing the DA ML-TED for sample-by-sample timing recovery, let us first derive the one-shot ML estimator of the phase-error Δ based on the observation of the overall detector input sequence x_1,...,x_N. To this aim, we assume in this section that noise statistics are known and fixed during the transmission of the N symbols $\underline{b}_1^N$. The DA ML estimate of the phase-error Δ is obtained by maximizing the likelihood function, i.e.

$$\Delta^{\mathrm{ML}} = \arg\max_{\delta} p(x_1,...,x_N|\underline{b}_1^N,\Delta=\delta), \tag{5.5}$$

over all possible phase-errors δ, where the likelihood function $p(x_1,...,x_N|\underline{b}_1^N,\delta)$ is the joint probability density function of the received samples x_1,...,x_N conditioned on the transmitted symbols $\underline{b}_1^N$ and on the phase-error $\Delta=\delta$.

If prior knowledge on the probability density function of the phase-error Δ is available, than the optimal estimation technique is based on the maximum a posteriori (MAP) criterion. This boils down to replacing the maximization argument in (5.5) by $p(x_1,...,x_N|\underline{b}_1^N,\Delta=\delta)p(\Delta=\delta)$. For simplicity we assume that no such prior information is available, or equivalently, that Δ has a uniform distribution.

In order to derive a practical criterion from (5.5) a few classical steps are needed. We first apply Bayes rule and obtain

$$\begin{aligned} p(x_1,...,x_N|\underline{b}_1^N,\delta) &= p(x_N|x_{N-1},...,x_1,\underline{b}_1^N,\delta)p(x_{N-1},...,x_1|\underline{b}_1^N,\delta) \\ &= \prod_{k=1}^{N} p(x_k|x_{k-1},...,x_1,\underline{b}_1^N,\delta). \end{aligned} \tag{5.6}$$

Then upon invoking (5.1) and the *finite correlation length* property of the noise, i.e. (5.2), (5.6) can be written as

$$p(x_1,...,x_N|\underline{b}_1^N,\delta)=\prod_{k=1}^{N} p(x_k|x_{k-1},...,x_{k-L},\underline{b}_1^N,\delta),$$

which leads by using the *finite data-dependent span* property, i.e. (5.3), to

$$p(x_1,...,x_N|\underline{b}_1^N,\delta)=\prod_{k=1}^{N} p(x_k|x_{k-1},...,x_{k-L},\underline{b}_{k-K_1}^{k+K_2},\delta).$$

Applying Bayes rule once again, (5.6) can then be factorized into

$$p(x_1,...,x_N|\underline{b}_1^N,\delta)=\prod_{k=1}^{N}\frac{p(x_k,x_{k-1},...,x_{k-L}|\underline{b}_{k-L-K_1}^{k+K_2},\delta)}{p(x_{k-1},...,x_{k-L}|\underline{b}_{k-L-K_1}^{k+K_2},\delta)}. \tag{5.7}$$

The right-hand factors in (5.7) can be rewritten using (5.4) as:

$$\frac{p(x_k,..,x_{k-L}|\underline{b}_{k-L-K_1}^{k+K_2},\delta)}{p(x_{k-1},..,x_{k-L}|\underline{b}_{k-L-K_1}^{k+K_2},\delta)} \propto \frac{\exp[-(\underline{E}_k-\delta\underline{S}_k)^{\mathrm{T}}\mathbf{C}_k^{-1}(\underline{E}_k-\delta\underline{S}_k)]}{\exp[-(\underline{e}_k-\delta\underline{s}_k)^{\mathrm{T}}\mathbf{c}_k^{-1}(\underline{e}_k-\delta\underline{s}_k)]}, \tag{5.8}$$

where the $L\times L$ matrix $\mathbf{c}_k$ is the lower principal submatrix of $\mathbf{C}_k$, i.e.

$$\mathbf{C}_k=\begin{bmatrix} \alpha_k & \underline{\nu}_k^{\mathrm{T}} \\ \underline{\nu}_k & \mathbf{c}_k \end{bmatrix}$$

and where the column vectors $\underline{E}_k$, $\underline{e}_k$, $\underline{S}_k$ and $\underline{s}_k$ are given, as function of the error signal $\varepsilon_k=x_k-(q^0*b)_k$ and the so called signature signal $s_k=(q'*b)_k$, by

$\underline{E}_k = [\varepsilon_k, ..., \varepsilon_{k-L}]^{\mathrm{T}}$, $\underline{e}_k = [\varepsilon_{k-1}, ..., \varepsilon_{k-L}]^{\mathrm{T}}$,
$\underline{S}_k = [s_k, ..., s_{k-L}]^{\mathrm{T}}$ and $\underline{s}_k = [s_{k-1}, ..., s_{k-L}]^{\mathrm{T}}$.

The proportionality factor in (5.8) equals $\sqrt{\frac{(2\pi)^L \det \mathbf{c}_k}{(2\pi)^{L+1} \det \mathbf{C}_k}}$ which is independent of δ and thus can be simply ignored. It follows, by taking the logarithm of (5.7) and invoking (5.8), that ML phase-error estimation is obtained by minimizing the following cost function:

$$\Lambda(\delta) = \sum_{k=1}^{N} (\underline{E}_k - \delta \underline{S}_k)^{\mathrm{T}} \mathbf{C}_k^{-1} (\underline{E}_k - \delta \underline{S}_k) - (\underline{e}_k - \delta \underline{s}_k)^{\mathrm{T}} \mathbf{c}_k^{-1} (\underline{e}_k - \delta \underline{s}_k). \tag{5.9}$$

This expression of $\Lambda(\delta)$ is still quite complex in that it involves inversions of the matrices $\mathbf{C}_k$ and $\mathbf{c}_k$ for all possible symbol clusters $\underline{b}_{k-L-K_1}^{k+K_2}$. A simplified expression of $\Lambda(\delta)$ can be derived via the matrix inversion lemma [108]. In fact using this lemma, one can prove that the inverse of $\mathbf{C}_k = \begin{bmatrix} \alpha_k & \underline{\nu}_k^{\mathrm{T}} \\ \underline{\nu}_k & \mathbf{c}_k \end{bmatrix}$ simplifies as

$$\mathbf{C}_k^{-1} = \begin{bmatrix} 0 & 0 \\ 0 & \mathbf{c}_k^{-1} \end{bmatrix} + \frac{1}{\alpha_k - \underline{\nu}_k^{\mathrm{T}} \mathbf{c}_k^{-1} \underline{\nu}_k} \begin{bmatrix} 1 \\ -\mathbf{c}_k^{-1} \underline{\nu}_k \end{bmatrix} \begin{bmatrix} 1 \\ -\mathbf{c}_k^{-1} \underline{\nu}_k \end{bmatrix}^{\mathrm{T}}.$$

This leads to the following simplified version of $\Lambda(\delta)$

$$\Lambda(\delta) = \sum_{k=1}^{N} \frac{1}{\sigma_k^2} (\underline{w}_k^{\mathrm{T}} (\underline{E}_k - \delta \underline{S}_k))^2, \tag{5.10}$$

where the $(L+1) \times 1$ vector $\underline{w}_k = \begin{bmatrix} 1 \\ -\underline{\rho}(\underline{b}_{k-L-K_1}^{k+K_2}) \end{bmatrix}$ and the positive scalar σ_k^2 are given by

$$\begin{cases} \underline{\rho}(\underline{b}_{k-L-K_1}^{k+K_2}) &= \mathbf{c}_k^{-1} \underline{\nu}_k \\ \sigma_k^2 &= \alpha_k - \underline{\nu}_k^{\mathrm{T}} \mathbf{c}_k^{-1} \underline{\nu}_k. \end{cases} \tag{5.11}$$

The complexity to compute $\Lambda(\delta)$ is brought down to $O(N(L+1))$ in (5.10) instead of $O(N(L+1)^2)$ in (5.9). The vectors $\underline{\rho}(\underline{b}_{k-L-K_1}^{k+K_2})$ can be interpreted as data-dependent noise predictors and the values σ_k^2 as noise-prediction variances. In fact, for a given symbol cluster $\underline{b}_{k-L-K_1}^{k+K_2}$, $\underline{w}_k = \underline{w}(\underline{b}_{k-L-K_1}^{k+K_2})$ acts to whiten the noise n_k by substracting from n_k the predicted component from the past noise samples. The variance of the whitened noise, i.e. of $\underline{w}_k^{\mathrm{T}} \underline{N}_k$, equals σ_k^2.

The ML one-shot phase-error estimate Δ^{ML} can be easily derived from (5.10) and is given by

$$\Delta^{\mathrm{ML}} = \frac{1}{\sum_{k=1}^{N} \frac{1}{\sigma_k^2} (\underline{w}_k^{\mathrm{T}} \underline{S}_k)^2} \sum_{k=1}^{N} \frac{1}{\sigma_k^2} (\underline{w}_k^{\mathrm{T}} \underline{E}_k)(\underline{w}_k^{\mathrm{T}} \underline{S}_k). \tag{5.12}$$

The ML phase-error estimate (5.12) can be seen as a normalized average of an instantaneous timing error function given by $\frac{1}{\sigma_k^2}(\underline{w}_k^{\mathrm{T}} \underline{E}_k)(\underline{w}_k^{\mathrm{T}} \underline{S}_k)$. Because, in a PLL based timing recovery scheme, the averaging operation is ensured by the loop filter, the ML timing error detector (ML-TED) can be simply written as

$$\chi_k^{\mathrm{ML}} = \frac{1}{\sigma_k^2} (\underline{w}_k^{\mathrm{T}} \underline{E}_k)(\underline{w}_k^{\mathrm{T}} \underline{S}_k), \tag{5.13}$$

where the vector $\underline{w}_k = \underline{w}(\underline{b}_{k-L-K_1}^{k+K_2})$ and the scalar $\sigma_k^2 = \sigma^2(\underline{b}_{k-L-K_1}^{k+K_2})$ correspond to the cluster $\underline{b}_{k-L-K_1}^{k+K_2}$.

Equation (5.13) presents two interesting properties.

- First, the division with σ_k^2 provides a weighing for every cluster of symbols $b_{k-L-K_1}^{k+K_2}$. The weight of a given cluster is inversely proportional to σ_k^2. More reliable symbol clusters that have smaller 'unpredictable' noise variance will be attributed higher gains in the extraction of timing information than noisy clusters and vice versa.

- Second, the 'predictable' component of n_k from n_{k-1},...,n_{k-L} is removed via the scalar product with $\underline{w}_k$, thus allowing less noise power to be sensed by the timing recovery subsystem. For example, in the extreme case where n_k is a deterministic linear combination of n_{k-1},...,n_{k-L}, the filtered noise $\underline{w}_k^{\mathrm{T}} \underline{N}_k$ is simply zero.

These two properties together make up the strength of the proposed TED.

A block diagram of the ML-TED is shown in Figure 5.2. This TED has attractive practical properties. First, from an implementation standpoint, the proposed TED is quite simple in that it requires only two additional FIR filters of length $(L+1)$ and one division. Second, the causal and minimum phase structure of $\underline{w}_k$ causes the latency of the ML-TED to be small. This limits the increase in the overall delay of the timing recovery loop due to the ML-TED. This property is very crucial in view of the impact of the overall delay of the timing-recovery loop on its stability margin and convergence speed [85].

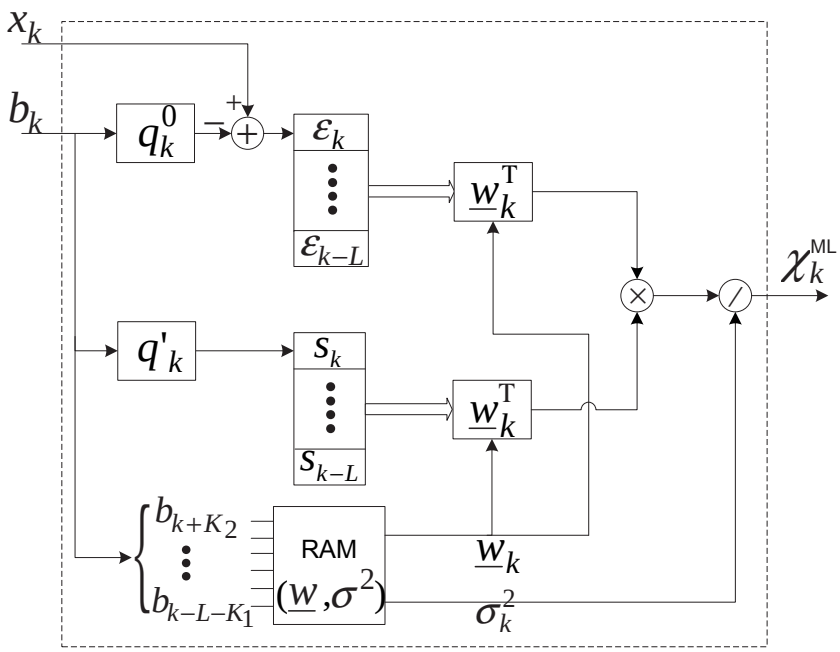

Figure 5.2: *The ML-TED. The vector $\underline{w}_k$ and the variance σ_k^2 are varied as function of the symbol cluster $\underline{b}_{k-L-K_1}^{k+K_2}$.*

Example 5.1 :

In the case of zero-mean additive white and data-independent noise with a variance σ^2, we have $L = 0$, $\sigma_k^2 = \sigma^2$ and $\underline{w}_k = 1$. Equation (5.10) boils down to

$$\Lambda(\delta) = \frac{1}{\sigma^2}\sum_{k=1}^{N}(\varepsilon_k - \delta(q' * b)_k)^2,$$

where $\varepsilon_k = x_k - (q^0 * b)_k$.

The optimum TED in this case is the Zero-Forcing (ZF) TED [86]. Its output, multiplied by σ^2, is given by

$$\chi_k^{ZF} = \varepsilon_k(q' * b)_k. \tag{5.14}$$

Because the ZF-TED achieves maximum-likelihood when noise is data-independent AWGN, we consider, throughout this chapter, the ZF-TED as baseline of comparison.$\diamondsuit$

Example 5.2 :

As explained in Chapter 1, media noise is one of the most important disturbances in optical storage. This is modelled for rewritable systems as a data-dependent AWGN

noise process m_k that is injected at the channel input. The variance of m_k, denoted by $\sigma_m^2(b_k)$, is dependent on the bit b_k.

At ideal sampling the noise component n_k of (5.1) equals $n_k = (q^0 * m)_k$. Assuming that the channel is invertible, i.e. that q_k^0 does not have spectral nulls, and has a minimum phase, it can be easily shown that $\underline{w}_k$ is data independent and is given by $(w * q^0)_k = \delta_k$ where δ_k denotes the Kronecker delta function. The variance of the whitened noise $(w * n)_k$ equals $\sigma_m^2(b_k)$. The ML-TED (5.13) simplifies in this case to

$$\chi_k^{\mathrm{ML}} = \frac{((w * x)_k - b_k)(c * b)_k}{\sigma_m^2(b_k)},$$

where c_k is the impulse response of the discrete derivative, i.e. $c_k = \frac{(-1)^k}{k}$, for $k \neq 0$ and $c_0 = 0$. The filtering with w_k achieves full equalization of the channel and the factors $1/\sigma_m^2(b_k)$ makes the loop gain higher for the less noisy bits.$\diamondsuit$

5.4 Efficiency of Data-Dependent Timing Recovery

The objective of any timing error detector is to provide an indication of the phase-error present at the detector input. The capability of the timing recovery loop to track fast timing variations depends heavily on how much timing information the TED can extract from the incoming signal, while rejecting the noise as much as possible. Good noise suppression requires the loop bandwidth to be as small as possible, whereas a wide bandwidth is required in order to track fast timing variations. In order to quantify this trade-off, a measure of efficiency was introduced in [87]. The efficiency of a TED was defined as the amount of the timing information that the TED is able to extract from the incoming signal per unit of time and SNR. In this section we extend the efficiency analysis of [87] to the ML-TED and show that this efficiency exceeds that of the ZF-TED.

The ML-TED (5.12) can be linearized as indicated in Figure 5.3 where

$$K_d(\underline{b}) \;=\; \frac{(\underline{w}(\underline{b})^T \underline{S}(\underline{b}))^2}{\sigma^2(\underline{b})}$$

denotes the TED gain and $v_k(\underline{b})$ is the TED additive noise which induces jitter in the PLL. Both quantities are symbol cluster dependent. The TED noise and average gain

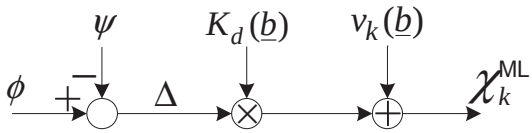

Figure 5.3: *Phase-domain model of the ML-TED. The TED gain $K_d(\underline{b})$ and additive noise $v_k(\underline{b})$ are dependent on the symbol cluster $\underline{b} = \underline{b}_{k-L-K_1}^{k+K_2}$.*

can be written as

$$\begin{cases} K_d &= E_{\underline{b}}\left[\frac{(\underline{w}(\underline{b})^T\underline{S}(\underline{b}))^2}{\sigma^2(\underline{b})}\right] \\ v_k &= \frac{(\underline{w}_k^T\underline{S}_k)(\underline{w}_k^T\underline{N}_k)}{\sigma_k^2} \end{cases} \tag{5.15}$$

where $E_{\underline{b}}[.]$ denotes averaging over all possible symbol clusters $\underline{b}$ of length K_1+K_2+L+1 and where, for clarity, the two equivalent notations $\underline{X}(\underline{b}_{k-L-K_1}^{k+K_2})$ and $\underline{X}_k$ are used.

The efficiency of a TED was defined in [87] as

$$\gamma = \frac{1}{\mathrm{SNR}}\frac{K_d^2}{\mathcal{V}(0)},$$

where $\mathcal{V}(0)$ is the power spectral density of v_k at DC. Invoking (5.15) and remarking that $\underline{w}_k^T\underline{N}_k$ is white with variance σ_k^2, the expression of the ML-TED efficiency can be simplified as

$$\gamma^{\mathrm{ML}} = \frac{1}{\mathrm{SNR}}E_{\underline{b}}\left[\frac{(\underline{w}(\underline{b})^T\underline{S}(\underline{b}))^2}{\sigma^2(\underline{b})}\right]. \tag{5.16}$$

This efficiency does not only include a measure of the high frequency spectrum of the transmitted data, i.e. $E[s_k^2] = \int(2\pi\Omega)^2|Q(e^{j2\pi\Omega})|^2\mathcal{A}(e^{j2\pi\Omega})d\Omega$ where Q denotes the Fourier transform of q_k^0 and $\mathcal{A}$ is the data power spectral density, but does also include a measure of how noisy every symbol cluster is. The efficiency γ^{ML} can be seen as the average of a per-cluster efficiency $\gamma(\underline{b}) = \frac{1}{\mathrm{SNR}}\frac{(\underline{w}(\underline{b})^T\underline{S}(\underline{b}))^2}{\sigma^2(\underline{b})}$. Good symbol clusters for timing recovery are clusters $\underline{b}$ for which $\gamma(\underline{b})$ is maximized. This result can be exploited to design optimal preamble patterns. This must be subject to maximizing the average per-cluster efficiency over all possible clusters in the preamble pattern, i.e. $E_{\underline{b}\in\mathrm{preamble}}[\gamma(\underline{b})]$.

Example 5.3 :

For the sake of comparison between the ZF-TED and the ML-TED, let us consider

the case when the noise n_k is white, i.e. $L = 0$, but with a data-dependent variance $\sigma^2(\underline{b})$. The ML-TED efficiency simplifies then to

$$\gamma^{\mathrm{ML}} = \frac{1}{\mathrm{SNR}} E_{\underline{b}} \left[\frac{s_k^2}{\sigma^2(\underline{b})} \right].$$

The ZF-TED has a gain $K_d = E_{\underline{b}}[s_k^2]$ and noise $v_k = s_k n_k$. Its efficiency in this case can be written as

$$\gamma^{ZF} = \frac{1}{\mathrm{SNR}} \frac{E_{\underline{b}}[s_k^2]^2}{E_{\underline{b}}[s_k^2 \sigma^2(\underline{b})]}.$$

Now using the Cauchy-Schwarz inequality, it is easy to prove that

$$\gamma^{\mathrm{ML}} \geq \gamma^{\mathrm{ZF}},$$

with equality only when the noise variance is data-independent, i.e. $\sigma^2(\underline{b}) = \mathrm{C}^{\mathrm{st}}$.

For the sake of illustration, let us consider, in this example, the simplifying case where the data is uncoded and the noise variance of the symbol cluster $\underline{b}_{k-K_1}^{k+K_2}$ is only dependent on the central bit b_k, i.e. $\sigma^2(\underline{b}_{k-K_1}^{k+K_2}) = \sigma^2(b_k)$.
The efficiency of the ML-TED simplifies in this case to $\gamma^{\mathrm{ML}} = \frac{1}{\mathrm{SNR}} E_{\underline{b}}[s_k^2] E_{\underline{b}} \left[\frac{1}{\sigma^2(b_k)} \right]$ because s_k is independent of b_k due to the fact that $q_0' = 0$. Similarly, the ZF-TED efficiency can be written as $\gamma^{\mathrm{ZF}} = \frac{1}{\mathrm{SNR}} \frac{E_{\underline{b}}[s_k^2]}{E_{\underline{b}}[\sigma^2(b_k)]}$. The gain in efficiency brought by the ML-TED over the ZF-TED can be expressed as function of $\beta = \sigma^2(-1)/\sigma^2(1)$ as follows

$$\frac{\gamma^{\mathrm{ML}}}{\gamma^{\mathrm{ZF}}}(\beta) = E\left[1/\sigma^2(b_k)\right] E[\sigma^2(b_k)] = \frac{1}{4}\left(2 + \beta + \frac{1}{\beta}\right).$$

Figure 5.4 shows this gain as function of β. It shows in particular that for $\beta >> 1$ or $\beta << 1$ a substantial improvement in efficiency is obtained using the ML-TED compared to the ZF-TED. For $\beta >> 1$ we have $\frac{\gamma^{\mathrm{ML}}}{\gamma^{\mathrm{ZF}}} \propto \beta$ and $\frac{\gamma^{\mathrm{ML}}}{\gamma^{\mathrm{ZF}}} \propto \frac{1}{\beta}$ for $\beta << 1$.$\diamondsuit$

5.5 Adaptive Data-Dependent Noise Characterization

In the previous section, we assumed that $\underline{w}(\underline{b}_{k-L-K_1}^{k+K_2})$ and $\sigma^2(\underline{b}_{k-L-K_1}^{k+K_2})$ are known for all symbol clusters. However, the statistics of the noise are not known in practice and need to be estimated from the received signal. Moreover, tracking these statistics adaptively is preferable in many applications because the noise may be nonstationary. This section presents an estimation scheme of the noise model parameters.

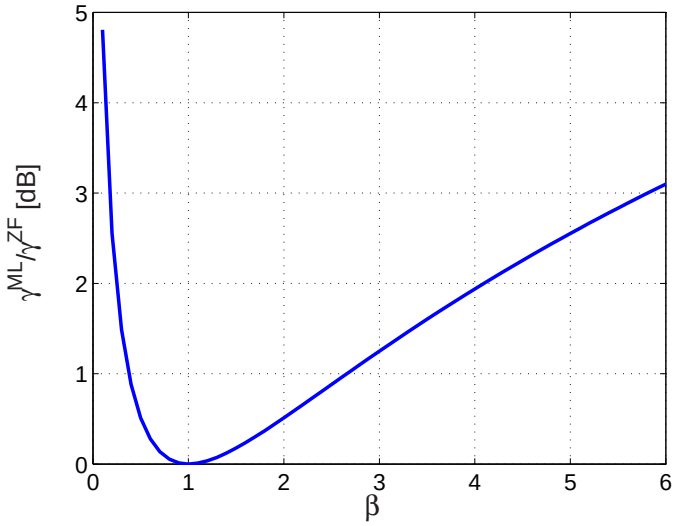

Figure 5.4: *The gain in efficiency of the ML-TED over the ZF-TED as function of* $\beta = \sigma^2(-1)/\sigma^2(1)$*, for the case that data is uncoded and* $L = K_1 = K_2 = 0$ *as considered in the illustration of* Example 5.3.

The noise model parameters, $\underline{w}(\underline{b}_{k-L-K_1}^{k+K_2}) = \begin{bmatrix} 1 \\ -\underline{\rho}(\underline{b}_{k-L-K_1}^{k+K_2}) \end{bmatrix}$ and $\sigma^2(\underline{b}_{k-L-K_1}^{k+K_2})$, are given by equation (5.11) for every cluster of symbols $\underline{b}_{k-L-K_1}^{k+K_2}$. This can be written as

$$\begin{bmatrix} \alpha_k & \underline{\nu}_k^{\mathrm{T}} \\ \underline{\nu}_k & \mathbf{c}_k \end{bmatrix} \begin{bmatrix} 1 \\ -\underline{\rho}_k \end{bmatrix} = \begin{bmatrix} \sigma_k^2 \\ 0 \end{bmatrix}$$

where $\underline{\rho}_k = \underline{\rho}(\underline{b}_{k-L-K_1}^{k+K_2})$. Which is interpreted as the data-dependent version of the well known Yule-Walker equations encountered in autoregressive modelling problems [5, 136]. The estimation of the noise model parameters can be based on first estimating, for all symbol clusters $\underline{b}$, the covariance matrices $\mathbf{C}(\underline{b})$ and then deriving the vectors $\underline{w}(\underline{b})$ and the variances $\sigma^2(\underline{b})$ via solving the different Yule-Walker equations for the different data clusters [5]. This means that at every estimation of one $\underline{w}(\underline{b})$ a covariance matrix needs to be inverted which can be prohibitively complex especially for high values of L.

A simpler alternative that does not involve estimating and inverting the covariance matrices can be proposed. In fact, as mentioned in Section 5.3, the scalar product with

$\underline{w}(\underline{b}_{k-L-K_1}^{k+K_2}) = \begin{bmatrix} 1 \\ -\underline{\rho}(\underline{b}_{k-L-K_1}^{k+K_2}) \end{bmatrix}$ is meant to whiten the noise samples n_k,...,n_{k-L}, for the symbol cluster $\underline{b}_{k-L-K_1}^{k+K_2}$, and $\sigma^2(\underline{b}_{k-L-K_1}^{k+K_2})$ is the variance of the whitened noise. Thus a scheme to estimate and track the prediction vector $\underline{\rho}(\underline{b}_{k-L-K_1}^{k+K_2})$ can be simply based on minimizing $E[(\underline{w}_k^T \underline{N}_k)^2]$. It is a simple exercise to prove that this estimation is unbiased. In order to minimize $E[(\underline{w}_k^T \underline{N}_k)^2] = E[(n_k - \underline{\rho}_k^T \underline{n}_k)^2]$, where $\underline{n}_k = [n_{k-1}, ..., n_{k-L}]^{\mathrm{T}}$, a least mean square (LMS) type of algorithm can be adopted. This consists of updating $\underline{\rho}_k$ in the opposite direction of the gradient of $E[(\underline{w}_k^T \underline{N}_k)^2]$ and replacing the expectation of $(\underline{w}_k^T \underline{N}_k)^2$ by its instantaneous realization. The variance σ_k^2 is then simply the variance of the whitened noise, i.e. $\sigma_k^2 = E[(\underline{w}_k^T \underline{N}_k)^2] = E[(\underline{w}_k^T \underline{N}_k)(n_k - \underline{\rho}_k^T \underline{n}_k)]$, which can be written as

$$\sigma_k^2 = E[(\underline{w}_k^T \underline{N}_k) n_k]$$

because the estimation of $\underline{\rho}_k$ acts to force $E[(\underline{w}_k^T \underline{N}_k)(\underline{\rho}_k^T \underline{n}_k)]$ to zero.

The overall estimation scheme is shown in Figure 5.5. At every clock cycle, one prediction vector $\underline{\rho}(\underline{b}_{k-L-K_1}^{k+K_2})$ and one variance $\sigma^2(\underline{b}_{k-L-K_1}^{k+K_2})$ are adapted. The adaptation of the prediction vector is based on the LMS technique as explained earlier. The adaptation of $\underline{\rho}(\underline{b}_{k-L-K_1}^{k+K_2})$ and estimation of $\sigma^2(\underline{b}_{k-L-K_1}^{k+K_2})$ are given by:

$$\begin{aligned} \underline{\rho}(\underline{b})^{\mathrm{new}} &= \underline{\rho}(\underline{b})^{\mathrm{old}} + \mu_\rho (\underline{w}^{\mathrm{old}}(\underline{b})^{\mathrm{T}} \underline{N}_k) \underline{n}_k \\ \sigma^2(\underline{b})^{\mathrm{new}} &= (1-\mu_{\sigma^2})\sigma^2(\underline{b})^{\mathrm{old}} + \mu_{\sigma^2} (\underline{w}^{\mathrm{old}}(\underline{b})^{\mathrm{T}} \underline{N}_k) n_k, \end{aligned} \tag{5.17}$$

where μ_ρ and μ_{σ^2} denote the adaptation constants for the adaptation of $\underline{\rho}(\underline{b}_{k-L-K_1}^{k+K_2})$ and estimation of $\sigma^2(\underline{b}_{k-L-K_1}^{k+K_2})$, $\underline{n}_k = [n_{k-1}, ..., n_{k-L}]^{\mathrm{T}}$ and $\underline{b} = \underline{b}_{k-L-K_1}^{k+K_2}$.

In practice, n_k is not available to the receiver and the adaptation of the prediction parameters has to be based on the error signal ε_k. In this case, one would like to ensure a proper dimensioning of the timing recovery loop. In fact, in order to ensure that average TED gain is well defined, one must include in the characterization of the prediction parameters, used by the ML-TED, a constraint on the average TED gain. A simple solution to this issue is presented in Section 5.6.

5.6 Dimensioning of the ML timing recovery loop

We described in Section 5.3 the ML-TED (5.13). This TED uses knowledge about noise in the form of a data-dependent whitening vector $\underline{w}_k^{\mathrm{T}} = \underline{w}^{\mathrm{T}}(\underline{b}_{k-L-K_1}^{k+K_2})$ and whitened

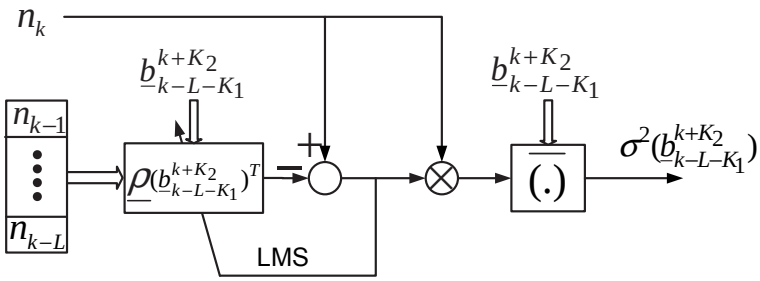

Figure 5.5: *Adaptation of* $\underline{\rho}(\underline{b}_{k-L-K_1}^{k+K_2})$ *and estimation of* $\sigma^2(\underline{b}_{k-L-K_1}^{k+K_2})$. *The averaging* $\overline{(.)}$ *is symbol cluster dependent.*

noise variance $\sigma^2(\underline{b}_{k-L-K_1}^{k+K_2})$. The characterization of the whitening vector and whitened noise variance was presented in Section 5.5. This characterization does not involve any constraint on the TED gain and thus the overall gain of the timing recovery loop is 'ill-defined'. However, for proper dimensioning of the timing recovery loop, one would like to have a controlled TED gain. This section describes how noise characterization (5.17) can be modified to include a constraint on the TED gain.

Figure 5.3 describes the phase-domain model of the TED of (5.13) where the TED gain is given by

$$K_d(\underline{b}_{k-L-K_1}^{k+K_2}) = \frac{(\underline{w}(\underline{b})^{\mathrm{T}}\underline{S}(\underline{b}))^2}{\sigma^2(\underline{b})},$$

and the TED noise $v_k(\underline{b}_{k-L-K_1}^{k+K_2})$ is given by

$$v_k(\underline{b}_{k-L-K_1}^{k+K_2}) = \frac{(\underline{w}(\underline{b})^{\mathrm{T}}\underline{N}_k)(\underline{w}(\underline{b})^{\mathrm{T}}\underline{S}(\underline{b}))}{\sigma^2(\underline{b})}.$$

The average TED gain $\overline{K_d}$ is defined as the average of $K_d(\underline{b})$ over all possible symbol clusters, i.e.

$$\begin{aligned} \overline{K_d} &= \textstyle\sum_{\underline{b}} p(\underline{b}) K_d(\underline{b}) \\ &= \textstyle\sum_{\underline{b}} p(\underline{b}) \frac{(\underline{w}(\underline{b})^{\mathrm{T}}\underline{S}(\underline{b}))^2}{\sigma^2(\underline{b})}, \end{aligned} \tag{5.18}$$

where $p(\underline{b})$ is the probability of occurrence of the symbol cluster $\underline{b}$. This probability depends only on the coding scheme and is assumed to be known a priori.

In order to constrain the average TED gain (5.18) to a fixed value, e.g. 1, while characterizing the data-dependent noise, the variances $\sigma^2(\underline{b})$ for all symbol clusters $\underline{b}$ must be scaled with the same value such that $\overline{K_d} = 1$. The adaptation of $\underline{\rho}(\underline{b})$

(equivalently $\underline{w}(\underline{b})$) is unchanged and is given by (5.17). The estimation of $\sigma^2(\underline{b})$ is modified to

$$\begin{aligned} \lambda &= \textstyle\sum_{\underline{b}' \in I} p(\underline{b}') \frac{(\underline{w}^{\text{old}}(\underline{b}')^{\text{T}} \underline{S}(\underline{b}'))^2}{\sigma^{2^{\text{old}}}(\underline{b}')} \\ \sigma^{2^{\text{new}}}(\underline{b}) &= (1-\mu_{\sigma^2})\sigma^{2^{\text{old}}}(\underline{b}) + \mu_{\sigma^2}\lambda(\underline{w}^{\text{old}}(\underline{b})^{\text{T}} \underline{N}_k) n_k, \end{aligned} \tag{5.19}$$

where we introduced the data-independent variable λ in order to force $\overline{K_d}$ to 1.

In order to reduce implementation complexity, the variable λ can be computed on a subset I of symbol clusters (not necessary all symbol clusters). In this case $p(\underline{b})$ must be normalized such that $\sum_{\underline{b}' \in I} p(\underline{b}') = 1$. The variable λ needs to be updated only if the prediction parameters of one of the symbol clusters of I is updated.

In practice the set I may be chosen to contain few symbol clusters. A particular case is $I = \{\underline{b}_0\}$, where the TED gain is then constrained to be unity for the symbol cluster $\underline{b}_0$. This is of interest when the symbol cluster $\underline{b}_0$ is often present in the transmitted data, e.g. part of a preamble sequence. In this case, λ is computed as

$$\lambda = \frac{(\underline{w}(\underline{b}_0)^{\text{T}} \underline{S}(\underline{b}_0))^2}{\sigma^2(\underline{b}_0)}$$

and needs to be recomputed only if $\underline{w}(\underline{b}_0)$ or $\sigma^2(\underline{b}_0)$ are changed. Note that $\underline{w}(\underline{b}_0)^{\text{T}} \underline{S}(\underline{b}_0)$ is computed in the TED (5.13) and thus does not require any extra circuitry.

5.7 Simulation Results For a PRML System

Receivers for PRML systems typically use a linear equalizer followed by a Viterbi detector (VD), see Chapter 1. The equalizer aims at shaping the channel response h_k to an acceptably shorter target response g_k in order to limit the implementation complexity of the detector. A discrete-time model of a PRML system is shown in Figure 5.6.

By way of illustration we consider run-length-limited data with run-length parameters $(\text{d}, \text{k}) = (1, 7)$ transmitted over an idealized optical storage channel according to the Braat-Hopkins model [42]

$$H(\Omega) = \begin{cases} \frac{2T}{\pi} \frac{\sin(\pi\Omega)}{\pi\Omega} \left(\cos^{-1} |\frac{\Omega}{\Omega_c}| - \frac{\Omega}{\Omega_c} \sqrt{1 - (\frac{\Omega}{\Omega_c})^2} \right), & |\Omega| < \Omega_c, \\ 0, & |\Omega| \geq \Omega_c. \end{cases}$$

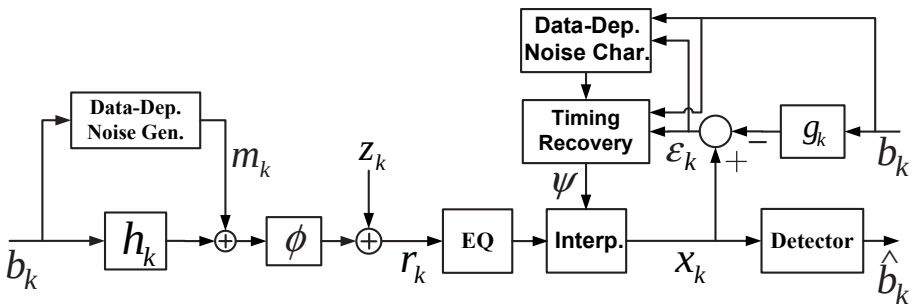

Figure 5.6: *A discrete-time model of a PRML system including a data-dependent noise generator.*

where Ω_c denotes the optical cut-off frequency normalized to the baud frequency, fixed at $1/3$ in the sequel. These choices reflect the system described in [115]. The channel output is corrupted by two different noise components. The first one is data-dependent noise m_k (media noise) and the second noise component is additive white Gaussian noise z_k (electronic noise) with zero mean and variance σ_z^2. As explained in Chapter 1, media noise can be equivalently seen as if the pits on the disc represent fuzzy ones, i.e. values of the form $1+u_k$. The lands, representing -1 on the disc, are not hampered by media noise. The data-dependent noise m_k results then from a noise source u_k that is injected at the channel input, i.e. $m_k = (h*u)_k$. The noise u_k is modelled as additive white Gaussian noise with a variance that depends on the bit b_k, $\sigma_{u,-1}^2 = 0$ for $b_k = -1$ and $\sigma_u^2 = \sigma_{u,1}^2 \neq 0$ for $b_k = 1$. Two SNR measures are defined: a signal to media noise ratio (SMNR) and a signal to additive noise ratio (SANR) given by

$$\text{SMNR} = \frac{2}{\sigma_u^2} \quad \text{and} \quad \text{SANR} = \frac{\sum_k h_k^2}{\sigma_z^2}.$$

The channel output is subject to a delay ϕ as shown in Figure 5.6. The channel output r_k is first filtered by the equalizer and then interpolated at a delay $-\psi$ where ψ is provided by the timing recovery subsystem. The interpolator is implemented via a six-tap Lagrange filter [110]. The equalized and interpolated signal x_k is subtracted from a reference signal $(g*b)_k$ to produce an error signal ε_k where g_k denotes the detector target response. This error signal is used by the timing recovery subsystem to adjust the interpolation phase and by the noise characterization block to estimate the noise prediction parameters. The 5-tap target response $g = [0.17, 0.5, 0.67, 0.5, 0.17]$ and a 9-tap equalizer are used. Bit detection is implemented via a Viterbi detector.

Because of the d=1 constraint, the number of states in the Viterbi trellis reduces to 10 which is standard for nowadays optical storage systems.

Before comparing the new timing recovery algorithm with the ZF algorithm, a few steps are needed. First, the equalizer taps are trained using the LMS algorithm at $\phi = \psi = 0$ and noise characterization is achieved as explained in Section 5.5. The noise characterization parameters are fixed to $L = 3$ and $K_1 = K_2 = 1$. Second, a calibration process is used in order to ensure that both the ZF-TED and the ML-TED have the same open-loop gain. To this aim, we fix ϕ at a given value and normalize the ML-TED and the ZF-TED such that their open-loop average output equals Δ.

The open-loop characteristics of both the ZF and the ML TEDs after calibration are shown in Figure 5.7 for the case where media noise is dominant, e.g. SMNR=12 dB and SANR=16 dB. The left plot shows the average of the open-loop TED output χ_k where it is apparent that after calibration, both ZF and ML TEDs have the same gain especially near $\Delta = 0$. However, as shown in the right plot of Figure 5.7, the variance of χ_k for the ZF-TED is always higher than that of the ML-TED. The reduction in the variance of the open-loop TED output amounts in this case to around 2.5 dB at $\Delta = 0$. One should recall that in closed-loop and when the PLL is in tracking mode, only the TED behavior for $\Delta \simeq 0$ matters. The increase in the open-loop noise variance around $\Delta = 0.5$ can be explained by the fact that the first order approximation of x_k as function of Δ given in (5.1) holds only for $\Delta \simeq 0$.

The gain in the open-loop TED variance depends obviously on SANR and SMNR. This gain as function of SANR and SMNR follows the same trend as the gain in timing jitter in closed-loop simulations. This is the subject of the next paragraph.

In order to assess the performance gain of the ML-TED over the ZF-TED in closed-loop as function of SMNR and SANR, we force the delay ϕ to be a step function of time, i.e. $\phi_k = 0$ for $k < k_0$ and $\phi_k = 0.1$ for $k \geq k_0$ where the timing recovery loop is closed at $k = k_0$. The loop filter parameters, i.e. natural frequency w_n and damping factor ζ, are optimized in order to achieve the best BER. This optimization was carried out at SANR=SMNR=16 dB. The optimal BER was achieved for $w_n = 0.03$ and $\zeta = 2$. Because optimization of the loop filter parameters at different values of SANR and SMNR did not show any important performance improvement, we simply fix the loop filter parameters throughout the simulations.

A first measure to estimate the performance of a timing recovery scheme is the timing jitter defined as the interpolation phase-error variance, i.e. $\sigma_\Delta^2 = E[(\phi - \psi)^2]$.

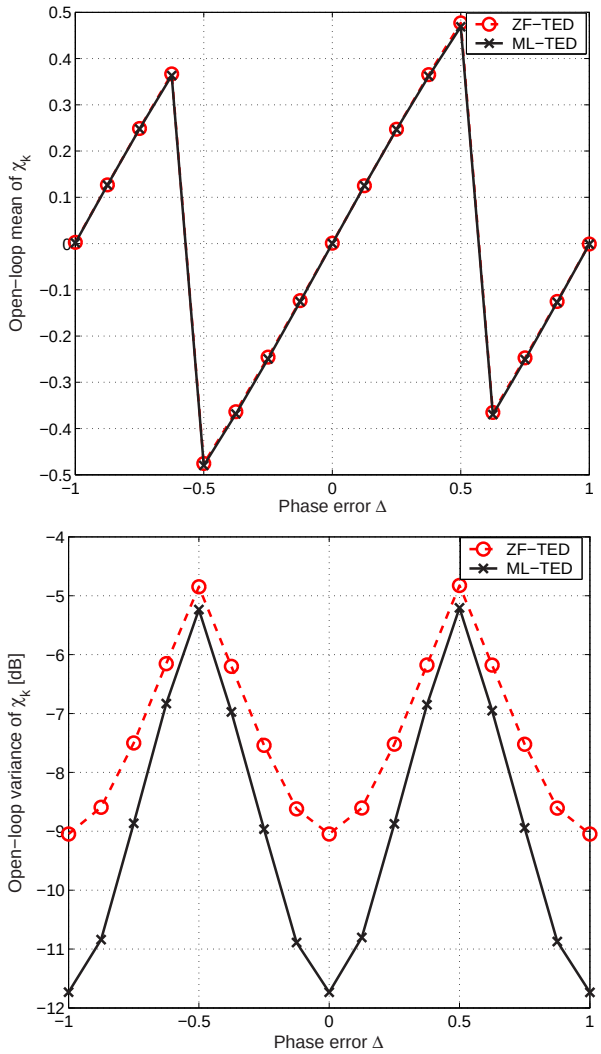

Figure 5.7: *Open-loop characteristics of the ZF and ML TEDs at SMNR=12 dB and SANR=16 dB.*

Figure 5.8 shows timing jitter as function of SMNR for different values of SANR for the ZF and the ML timing recovery schemes. First, it is apparent that the ML timing recovery is always superior to the ZF timing recovery. Second, the gain of the new scheme over the ZF scheme is highly dependent on the ratio of SMNR and SANR. For a given SANR, the gain is higher at low SMNR and vice versa. This gain goes from 0.3 dB at SANR=10 dB and SMNR=22 dB to around 2.5 dB for SANR=16 dB and SMNR=12 dB. This is in accordance with the open-loop gain in TED output

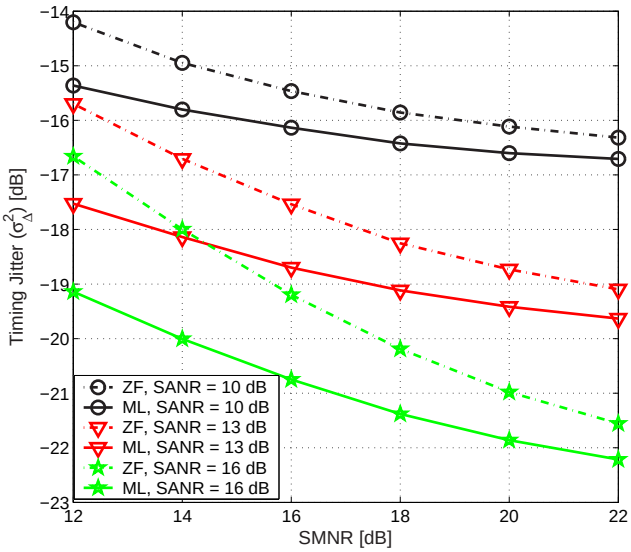

Figure 5.8: *Timing jitter as function of SMNR for different values of SANR.*

variance around $\Delta = 0$ shown in Figure 5.7.

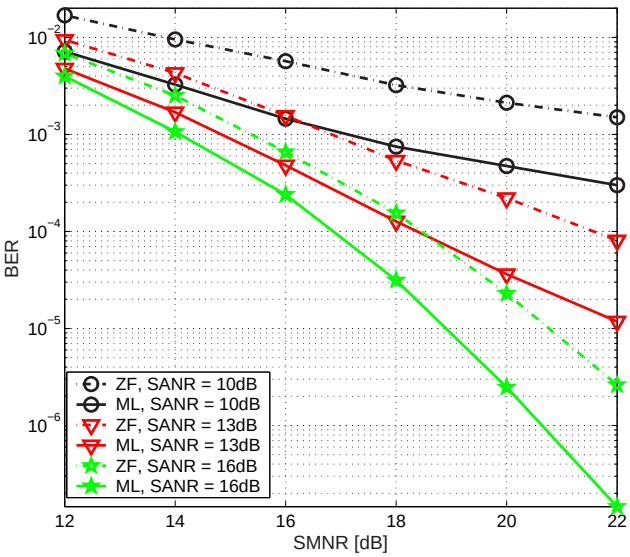

Figure 5.9: *Simulated BER as function of SMNR for different values of SANR.*

In terms of BER, Figure 5.9 shows simulated BER as function of SMNR for different values of SANR. At low SANR values, e.g. SANR=10 dB, the BER curve

is not a steep function of SMNR and thus a little gain in timing jitter translates into a big gain in SMNR, e.g. 6 dB gain at BER $= 10^{-3}$. At high SANR values, e.g. SANR=16 dB, the BER is mainly determined by the data-dependent media noise. For this reason, a substantial gain in timing jitter does not translate directly into a relatively big gain in BER. Still, a gain of more than 1 dB in SMNR is achieved at BER $= 10^{-3}$. At higher SMNR values the impact of timing jitter is much more visible and the new timing recovery scheme allows a gain of 2 dB in SMNR.

5.8 Conclusions

In this chapter a new timing recovery algorithm for storage channels with data-dependent noise was presented. Based on a Gauss-Markov correlated noise model, a maximum-likelihood timing recovery algorithm was derived and analyzed. The new algorithm incorporates, on the one hand, data-dependent noise prediction and on the other hand a data-dependent weighing. The noise prediction aims at whitening the data-dependent noise and the weighing makes the gain of the timing error detector data-dependent, i.e. smaller gain for noisier data patterns and vice versa. Moreover, because in practice noise can be nonstationary, a simple adaptation scheme is proposed to estimate and track the noise prediction parameters. Simulation results for a partial response maximum-likelihood system show that the proposed algorithm allows significant improvements in performance in the presence of data-dependent noise.

Chapter 6

Equalizing Sampling Rate Converter

Data receivers for storage systems normally operate at a fixed sampling rate $1/T_s$ that is asynchronous to the baud rate $1/T$. A sampling-rate converter (SRC) serves to convert the incoming signal from the asynchronous to the synchronous clock domain. These receivers also contain an equalizer that serves to suppress or condition intersymbol interference and noise. To limit receiver complexity, the equalization burden can be shifted partially towards the SRC. This possibility is not exploited in any existing SRC. This chapter presents SRC design methods that combine group delay flatness and out-of-band rejection criteria with the minimum mean square error equalization criterion. Numerical examples for an idealized optical storage channel validate the design methods.

6.1 Introduction

Receivers for data storage systems are often realized with the aid of digital IC technology. To profit optimally from the rapid advances of this technology, analog-to-digital conversion is ideally performed early on in the receiver. A common baseband topology for existing storage systems is depicted in Figure 6.1. A replay signal $r(t)$ is applied to an analog low-pass filter (LPF) which suppresses out-of-band noise. The LPF output is digitized by an analog-to-digital converter (ADC) which operates at a crystal-controlled free-running frequency $1/T_s$ that is high enough to prevent aliasing. The ADC output is applied to an equalizer (EQ) which conditions intersymbol interference (ISI) and noise. The equalizer operates at the sampling rate $1/T_s$, i.e asynchronously to the baud rate $1/T$ [21]. It is controlled by an adaptation scheme that is not depicted for simplicity. Asynchronous equalizer adaptation is treated in

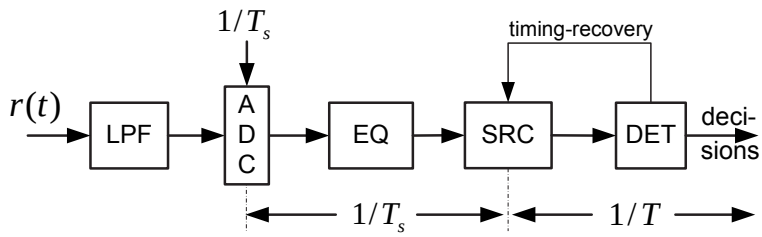

Figure 6.1: *Baseband receiver with asynchronous equalizer. Asynchronous and synchronous clock domains are indicated with the symbols* $1/T_s$ *and* $1/T$*, respectively.*

Chapter 4. A sampling-rate converter (SRC) [86], which forms part of a timing-recovery loop, produces an equivalent synchronous output which serves as the input of a bit detector (DET). Rather than placing the equalizer before the SRC, it would be possible to reverse their order. That would, however, cause the latency of the equalizer to contribute to the overall delay of the timing-recovery loop, thus significantly lowering its stability margin and attainable acquisition speed [85]. Also, the sampling rate $1/T_s$ can be lower than the baud rate $1/T$ whenever the channel has negative excess bandwidth. This is so, for example, in existing optical storage systems, e.g. DVD, Blu-Ray Disc. In such cases the asynchronous equalizer can have fewer taps and a lower operating speed than its synchronous counterpart, thereby lowering complexity and power dissipation.

At the heart of the SRC is an interpolation filter that mimics fractional delays, i.e. delays of a fraction μ of the sampling interval T_s. A shift register that precedes the interpolation filter produces an additional integer delay m, and the overall delay $\tau = (m+\mu)T_s$ is re-determined at every symbol interval by the timing-recovery subsystem [86].

Design of the interpolator filter is a compromise between complexity and interpolation accuracy. Conventionally, this accuracy has two complementary aspects. First, the filter should mimic a fractional delay, i.e. its group delay characteristics should be almost flat. Second, the filter should introduce as little amplitude distortion as possible. This generally requires a long filter. These requirements only pertain to the pass-band of the storage channel, i.e. the range of frequencies in which actual data information is received. Outside that range the interpolator filter should ideally exhibit a large attenuation, and its group delay characteristics become irrelevant.

The equalizer (EQ) in Figure 6.1 is complementary to the SRC in that it is con-

ventionally meant to counteract all amplitude distortion as well as all phase distortion except for pure delays. In practice, digital storage channels have a nominal behavior that is relatively well known [86]. For this reason it is, in principle, possible to compensate for the nominal channel characteristics (amplitude as well as phase) within the SRC. This would relieve, and thereby simplify, the equalizer in that it would now only have to deal with variations of the actual channel characteristics relative to the nominal ones. Moreover, it should also simplify the interpolator filter in that it no longer requires a very flat amplitude characteristic and a steep transition between pass-band and stop-band. Hence, by shifting a part of the burden of the equalizer towards the SRC both blocks will be made simpler.

Because interpolation filters and anti-aliasing filters constitute the heart of any practical SRC, the remainder of this chapter is divided into two main sections. Section 6.2 describes the design of equalizing interpolators. Section 6.3 treats the problem of designing equalizing anti-aliasing filters.

6.2 Equalizing Interpolator

In order to explain the principle and the design of an equalizing interpolation filter, let us first consider, in this section, the case where the ADC frequency $1/T_s$ is equal to the baud rate, i.e. $R = T/T_s = 1$. The replay signal, in Figure 6.1, can be written as

$$r(t) = \sum_i b_i h(t - iT) + n(t),$$

where b_i denotes channel data, $h(t)$ is the continuous-time channel symbol response and $n(t)$ is additive noise. We denote by r_k the ADC output at the sampling instant $t_k^s = (k+\mu)T$ where μT denotes the sampling phase, i.e.

$$r_k = (h^\mu * b)_k + n_k,$$

where $h_k^\mu \doteq h((k+\mu)T)$ and n_k is pre-filtered and sampled noise. The signal r_k is applied to a FIR filter c^μ of length L_c, which we call equalizing interpolator, that is principally meant to compensate for the sampling phase μT and secondarily to equalize the channel impulse response h_k^μ towards a target response g_k of length L_g, see Figure 6.2. The following subsections present two design methods for the equalizing interpolator c^μ.

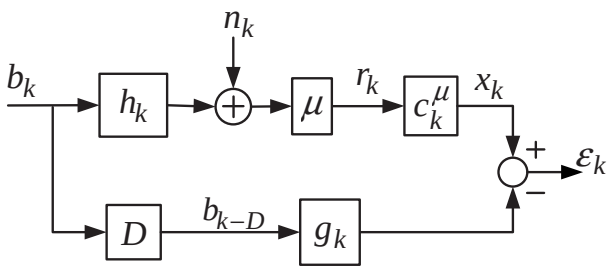

Figure 6.2: *Discrete-time system model for* $1/T_s = 1/T$.

6.2.1 MMSE equalizing interpolator

For a given sampling phase μ, the first design method of the equalizing interpolator c^μ is based on the minimum mean square error (MMSE) criterion. This method consists of optimizing the taps of c^μ to minimize the mean square error (MSE), i.e. $E[\varepsilon_k^2]$, where ε_k denotes the error signal (see Figure 6.2) given by

$$\varepsilon_k = x_k - (g * b)_{k-D}.$$

For a given equalizing interpolator c^μ, the MSE can be written as

$$E[\varepsilon_k^2] = \underline{c}^{\mu\mathrm{T}}\mathbf{Q}\underline{c}^\mu - 2\underline{c}^{\mu\mathrm{T}}\underline{v} + E[(g*b)_{k-D}^2], \tag{6.1}$$

where the matrix $\mathbf{Q}$ is given by $\mathbf{Q}_{i,j} = E[r_{k-i}r_{k-j}]$ and the vectors $\underline{c}^\mu$ and $\underline{v}$ are given by $(\underline{c}^\mu)_k = c_k^\mu$ and $(\underline{v})_i = E[r_{k-i}(g*b)_{k-D}]$, respectively. In case the noise n_k is zero-mean and white with a variance σ_n^2 and the data is uncoded, it can be easily shown that

$$\mathbf{Q}_{i,j} = \left(\sum_m h_m^\mu h_{m+i-j}^\mu\right) + \sigma_n^2\delta(i-j),$$

and

$$(\underline{v})_i = \sum_m h_m^\mu g_{i+m-D}$$

where $\delta(.)$ denotes the delta Kronecker function.

The MMSE equalizing interpolator can be derived by setting the gradient of (6.1) with respect to $\underline{c}^\mu$ to zero. This yields

$$\underline{c}_{\mathrm{MMSE}}^\mu = \mathbf{Q}^{-1}\underline{v}. \tag{6.2}$$

Numerical Example :

By way of illustration we consider an idealized optical storage channel according to the Braat-Hopkins model [42], see Chapter 1, where the normalized optical channel cut-off frequency is $\Omega_c = 1/3$. *The target response has 5 taps* $g = [0.17, 0.5, 0.67, 0.5, 0.17]$. *The noise* n_k *is taken to be white and the signal to noise ratio, as defined in Chapter 1, is fixed to 15 dB. Figure 6.3 shows the amplitude and group delay of a 7-tap MMSE equalizing interpolator for* $\mu = 0.3$. *The error in group delay inside the channel pass-band is around 5% of the bit length.*

The previous example illustrates that the MMSE design method does not lead to a flat group delay and that a method that constrains the group delay is needed. This is presented in the next subsection.

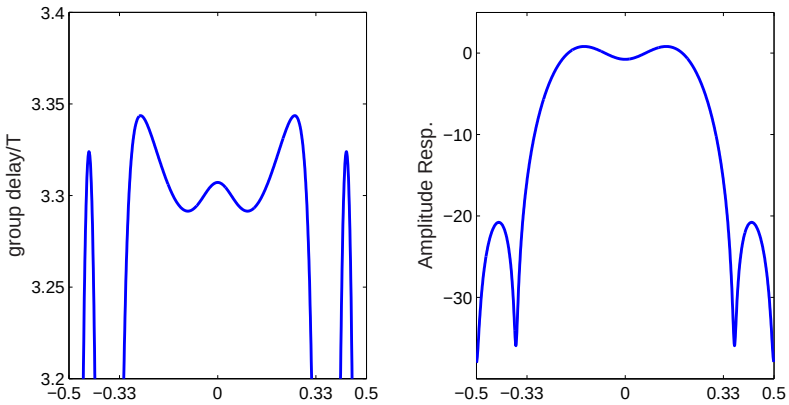

Figure 6.3: *group delay (left plot) and amplitude response (right plot) of the 7-tap MMSE equalizing interpolator for* $\mu = 0.3$.

6.2.2 Group delay constrained equalizing interpolator

The group delay of the interpolation filter c_k^μ must be as close as possible to $(\frac{L_c-1}{2} + \mu)T$ at all frequencies inside the channel pass-band, i.e. $|\Omega| < \Omega_c$ where Ω_c is the channel cut-off frequency. Upon writing the frequency response of c_k^μ as $C^\mu(e^{j2\pi T\Omega}) = A(\Omega)e^{-j2\pi\varphi(\Omega)}$ where $A(\Omega)$ and $\varphi(\Omega)$ denote the amplitude and phase response of c_k^μ respectively, it can be easily shown that the group delay of c_k^μ satisfies

$$\varphi'(\Omega) = -\frac{1}{2\pi}\frac{\mathrm{Im}(C^{\mu\prime}C^{\mu *})}{|C^\mu|^2},$$

where $C^{\mu\prime}$ and $C^{\mu *}$ denote the derivative and the conjugate of $C^{\mu}(e^{j2\pi T\Omega})$ respectively and $\mathrm{Im}(.)$ is the imaginary part. This expression can be simplified into

$$\varphi'(\Omega) = \frac{\underline{c}^{\mu\mathrm{T}} G(\Omega)\Lambda \underline{c}^{\mu}}{\underline{c}^{\mu\mathrm{T}} G(\Omega)\underline{c}^{\mu}}, \tag{6.3}$$

where $G(\Omega) = v_c v_c^{\mathrm{T}} + v_s v_s^{\mathrm{T}}$, given by
$v_c = [1, \cos(2\pi\Omega T), \ldots, \cos(2\pi(L_c-1)\Omega T)]^{\mathrm{T}}$ and
$v_s = [0, \sin(2\pi\Omega T), \ldots, \sin(2\pi(L_c-1)\Omega T)]^{\mathrm{T}}$. The matrix Λ is diagonal and its diagonal is equal to $[0, 1, \ldots, L_c-1]$.

The mismatch in group delay of c_k^{μ} with respect to its ideal value, i.e. $(\frac{L_c-1}{2}+\mu)T$, needs in practice to stays below a predefined margin $\delta_g T$ where δ_g depends on system sensitivity to phase errors. In other words, the interpolation filter needs to meet

$$\tau_1 \leq \varphi'(\Omega) \leq \tau_2, \quad \forall |\Omega| < \Omega_c \tag{6.4}$$

where $\tau_1 = (\frac{L_c-1}{2}+\mu)T - \delta_g T$ and $\tau_2 = (\frac{L_c-1}{2}+\mu)T + \delta_g T$. We introduce a finite frequency grid $\Omega_i \in [0, \Omega_c]$, $i = 1 \ldots N_c$, and define the corresponding constraints sets as

$$\mathcal{S}_i = \{\underline{c} : \tau_1 \leq \frac{\underline{c}^{\mathrm{T}} G(\Omega_i)\Lambda \underline{c}}{\underline{c}^{\mathrm{T}} G(\Omega_i)\underline{c}} \leq \tau_2\}. \tag{6.5}$$

The problem of equalizing interpolation boils down to designing the filter $c_k^{\mu} \in \mathcal{S}_i, \forall i$, while achieving amplitude equalization. Amplitude equalization is achieved by the MMSE technique, i.e. via minimization of

$$J(\underline{c}^{\mu}) = E[\varepsilon_k^2] = \underline{c}^{\mu\mathrm{T}} \mathbf{Q} \underline{c}^{\mu} - 2\underline{c}^{\mu\mathrm{T}} \underline{v} + \underline{g}^{\mathrm{T}} \mathbf{R}_b \underline{g}, \tag{6.6}$$

where $\underline{c}^{\mu} = [c_0^{\mu}, \ldots, c_{L_c-1}^{\mu}]^{\mathrm{T}}$, $\underline{g} = [g_0, \ldots, g_{L_g-1}]^{\mathrm{T}}$, $\mathbf{Q} = \mathbf{H}\mathbf{R}_b\mathbf{H}^{\mathrm{T}} + \mathbf{R}_n$ and $\underline{v} = \mathbf{H}\mathbf{R}_b\underline{g}$ where the matrix $\mathbf{H}$ has entries $H_{p,q} = h((q-p+\mu)T)$ and $\mathbf{R}_b$ and $\mathbf{R}_n$ denote the autocorrelation matrices of the input data and noise respectively. The design of the equalizing interpolator can now be formulated as

$$\underline{c}^{\mu} = \arg \min_{\underline{c} \in \bigcap_{i=1}^{N_c} \mathcal{S}_i} J(\underline{c}). \tag{6.7}$$

It should be noted that the group delay of (6.3) is related to the filter coefficients in a nonconvex rational manner, hence the constraints sets $\mathcal{S}_i$ are nonconvex in general. It follows that standard optimization techniques that hold for convex constraints sets

do not apply to our problem (6.7). However, we will show that, modulo a linear transformation, (6.7) is equivalent to finding the orthogonal projection of the MMSE solution, i.e. the minima of (6.6), over an intersection of nonconvex sets. The vector space projection method (VSPM) [141] extended to nonconvex sets [126] can then be applied. The VSPM deals with the problem of finding an optimal point in a vector space that satisfies multiple constraints. The theory of VSPM was initially developed for intersecting convex constraints sets in [109] and [107]. In recent years the theory was extended to non-convex, non-intersecting sets in [126]. In [126] a parallel projection algorithm, also known in literature as the Parallel Generalized Projection Algorithm (PGPA), was shown to ensure weak convergence even if the constraint sets are non-intersecting. As an example, this theorem was used in [97] to design allpass filters under group delay constraints.

Via decomposing the positive definite matrix $\mathbf{Q}$ into $\Gamma^{\mathrm{T}}\Gamma$, where Γ is positive definite, one can show that (6.7) yields

$$\underline{c}^{\mu\prime} = \Gamma\underline{c}^{\mu} = \arg\min_{\underline{c}'\in\bigcap_{i=1}^{N_c}\mathcal{S}_i'} \|\underline{c}' - \Gamma\underline{c}_0\|^2, \tag{6.8}$$

where $\|.\|$ denotes the L_2-norm and $\underline{c}_0 = \mathbf{Q}^{-1}\underline{v}$ is the MMSE solution. The definition of the new constraints sets $\mathcal{S}_i'$ is similar to (6.5) by replacing $G(\Omega_i)$ with $G'(\Omega_i) = \Gamma^{\mathrm{T}^{-1}}G(\Omega_i)\Gamma^{-1}$ and Λ with $\Lambda' = \Gamma\Lambda\Gamma^{-1}$. According to (6.8), $\Gamma\underline{c}^{\mu}$ can be interpreted as the orthogonal projection of $\Gamma\underline{c}_0$ over $\bigcap_{i=1}^{N_c}\mathcal{S}_i'$. The sets $\mathcal{S}_i'$ can be written as $\mathcal{S}_i' = \mathcal{S}'^1_i \cap \mathcal{S}'^2_i$ where $\mathcal{S}'^1_i = \{\underline{c}' : \tau_1 \leq \frac{\underline{c}'^{\mathrm{T}}G(\Omega_i)'\Lambda'\underline{c}'}{\underline{c}'^{\mathrm{T}}G(\Omega_i)'\underline{c}'}\}$ and $\mathcal{S}'^2_i = \{\underline{c}' : \frac{\underline{c}'^{\mathrm{T}}G(\Omega_i)'\Lambda'\underline{c}'}{\underline{c}'^{\mathrm{T}}G(\Omega_i)'\underline{c}'} \leq \tau_2\}$. The solution of (6.8) can then be based on the PGPA theorem which consists of iteratively applying a weighted sum of the orthogonal projections $P_i^{1,2}$ over $\mathcal{S}'^{1,2}_i$. For the sake of conciseness, we refer to [97] where a very similar derivation of $P_i^{1,2}$ can be found. The algorithm of designing an equalizing interpolator can be summarized as follows:

Step 1. we initially set $\underline{c}_0' = \Gamma\underline{c}_0$.
Step 2. $\forall n \geq 0$, $\underline{c}_{n+1}' = \sum_{j=1}^{2}\sum_{i=1}^{N_c} w_i^j P_i^j \underline{c}_n'$.
If $\underline{c}_{n+1}' \in \bigcap_{i=1}^{N_c}\mathcal{S}_i'$ then go to step 3 otherwise repeat step 2.
Step 3. after convergence, $\underline{c}^{\mu} = \Gamma^{-1}\underline{c}'_{\infty}$.

The weights w_i^j must satisfy $\sum_{i,j} w_i^j = 1$. An obvious choice is $w_i^j = \frac{1}{2N_c}$. However, in our application it was observed that a much faster convergence is obtained by choos-

ing

$$w_i^j = \frac{\|\underline{c}'_n - P_i^j \underline{c}'_n\|^2}{\sum_{l,m} \|\underline{c}'_n - P_l^m \underline{c}'_n\|^2}.$$

Numerical Example :

Using the same channel as in the numerical example of Section 6.2.1, Figures 6.4 and 6.5 show the amplitude and group delay of a 7-tap and 9-tap group delay constrained equalizing interpolator for $\mu = 0.3$ *and* $\delta_g = 0.003$*, i.e.* 0.3% *of the bit interval. The signal to noise ratio is fixed to 15 dB. Compared to a 7-tap MMSE equalizer together with a 6-tap Lagrange interpolation [110], the equalizing interpolator has a negligible loss in MSE of only* 0.05 *dB. This means that the equalizer of Figure 6.1 becomes superfluous.*

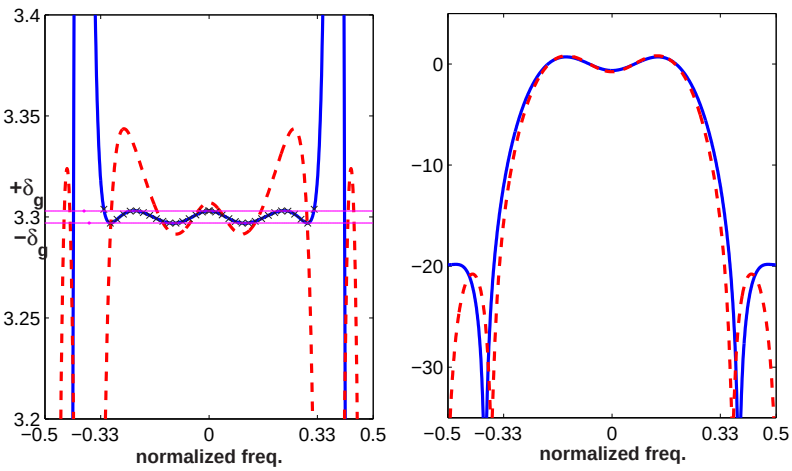

Figure 6.4: *left plot: group delay of the 7-tap group delay constrained equalizing interpolator for* $\mu = 0.3$ *and* $\delta_g = 0.0003$ *(solid) and the 7-tap MMSE equalizing interpolator (dashed). The crosses denote the frequencies* Ω_i*. right plot: amplitude responses of the two equalizers.*

6.3 Equalizing anti-aliasing filters

In many practical systems, the SRC filters are split into two filters, see Figure 6.6. A first anti-aliasing filter p_n, of length L_p, rejects a specific frequency band in order to

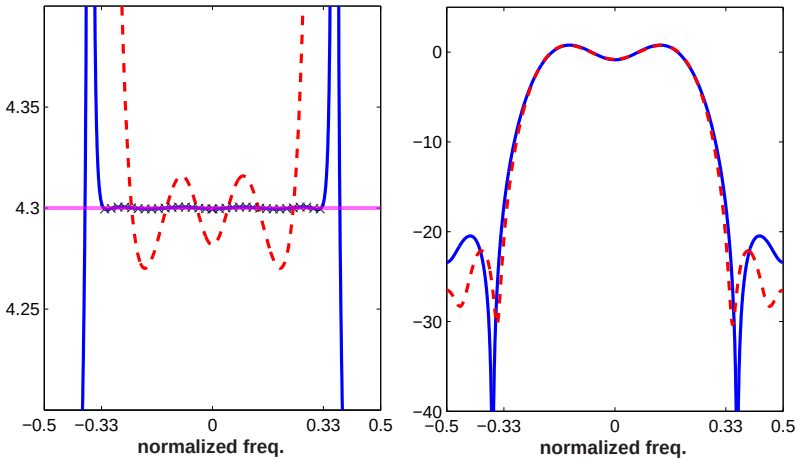

Figure 6.5: *left plot: group delay of the 9-tap group delay constrained equalizing interpolator for* $\mu = 0.3$ *and* $\delta_g = 0.003$ *(solid) and the 9-tap MMSE equalizing interpolator (dashed). The crosses denote the frequencies* Ω_i*. right plot: amplitude responses of the two equalizers.*

prevent noise and data aliasing. A second filter $c^{t_k^r}$ that depends on t_k^r resamples the filtered signal at the sampling instants t_k^r, provided by the timing-recovery subsystem. Such a structure allows a relaxation on the stop-band constraints of $c^{t_k^r}$. This simplifies greatly the SRC. It is important to mention here that depending on the channel cut-off frequency and the oversampling rate $R = T/T_s$, $c^{t_k^r}$ can precede the filter p_n. The results of this section can be easily translated to this case. The SRC filter $c^{t_k^r}$ is implemented via a sample selector and an interpolation filter [86]. The interpolation filter can be designed as explained in the previous section. The filter p_n should then tackle all phase distortions and the remaining amplitude distortions, left by the equalizing interpolator, while providing enough attenuation at the stop-band.

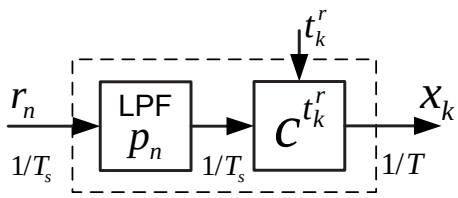

Figure 6.6: *a practical implementation of the SRC.*

The MSE of a system employing the SRC architecture of Figure 6.6 can be found in [114]. It is given by

$$J(\underline{p}) = \underline{p}^T \mathbf{Q}_R \underline{p} - 2\underline{p}^T \underline{v}_R + \underline{g}^T \mathbf{R_b} \underline{g}, \tag{6.9}$$

where $\underline{p} = [p_0, ..., p_{L_p-1}]^T$, the matrix $\mathbf{Q}_R$ and the vector $\underline{v}_R$ depend on the oversampling rate R and are given by

$$\mathbf{Q}_R \quad = \quad \mathbf{F}\mathbf{R}_b\mathbf{F}^{\mathrm{T}} + \mathbf{C}\mathbf{R}_u\mathbf{C}^{\mathrm{T}}; \quad \underline{v}_R = \mathbf{F}\mathbf{R}_b\mathbf{g},$$

where the matrix $\mathbf{F}$ has entries $\mathbf{F}_{p,q} = \sum_n c(nT_s - pT_s)h(qT - nT_s)$, $\mathbf{C}$ is given by $\mathbf{C}_{p,q} = c(-pT_s - qT_s)$ and the autocorrelation matrices of the input data and noise are denoted by $\mathbf{R}_b$ and $\mathbf{R}_u$ respectively. The symbol response of the SRC interpolation filter is denoted by $c(t)$. Similarly to Section 6.2, we introduce a finite frequency grid Ω_i, $i = 1...N_c$ in the stop-band, and constrain the filter p_n to meet

$$|P(e^{j2\pi\Omega_i T_s})|^2 \leq \delta_a, \;\; i = 1...N_c$$

where $P(e^{j2\pi f T_s}) = \sum_{n=0}^{L_p-1} p_n e^{-j2\pi n f T_s}$ and $10\log(\delta_a)$ is the desired stop-band attenuation. This amplitude constraint can be written as $\underline{p}^{\mathrm{T}}\underline{m}_i\underline{m}_i^{\mathrm{H}}\underline{p} \leq \delta_a$ where $\underline{m}_i = [1, e^{-j2\pi\Omega_i T_s}, \ldots, e^{-j2\pi(L_p-1)\Omega_i T_s}]^{\mathrm{T}}$ and $[.]^{\mathrm{H}}$ denotes transpose conjugate. The optimization problem related to $\underline{p}$ can be formulated as

$$\underline{p} = \arg \min_{\forall i \; F_i(\underline{p}) \leq 0} J(\underline{p}), \tag{6.10}$$

where $F_i(\underline{p}) = \underline{p}^{\mathrm{T}}\underline{m}_i\underline{m}_i^{\mathrm{H}}\underline{p} - \delta_a$. The equalizing anti-aliasing filters problem can now be stated in terms of minimizing the quadratic function $J(\underline{p})$ subject to the inequalities constraints $F_i(\underline{p}) \leq 0$ where $F_i(\underline{p})$ are real differentiable and convex functions because the real matrices $\underline{m}_i\underline{m}_i^{\mathrm{H}}$ are positive. Because the function $J(\underline{p})$ is also convex, we know that if a solution of (6.10) exists then it is unique and it is characterized by the Kuhn-Tucker (KT) conditions [39]. However, solving the KT conditions can be quite complex in general. For this purpose we propose to use the Uzawa algorithm [90] which is an iterative method allowing one to solve an inequality constrained minimization problem, of a structure as in (6.10) by replacing it with a sequence of unconstrained minimization problems. If we denote the Lagrangian $\mathcal{L}(\underline{p}, \underline{\lambda}) =$

$J(\underline{p}) + \sum_{i=1}^{N_c} \lambda_i F_i(\underline{p})$, the Uzawa algorithm in our context is written as:

$$\mathcal{L}(\underline{p}^{(n)}, \underline{\lambda}^{(n)}) = \min_{\underline{p}} \mathcal{L}(\underline{p}, \underline{\lambda}^{(n)}) \tag{6.11}$$

$$\forall i \quad \lambda_i^{(n+1)} = \max(0, \lambda_i^{(n)} + \eta F_i(\underline{p}^{(n)})), \tag{6.12}$$

where $\eta > 0$ is a fixed adaptation constant and the superscript (n) indicates the nth iteration. Equation (6.12) ensures that the Lagrange multipliers are always positive. The unconstrained minimization in (6.11) yields a simple linear system. In fact, it can be easily shown that (6.11) is equivalent to

$$\underline{p}^{(n)} = \left(\mathbf{Q}_R + \sum_{i=1}^{N_c} \lambda_i^{(n)} \underline{m}_i \underline{m}_i^{\mathrm{H}} \right)^{-1} \underline{v}_R. \tag{6.13}$$

Initially we set $\lambda_i^{(0)} = 0$ and $\underline{p}^{(0)} = \mathbf{Q}_R^{-1} \underline{v}_R$ (the MMSE equalizer). At every iteration, we apply (6.13) and (6.12) and check if $F_i(\underline{p}^{(n)}) \leq 0$, $\forall i$. The algorithm is stopped if this latter condition is met.

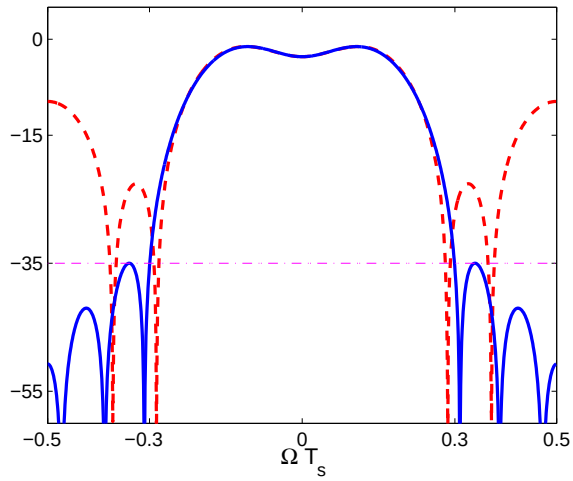

Figure 6.7: *The Amplitude response of the 9-tap filter p_n (solid) and the 9-tap MMSE equalizer (dashed).*

Numerical Example :

Using the same channel as in the example of Section 6.2 at an oversampling rate

R=1.25, Figure 6.7 shows the amplitude response of a 9-tap filter p_n for an attenuation of -35 dB in $[0.3/T_s, 0.5/T_s]$. The MSE difference between the filter p_n and the MMSE equalizer is less than 0.1 dB. This shows that the equalization burden can be shifted towards the SRC which means that the equalizer of Figure 6.1 can be omitted.

6.4 Conclusions

For all-digital timing-recovery loops, design of efficient sampling-rate converter filters is very important for performance optimization and complexity limitation. In fact, to limit the overall receiver complexity, sampling-rate converter filters can be designed to also perform channel equalization. This presents a two-fold attractive feature. First, it helps to reduce complexity by shifting a big part of channel equalization towards the SRC filters and thus shortens significantly the equalizer length for the same performance. Second, for systems employing a digital synchronous equalizer, shortening the equalizer length limits the delay inside the timing-recovery loop which is crucial for its proper functioning.

This chapter presents design methods that combine group delay flatness and out-of-band rejection criteria, required for sampling-rate converter filters, together with minimum mean square error equalization. This approach and the corresponding design methods are validated for an idealized optical storage system.

Chapter 7

Summary and Conclusions

The objectives of this thesis are the study and development of adaptive equalization and timing recovery techniques that meet the key future challenges in high-density optical storage systems. These challenges stem from the increase in linear and nonlinear intersymbol interference, the nature of noise and fast channel variations. In this thesis we study issues related to equalization and timing recovery and present practical schemes that are of potential interest for future systems.

The work in this thesis should open new doors for research in the field of adaptive equalization and timing recovery for optical storage systems. In fact, as most of the adaptation techniques used in todays optical storage systems do not fully exploit the nature of the optical storage channel in terms of noise and nonlinearities, the different adaptation schemes proposed in this thesis, and in particular the selective equalizer adaptation and the data-dependent timing-recovery, can be an important contribution to the state of the art.

This chapter summarizes the thesis work and provides suggestions for future research. This thesis contains seven chapters. Chapter 1 gives an introduction to optical storage technology and a review of signal processing techniques for read channels. It presents the main challenges in terms of linear and nonlinear ISI, noise and fast channel variations for future high-density optical storage systems. Then it points out the implications of these challenges for equalization and timing recovery.

In Chapter 2 we introduce a new adaptive equalization technique that seeks to minimize detection bit-error rate (BER). The proposed algorithm incorporates a selection mechanism that enables equalizer adaptation only when bit-detection becomes not reliable. Compared to existing equalization schemes, the proposed algorithm provides an important performance improvement, with no increment of com-

plexity. The superiority of the proposed algorithm is demonstrated analytically and verified based on computer simulations.

Chapter 3 can be seen as an extension of Chapter 2 in the sense that it covers the problem of joint equalizer and target response adaptation. We generalize and apply the near minimum-BER adaptation technique to joint target response and equalizer adaptation. This is achieved by focusing target-response adaptation on the most likely bit-error events and acting towards decreasing their probability of occurrence. Relative to existing adaptation methods, the near minimum-BER scheme is comparable in terms of implementation complexity. However, in terms of performance, it allows significant improvements especially for short target or equalizer lengths or in the presence of channel nonlinearities and media noise. This can be important for high-density storage systems in terms of system complexity reduction, by allowing the use of a short target response without significant performance degradation, or in terms of mitigating nonlinearities and media noise.

Chapter 4 tackles the problem of minimizing latencies inside the timing-recovery loop by shifting the equalizer to the asynchronous clock domain. This involves an equalizer that operates at a sampling-rate asynchronous to the data rate. Chapter 4 explains, first, the implication of this scheme for equalizer adaptation and then proposes a highly simple yet efficient method for asynchronous equalizer adaptation. Although Chapter 4 focuses on LMS adaptation for simplicity, its results carry over to other adaptation criteria as well, e.g. the minimum-BER criterion proposed in Chapter 2. The main result of this chapter is that asynchronous equalization is now made as simple as its synchronous counterpart.

With respect to the objective of strengthening the timing-recovery loop, Chapter 5 focuses on designing an optimal timing-recovery scheme for channels with data-dependent noise. This chapter presents a new data-aided timing recovery algorithm based on a data-dependent Gauss-Markov model of the noise. The proposed timing recovery algorithm incorporates data-dependent noise prediction parameters in the form of linear prediction filters and prediction error variances. Compared to the state of the art, the proposed scheme allows an important performance gain in the presence of media noise.

As recently all-digital timing recovery is often employed, design of efficient sampling-rate converter (SRC) digital filters is very important for performance optimization and complexity limitation. More precisely, design of SRC filters that also

realize channel equalization presents attractive features. First, it helps to reduce complexity by shifting a big part of channel equalization towards the SRC filters and thus shortens significantly the equalizer length for the same performance. Second, for systems employing a digital synchronous equalizer, shortening the equalizer length limits the delay inside the timing-recovery loop which is crucial for its proper functioning. Chapter 6 explains first the problem of equalizing SRC filters and then presents algorithms for designing such filters.

7.1 Future Research

With respect to the objective of improving the signal-processing part of future optical storage systems, we can distinguish between two steps. First, improvement of the write subsystem via development of accurate write-strategy optimization. Second, amelioration of the read channel which requires dealing with linear and nonlinear ISI and strengthening the adaptive equalization and timing recovery loop.

Regarding the second step, a possible future research work can aim at enhancing the performance of the different equalization and timing recovery algorithms proposed in this thesis. In particular, tailoring the near-minimum BER adaptation algorithms to decision-directed mode and combining the different algorithms with soft-decision and iterative techniques could provide some interesting performance improvements. Also, combination of the near-minimum BER adaptation with post-processing detection techniques, which focus on the dominant bit-error events provided by the equalization algorithm, should be investigated. Moreover, extension of the different algorithms to two-dimensional systems can be a good topic for future work.

An other topic of future research can be the investigation of nonlinear equalization methods to deal with nonlinear ISI. This should also include a generalization of the selective adaptation criterion of Chapters 2 and 3. Also nonlinearity compensation in combination with a linear or nonlinear equalizer needs to be thoroughly investigated.

In order to further strengthen the timing recovery loop at low signal to noise ratios, a possible future work consists of incorporating in our timing error detector knowledge of the timing errors models. This involves developing proper timing error models by taking into account the different timing uncertainty sources and then

designing the corresponding optimal timing error detectors.

An other topic of future work might be the investigation of the interaction problem between the equalizer adaptation and the timing recovery loop. This is caused by the fact that a linear phase distortion in the channel can be either compensated by timing recovery or by the adaptive equalizer. This makes the phase response of the equalizer ill-defined and causes a degradation of system performance. Although there exist some constraint-based interaction mitigation algorithms, e.g. [50, 128], they mainly try, with more or less success, to patch up the problem instead of preventing the source of interaction by decreasing the receiver degrees of freedom. This subject still needs to be fully explored especially in the case of selective equalizer adaptation that we developed in Chapters 2 and 3.

Although this thesis focused on optical storage systems, the applicability of the main results extends well beyond optical storage. A first possible extension of this thesis, is thus the application of its main results in the field of equalization and timing recovery to other communication and storage systems. In particular, the near-minimum BER adaptation scheme developed in Chapters 2,3 and the new timing recovery scheme of Chapter 5 can be of great interest for high-density magnetic storage systems as these suffer from similar artifacts as optical storage systems. Also, with modest changes, the new ideas of this thesis might be applicable, among other systems, to wireless and optical communication systems.

Bibliography

[1] "The Philips and MCA Optical Video Disc System," *Issued by the Audio VLP Group. N.V. Philips' Gloeilampenfabriek Eindhoven, Netherlands*.

[2] A. Gameiro, "Baud sampling bit synchroniser for channels with data dependent noise," *Electronics Letters*, vol. 34, no. 21, pp. 2000–2002, 15th Oct. 1998.

[3] A. Gersho, "Adaptive equalization of highly dispersive channels," *Bell Syst. Tech. J.*, vol. 48, pp. 55–70, Jan. 1969.

[4] A. Jennings and B.R. Clarke, "Data-sequence selective timing recovery for PAM systems," *IEEE Trans. on Commun.*, vol. 33, pp. 729–731, July 1985.

[5] A. Kavcic and A. Patapoutian, "A Signal-Dependent Autoregressive Channel Model," *IEEE Trans. Magn.*, vol. 35, no. 5, pp. 2316–2318, Sep. 1999.

[6] A. Kavcic and J.M.F. Moura, "The Viterbi Algorithm and Markov Noise Memory," *IEEE Trans. Inf. Theory*, vol. 46, no. 1, pp. 291–301, Jan. 2000.

[7] ——, "Correlation-Sensitive Adaptive Sequence Detection," *IEEE Trans. Magn.*, vol. 34, no. 3, pp. 763–771, May 1998.

[8] A. Kavčić and A. Patapoutian, "A signal-dependent autoregressive channel model," *IEEE Trans. on Magn.*, vol. 35, no. 5, pp. 2316–2318, 1999.

[9] A. Lender, "The Duobinary technique for high-speed data transmission," *IEEE Trans. on Commun. Electron.*, vol. 82, pp. 214–218, May 1963.

[10] A.B. Marchant, *Optical Recording*. Reading, MA: Addison Wesley, 1990.

[11] A.H.J. Immink and B. Yin, "Method and system for providing timing recovery in an optical system," *Patent application WO 2005/060146 A1*, June 2005.

[12] A.R. Nayak, J.R. Barry and S.W. McLaughlin, "Joint Timing Recovery and Turbo Equalization for Coded Partial Response Channels," *IEEE Trans. Magn.*, vol. 38, no. 5, pp. 2295–2297, Sep. 2002.

[13] B. Bloodworth, P. Siniscalchi, G. De Veirman, A. Jezdic, R. Pierson and R. Sundararaman, "A 450Mb/s analog front-end for PRML read channels," *Proc. IEEE Int. Conf. Solid-State Circuits (ISSCC)*, pp. 34–35, Feb. 1999.

[14] B. Widrow, J.M. McCool, M.G. Larimore and R. Johnson, Jr., "Stationary and nonstationary learning characteristics of the LMS adaptive filter," *Proc. IEEE*, vol. 64, no. 8, pp. 1151–1162, Aug. 1976.

[15] J. W. M. Bergmans, "Effect of Loop Delay on Phase Margin of First-Order and Second-Order Control Loops," *Submitted for publication*, 2004.

[16] J. J. M. Braat, P. Dirksen, and A. J. E. M. Janssen, "Diffractive Read-out of Optical Disks," *Focus on Microscopy (P. Török, F.J. Kao eds.), Springer*, pp. 45–85, 2002.

[17] D. M. Bruls, A. M. van der Lee, A. H. J. Immink, and W. M. J. Coene, "Two-Dimensional Optical Storage (TwoDOS)," *Techn. Dig. ISOM 2004*, no. WE-E-06, pp. 60–61, 2004.

[18] C. Peng and M. Mansuripur, "Sources of noise in erasable optical disk data storage," *App. Opt.*, vol. 37, no. 5, pp. 921–928, Feb. 1998.

[19] C. Yeh and J. Barry, "Adaptive Minimum Bit-Error Rate Equalization for Binary Signaling," *IEEE Trans. on Communications*, vol. 48, no. 7, pp. 1226–1235, July 2000.

[20] R. D. Cideciyan, F. Dolivo, R. Hermann, W. Hirt, and W. Schott, "A PRML system for digital magnetic recording," *IEEE J. Sel. Areas Commun.*, vol. 10, pp. 38–56, Jan. 1992.

[21] C.M. Melas and P. Sutardja, "An asynchronous fully digital channel for magnetic recording," *IEEE Global Telecomm. Conf. (Globecom)*, vol. 2, pp. 1144–1147, 1994.

[22] W. M. J. Coene, “NonLinear signal-processing model for scalar diffraction in optical recording,” *Applied Optics*, vol. 42, no. 32, p. 6525, 2003.

[23] J. D. Coker, E. Eleftheriou, R. L. Galbraith, and W. Hirt, “Noise-Predictive Maximum Likelihood (NPML) Detection,” *IEEE Trans. Magn.*, vol. 34, no. 1, pp. 110–117, Jan. 1998.

[24] K. Compaan and P. Kramer, “The Philips ‘VLP’ System,” *Philips Tech. Rev.*, vol. 33, no. 7, pp. 178–180, 1973.

[25] C.T. Beare, “The choice of the desired impulse response in combined linear-Viterbi algorithm equalizers,” *IEEE Trans. Commun.*, vol. COM-26, pp. 1301–1307, Aug. 1978.

[26] D. D. Falconer, “Adaptive equalization of channel nonlinearities in QAM data transmission systems,” *Bell Syst. Tech. J.*, vol. 57, no. 7, pp. 2589–2611, 1978.

[27] D. G. Messerschmitt, “Design of finite impulse response for the viterbi algorithm and decision feedback equalizer,” *Proc. ICC*, June 1974.

[28] D. Modrie and R. Otte, “Adaptive equalizer operating at a sampling rate asynchronous to the data rate,” *US Patent No. 2005/0111540A1*, May 2005.

[29] D.D. Falconer and J.F.R. Magee, “Adaptive channel memory truncation for maximum likelihood sequence estimation,” *Bell Syst. Tech. J.*, vol. 52, pp. 1541–1562, Nov. 1973.

[30] D.J. Costello, J. Hagenauer, H. Imai and S.B. Wicker, “Applications of Error-Control Coding,” *IEEE Trans. Inf. Theory*, vol. 44, no. 6, pp. 2531–2560, Oct. 1998.

[31] D.J. Parker, “Defining DVD,” *IEEE Multimedia*, vol. 6, no. 1, pp. 80–84, 1999.

[32] E. Eleftheriou and W. Hirt, “Noise-Predictive Maximum-Likelihood (NPML) Detection for the Magnetic Recording Channel,” *IEEE Conf. Record ICC’96*, vol. 1, pp. 23–27, June 1996.

[33] E. F. Haratsch and Z. A. Keirn, “Digital Signal Processing in Read Channels,” *IEEE Custom Integrated Circuits Conference*, pp. 683–690, 2005.

[34] E.F. Stikvoort and J.A.C.v. Rens, "An all-digital bit detector for compact disc players," *IEEE J. on Select. Areas in Commun.*, vol. 10, no. 1, pp. 191–200, Jan. 1992.

[35] R. B. *et al.*, "Gain and Phase Constrained Adaptive Equalizer in a Sampled Amplitude Read Channel for Magnetic Recording," *US Patent No. 5,999,355*, Dec. 7, 1999.

[36] E.R. Kretzmer, "Generalization of a technique for binary data transmission," *IEEE Trans. on Commun. Technol.*, vol. COM-14, pp. 67–68, Feb. 1966.

[37] W. S. F. Dolivo and G. Ungerboeck, "Fast Timing Recovery for Partial-Response Signaling Systems," *Int. Conf. on Commun. (ICC)*, pp. 573–577, June 1989.

[38] F. Dolivo, R. Hermann and S. Ölcer, "Performance and sensitivity analysis of maximum-likelihood sequence detection on magnetic recording channels," *IEEE Trans. on Magn.*, vol. 25, no. 5, pp. 4072–4074, Sep. 1989.

[39] R. Fletcher, *Practical Methods of Optimization*. New York: Wiley, 1987.

[40] F.M. Gardner, "Interpolation in Digital Modems - Part I: Fundamentals," *IEEE Trans. Commun.*, vol. COM-41, no. 3, pp. 501–507, Mar. 1993.

[41] G. D. Forney, "Maximum-Likelihood Sequence Estimation of Digital Sequences in the Presence of Intersymbol Interference," *IEEE Trans. Inform. Theory*, vol. IT-18, pp. 363–378, May 1972.

[42] G. Bouwhuis, J. Braat, A. Huijser, J. Pasman, G. van Rosmalen and K. Schouhamer Immink, *Principles of Optical Disc Systems*. Adam Hilger Ltd, Bristol, UK, 1985.

[43] G. Ungerboeck, "Fractional tap-spacing equalizer and consequences for clock recovery in data modems," *IEEE Trans. Commun.*, vol. COM-24, no. 8, pp. 856–864, Aug. 1976.

[44] ——, "Theory on the speed of convergence in adaptive equalizers for digital communication," *IBM J. Res. Dev.*, vol. 16, pp. 546–555, Nov. 1972.

[45] F. Gardner, *Phaselock Techniques. 2nd ed.* New York: Wiley, 1979.

[46] R. D. Gitlin, H. C. Meadors Jr., and S. B. Weinstein, "The Tap-Lekeage Algorithm: An Algorithm for the Stable Operation of a Digitally Implemented Fractionally-Spaced Adaptive Equalizer," *Bell Syst. Techn. J.*, vol. 61, pp. 1817–1839, 1982.

[47] G.J. van den Enden, "Transmission system and recording system having a simplified symbol detector," *European Patent Application*, no. EP-885 499, Dec. 1998.

[48] D. Goldberg, *Genetic Algorithms in Search, Optimization and Machine Learning*. Addison-Wesley Pub. Co. Hardcover, 1989.

[49] D. P. Gregg, "Transparent Recording Disc," *U.S. Patent no. 3,430,966*, March 1969.

[50] G.S. Christiansen, "An LMS adaptation technique to prevent ADC saturation and loop interaction," *Inter. Conf. on Comm.*, vol. 3, pp. 1558–1562, May 2002.

[51] H. Kobayashi, "Application of probabilistic decoding to digital magnetic recording systems," *IBM J. Res. Dev.*, vol. 15, pp. 65–74, Jan. 1971.

[52] ——, "Simultaneous adaptive estimation and decision algorithm for carrier modulated data transmission systems," *IEEE Trans. on Commun.*, vol. 19, pp. 268–280, June 1971.

[53] ——, "Correlative level coding and maximum-likelihood decoding," *IEEE Trans. Inf. Theory*, vol. IT-17, no. 5, pp. 586–594, Sep. 1971.

[54] H. Kobayashi and D.T. Tang, "Application of partial-response channel coding to magnetic recording systems," *IBM J. Res. Dev.*, vol. 14, pp. 368–375, July 1970.

[55] H. Meyr and G. Ascheid, *Synchronization in Digital Communications - Volume I*. New York: Wiley, 1990.

[56] H. Meyr, M. Moeneclaey and S. A. Fechtel, *Digital Communication Receivers*. New York: Wiley & Sons, 1998.

[57] H. Minemura, “A Write Shift Compensation Method for High Density Optical Disc Drives,” *in Proc. 12th Symp. Phase Change Optical Information Storage (PCOS2000)*, pp. 76–78, 2000.

[58] H. Nyquist, “Certain factors affecting telegraph speed,” *Bell Syst. Tech. J.*, vol. 3, no. 2, pp. 324–346, Apr. 1924.

[59] ——, “Certain topics in telegraph transmission theory,” *Trans. AIEE*, vol. 47, pp. 617–644, Apr. 1928.

[60] H. Pozidis, J.W.M. Bergmans and W.M.J. Coene, “Modeling and compensation of asymmetry in optical recording,” *IEEE Trans. Commun.*, vol. 50, no. 12, pp. 2052–2063, Dec. 2000.

[61] H. Pozidis, W.M.J. Coene and J.W.M. Bergmans, “A simple nonlinear channel model for the optical recording channel,” *IEEE International Conference on Communications*, vol. 1, pp. 99–103, 2000.

[62] H. Pozidis, W.M.J. Coene and M.J. Dekker, “A simple detection method for high-density d=1 optical recording,” *Int. Conf. on Consumer Electronics*, pp. 156 – 157, June 2000.

[63] H. Sawaguchi, M. Kondou, N. Kobayashi and S. Mita, “Concatenated error correction coding for high-order PRML channels,” *In Proc. Globecom 98*, vol. 5, pp. 2694 – 2699, Nov. 1998.

[64] H. Song, J. Liu, B. Kumar and Y. Yuan, “Application of soft output viterbi algorithm (SOVA) in timing recovery for iterative soft decoded magnetic recording channels,” *IEEE Int. Magnetics Conf.*, Jan. 2001.

[65] H. Sun, G. Mathew and B. Farhang-Boroujeny, “Detection techniques for high-density magnetic recording,” *IEEE Trans. on Magn.*, vol. 41, no. 3, pp. 1193–1199, 2005.

[66] H. Thapar, Sang-Soo Lee, C. Conroy, R. Contreras, A. Yeung, Jenn-Gang Chern, T. Pan and Shih-Ming Shih, “Hard disk drive read channels: technology and trends,” *Proceedings of the IEEE Custom Integrated Circuits Conference*, pp. 309–316, 16-19 May 1999.

[67] H.C. Patel, R.H. Noyau and E.W. Williams, "A review of noise in magneto-optic recording," *Int. Conf. on Video, Audio and Data Recording*, pp. 1–6, Apr. 1990.

[68] H.H. Hopkins, "Diffraction theory of laser read-out systems for optical video discs," *J. Opt. Soc. Am.*, vol. 69, no. 1, pp. 4–24, Jan. 1979.

[69] H.J. Ki, C.S Lee, M.H. Song and S.W. Kim, "Folding Viterbi detector with reduced complexity for EPRML system applications," *Electronic letters*, vol. 36, no. 4, pp. 330–331, Feb. 2000.

[70] H.K. Thapar and T.D. Howell, "On the performance of partial response maximum-likelihood and peak detection methods in digital recording," *Tech. Dig. Magn. Recording Conf. Hidden Valley, Pennsylvania.*, June 12-15, 1991.

[71] I. Lee and J.M. Cioffi, "Equalized maximum likelihood receiver with a unit energy constraint," *IEEE Trans. Magn.*, vol. 33, no. 1, pp. 855–862, Jan. 1997.

[72] I. Lee, C. Modlin and J. M. Cioffi, "Equalized maximum likelihood receiver in a magnetic recording channel," *In Proc. Globecom 93*, pp. 1970–1973, Nov. 1993.

[73] A. H. J. Immink, W. M. J. Coene, A. M. van der Lee, C. Busch, A. P. Hekstra, J. W. M. Bergmans, J. Riani, S. J. L. van Beneden, and T. Conway, "Signal Processing and Coding for Two-Dimensional Optical Storage," *Global Telecommunications Conference, GLOBECOM, IEEE*, vol. 7, pp. 3904–3908, 2003.

[74] A. Immink, *System and Receiver Design for Two-Dimensional Optical Storage*. PhD thesis, Technische Universiteit Eindhoven. ISBN 90-386-1773-9, 2005.

[75] A. Immink, J. Riani, S. J. L. van Beneden, J. W. M. Bergmans, M. Ciacci, A. Nowbakht Irani, W. M. J. Coene, A. M. van der Lee, and D. Bruls, "Adaptation and timing recovery for two-dimensional optical storage," *Optical Data Storage, Proceedings of SPIE*, vol. 5380, pp. 90–104, 2004.

[76] J. Armstrong, "Symbol synchronization using baud-rate sampling and data-sequence-dependent signal processing," *IEEE Trans. on Commun.*, vol. 39, no. 1, pp. 127–132, Jan. 1991.

[77] J. Fitzpatrick, J.K. Wolf and L. Barbosa, “New equalizer targets for sampled magnetic recording systems,” *Proc. of the 25th Asilomar Conf. on Signals, Systems and Computers*, pp. 30–34, Nov, 1991.

[78] J. Moon and W. Zeng, “Equalization for maximum likelihood detectors,” *IEEE Trans. on Magn.*, vol. 31, no. 2, pp. 1083–1088, March 1995.

[79] J. Moon, H. Thapar, B.V.K.V. Kumar and K.A.S. Immink, “Editorial signal processing for high density storage channels,” *IEEE Journal on Sel. Areas in Commun.*, vol. 19, no. 4, pp. 577–581, Apr. 2001.

[80] J. Proakis, *Digital Communications*. McGraw-Hill, New York.

[81] J. Stander and A. Patapoutian, “Performance of a Signal-Dependent Autoregressive Channel Model,” *IEEE Trans. Magn.*, vol. 36, no. 5, pp. 2197–2199, Sep. 2000.

[82] J. W. Freedoby, *Telegraphy*. Sir Isaac Pitman & Sons, Ltd., London.

[83] J.G. Proakis and J.H. Miller, “An adaptive receiver for digital signaling through channels with intersymbol interference,” *IEEE Trans. Inf. Theory*, vol. IT-15, pp. 484–497, July 1969.

[84] J.R. Barry, A. Kavcic *et al*, “Iterative timing recovery,” *IEEE Signal Processing Magazine*, vol. 21, no. 1, pp. 89–102, Jan. 2004.

[85] J.W.M. Bergmans, “Effect of loop delay on stability of discrete-time PLL,” *IEEE Trans. on Circuits and Systems-I: Fundamental theory and applications*, vol. 42, no. 4, pp. 229–231, 1995.

[86] J.W.M. Bergmans, *Digital Baseband Transmission and Recording*. Kluwer Academic Publishers, 1996.

[87] J.W.M. Bergmans, “Efficiency of data-aided timing recovery techniques,” *IEEE Trans. Inf. Theory*, vol. 41, no. 5, pp. 1397–1408, Sep. 1995.

[88] J.W.M. Bergmans and H.W. Wong-Lam, “A Class of Data-Aided Timing-Recovery Schemes,” *IEEE Trans. Commun.*, vol. 43, no. 2/3/4, pp. 1819–1827, Feb./Mar./Apr. 1995.

[89] J.W.M. Bergmans, W.M.J. Coene, R. Otte and S. Bramwell, “Transition detector for CD and DVD,” *IEEE Trans. Consumer Electronics*, vol. 46, no. 1, pp. 16–19, Feb. 2000.

[90] K. Arrow, L. Hurwicz and H. Uzawa, *Studies in Nonlinear Programming*. Stanford University Press, Stanford, CA, 1958.

[91] K. H. Mueller and M.S. Muller, “Timing Recovery in Digital Synchronous Data Receivers,” *IEEE Trans. on Commun.*, vol. 24, no. 5, pp. 516–531, May 1976.

[92] K. Küpfmüller, “Transient Phenomena in Wave Filters,” *Elek. Nach. Tech.*, vol. 1, p. 141, 1924.

[93] K.A.S. Immink, *Codes for Mass Data Storage Systems*. Shannon Foundation Publishers, The Netherlands, 1999.

[94] K.A.S. Immink, “EFMPlus: The coding format of the multimedia compact disc,” *IEEE Trans. Consumer Electronics*, vol. 41, no. 3, pp. 491–497, Aug. 1995.

[95] K.A.S. Immink and H. Ogawa, “Method for encoding binary data,” *US patent 4,501,000*, Feb. 1985.

[96] K.A.S. Immink, P.H. Siegel and J.K. Wolf, “Codes for Digital Recorders,” *IEEE Trans. Inf. Theory*, vol. 44, no. 6, pp. 2260–2299, Oct. 1998.

[97] K.C. Haddad, Y. Yang, N.P. Galatsanos and H. Stark, “Allpass filter design using projection-based method under group delay constraints,” *IEEE Int. Conf. on Acoustics, Speech, and Signal Processing (ICASP)*, vol. 6, pp. 3833–3836, 2001.

[98] K.K. Fitzpatrick, “A Reduced Complexity EPR4 Post-Processor,” *IEEE Trans. on Magn.*, vol. 34, no. 1, pp. 135–140, Jan. 1998.

[99] P. Kramer, “Reflective, optical record carrier,” *U.S. Patent no. 5,068,846*, 1988.

[100] L. Agarossi, S. Bellini, C. Beoni and P. Migliorati, “A Volterra model for the high density optical disc,” *Proc. ICASSP*, May 1998.

[101] ——, "Non linear effects in high density optical recording," *Proc. Int. Workshop on HDTV*, Oct. 1996.

[102] L. Agarossi, S. Bellini, F. Bregoli and P. Migliorati, "Equalization of nonlinear optical channels," *IEEE International Conference on Communications (ICC)*, vol. 2, pp. 662–667, June 1998.

[103] L. Guidoux, "Egaliseur autoadaptif a double echantillonnage," *Ann. Telecommun.*, vol. 30, no. 9/10, pp. 331–338, 1975.

[104] P. V. Laarhoven and E. Aarts, *Simulated Annealing: Theory and Applications*. D. Reidel Publishing Company, Holland, 1987.

[105] L.E. Franks, "Carrier and bit synchronization in data communication- a tutorial review," *IEEE Trans. on Commun.*, vol. 28, no. 8, pp. 1107–1120, Aug. 1980.

[106] E. Lee and D. Messerschmitt, *Digital Communication, 2nd edition*. Kluwter Academic Publishers, Boston, Massachusetts, 1994.

[107] L.G. Gubin, B.T. Polyak, E.V. Raik, "The method of projections for finding the common point of convex sets," *USSR Comput. Math. Phys.*, vol. 7, no. 1, 1967.

[108] L.L. Scharf, *Statistical Signal Processing: Detection, Estimation and Time Series Analysis*. New York, NY: Addison-Wesley, 1991.

[109] L.M. Bregman, "Finding the common point of convex sets by the method of successive projections," *Dokl. Akad. Nauk. USSR*, vol. 162, 1965.

[110] M. Abramowitz and I. Stegun, *Handbook of Mathematical Functions (9th edition)*. Dover Publications, New York, 1970.

[111] M. Mansuripur and G. Sincerbox, "Principles and techniques of optical data storage," *Proceedings of the IEEE*, vol. 85, no. 11, pp. 1780 – 1796, Nov. 1997.

[112] M. Spurbeck and R.T. Behrens, "Interpolated Timing Recovery for Hard Disk Drive Read Channels," *IEEE Int. Conf. on Commun. (ICC)*, vol. 3, pp. 1618–1624, Jun. 1997.

[113] J. Moon, “The Role of SP in Data-Storage,” *IEEE Sig. Proc. Mag.*, pp. 54–72, July 1998.

[114] M.Y. Lin, *Synchronous/Asynchronous Adaptive Signal Processing For Recording Channels*. PHD Thesis: National University of Singapore, 2002.

[115] T. Narahara, S. Kobayashi, M. Hattori, Y. Shimpuku, G. van den Enden, J. Kahlman, M. van Dijk, and R. van Woudenberg, “Optical Disc System for Digital Video Recording,” *Jpn. J. Appl. Phys.*, vol. 39, Pt. 1, no. 2B, pp. 912–919, Feb. 2000.

[116] N.M. Zayed and L.R. Carley, “Equalization and Detection for Nonlinear Recording Channels with Correlated Noise,” *IEEE Trans. on Magn.*, vol. 35, no. 5, pp. 2295–2297, Sept. 1999.

[117] T. Okumura, J. Akiyama, S. Maeda, T. Yamaguchi, and A. Takahashi, “New Adaptive Equalization Method for Partial Response Maximum Likelihood System Optimizing Error Rate Performance,” *Jpn. J. Appl. Phys.*, vol. 43, no. 10, pp. 7097–7101, 2004.

[118] T. Okumura, T. Numata, J. Akiyama, S. Maeda, T. Yamaguchi, and A. Takahashi, “Method for evaluating partial response maximum likelihood system performance using sequenced amplitude margin,” *Jpn. J. Appl. Phys.*, vol. 41, no. 3B, pp. 1783–1784, 2002.

[119] P. Kabal and S. Pasupathy, “Partial response signaling,” *IEEE Trans. Commun.*, vol. 23, no. 9, pp. 921–934, 1975.

[120] P.A. Ziperovich, “Performance degradation of PRML channels due to nonlinear distortions,” *IEEE Trans. Magn.*, vol. 27, no. 6, pp. 4825–4827, Nov. 1991.

[121] A. Padiy, B. Yin, C. Verschuren, J. Lee, R. Vlutters, and T. Jansen, “Signal Processing for 35GB on a single-layer Blu-ray Disc,” *Proc. of SPIE, Optical Data Storage*, vol. 5380, pp. 56–70, 2004.

[122] T. Perkins and Z. A. Keirn, “A window-margin-like procedure for evaluating PRML channel performance,” *IEEE Trans. Magn.*, vol. 31, no. 2, pp. 1109–1114, March 1995.

[123] P.G. Ogmundson, “Zero-crossing DPLL bit synchronization with pattern jitter compensation,” *IEEE Trans. on Commun.*, vol. 39, no. 4, pp. 603–612, Apr. 1991.

[124] P.H. Siegel, “Applications of a peak detection channel model,” *IEEE Trans. on Magn.*, vol. MAG-18, no. 6, pp. 1250–1252, Nov. 1982.

[125] P.H. Siegel and J.K. Wolf, “Modulation and Coding for Information Storage,” *IEEE Comm. Magazine*, vol. 29, no. 12, pp. 68–86, Dec. 1991.

[126] P.L. Combettes, “Inconsistent signal feasability problem: Least-squares solutions in a product space,” *IEEE Trans. Signal Processing*, vol. 42, pp. 2955–2866, Nov. 1994.

[127] S. U. H. Qureshi, “Timing recovery for equalized partial-response systems,” *IEEE Trans. on Commun.*, vol. 24, no. 12, pp. 1326–1331, Dec. 1976.

[128] R.B. Staszewski, K. Muhammad, and P.T. Balsara, “A constrained asymmetry LMS algorithm for PRML disk drive read channels,” *IEEE Trans. on Circuits and Systems*, vol. 48, no. 8, pp. 793–798, Aug. 2001.

[129] R.D. Gitlin and J. Salz, “Timing recovery in PAM-systems,” *Bell Syst. Tech. J.*, vol. 50, pp. 1645–1669, May-June 1971.

[130] R.D. Gitlin and S.B. Weinstein, “On the required tap-weight precision for digitally implemented adaptive mean-squared equalizers,” *Bell Syst. Tech. J.*, vol. 58, pp. 301–321, Feb. 1979.

[131] R.W. Lucky, “Automatic equalization for digital communications,” *Bell Syst. Tech. J.*, vol. 44, pp. 547–588, April 1965.

[132] J. S. R.W. Lucky and J. E.J. Weldon, *Principles of Data Communications*. New York: McGraw-Hill, 1968.

[133] R.W. Lucky and H.R. Rudin, “An automatic equalizer for general-purpose communication channels,” *Bell Syst. Tech. J.*, vol. 46, pp. 2179–2208, Nov. 1967.

[134] S. Chen, E. Chng, B. Mulgrew and G. Gibson, “Minimum-BER linear-combiner DFE,” *in Proc. Int. Conf. on Communications*, pp. 1173–1177, 1996.

[135] S. Furumiya, S. Kobayashi, B. Stek, H. Ishibashi, T. Yamagami and K. Schep, "Wobble-address format of the Blu-ray Disc," *Int. Symp. on Opt. Mem. and Opt. Data Storage Topical Meeting*, pp. 266 – 268, July 2002.

[136] S. Haykin, *Adaptive Filter Theory*. Prentice Hall Inc., 1986.

[137] S. Kobayashi, "Nonlinear model for an optical read-only-memory disk readout channel based on an edge-spread function," *Appl. Optics*, vol. 41, pp. 2679–2685, 2002.

[138] S. Lin and D.J. Costello, *Error Control Coding: Fundamentals and Applications*. Prentice Hall, 1983.

[139] S. Van Beneden, J. Riani and J.W.M. Bergmans, "Adaptive decomposition of noise sources in digital recording systems with media noise," *Submitted to IEEE Trans. on Magn*, 2006.

[140] S.J. Ko, P.S. Kim, H.J. Choi, J.W. Lee and J. Lee, "A robust digital timing recovery with asymmetry compensator for high speed optical drive systems," *IEEE Trans. on Consumer Electronics*, vol. 47, no. 4, pp. 821 – 830, Nov. 2001.

[141] H. Stark and Y. Yang, *Vector Space Projection Methods: A Numerical Approach to Signal and Image Processing, Neural Nets and Optics*. Wiley, 1998.

[142] A. Stek, G. W. de Jong, T. P. H. G. Jansen, J. R. M. Bergervoet, and P. H. Woerlee, "Circuit Design and Noise Considerations for Future Blu-ray Disc Optical Storage Technology," *Digest of Technical Papers. ISSCC 15-19 Feb.*, vol. 1, pp. 136–137, 2004.

[143] S.U. Qureshi and E.E. Newhall, "An adaptive receiver for data transmission over time-dispersive channels," *IEEE Trans. Inf. Theory*, vol. 19, pp. 448–457, July 1973.

[144] S.U.H. Qureshi, "Adaptive equalization," *Proc. IEEE*, vol. 73, no. 9, pp. 1349–1387, Sept. 1985.

[145] T. Maeda, H. Minemura and T. Shimano, "Nonlinear Components in Optical Disk Signals: Analysis and Compensation," *IEEE Trans. on Magn.*, vol. 41, no. 2, pp. 992–996, 2005.

[146] T. Maeda, T. Toda, H. Ide, F. Kirino, S. Mita and K. Shigematsu, "Write control method for high density magneto-optical disk system," *IEEE Trans. Magn.*, vol. 29, no. 6, pp. 3787–3789, Nov. 1993.

[147] T. Nakagawa, "A simple detection method for RLL codes (run detector)," *IEEE Trans. on Magn.*, vol. 33, no. 5, pp. 3262–3264, Sep. 1997.

[148] S. van Beneden and A. I. J.W.M. Bergmans, J. Riani, "Minimum-latency tracking of rapid variations in two-dimensional storage systems," *IEEE Trans. on Magn.*, 2005.

[149] W. van den Busche, A. H. Hoogendijk, and J. H. Wessels, "Signal Processing in the Philips 'VLP' System," *Philips Tech. Rev.*, vol. 33, no. 7, pp. 181–185, 1973.

[150] H. van Houten and W. Leibbrandt, "Phase Change Recording," *Communications on the ACM*, vol. 43, no. 11, pp. 64–71, 2000.

[151] R. Vermeulen, "Het Philips-Miller-Systeem voor Geluidsregistratie," *Philips Technisch Tijdschrift*, vol. 1, no. 4, pp. 107–114, April 1936.

[152] W. Coene, H. Pozidis, M. van Dijk, J. Kahlman, R. van Woudenberg and B. Stek, "Channel Coding and Signal Processing for Optical Recording Systems Beyond DVD," *IEEE Trans. on Magn.*, vol. 37, no. 2, pp. 682–688, Mar. 2001.

[153] W.C. Lindsey and M.K. Simon, *Telecommunication systems engineering*. Englewood Cliffs, NJ: Prentice-Hall, 1973.

[154] W.M.J. Coene, "Combi-codes for DC-free runlength-limited coding," *IEEE Trans. Cons. Electronics*, vol. 46, pp. 1082–1087, Nov. 2000.

[155] Y. Tanaka et al, "High density magneto-optical disk technologies," *IEEE Trans. on Cons. Elec.*, vol. 43, no. 3, pp. 475–481, 1997.

Acknowledgment

This work is substantially inspired from my activities in the European project TwoDOS and the co-operation with the different partners. For this reason I would like to thank the different TwoDOS partners: Philips Research Laboratories, Philips ODTC, University of Limerick in Ireland, Lancaster University in the UK and HW Communications in the UK.

The person I would like to thank most is my promotor Prof. Jan Bergmans from the Eindhoven University of Technology (TU/e). His high quality supervision and advises on all levels, were more than necessary for my Ph.D. work. His tremendous knowledge and deep insights were sources of inspiration to me during my Ph.D. period. Moreover, his availability, his high quality guidance and his challenge-based supervision approach allowed me to grow professionally during the last years.

I also would like to thank the TwoDOS research team at TU/e for the enormous team spirit and friendship that I already miss. A special thank goes to my colleague and friend Steven van Beneden for all the discussions, the mutual reviews and the pleasant co-operation. I also thank very warmly Massimo Ciacci and Ali Nowbakht Irani for all their support and their friendship. They were always available for technical and non-technical discussions and made the TwoDOS room at TU/e one of the most pleasant rooms.

Thanks also for the TwoDOS team at Philips research for the pleasant co-operation. I would like to thank Dr. Andre Immink. With his broad knowledge, efficiency at work and deep insights into implementation issues he was always a model for me to follow. Thanks also to Dr. Wim Coene for his enthusiastic project leading and for the exciting discussions during the TwoDOS meetings. Many thanks also to the other TwoDOS project teammates from Philips research for the valuable discussions: Dominique Bruls, Alexander van der Lee, Christopher Busch, Peter Linotte, Floris Crompvoets and Andries Hekstra. Appreciation also goes to the other partners in the European TwoDOS team: Philips ODTC, University of Limerick in Ireland, Lan-

caster University in the UK and HW Communications in the UK. In particular I would like to mention Dr. Thomas Conway for being a source of inspiration and for all his new ideas.

I would never be able to thank enough my parents: Yemma and Babba, for all their sacrifices and their support. I would also like to mention my brothers (Kamal, Said, Otman and Youssef) and my sisters (Jamila and Malika) and their husbands (Said and Abdessalam).

My special acknowledgements to all my dear friends and their families. I would like to mention Mohammed Ali (Allah yerehemou), Rachid, Aziz, Hakim, Hassan, Bilal, Issam, Saad, Tarik, Nabil and all others.

At the end, I would like to thank my dear wife Zoulikha for all her support, her love and for being patient during my Ph.D. period. Thanks for everything and for making me the happiest papa ever. For my little star Safae: thanks for your encouraging sweet smiles.

Curriculum Vitae

Jamal Riani was born in Tétouan, Morocco, on July 3, 1977. In 1997, he entered the Ecole Polytechnique in Palaiseau-France, the most renowned and prestigious engineering school in France. He then joined l'Ecole National Supérieure des Télécommunications (ENST) in Paris to specialize in telecommunication systems.

In 2001, he did an internship at Qualcomm Inc. in San Diego, USA, where he worked on Ultra Wide Band (UWB) systems. He specially analyzed the effect of UWB signals on Code Division Multiple Access (CDMA) systems and focused on the impact of aggregate of UWB transmitters on the IS-95 system.

In 2002, he joined the Eindhoven University of Technology as a Ph.D. student. During the first two years of his Ph.D. period he worked on a European project to develop a two-dimensional optical storage system (TwoDOS). The work was carried out in cooperation with Philips research laboratories and 4 other European partners with the goal of realizing at least a doubling of the storage density compared to the 25 GB Blu-ray Disc system and an increase in data rate by one order of magnitude.

Inspired by the work on TwoDOS, he then focused, in the second part of his Ph.D. period, on equalization and timing recovery for optical storage systems. The results of his research are reported in this thesis.

Currently he is working for Marvell Semiconductor, Inc. in the field of digital signal processing for different communication systems.